**University of Alberta**

# Multirate Control and Multiscale Monitoring of Chemical Processes

by

**Arun K. Tangirala** 

A thesis submitted to the Faculty of Graduate Studies and Research in partial fulfillment of the requirements for the degree of **Doctor of Philosophy**.

in

Process Control

Department of Chemical and Materials Engineering

Edmonton, Alberta
Fall 2001

National Library of Canada
Acquisitions and Bibliographic Services
395 Wellington Street
Ottawa ON K1A 0N4
Canada

Bibliothèque nationale du Canada
Acquisitions et services bibliographiques
395, rue Wellington
Ottawa ON K1A 0N4
Canada

*Your file Votre référence*

*Our file Notre référence*

The author has granted a non-exclusive licence allowing the National Library of Canada to reproduce, loan, distribute or sell copies of this thesis in microform, paper or electronic formats.

L'auteur a accordé une licence non exclusive permettant à la Bibliothèque nationale du Canada de reproduire, prêter, distribuer ou vendre des copies de cette thèse sous la forme de microfiche/film, de reproduction sur papier ou sur format électronique.

The author retains ownership of the copyright in this thesis. Neither the thesis nor substantial extracts from it may be printed or otherwise reproduced without the author's permission.

L'auteur conserve la propriété du droit d'auteur qui protège cette thèse. Ni la thèse ni des extraits substantiels de celle-ci ne doivent être imprimés ou autrement reproduits sans son autorisation.

0-612-69003-2

Canada

**University of Alberta**

**Library Release Form**

**Name of Author**: Arun K. Tangirala

**Title of Thesis**: Multirate Control and Multiscale Monitoring of Chemical Processes

**Degree**: Doctor of Philosophy

**Year this Degree Granted**: 2001

Permission is hereby granted to the University of Alberta Library to reproduce single copies of this thesis and to lend or sell such copies for private, scholarly or scientific research purposes only.

The author reserves all other publication and other rights in association with the copyright in the thesis, and except as hereinbefore provided, neither the thesis nor any substantial portion thereof may be printed or otherwise reproduced in any material form whatever without the author's prior written permission.

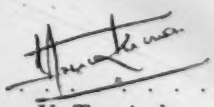

Arun K. Tangirala
CME 536
University of Alberta
Edmonton, AB
Canada, T6G 2G6

**Date**: 31-Aug-2001

**University of Alberta**

**Faculty of Graduate Studies and Research**

The undersigned certify that they have read, and recommend to the Faculty of Graduate Studies and Research for acceptance, a thesis entitled **Multirate Control and Multiscale Monitoring of Chemical Processes** submitted by Arun K. Tangirala in partial fulfillment of the requirements for the degree of **Doctor of Philosophy** in *Process Control*.

Sirish L. Shah
(Dept. of Chemical & Materials Engineering)

Tongwen Chen
(Dept. of Electrical & Computer Engineering)

Bhavik R. Bakshi
(Dept. of Chemical Engineering)
(The Ohio-State University, Columbus, OH, USA)

Behrouz Nowrouzian
(Dept. of Electrical & Computer Engineering)

Fraser Forbes
(Dept. of Chemical & Materials Engineering)

Scott Meadows
(Dept. of Chemical & Materials Engineering)

**Date:** 30-Aug-2001

I dedicate this thesis to my late Father

# Abstract

Multirate (MR) systems arise due to the limitations on the output sampling rates and input adjustment rates of the physical variables. They are inherently more complex and challenging than single-rate (SR) systems and yet, practically important.

The concept of 'lifting', is used in this thesis to analyze multirate systems. It is shown that *lifting* techniques can give rise to intersample ripples in the closed-loop outputs of the MR system. These ripples can be eliminated if the lifted controller satisfies certain gain constraints or by incorporating an integrator at the input rate.

Due to the limitation on the sampling rates, control of multirate systems can be limited by the slowest available measurement, defined here as slow single rate (SSR) control. A natural problem of interest is to explore the benefits that lifted MR control systems can offer over SSR control systems. In this thesis, we address the performance issue: *what are the upper and lower bounds on the performance of multirate systems?* We also answer the question: *can we get better performance with fast single-rate control (FSR) (sampling at faster rates)?* The main contribution of this thesis is a proof that the optimal performance of MR systems is bounded above by that of SSR systems and bounded below by that of FSR systems, with the continuous-time LQR cost function and the generalized $\mathcal{H}_2$-norm as the benchmarks. In the presence of a model-plant mismatch. the sensitivity of the performance benefits is analyzed for first-order SISO systems.

Multirate representations of data are a special case of a more general class of representations, known as *multiscale* representations, which can capture the inherent different/multiple time-frequency scales. These representations are obtained by employing wavelet transforms.

The last part of this thesis focusses on monitoring of multiscale systems using a combination of wavelet transformation with PCA, known as Multiscale PCA

(MSPCA). It is shown that MSPCA has several advantages over conventional PCA both in the theoretical and practical aspects. MSPCA provides an enhanced sensitivity towards and discrimination between detection of incipient and abrupt faults. Application of MSPCA to sheet-break diagnosis using data from a major pulp and paper mill is presented to highlight the potential of this technique.

*"...The science of today is a light matter; the revolutions and evolutions which it will experience in a hundred thousand years will far exceed the most daring anticipations. The truths - those surprising, amazing, unforeseen truths - which our descendants will discover, are even now all around us, staring us in the eyes, so to speak, and yet we do not see them. But it is not enough to say that we do not see them; we do not wish to see them; for as soon as an unexpected and unfamiliar fact appears, we try to fit it into the framework of the commonplaces of acquired knowledge, and we are indignant that anyone should dare to experiment further."*

- Charles Robert Richet, Nobel Laureate in Medicine

*You can control a mad elephant;*
*You can shut the mouth of the bear and the tiger;*
*You can ride a lion;*
*You can play with the cobra;*
*By alchemy you can eke out your livelihood;*
*You can wander through the universe incognito;*
*You can make vassals of the gods;*
*You can be ever youthful;*
*You can walk on water and live in fire;*
*But control of the mind is better and more difficult.*

- Sage Thayumanavar

# Acknowledgements

I wish to express my deep gratitude towards my supervisors Prof. Shah and Prof. Chen for their invaluable guidance, motivation and support mixed with kindness, gentleness and humility. My special thanks to them for their promptness and sparing their invaluable time to help me make the right decisions on several occasions. I will be always grateful to them for sowing the seeds of research in me and nourishing them with a keen inspiration. I am greatly indebted to Prof. Shah for his benevolent and unfailing financial support without which this work would not have been possible.

I am grateful to Prof. Fisher for providing me with the computing facilities and the readiness in providing the needful software. I can never forget his wonderful words of advice and his sense of wit that I have enjoyed in his presence. I am thankful to Prof. Forbes for his wonderful inspiration, and the enjoyable times I have had while assisting him with his teaching. I would also like to express my thanks to Prof. Guay who has influenced me with his novel ideas and his useful comments on my work. I am grateful to Prof. Nandakumar and his family for their valuable advice and moral support that they have provided at crucial times. I would like to express my special thanks to all those Professors who have imparted their priceless knowledge through the courses that I have taken and the seminars that I have attended.

I would like to gratefully acknowledge the Department of Chemical Engineering, University of Alberta, for giving me an opportunity to pursue my Doctoral degree and providing me with the best of the resources and a friendly atmosphere. Special thanks to all the administrative staff who have cheerfully and politely helped me on several occasions.

I will always cherish the warmth and affection that I have received from my present and past colleagues Laksh, Biao, Anand, Rohit, Aseema, Misha, Daniel, Lisa, Bhushan, Kamrun, Dongguang, Ramesh, Ashish, Lanny, Abhishek, Haitao, Xin, Shoukat, Weihua, Mike, Hui Lan, Yale, Giti, Hari, Raghu, Vikas and Zhengang. Special words of gratitude to my ex-colleagues, Laksh and Rohit, who gave me the right impetus during my early days of research. The long and enlightening occasions of blackboard discussions that I have had with Dongguang, Bhushan, Rohit, Haitao

and Xin are unforgettable memories that I carry along. Equally cherishable are those days of preparation for the qualifying exams that I spent in Kamrun's company.

My wonderful friends outside the CPC group, to list whose names would be endless, have been a great source of solace and comfort for me in times of need besides the enjoyment they have given me in their company. I am immensely thankful to all of them for the role each of them has played in making me feel at home in Edmonton. I would like to thank Haitao for his comments on Chapters 6 and 7 of this thesis. I express my deep gratitude towards my friends Bhushan, Abdul, Brian and Riaz for their affectionate and brotherly support during my stay in Edmonton. Special thanks to Kalpana, Janice, Razia, Vishala, Srinivas and Lanny for the precious hands of friendship that they have extended and sharing their valuable knowledge.

I fall short of words to express my immense thanks to Sirinda, my best friend, for showering me with an unconditional wonderful affection, and for being a source of inspiration on many levels.

I also wish to express my gratitude towards all those unknown hands that have worked through their way in making this work successful. I am grateful to Matrikon Consulting Inc. and Prof. Shah, for giving me a golden opportunity in obtaining a hands-on experience on various industrial problems that we handled in the course of this program.

Without the wonderful support of my family members, this work would not have been possible. My endless gratitude towards my parents for bestowing their unconditional love and affection, and for the immense trust that they have placed in me. I am always indebted towards my brothers and my sisters-in-law for their affectionate love and friendship.

My sincerest and humble gratefulness to my Guru, Mathaji, whose everlasting love and guidance has induced in me a keen sense of respect, awe and humility necessary for learning. Through Her, I realize a deep sense of gratitude and responsibility towards the Almighty whose Omnipresence and Everlasting Love has helped me see light at the end of the tunnel.

# TABLE OF CONTENTS


**1 Introduction** 1

1.1 Why Study Multirate Control Systems? . . . . . 4

1.2 Multirate Control . . . . . 4

1.3 From Multirate Systems to Multiscale Systems . . . . . 8

1.4 Multiscale Monitoring . . . . . 11

1.5 Outline of this Thesis . . . . . 12

**2 Multirate Control Design via Lifting** 15

2.1 Background . . . . . 15

2.2 Discrete Lifting . . . . . 19

2.3 Application to Multirate Control . . . . . 25

**3 Ripple-Free Conditions for Lifted Multirate Control Systems** 37

3.1 Introduction . . . . . 37

3.2 Analysis of Gains . . . . . 38

3.3 Constraints on Controller Gains . . . . . 42

3.3.1 Intersample Behaviour in the Presence of Disturbances . . . . 61

3.4 Parametrization of Lifted Controllers . . . . . 62

3.4.1 Stable Plants with $L = 0, F = 0$ . . . . . 64

3.5 Causality Constraints . . . . . 66

3.6 Summary . . . . . 69

3.7 Future Work . . . . . 70

**4 Performance Comparison of Multirate Systems vs. Single-rate Systems** 71

4.1 Motivation . . . . . 71

4.2 LQR Cost Function for Performance Evaluation . . . . . 74

4.2.1 Choice of Benchmark . . . . . 74

4.2.2 Performance Based Multirate Controller Design . . . . . 76

4.2.3 Linking MR and SR Control Design . . . . . 79
4.3 Multirate Control vs. Single-Rate Control . . . . . 85
4.3.1 Regulatory Problem . . . . . 85
4.3.2 Servo Problem . . . . . 87
4.4 Results on an Experimental Model . . . . . 91
4.5 A Step Further: Output Feedback Control . . . . . 93
4.5.1 Main Result: Performance Comparison . . . . . 96
4.6 Conclusions and Summary . . . . . 100
4.7 Journey Ahead . . . . . 101

**5 Robustness Analysis of the Performance Comparison Problem 102**
5.1 Motivation . . . . . 102
5.2 Robustness Analysis . . . . . 103
5.2.1 FSR systems vs. MR systems . . . . . 104
5.2.2 MR vs. SSR systems . . . . . 110
5.3 Simulation Results . . . . . 111
5.4 Summary . . . . . 114
5.5 Future work . . . . . 115

**6 Multiscale Analysis Using Wavelets 116**
6.1 Multiscale Systems . . . . . 116
6.2 Introduction to Wavelets . . . . . 118
6.2.1 The Need for Wavelets: Why? . . . . . 119
6.2.2 Wedding Time and Frequency: Wavelets . . . . . 124
6.2.3 Wavelet Filtering . . . . . 129
6.3 Multiresolution/Multiscale Analysis . . . . . 132
6.3.1 Multiresolution Spaces . . . . . 132
6.3.2 Design of Wavelet Filters . . . . . 134
6.3.3 Fast Orthogonal WT and IWT . . . . . 137
6.4 Application of Wavelets . . . . . 140
6.4.1 Data Compression . . . . . 141
6.4.2 Wavelet Denoising . . . . . 142
6.4.3 Outlier Detection . . . . . 144
6.4.4 Process Identification, Control & Monitoring . . . . . 146
6.5 Summary . . . . . 147

**7 Multiscale Process Monitoring Using Wavelets** 148
7.1 Introduction . . . 148
7.2 PCA and Statistical Assumptions . . . 149
7.3 MSPCA for Dynamic Process Monitoring . . . 153
7.3.1 Philosophy . . . 153
7.3.2 Comparison with Dynamic PCA . . . 155
7.4 Conclusion & Discussion . . . 159

**8 Application of Multiscale PCA to Sheet Break Diagnosis** 161
8.1 Introduction . . . 161
8.2 Motivation . . . 162
8.3 Problem description . . . 164
8.4 Data Analysis . . . 166
8.4.1 Objective . . . 166
8.4.2 Variable Selection and Data Cleaning . . . 166
8.4.3 Wavelet Filtering . . . 168
8.4.4 Initial PCA Model . . . 169
8.4.5 Final PCA Model . . . 170
8.4.6 Remarks on PCA Implementation in the First Phase . . . 171
8.5 Results . . . 172
8.6 Conclusions . . . 172

**9 Conclusions and Future Work** 174

**Bibliography** 178

# List of Figures


2.1 *A multirate system (output/input sampling ratio = n, $n \in Z^+$) (high frequency dots indicate fast-rate signals, low frequency dots indicate slow-rate signals and solid lines correspond to continuous signals)* . . 15

2.2 *A typical multirate system ($T_a \neq T_b$)* . . . . . 17

2.3 *An example of a lifted system (high frequency dots indicate fast-rate signals; low frequency dots indicate slow-rate signals and solid line corresponds to continuous signals)* . . . . . 21

2.4 *(a) A multirate system (output/input sampling ratio = n, $n \in Z^+$) (b) Single-rate lifted system (high frequency dots indicate fast-rate signals; low frequency dots indicate slow-rate signals and solid line corresponds to continuous signals)* . . . . . 24

2.5 *A typical distillation column with the RV-configuration* . . . . . 27

2.6 *Comparison of the 82-state model and the 5-state model (shown for $x_D$) - hardly differ from each other* . . . . . 29

2.7 *Comparison of the non-linear and linear reduced-order models* . . . . 30

2.8 *Closed-loop response of $x_B$ with controller based on augmented plant* . 31

2.9 *Comparison of closed-loop response of $x_D$ and $x_B$ for multirate and single rate systems ($n = 2$)* . . . . . 32

2.10 *Comparison of closed-loop response of $x_D$ and $x_B$ for multirate and single rate systems ($n = 5$)* . . . . . 32

2.11 *Comparison of input profiles (reflux flow rate) for $n = 2$ and $n = 5$* . . 33

2.12 *Continuous-time composition plots for MR system without an integrator in the loop ($n = 2$)* . . . . . 34

2.13 *Slow sampled composition plots for MR system without an integrator in the loop ($n = 2$)* . . . . . 34

2.14 *Fast sampled composition plots for MR system without an integrator in the loop ($n = 2$)* . . . . . 35

3.1 *Typical closed-loop multirate system ($T_b/T_a = n$ ($n \in Z^+$))* . . . . . 42

3.2 *Outputs of the closed-loop system with identical & non-identical controller gains - set point tracking* ($n = 5$) . . . . . 46
3.3 *Inverse lifting of the lifted controller output signal introduces oscillations in the inputs* ($n = 5$) . . . . . 47
3.4 *Inputs to the plant for the closed-loop system with non-identical and identical controller gains - set point tracking* ($n = 5$) . . . . . 47
3.5 *Experimental Tank setup* . . . . . 48
3.6 *Experimental results - multirate level control: (solid) output, (dashed) setpoint* . . . . . 49
3.7 *Experimental results - multirate level control: (solid) output, (dashed) setpoint* . . . . . 49
3.8 *Output and input profiles for set-point tracking in a plant augmented with an integrator - set point tracking* ($n = 5$) . . . . . 50
3.9 *Output (solid) of the closed-loop system with identical & unidentical sums of controller gains - set point (dashdot) tracking; rational sampling ratio* ($n/m = 5/2$) . . . . . 52
3.10 *Output (solid) of the closed-loop MIMO* ($2 \times 2$) *system with identical & non-identical controller gains - set point (dashdot) tracking; integer sampling ratio* ($n = 5$) . . . . . 53
3.11 *Output (solid) of the closed-loop MIMO* ($2 \times 2$) *system with identical & non-identical sums of controller gains - set point (dashdot) tracking; integer sampling ratio* ($n/m = 3/2$) . . . . . 54
3.12 *Closed-loop multirate system with augmented discrete integrator* ($T_b/T_a = n\ (n \in Z^+)$) . . . . . 60
3.13 *Outputs (solid and dash) of the closed-loop MIMO* ($2 \times 2$) *system when the lifted system is augmented with a lifted integrator - unit set point (dashdot) tracking; integer sampling ratio* ($n/m = 3/2$) . . . . . 61
3.14 *Generalized setup of a discrete-time control system* . . . . . 63
3.15 *Parametrization of controllers - LFT of Q* . . . . . 64

4.1 *General closed-loop multirate system* ($T_b/T_a = n/m$) . . . . . 75
4.2 *Equivalent multirate system (SISO G and integer sampling ratio)* . . 78
4.3 *Variation of relative improvement in the closed-loop performance of FSR over MR systems with input weight* $R_c$ *and sampling ratio* $n/m$. 92
4.4 *Variation of relative improvement in the closed-loop performance of MR over SSR systems with input weight* $R_c$ *and sampling ratio* $n/m$. 93
4.5 *A general sampled-data system* . . . . . 94

4.6 *MR system with integer sampling ratio and its associated SSR system* 96
(a) MR sampled-data system . . . . . 96
(b) Associated SSR sampled-data system . . . . . 96
4.7 *Introducing lifting operators in the fast-rate channels of MR and SSR systems* . . . . . 97
(a) Lifted MR system . . . . . 97
(b) Lifted SSR system . . . . . 97
4.8 *Associated finite-dimensional systems for the lifted MR and SSR control systems* . . . . . 99
(a) Lifted MR system . . . . . 99
(b) Lifted SSR system . . . . . 99

5.1 *FSR vs. MR systems - performance comparison* . . . . . 112
(a) Variation of $\tilde{p}$, $\tilde{q}$ and $\tilde{r}$ with $R_c$ . . . . . 112
(b) Trajectory of roots with $R_c$ . . . . . 112
5.2 *Effect of input weighting on MR and FSR systems (robustness analysis)* 113
(a) Intervals for robust stability and optimal performance . . . . . 113
(b) Comparison of robust stability of FSR & MR systems - $\tilde{\beta}$ and $k_f$ vs. $R_c$ . . . . . 113
5.3 *Effect of input weighting on MR and SSR systems (robustness analysis)* 113
(a) Variation of $\tilde{p}$, $\tilde{q}$ and $\tilde{r}$ with $R_c$ . . . . . 113
(b) Trajectory of roots with $R_c$ . . . . . 113
5.4 *MR vs. SSR systems - performance comparison* . . . . . 114
(a) Intervals for robust stability and optimal performance . . . . . 114
(b) Comparison of robust stability of MR & SSR systems - $\tilde{\beta}$ and $\tilde{\Omega}$ vs. $R_c$ . . . . . 114

6.1 *Fourier transform of signal:* $f(t) = sin(2\pi 10t)+sin(2\pi 50t)+sin(2\pi 200t)+sin(2\pi 300t)$ *- provides good frequency resolution* . . . . . 120
6.2 *Fourier transforms of two signals - look almost identical* . . . . . 121
(a) Fourier transform of signal 1 . . . . . 121
(b) Fourier transform of signal 2 . . . . . 121
6.3 *Signals 1 & 2 - quite different from each other* . . . . . 122
(a) Signal 1 . . . . . 122
(b) Signal 2 . . . . . 122
6.4 *STFT of signals 1 & 2 using Hanning window (window width = 32 units) - capable of distinguishing signals 1 & 2* . . . . . 123
(a) STFT of signal 1 . . . . . 123

(b) STFT of signal 2 . . . . . 123
6.5 *STFT of signals 1 & 2 using Hanning window (window width = 512 units) - loss in time resolution with increase in frequency resolution* . 123
(a) STFT of signal 1 . . . . . 123
(b) STFT of signal 2 . . . . . 123
6.6 *Time frequency tiling with Delta, Fourier, STFT and Wavelet basis functions* . . . . . 127
(a) Best time resolution; Poor frequency resolution . . . . . 127
(b) Best frequency resolution; Poor time resolution . . . . . 127
(c) Fixed time-frequency resolution . . . . . 127
(d) Ideal time-frequency resolution . . . . . 127
6.7 *Splitting data into low and high frequency components - Wavelet filtering tree: Mallat's pyramidal algorithm* . . . . . 130
6.8 *Wavelet transformation of signal 2 using D8 wavelets* . . . . . 131
6.9 *Daubechies scaling function $\phi$ and wavelet $\psi$ with p vanishing moments* 137
6.10 *Reconstruction at each level starting from the coarsest level - using Haar basis* . . . . . 139
6.11 *Reconstruction at each level starting from the coarsest level - using Daubechies basis* . . . . . 139
6.12 *IWT - reconstruction of each component of the wavelet decomposition of signal 2 using D8 wavelets* . . . . . 140
6.13 *MRA of signal 2 using D8 wavelets* . . . . . 141

7.1 *ACF plots of z and the scores from PCA* . . . . . 152
(a) Autocorrelation function for $z$ . . . . . 152
(b) Autocorrelation function for PC-1 . . . . . 152
7.2 *Autocorrelation function of PC-1 from DPCA* . . . . . 153
7.3 *ACF plots of wavelet coefficients and their reconstruction* . . . . . 154
(a) Autocorrelation function of the wavelet coefficients $d_{4,z}$ . . . . . 154
(b) Autocorrelation function of reconstructed data from $d_{4,z}$ . . . . 154
7.4 *Typical illustration of the MSPCA methodology* . . . . . 155
7.5 *Results from DPCA* . . . . . 156
(a) $T^2$ plot from DPCA . . . . . 156
(b) SPE plot from DPCA . . . . . 156
7.6 *Results from MSPCA - highest frequency band* . . . . . 157
(a) SPE plot from MSPCA . . . . . 157
(b) $T^2$ plot from MSPCA . . . . . 157

7.7 *MSPCA - lowest frequency band; SPE chart clearly captures the fault* 157
(a) SPE plot from MSPCA . . . . . 157
(b) $T^2$ plot from MSPCA . . . . . 157
7.8 *ACF of the scaling function coefficients - approximately decorrelated* 158
7.9 *MSPCA - lowest frequency band; 1-PC SPE is unable to capture the persistent fault* . . . . . 158
(a) SPE plot from MSPCA . . . . . 158
(b) $T^2$ plot from MSPCA . . . . . 158

8.1 *Typical flowsheet of a paper machine* . . . . . 164
8.2 *Procedure for data analysis* . . . . . 167
8.3 *2-level wavelet transformation and decomposition of a process measurement* . . . . . 168
(a) 2-level wavelet transformation . . . . . 168
(b) 2-level wavelet decomposition . . . . . 168
8.4 *MSPCA revealing the process drifts due to a sheet break* . . . . . 170
8.5 *Scores plots due to initial and final phases of PCA* . . . . . 171
(a) PC3 scores based on 70-variable PCA model . . . . . 171
(b) PC1 scores based on 10-variable PCA model . . . . . 171

# Chapter 1

# Introduction

From a philosophical perspective, the objective of control can be termed analogous to the basic inherent human objective of maintaining a state of mind. The objectives could be, *(i)* holding the current state of mind for a desired period of time in the presence of disturbances both external and internal, and *(ii)* maintaining the stability of mind *(iii)* reaching another state of mind from the present one in the absence or presence of disturbances. The first objective is analogous to controlling a given system at its current state (for now we use state in a general sense) over a finite time in presence of disturbances (*regulatory problem*). The second one is concerned with the stability of a system or analogous to the design of a controller to stabilize a given system while the third objective is equivalent to taking a system from one state to another or tracking a given signal (a combination of both *servo problem* and *regulatory problem*).

From a practical perspective, control objectives mainly arise due to the need for *(i)* quality control, *(ii)* safety measures, and *(iii)* economic reasons, all of which give rise to a combination of both *servo* and *regulatory* problems. Quality control is more than a rule in process industry. Quality may be described in innumerable terms such as composition, temperature, hardness, strength, density, volume, etc. Each quality control problem is a challenge in its own due to the nature of each quality variable and its relationship with other process variables. Besides the quality variable, many a time it becomes necessary to control the quantity (or differential quantity) variables such as pressure, flow rate, production rate etc. Safety is a great motivating factor to constrain several process variables within certain operating limits. The importance of this problem in the operation of a plant requires no elaboration as it is well understood to be one among the foremost operating requirements. Economic reasons could be a combination of both quality and quantity factors, safety measures, meeting the market and supplier demands, cost-effective operations, etc. All control problems

arising due to these factors could be classified either as *servo* or *regulatory* problems or a combination of both. In order to maintain a state of mind, it is necessary to know the functioning of our mind. In process control, this is equivalent to identifying the process (or the evolution of process states), preferably in a mathematical form.

Although identification can be performed in both the continuous-time domain and discrete-time domain, for all practical purposes, modern control theory demands analysis in the discrete domain implying the requirement of sampled signals. The fundamental principle of sampling (Nyquist 1928, Whittaker 1935, Shannon 1949) states that a continuous-time signal can be reconstructed from its discrete-time counterpart without loss of information if the sampling frequency is *at least* twice as fast as the maximum frequency in the original signal. This is known as the Nyquist frequency or sampling rate. The theory of sampling is fundamental to discrete-time control and identification. Sampled models are natural descriptions for many natural phenomena in several areas besides the field of digital control. Examples of such situations are the rotation of a radar antenna, stock information, measurements using analytical instruments, etc. In practice, the sampling frequencies are 5-10 times faster than the Nyquist sampling frequency (twice the maximum frequency present in the continuous-time signal). Ideally, it is desirable to carry out both identification and control in the continuous-time domain. For this reason, it would be beneficial to sample signals at faster rates so that maximum process information can be extracted.

However fast we wish to sample a signal, limitations exist on the fastest possible sampling rate for a signal governed by the physical variable sampled, the hardware, *etc.* For example, in distillation columns, composition estimates can take anywhere between 5-30 minutes; molecular weight estimates in a polymerization reactor can take about 30-60 minutes of analysis time. This is a constraint imposed mainly by the physical variable which is being sampled. On the other hand, temperature, pressure and flow measurements can be obtained at a relatively faster rate. Therefore, if we consider a distillation column, for example, we would have different signals at different sampling intervals (or different sampling rates). Such examples with different sampling rates for different signals comprising a given system are common and given the term **multirate systems**. The term **single-rate systems** applies to those systems whose signals are all sampled at one identical rate.

Single-rate (SR) systems present relatively less complexity in terms of controller design, identification or monitoring than multirate (MR) systems. This is mainly because the mathematical complexity involved in dealing with SR systems is less intriguing than MR systems and also that MR systems are not as transparent as SR systems. Besides, MR systems are a more general case and include SR systems as a

special case. There is a wide body of literature and theoretical framework on simple to advanced techniques for these SR systems.

On a relative basis, controller design techniques for MR systems have evolved at a slower pace and received less attention. The main hindrance being the increase in mathematical complexity and the scarcity of design tools as one moves from SR to MR systems. Moreover, it has been only in the recent two decades that technology has emerged to meet the hardware requirements for faster sampling. With the advent of multiprocessors capable of operating at much faster sampling rates, it is now both feasible and practical to focus on design of multirate controllers. In addition, performance requirements increasingly stress the need for sampling at a faster rate because it can greatly aid in improving intersample performance.

The *first half* of this thesis focuses on issues related to MR control systems, particularly, *(i)* controller constraints arising in the design of MR lifted (the term *lifting* will be explained later) control systems, *(ii)* the benefits of MR control in comparison with the SR control and *(iii)* robustness analysis of MR systems vs. SR systems. The entire set of ideas on multirate controller design and performance analysis is built on the lifting framework (see section 2.2 for lifting techniques). It is shown that a set of constraints exists on the resulting controller in order to ensure ripple-free outputs. In the context of performance, it is shown in both cases of state feedback and output feedback control that MR systems are practically superior to the slow SR (SSR) systems both for the regulatory and the tracking problem in the absence of model-plant mismatch. Besides, we prove that the lower bound on the optimal performance of MR systems is the optimal performance of the fast single-rate (FSR) (operating at the *greatest common divisor (g.c.d.)* of all the sampling rates) systems.

In the presence of a mismatch, we consider a complementary but an interesting performance comparison problem. Our objective is to evaluate the commonly held belief that faster sampling rates, in general, can yield better performance. Therefore, we compare the superiority of fast single-rate systems over multirate systems in the presence of uncertainties. It is shown for first-order SISO systems that multirate systems can perform better than FSR systems. Theoretical expressions for those regions of uncertainty are established under which the superiority of MR systems holds.

The choice of lifting framework is due to the mathematical tractability and convenience it provides in viewing MR systems as fictitious SR systems with increased input-output dimensionality. The practicality of lifting methodology lies in the fact that it does not require the aid of a fast-rate model and encourages its use in chemical

processes, such as distillation, polymerization, etc.

## 1.1 Why Study Multirate Control Systems?

One of the most important factors motivating the study of MR systems is the practical limitations that not all process variables can be sampled at the same rate. As discussed earlier, in a distillation column, the composition estimates take relatively longer times than the flow or temperature measurements. The presence of these multiple sampling rates renders the controller design problem challenging and complex. In such situations, control moves are usually limited by the slowest available measurement(s). In such a strategy, only the information at the slowest rate is utilized. On the other hand, from a performance point of view, it is motivating to make faster control moves and also improve intersample performance, see for *e.g.*, Åström and Wittenmark (1984). These requirements are met by a multirate controller that utilizes the entire information available in the multirate measurement set.

Then, it is intuitive that the multirate controller can yield a better closed-loop performance than a SSR controller. However, in making such a judgement it should not be forgotten that in practice, we can seldom obtain a perfect or accurate knowledge of the process, meaning that model-plant mismatch is inevitable. Therefore, the question that arises is: *Do faster sampling rates necessarily imply improved performance in the presence of model-plant mismatch?* This question arises from the question: *is it necessary to respond to every process change when the complete process knowledge is unavailable?* Also, in applying data analysis techniques, changes in a chemical process are usually observed by looking at changes in measurements which are typically corrupted with measurement and sensor noise. These questions leads us to acquire knowledge of an appropriate basis for a fair comparison and the measure of performance, indicating that the comparison problem is non-trivial.

The above factors therefore motivate and necessitate the study of MR systems, the related controller design techniques, the performance benefits that one can achieve over SR systems.

In the following section, a detailed introduction to multirate control is presented which highlights the uniqueness of MR control system analysis.

## 1.2 Multirate Control

Several types of multirate systems arise due to *(i)* uniform input and non-uniform output sampling, *(ii)* non-uniform input and uniform output sampling and *(iii)* non-

uniform input and output sampling rates. Other cases of multirate systems arise when certain signals are irregularly sampled, such as the Melt Flow Index of a polymer in a Low Density PolyEthylene (LDPE) reactor (Lakshminarayanan *et al.* 1998). In this work, we particularly focus on the case when the outputs are sampled at a slower rate than that at which the control moves are made. This case is more practically appealing since in chemical processes usually the outputs are available at a rate slower than the rate at which the control moves are updated. However, it is assumed the sampling rate is fixed in time.

Multirate control systems pose challenging problems because of their time-varying nature. The time-varying nature is attributed to the disparity in the sampling periods of the sampler and the hold elements, regardless of the time-invariance of the continuous-time system. Simply speaking, the challenge in the multirate control problem occurs because the control moves have to be designed at a rate different from the rate at which the information is available. In an optimal sense, the problem is exciting because two questions arise: *(i)* what is the optimal criterion? and *(ii)* how do we design the control moves in this optimal sense? The lack of available information at the same sample rate as the control signals in MR systems is a handicap in using SR control techniques. In order to overcome this drawback, from a traditional point of view, inferential control schemes have been developed to estimate the intersample output signals. Inferential schemes are mainly based on two methods: *(i)* intersample estimates based on a fast-rate process model, and *(ii)* intersample estimates based on other secondary measurements. By secondary measurements, it is meant they are not of primary interest to the control problem, but only used to estimate the primary measurements (the output signals). For example, in a distillation column, since the composition measurements take relatively longer periods of times, tray temperatures are used as secondary estimates to infer the primary composition measurements. Estimation schemes that do not accommodate the infrequently measured output or the primary process variables were used by Brosilow and Tong (1978). Such estimation schemes often give biased estimates of the process output because of model-plant mismatch and the presence of disturbances. Estimation schemes that incorporate the infrequently measured primary process output into estimation schemes were first proposed by D'Hulster and van Cauwenberghe (1981). Guilandoust *et al.* (1987) proposed a multirate scheme that uses the infrequent primary measurements to update a transfer function based inferential process model which can be then used to update the primary variables from the secondary outputs.

Inferential relationships that are shown to have convergence properties have been stated formally and entirely as a multirate estimation problem by Lu and Fisher

(1990). Another method for estimation and filtering frequently used in chemical processes is the Kalman filtering strategy (Kalman 1960). The process models used in the Kalman filter approach are state-space models that result from writing a dynamic balance on the system states. In the multirate case, the multirate Kalman filtering strategy is employed. Glasson (1983) proposed the multirate Kalman filter algorithm with regard to applications in aerospace engineering. The extension of this multirate Kalman filter algorithm to non-linear/time-varying processes is discussed in Gudi (1995) with application to a fed-batch fermentation process.

Robustness issues of control systems with measurement difficulties, actuator or measurement failures are analyzed in the generalized inferential framework that takes into account both primary and secondary measurements by Lee and Morari (1992). In their work, the authors give a detailed analysis of various $\mathcal{H}_2$ based optimal control schemes that make use of the separation principle and modified Kalman filtering approaches. The authors also make a comparison of the various design approaches on a high purity distillation column.

Inferential control based on a fast-rate model assumes the availability of a fast-rate model for direct use. The fast-rate models can be either obtained by fast discretization of a continuous-time model or by using multirate data by lifting schemes (Li *et al.* 2000*b*). The second method actually overcomes the practical limitation of obtaining a fast-rate model by other means. In the lifting scheme, the fast-rate model is essentially obtained by using only the multirate data, whereas otherwise it is necessary to have a continuous-time model which is not always practical. Moreover, the lifting approach does not involve the use of secondary measurements.

On a parallel note, other disciplines of engineering witnessed the evolution of several other schemes for the analysis of MR systems in a rigorous theoretical fashion. The origins of such work dates back to early 1950's (Sklansky and Ragazzini 1955, Kranc 1957, Kalman and Bertram 1959, Jury and Mullin 1959, Freidland 1961). Classical time-varying periodic discrete models have been used to describe MR systems because of their periodic nature, see for example, Berg *et al.* (1988) and Grasselli *et al.* (1995). In Berg *et al.* (1988), the design of multirate controllers is performed using mainly two methods, *(i)* Discretization methods: (a) Discretization of the plant model and (b) Discretization of continuous-time LQG cost function; *(ii)* Synthesis methods: (a) Successive loop closure methods, (b) LQG method and (c) Constrained Optimization method. The LQG method synthesizes a multirate controller by representing each hold as a state in an augmented system, and "switching logic" matrices are used to coordinate the various sampling activities. A lifting approach to $\mathcal{H}_2$ optimal synthesis for *dual-rate* sampled data systems is discussed in

Chen and Francis (1991*a*). The term *dual-rate* is given to the system whose inputs are all sampled at a uniform rate while all the outputs are sampled uniformly at a different rate. Multirate systems can also arise when the sampler and hold functions are chosen as a part of the controller design process for a continuous-time plant. This view arises from the idea of generalized sampled-data hold functions, see for example, Arvanitis (1998) and Mirkin and Rotstein (1997). However, the last two decades witnessed the emergence of a convenient framework for the analysis of MR control systems known as *lifting* (Khargonekar *et al.* 1985, Araki and Yamamoto 1986, Meyer and Burrus 1975, Bamieh *et al.* 1991, Chen and Qiu 1994, Sagfors and Toivonen 1998). Khargonekar *et al.* (1985) showed how closed-loop zeros could be assigned by periodic controllers, concluding, for example, that the system gain margin could be increased without bound (even if there is a bound for time-invariant controllers). In Araki and Yamamoto (1986), the authors analyze multirate pole-placement assuming that the inputs and outputs can be paired off into loops having the same rate.

Ideas discussed in Kranc (1957) and Freidland (1961) are key to the development of *lifting* schemes which are used extensively in this work. The lifting framework was developed by Khargonekar *et al.* (1985). Lifting converts a given MR systems to a fictitious single-rate system by making use of the periodic nature of the multirate system. The fundamental idea is to express each fast-rate signal as a vector and rearrange them suitably to give rise to a new vector at a slow-rate, but with increased dimensionality. Therefore, the resulting fictitious SR system has an increased input-output dimensionality and given the name *lifted system*. The controller is then designed for the lifted system using the rich theoretical framework established for the SR based control design techniques. The resulting controller is given the name *lifted controller*. Input moves designed using the lifted controller are inverse lifted taking into account the rearrangement involved during lifting and then passed through the zero-order hold. This method is superior to methods of inferential control in the sense that it eliminates the necessity of a fast-rate model since the lifted system can be identified directly from the multirate data. Additionally, the identified lifted system can provide information regarding the underlying fast-rate model (Li *et al.* 2001). Chapter 2 discusses the notion of lifting and its applications in greater detail. A more detailed and formal treatment is presented in Chen and Francis (1995).

A key motivating factor for MR control as discussed earlier is the closed-loop performance factor. It appears intuitive that MR systems should give better closed-loop performance than SR systems at the slow rate. However, to understand the effect of sampling rates on the closed-loop performance, a rigorous and fundamental analysis of the closed-loop performance of MR systems relative to SR systems is

required. Issues such as the choice of a suitable benchmark, conditions under which such a comparison can be established, etc., have to be resolved prior to arriving at a theoretical conclusion to the comparison problem. For example, what signal in the system or its transformation would give a measure of the performance of MR vs. SR systems? Despite the practicality of this issue, until recently (Tangirala *et al.* 2000), only a handful of papers have addressed a closely related issue (McEachen and Meyer 1991, Berg *et al.* 1988). In both papers (McEachen and Meyer 1991, Berg *et al.* 1988), the comparison is purely on the basis of simulation. The main drawback of the work reported in McEachen and Meyer (1991) is that it lacks a common ground for comparison. For instance, equal importance to input weights in the MR and SSR systems is not ensured because the design problem does not start from a continuous-time cost function, bur rather with a discrete-time one. In Berg *et al.* (1988), although the controllers are derived from the same continuous-time LQG cost function, the comparison is made only on the basis of simulation. Moreover, the MR system is modelled as a periodic discrete-time system, yielding a periodic LQG controller. In contrast, in this work, we give a theoretical proof that MR systems indeed give a better performance than SSR systems with their worst-case performance identical to that of SSR systems. Also, we show that the optimal performance of MR systems is bounded below by the optimal performance of FSR systems. The proof is built on an LTI framework using lifting techniques, with the continuous-time LQR cost function (state-feedback) as a benchmark.

These issues are discussed in Chapter 4 in a theoretical fashion with appropriate simulation results.

## 1.3 From Multirate Systems to Multiscale Systems

We begin this section by understanding the terms *multiscale* and *multiscale representation* with a simple practical example.

Consider a geographical map of a city drawn to a low scale. At this scale, the resolution in the map is good, meaning two places actually close in distance can be seen distinctly on the map. However, the low scale would make the map dense and possibly illegible. But if the finer details are irrelevant, then the scale can be increased. Evidently, the resolution of the map becomes poorer, but with a better overall picture of the city. In this way, we can build multiscale representations starting from the fine representations to the very coarse representation.

The above analogy closely resembles the method of representing a continuous-time signal with a sampled signal. In digital systems, the sampling interval decides the

scale of the signal (as the scale in the map), and therefore the time resolution. Hence, the sampled signal is said to be a single-scale representation of the continuous-time signal. All process measurements can be said to fall under this category unless under rare situations where the sampling times are irregular. In a multirate sampling scheme, the sampled signals are at different scales (time resolutions). The finest resolution for each signal is given by its sampling interval. Each signals is in fact an approximation of the underlying signal at that resolution. However, this way of multiscale representation is elementary and a special case of the general multiscale representations. In a multiscale representation, we start from the finest resolution in time and go to coarser representations (approximations) of the signal using suitable transformations. The importance of multiscale representation is clear from the following discussion.

In the earlier section, we indicated how closed-loop performance analysis could reveal the choice of sampling rates in a given system. Besides the performance issue, it is commonly known that variables in a chemical process that evolve slowly with time do not require fast sampling, whereas variables which change quickly with time require fast sampling. Many chemical processes in practice possess such characteristics where different physical variables have different rates of change. This behaviour is termed as **multiscale** since different time scales exist in one process. The *multiscale* behaviour also means that different frequencies (since the frequency of a signal is related to its rate of change) exist over different periods of time for different signals. Therefore, the term *multiscale* also refers to the different frequency scales.

With wide variations in the evolution times, it is intuitive to sample signals in a multiscale system at different rates depending on their rate of change. These different sampling rates in turn give rise to multirate systems. Thus, multirate systems also arise because of the multiscale behaviour of chemical processes.

In other words, multirate systems can be viewed as a special case of multiscale systems. This is because although the process is single-scale (all variables evolve approximately at the same rate) in nature, the multiscale nature could be introduced in the data due to different sampling intervals. It should be noted that the term multiscale is not limited to describing processes. Rather, the multiscale nature can also be introduced due to the representation of data with different sampling rates. From this angle, multirate systems can be considered as a subset of multiscale systems. This motivates us to consider a more general analysis of multirate systems, *i.e.*, multiscale systems.

An example of a multiscale system is a fluidized catalytic cracker where the residence time in the reactor is significantly smaller than that in the regenerator. Other

examples include chemical reactors in series with different residence times, chemical vapour deposition reactors (where coupling of fast and slow reaction occurs), etc.. Methods that extract information by representing the measured variables at various scales are more congenial for analysis of such data than conventional methods which perform analysis at a single scale. Besides, it is well-established that a direct application of standard control methods to multiscale processes, without accounting for the multiple time-scales may lead to controller ill-conditioning, stiffness and closed-loop instability due to slightly non-minimum phase behaviour of the process (Kokotovic *et al.* 1986, Christofides and Daoutidis 1996*a*, Christofides 1998).

Multiscale analysis of systems involves integration of both time and frequency (scale) domain techniques providing a more general framework for modelling, control and monitoring of several multiscale systems. Multiscale modelling, control and monitoring based on wavelet analysis has been receiving increasing attention due to the attractive properties of wavelets in an integrated time-frequency domain. Wavelet transformations have come into play to overcome the shortcoming of Fourier transforms in providing simultaneous time-frequency projection of a signal. Wavelets are not totally new to mathematicians or physicists but they were formalized in the early 1980's (Grossman and Morlet 1984) as a result of the reactivating fundamental collaboration between researchers in theoretical physics and signal processing. Wavelet transforms (Daubechies 1990, Daubechies 1988) have been shown to offer very good time-frequency localization properties over other techniques. Wavelets have also emerged as novel tools for analysis of non-stationary signals, data compression, multirate signal processing, etc..

Wavelet filters offer several advantages over other linear filters (Bakshi 1999, Bakshi 1998) due to their ability to represent data at various scales or different resolutions. Multiresolution representation or decomposition of data via wavelets (Mallat 1989) is a very useful property that forms the basis for multiscale estimation, control and analysis of systems using wavelets (Stephanopoulos *et al.* 1997, Dyer *et al.* 1998). Wavelet transforms of cross-spectrum data are shown to be useful in the detection of time delays for linear systems (Tabaru and Shin 1997). Identification of time-varying systems and model validation using wavelet techniques are discussed in Tsatsanis and Giannakis (1993) and Doroslovacki and Fan (1996). Although wavelet transforms cannot be directly employed to identify processes in the frequency domain, with certain approximations they can be used to identify two time-scale systems. These ideas were recently coined by Chaplais and Alaoui (1996). Multiscale MPC is obtained by formulating the MPC problem in the multiscale domain in order to overcome certain weaknesses of traditional MPC such as limited representation of

model-plant mismatch, the inability to shape frequency response characteristics of the outputs through systematically selected weights in the objective function, just to mention a few (Karsligil *et al.* 1999). Applications of wavelets to other areas such as monitoring, pattern recognition and fault detection have also received wide attention in the last decade.

## 1.4 Multiscale Monitoring

Process Monitoring (PM) is usually on a higher level in the hierarchy of plant operation. Monitoring typically involves governing the safe operation, supervising situations involving equipment failure, abnormal operating conditions, sensor failures, process drifts, etc. Many a time, it is of crucial importance to equip a chemical plant with sensitive monitoring instrumentation involving advanced strategies. The area of process monitoring has been receiving increasing attention over the years. This area is formally defined as Fault Detection, Diagnosis and Isolation. Each of these areas involves intricate complex analysis with various ideas borrowed from pattern recognition. Monitoring can be in general more challenging than a control or identification problem.

Among the well-established multivariate statistical techniques for statistical monitoring of chemical processes, Principal Component Analysis (PCA) (Kresta *et al.* 1991, MacGregor 1994) has gained widespread popularity. Several extensions of conventional PCA have been proposed to take into account various factors such as process dynamics (Ku *et al.* 1995), changing operating conditions (Li *et al.* 2000*c*), monitoring of large-scale and complex processes (Nomikos and MacGregor 1994), etc. However, all these techniques are based on single-scale representation (same time-frequency localizations at all locations) of the measurements and therefore suffer the disadvantages of single-scale methods (Bakshi 1999). Moreover, they do not exploit the advantages of multiscale representations. One of these disadvantages is their inability to adapt to the nature of the signal. They have a fixed time-frequency resolution which forces a trade-off between the extent of noise removal and the quality of retained features for signals with multiple scales. Other disadvantages occur with cases of non-stationary signals, presence of autocorrelated errors, etc. Some of these disadvantages will become clear when we discuss the Short Time Fourier Transform (STFT) in the ensuing sections. The multiscale nature of wavelet filters integrated with these multivariate statistical techniques offer certain attractive features such as improved detection of short-lived faults and incipient faults, automatic filtering of the scores and residuals at each scale (Bakshi 1998, Kosanovich and Piovoso 1997), etc. In addition, ap-

proximate decorrelation of stochastic components due to wavelet decomposition of signals provides a justified environment for using PCA for sensor fault detection on autocorrelated data (Zhang *et al.* 1999).

In addition to the above features, multirate data can be conveniently fused together with the help of wavelet transformations. Subsequently, one can apply a well-established single-scale monitoring technique such as PCA. This area of research is also recently emerging and gaining attention (Dyer *et al.* 1998).

In this work, the focus is on process monitoring in the multiscale framework. The advantage of multiscale framework is that it encompasses the case of multirate systems as well. Thus, measurements at different rates can be fused in an appropriate way to include all the available information for monitoring purposes. However, the present thesis highlights the use of wavelets for multiscale process monitoring only for single-rate systems. This is done by using a combination of wavelets and PCA, popularly known as Multiscale PCA (MSPCA). Future directions are also given to encompass multirate measurements for monitoring purposes.

## 1.5 Outline of this Thesis

The thesis is concerned with the discussion of: *(i)* multirate control, and *(ii)* multiscale monitoring of multivariate chemical processes. To enable easy travel through the thesis, each chapter begins with a statement of purpose giving the reader an overall picture of the substance present therein.

Chapter 2 deals with control of multirate systems. The focus of Chapter 2 is to present the notion of lifting from a chemical engineering point of view. In this chapter, first an introduction to lifting techniques is presented. The discussion is supplemented with an application of lifting techniques to multirate control of a binary distillation column.

Chapter 3 forms the first part of one of the main contributions of this thesis. This chapter presents the issues involved in the multirate controller design problem. The presentation highlights the constraints on the controller gains to ensure ripple-free closed-loop outputs for both the servo and regulatory types of problems. Following this discussion, causality constraints are briefly reviewed. Parametrization methods are employed to design multirate/lifted controllers satisfying the gain constraints in Section 3.4. Experimental work along with results from simulations is presented wherever appropriate to corroborate the theoretical findings in the earlier sections. Future trails are laid for the design issues involved in the area of multirate control using lifting techniques.

Chapter 4 presents the second part of contributions in the context of performance issues discussed in Section 1.2. Comparison of closed-loop performances of multirate and single-rate systems requires a benchmark that can provide a fair ground for both the systems. In this work, the continuous-time LQR cost function for LTI systems is considered for this purpose. Our objective is to give a theoretical proof that MR systems can perform better than single-rate systems at the slow rate in the absence of model-plant mismatch. Also, we give a lower bound for the performance of MR systems - the optimal performance of the associated fast-rate systems. We consider both set-point tracking and disturbance rejection problems. Tracking performance is compared for three classes of signals, namely, step, ramp and sinusoidal types of signals. The servo problem is tackled by converting it to a regular LQR problem and then using the results from the regulatory case. For the output-feedback case, the generalized $\mathcal{H}_2$-norm (Bamieh and Pearson 1992, Khargonekar and Sivashankar 1992) is chosen as a benchmark. The superiority of MR systems over SSR systems is still shown to hold good.

In Chapter 5, novel results on the robustness analysis of the closed-loop performance comparison problem are given. It is intuitive that faster sampling should give better performance. However, in presence of model-plant mismatch, drawing definite conclusions is a non-trivial problem as mentioned in Section 1.2. With the continuous-time LQR cost function as a benchmark, we establish conditions on the uncertainty intervals for which first-order SISO MR systems give better performance than their fast single-rate (FSR) counterparts. Uncertainty is introduced in the form of gain and pole mismatch. Sufficient and necessary conditions are given for MR systems with integer sampling ratios, while only sufficient conditions are established for MR systems with rational sampling ratios. These results provide a new direction to the assessment of benefits of MR systems from a performance point of view. Simulation results are presented in Section 5.3 to confirm the theoretical results established in this chapter. In conclusion, future directions for further research in this area are given.

Multiscale analysis first appears in Chapter 6 with a brief discussion on multiscale systems. Wavelets are introduced in Section 6.2 with emphasis on their applications to multiscale or multiresolution analysis.

Combination of wavelet analysis with PCA, termed as Multiscale PCA (MSPCA) applied to Multiscale Process Monitoring is presented in Chapter 7. Advantages of MSPCA over conventional single-scale techniques with regard to sensitivity to fault detection, adherence to theoretical assumptions for SPM, etc. are illustrated in Section 7.3.2.

A real-time application of MSPCA to industrial data for detecting sheet-breaks in a pulp and paper mill is presented in Chapter 8. The application illustrates the potential of MSPCA as an emerging multivariate statistical data analysis tool in extracting useful information supplementary to process knowledge in solving process problems.

Conclusions to this work appear in Chapter 9 giving an overall summary and drawing inferences based on the overall work reported in this thesis. Future directions to the research are proposed towards the end of that Chapter.

# Chapter 2

# Multirate Control Design via Lifting

**Purpose:** To introduce the reader to the concept of lifting techniques from a chemical engineering perspective, with an illustration on a binary distillation column.

## 2.1 Background

Multirate control, as the term suggests, is concerned with the control of multirate systems. The term multirate arises due to the simple reason that different signals of a system are sampled at different or multiple rates. A schematic of a typical multirate system is shown in Figure 2.1.

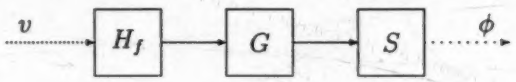


Figure 2.1: *A multirate system (output/input sampling ratio = $n$, $n \in Z^+$) (high frequency dots indicate fast-rate signals, low frequency dots indicate slow-rate signals and solid lines correspond to continuous signals)*

In Figure 2.1, $G$ represents a continuous-time SISO LTI system[1] with different sample rates for the output and input. In particular, the output is sampled $n$ times slower than the input or equivalently, the sampling interval of the output is $n$ times larger than the input sampling interval, $h$. Accordingly, $H_f$ stands for a fast-rate zero-order hold with sampling interval $h$ and $S$ denotes a slow-rate sampler with sampling

[1]In this work, in general, $G$ refers to a continuous-time LTI system, unless specifically stated otherwise.

interval $nh$. Throughout the analysis, we base our focus on those MR systems whose outputs are available at a slower rate than the inputs since these situations are practical and commonly encountered in the chemical process industry (e.g., distillation columns, polymerization reactors). Nevertheless, wherever appropriate, situations arising due to slow-control, and fast sampling are also considered for the sake of completeness.

For the original multirate system, it is appropriate here to introduce the definition of a single-rate system at the slow rate (SSR system) and a single-rate system at the fast rate (FSR system). An SSR system is a discrete-time system operating at the slowest sample rate of all the signal sampling rates in the corresponding MR system. In this case, the SSR system is defined as $SGH$, where $H$ is the fictitious zero-order hold at the slow sample interval $nh$. More generally, when the ratio of the sampling intervals are rational, *i.e.*, $n/m$ ($n$ and $m$ are relatively prime), the SSR system operates over the least common multiple ($l.c.m$) interval of all the sampling intervals in the system. Similarly, an FSR system is defined as a single-rate system operating at the greatest common divisor ($g.c.d$) intervals of all the sampling intervals in the corresponding MR system. In the case of Figure 2.1, the FSR system is defined as $S_fGH_f$ operating over the interval $h$. Both $S_f$ and $H$, as introduced here for the sake of analysis, are fictitious sampler and zero-order hold with sampling periods $h$ and $nh$ respectively.

A general multirate *control system* is shown in Figure 2.2, where $S_b$ represents the output sampler with period $nh$ and $H_a$ represents a zero-order hold with sampling interval $mh$. $G$ represents a continuous-time LTI system and $C_m$ represents the multirate controller. Signals $r$, $d$ and $y_k$ stand for the reference, disturbance and sampled output signals respectively. The simplest case of multirate system as depicted in Figure 2.1 is the case where the output sampling interval is an integer multiple of the input sampling interval.

Evidently, the major difference between single-rate and multirate systems is the non-uniformity in the sampling rates of the signals. Accordingly, if the continuous-time system is LTI, the corresponding multirate system is linearly periodically time-varying (LPTV) whereas the single-rate system is LTI. This major difference between MR and SR systems affects the course of analysis of MR systems in a way that makes the controller design more complicated and challenging than that of SR systems. Thus, it is more appropriate to analyze MR systems in the LPTV framework whereas SR systems can be analyzed in the LTI framework[2].

The LPTV nature of MR systems makes the control methodologies in the LTI

[2]It is assumed that the original continuous-time system is LTI.

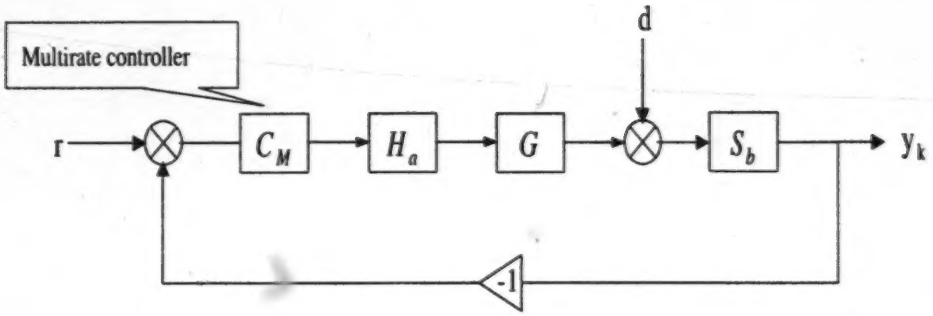


Figure 2.2: *A typical multirate system ($T_a \neq T_b$)*

framework inaccessible. In simple terms, the rate mismatch between the output and input samples is the primary source of complexities in MR systems. As explained in Section 1.2, one of the strategies to overcome this drawback is to estimate the missing or the intersample outputs so as to match the rate of manipulation of the inputs. Intersample estimation is the key to inferential control strategies. Estimation can be done either by means of a fast-rate model or with the aid of secondary variables. An example of the latter method is to estimate the distillate compositions (primary variable) in a distillation column using tray temperatures (secondary variables). Traditionally, Kalman filters (Kalman 1960) have been used for optimal estimation strategies (Glasson 1980, Glasson 1983, Gudi 1995). Among Kalman filtering strategies various classes exist such as the ordinary Kalman filter, extended Kalman filter, non-linear Kalman filter, etc. An alternative method as mentioned earlier is to employ a fast-rate model (available at the *g.c.d* of all the sampling intervals) to estimate the intersample outputs. A fast-rate model can be obtained by discretizing a continuous-time model at the fast sample rate. Practically, this approach might be infeasible since it is difficult to obtain a continuous-time model for many physical systems. Moreover, it is not always possible to locate secondary variables to infer primary variables. Both these methods share a common ground in that they estimate intersample outputs for controller design.

In this work, we base our controller design on a different strategy known as *lifting*. Lifting techniques have been in use since their origin from Kranc's concept of switch decomposition (Kranc 1957) and the work by Freidland (1961). Formal treatment of lifting techniques was given by Khargonekar *et al.* (1985). The lifting methodology has been since popular in analyzing multirate systems and has been employed extensively

in both controller design (Khargonekar *et al.* 1985, Araki and Yamamoto 1986, Ravi *et al.* 1990, Meyer 1990, Bamieh *et al.* 1991, Chen and Francis 1991*a*, Chen and Qiu 1994, Sagfors and Toivonen 1998, Tangirala *et al.* 2001) and performance analysis of multirate systems (Meyer 1992, Tangirala *et al.* 2000). The methodology is simple and offers powerful tools because of its capability of converting MR systems into time-invariant SR systems. However, the resulting SR systems have an increased dimensionality. For instance, lifting a SISO MR system whose outputs are sampled at a period $2h$ and inputs at a period $h$ results in a 2-input, 1-output single-rate system with a sampling interval $2h$. With the exception of increased dimensionality, the lifting operator serves a useful function of transforming an LPTV system to an LTI system. Lifting operators exist for continuous-time systems as well under the name of continuous lifting. Continuous-time lifting takes a finite-dimensional LTI (FDLTI) system in continuous-time to a discrete-time LTI system, but with infinite dimensional input/output spaces. In the following section, we discuss only discrete lifting with suitable illustrations since the work presented here extensively involves discrete domain analysis.

Multirate control using lifting methods is a three step design. The first step involves transforming all signals *available at different sampling rates* (multi-rate) to fictitious signals *available at a single uniform sampling rate* (single-rate). This is the lifting step which results in fictitious signals (termed as *lifted signals*) of increased dimensionality, but where the 2-norm of the signals is preserved. The second step consists of designing a controller (termed as the *lifted controller*) for the single-rate system comprised of the lifted signals, using techniques available for SR systems. Finally, since the lifted controller gives the lifted input moves, the outputs of the lifted controller have to be inverse lifted to obtain the fast-rate input signals to the plant. A more detailed explanation with suitable examples is illustrated in Section 2.3.

Multirate control performed this way has a number of advantages as discussed in Section 2.3. The concept of discrete lifting is discussed in detail in Section 2.2. Discrete lifting transforms a one-dimensional fast-rate signal to a set of slow-rate signals with increased dimensionality.

Design of lifted multirate control systems is concerned with two main issues. The first issue is that of causality, *i.e.*, the lifted controller designed has to be causal, thus calling for a set of causality constraints on the controller. While the source of this problem is lifting (as it is a non-causal operation), the second issue, which is novel in this work, is due to inverse lifting. Inverse lifting the lifted controller moves at steady state leads to the presence of intersample ripples in the closed-loop output.

It is shown in this work that intersample ripples can arise in the closed-loop outputs if the controller fails to satisfy certain gain constraints. Thus, the lifted controller in addition to satisfying the causality constraints is also required to satisfy the gain constraints for all stable systems. Chapter 3 highlights the issue of intersample ripples and discusses in detail the source of these ripples, the conditions under which they arise and methods to eliminate or avoid them. Section 3.5 discusses the problem of causality constraints. It should be noted that causality constraints arise in all cases except when the output is sampled $n$ ($n \in Z^+$) ($Z^+$ denotes the set of all positive integers) times slower than the input. The subsequent section utilizes parametric and optimal methods to design causal controllers which do not give rise to intersample ripples in the closed-loop outputs.

State-space design methods provide a convenient framework for design, especially to arrive at models for lifted systems. However, transfer functions formats are also used interchangeably with the state-space formats, whichever is more appropriate to the situation. The following notation is introduced in the discussions to follow. State-space matrices in the continuous-time are represented as $(A, B, C, D)$ and transfer functions are denoted by $\hat{g}(\lambda)$, where we have used $\lambda = z^{-1}$ for the sake of convenience.

## 2.2 Discrete Lifting

In this section, we introduce the concept of discrete lifting, *i.e.*, lifting signals in the discrete-time domain. We first discuss lifting discrete signals and subsequently extend it to lifting discrete-time systems.

Lifting techniques (Khargonekar *et al.* 1985) are essentially the result of concatenation of fast-rate signals to form slow-rate signals with increased dimensionality. The concept of lifting originates from Kranc's idea (Kranc 1957) of *switch decomposition*. It involves the simple idea of rearranging a fast-rate signal to give rise to a slow-rate signal with increased dimensionality. As an example, consider two multirate signals available at sample rates $2h$ and $3h$.

$$u = \{u(0), u(2h), u(4h), \cdots\}, \quad y = \{y(0), y(3h), y(6h), \cdots\}$$

A rearrangement of these signals would give rise to the following vectored input and output signals

$$\underline{u} = \left\{ \begin{bmatrix} u(0) \\ u(2h) \\ u(4h) \end{bmatrix}, \begin{bmatrix} u(6h) \\ u(8h) \\ u(10h) \end{bmatrix}, \cdots, \begin{bmatrix} u(6nh) \\ u((6n+2)h) \\ u((6n+4)h) \end{bmatrix}, \cdots \right\}.$$

and

$$\underline{y} = \left\{ \begin{bmatrix} y(0) \\ y(3h) \end{bmatrix}, \begin{bmatrix} y(6h) \\ y(9h) \end{bmatrix}, \cdots, \begin{bmatrix} y(6nh) \\ y((6n+3)h) \end{bmatrix}, \cdots \right\}$$

where $n$ is a non-negative integer. The idea is that both the resulting vectored signals $\underline{u}$ and $\underline{y}$ are available at a uniform single period $6h$, the *least common multiple or l.c.m.* of $2h$ and $3h$. The above rearrangement is formally termed as *lifting*, represented by the operator $L$. More generally, lifting is represented by $L_N$, where $N$ denotes the *order* of lifting. In the above example, the order of lifting was $N = 3$ in the first transformation, while $N = 2$ for the second transformation. In this work, the subscript $N$ is dropped for the sake of simplicity. The resulting signals are referred to as *lifted* signals. In the above example, note that the signals $\underline{u}$ and $\underline{y}$ have an increased dimensionality. Thus, lifting converts a SISO multirate system into a MIMO single-rate system, *i.e.* a 3-input, 2-output system in this illustrative example. The process of moving back to $u$ and $y$ from $\underline{u}$ and $\underline{y}$ is termed as *inverse lifting*, represented by the operator $L_N^{-1}$ or simply $L^{-1}$. The combined transformation of lifting and inverse lifting is an identity transformation. In all the ensuing discussions, all lifted signals are denoted with an underline.

Now, we present the mathematics of the lifting operation. A discrete signal $v$ on lifting yields a lifted signal represented by $\underline{v}$ and denoted as:

$$\underline{v} = Lv$$

If the order of lifting $v$ is for example, $N = 2$, the operation can be represented using the system matrix representation of $L$ as:

$$\begin{bmatrix} \underline{v}(0) \\ \underline{v}(1) \\ \underline{v}(2) \\ \vdots \end{bmatrix} = \left[\begin{array}{c|c|c|c|c|c} I & 0 & 0 & 0 & 0 & \cdots \\ 0 & I & 0 & 0 & 0 & \cdots \\ \hline 0 & 0 & I & 0 & 0 & \cdots \\ 0 & 0 & 0 & I & 0 & \cdots \\ \hline 0 & 0 & 0 & 0 & I & \cdots \\ 0 & 0 & 0 & 0 & 0 & \cdots \\ \hline \vdots & \vdots & \vdots & \vdots & \vdots & \end{array}\right] \begin{bmatrix} v(0) \\ v(1) \\ v(2) \\ \vdots \end{bmatrix} \tag{2.1}$$

where the identity matrix $I$ in equation (2.1) has the same dimensions as $v$ (in this example, $I = 1$). The dimension of $\underline{v}$ in equation (2.1) is $N = 2$ times the dimension of $v$ (in general, the dimension of $\underline{v}$ would be $N$ times the dimension of $v$). It is clear from (2.1) that lifting results in the localization signals in the time domain. It is an all-pass filter and changes the sampling interval of the original signal. Moreover, for the partition shown, $[L]$ is neither lower-triangular nor Toeplitz implying that as a system, $L$ is non-causal and time-varying. The non-causal property of the lifting

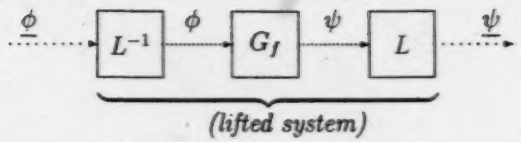


Figure 2.3: *An example of a lifted system (high frequency dots indicate fast-rate signals; low frequency dots indicate slow-rate signals and solid line corresponds to continuous signals)*

operator plays an important role in the design of lifted controllers. As explained later in Section 3.5, it is this property which gives rise to the undesired set of causality constraints. A very useful property of $L$ is that it is norm-preserving. Thus, in the case of $l_2$-norms, it can be shown that

$$\|Lv\|_2 = \|v\|_2 \tag{2.2}$$

In order to map the slow-rate signals (lifted signals) back to their fast-rate counterparts, we need to introduce another operation known as *inverse lifting* denoted by $L^{-1}$. Thus, $L^{-1}$ takes $\underline{v}$ to the space of $v$. Again choosing $N = 2$, the operator $L^{-1}$ can be represented using the system matrix representation as:

$$[L^{-1}] = \left[\begin{array}{cc|cc|cc|c} I & 0 & 0 & 0 & 0 & 0 & \cdots \\ \hline 0 & I & 0 & 0 & 0 & 0 & \cdots \\ \hline 0 & 0 & I & 0 & 0 & 0 & \cdots \\ \hline 0 & 0 & 0 & I & 0 & 0 & \cdots \\ \hline 0 & 0 & 0 & 0 & I & 0 & \cdots \\ \hline \vdots & \vdots & \vdots & \vdots & \vdots & \vdots & \end{array}\right] \tag{2.3}$$

The above representation of inverse lifting shows that as a system, $L^{-1}$ is causal and time-varying. The causal property of the inverse operation is essential to compensate for the non-causal operation involved during lifting. The time-varying nature is expected as the operation involves a change of sampling intervals (from slow to fast sampling interval). It should be noted that inverse lifting preserves the norms of signals as well. It is easy to see that $LL^{-1} = I_{MN}$ and $L^{-1}L = I_M$, where $M$ is the dimension of $v$. The former identity corresponds to mapping lifted signals back to the space of lifted signals, while the latter expression corresponds to mapping fast-rate signals back to the space of fast-rate signals.

So far we have discussed lifting (and inverse lifting) discrete signals. Now, we extend these ideas to lifting discrete-time systems, specifically FDLTI systems.

Lifting discrete-time systems is equivalent to lifting the input and output signals so that the resulting lifted signals have a sampling period equal to the *l.c.m.* of the sampling intervals of the original signals.

An important point to note here is that although we have discussed lifting with reference to MR systems, the operation is not limited to MR systems alone. In other words, lifting is concerned with signals (irrespective of whether they belong to MR or SR systems) rather than systems. Here, we are utilizing the potential of lifting by applying it to MR systems. Therefore, it should be kept in mind that the term *lifted systems* can be applied to systems resulting from lifting MR and SR systems as well.

For illustration purposes, we begin with the single-rate case, *i.e.*, both the input and output signals are sampled over one identical interval $h_b/n$, where $h_b$ is a base sampling period and $n$ is a positive integer. The purpose of doing so will become clear when we apply these results to lifting multirate systems subsequently. Now, we lift both the output $\psi$ and input $\phi$ such that the corresponding signals $\underline{\psi}$ and $\underline{\phi}$ are available over the sampling period $h_b$. Again, the output and input signals of the lifted system, $\underline{\psi}$ and $\underline{\phi}$ are fictitious signals.

If $G_f$ represents the fast-rate discrete-time system, then the lifted system is represented as $G_L = LG_dL^{-1}$ as shown in Figure 2.3. The dimension of the new system is increased by $n$-fold if the order of lifting is $n$. It is not difficult to show that $G_L$ is LTI as well.

Next, given $\hat{g}_f$, which is the transfer function for the fast-rate model $G_f$, we compute the transfer function for $G_L$, denoted as $\hat{g}_L$. First, we show the procedure for $n = 2$ and then extend it to a general $n \in Z^+$. Assuming that $\hat{g}_f(\lambda)$ is described in state-space terms as:

$$\hat{g}_f(\lambda) = \left[\begin{array}{c|c} A_f & B_f \\ \hline C & D \end{array}\right]$$

then the system matrix representation of $\hat{g}_f$ can be written as:

$$[G_f] = \begin{bmatrix} D & 0 & 0 & 0\cdots & \\ CB_f & D & 0 & 0 & \cdots \\ CA_fB_f & CB_f & D & 0 & \cdots \\ CA_f^2B_f & CA_fB_f & CB_f & D & \cdots \\ \vdots & \vdots & \vdots & \vdots & \end{bmatrix} \tag{2.4}$$

Each row (except the first one) of the system matrix is obtained by appending the beginning of previous row with the next impulse response coefficient. In a similar way, based on the functionality of lifting and inverse lifting operators, we can write system matrices for $L$ and $L^{-1}$ (equations (2.1) and (2.3) are given for $n = 2$). These derivations are clearly shown in Chen and Francis (1995). Then, for $n = 2$, the system

matrix representation of the lifted system can be represented as:

$$
\begin{aligned}
[G_L] &= [L][G_f][L^{-1}] \\
&= \left[\begin{array}{cc|cc|c}
D & 0 & 0 & 0 & \cdots \\
CB_f & D & 0 & 0 & \cdots \\
\hline
CA_fB_f & CB_f & D & 0 & \cdots \\
CA_f^2B_f & CAB_f & CB_f & D & \cdots \\
\hline
\vdots & \vdots & \vdots & \vdots &
\end{array}\right]
\end{aligned} \tag{2.5}
$$

It can be noticed that $[G_L]$ looks similar to $[G_f]$ excepting the repartition of the blocks. The transfer function for the lifted system can be then arrived from equation (2.5) as:

$$
\hat{g}_L(\lambda) = \left[\begin{array}{c|cc}
A_f^2 & A_fB_f & B_f \\
\hline
C & D & 0 \\
CA_f & CB_f & D
\end{array}\right] \tag{2.6}
$$

Observe that the state-space representation of $\hat{g}_L$ clearly indicates that $G_L$ is both FDLTI and causal. More generally, the following theorem is stated (Chen and Francis 1995).

**Theorem 1** *The lifted system $G_L$ in general, is FDLTI and written as,*

$$
\hat{g}_L(\lambda) = \left[\begin{array}{c|cccc}
A_f^n & A_f^{n-1}B_f & A_f^{n-2}B_f & \cdots & B_f \\
\hline
C & D & 0 & \cdots & 0 \\
CA_f & CB_f & D & \cdots & 0 \\
\vdots & \vdots & \vdots & \vdots & \\
CA_f^{n-1} & CA_f^{n-2}B_f & CA_f^{n-3}B_f & \cdots & D
\end{array}\right] \tag{2.7}
$$

**Proof.** Proof of this theorem follows from the observation made earlier from equation (2.6). ∎

Some important observation follow from the expression for the lifted system given by Theorem 1.

1. Lifting preserves the order of the system, *i.e.*, the lifted system has the same number of states as the original system. This is a useful property as most optimal controllers designed for the lifted system will be of the same order as the original system.

2. Lifting preserves the stability of the system, *i.e.*, if $A$ is stable, so is $A^n$.

3. Since lifting preserves the norms, $\|\hat{g}_f\|_2^2 = \|\hat{g}_L\|_2^2/n$. This property plays a great role in controller design, especially in minimizing intersample ripples in sampled-data systems.

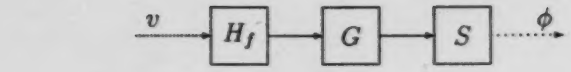


(a)

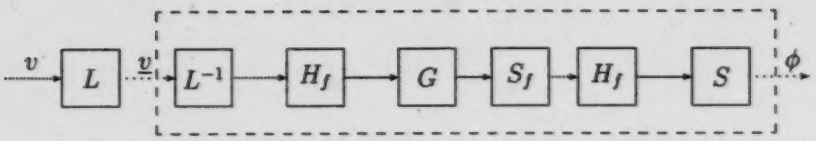


(b)

Figure 2.4: *(a) A multirate system (output/input sampling ratio = n, $n \in Z^+$) (b) Single-rate lifted system (high frequency dots indicate fast-rate signals; low frequency dots indicate slow-rate signals and solid line corresponds to continuous signals)*

4. The operation results in an increase in dimensionality. As evident from equation (2.7), the lifted system is an $(n \times n)$ system. This feature of lifting results in an increase in controller dimensionality and may be a disadvantage for the design technique.

In the above case, we considered lifting as applied to a single-rate system at the fast rate. Now, we illustrate the application of these ideas to lifting a simple multirate system whose inputs are sampled at a rate $n$ ($n \in Z^+$) times faster than the output. It is assumed that the input is sampled over the interval $h_b/n$ while the output is sampled at $h_b$, the base period. The multirate system then is appropriately described in Figure 2.4(a), where the symbols in the blocks have their usual meaning. Figure 2.4(b) is obtained from Figure 2.4(a) by using two properties: (i) the identity property of lifting and inverse lifting and (ii) $SH_fS_f = S$. The components consisted by the dashed box comprise the *lifted system* $\tilde{G}_L$ in this case. The tilde on the top of $G_L$ is used to differentiate from the lifted system obtained in the earlier case. The inputs and outputs of the lifted system are available at the slow rate, $h_b$. The major difference between the previous and the present situation is that we lifted both the signals in the former case whereas we lifted only the input in the latter one.

Having identified the corresponding lifted system, the next step is to arrive at a transfer function for the lifted system. For this purpose, again we use the system

matrix representations of the lifting and inverse lifting operators. In addition, we utilize the following relationship between $SH_f$ and the lifting operator, $L$:

$$SH_f = \begin{bmatrix} I & 0 & \cdots & 0 \end{bmatrix} L \tag{2.8}$$

The blocks comprising of $S_f G H_f$ is none other than $G_f$, the fast-rate discretized version of $G$. Therefore, the following equations follow in order:

$$\begin{aligned} \tilde{G}_L &= SH_f S_f G H_f L_n^{-1} \\ &= \underbrace{[I \ 0 \ \ldots \ 0]}_{n \ blocks} L_n G_f L^{-1} \\ &= \overbrace{[I \ 0 \ \ldots \ 0]} G_L \qquad (2.9) \\ & \qquad (2.10) \end{aligned}$$

Using the transfer function for $G_L$ from our earlier result in equation (2.7), the transfer function for $\tilde{G}_L$ can be written as:

$$\hat{\tilde{g}}_L(\lambda) = \left[\begin{array}{c|ccc} A_f^n & A_f^{n-1}B_f & A_f^{n-2}B_f & \cdots & B_f \\ \hline C & D & 0 & \cdots & 0 \end{array}\right] \tag{2.11}$$

Observe from equation (2.11) that the lifted system is a $(1 \times n)$ system, *i.e.*, one output and $n$ inputs respectively.

The reader should note that a continuous version of the above exists under the name of *continuous lifting*. This topic is beyond the scope of discussion here. Interested readers may refer to Chen and Francis (1995) for a discussion on continuous lifting. In the following section, we illustrate the above ideas to control a multirate binary distillation column.

## 2.3 Application to Multirate Control

The analysis and design of multirate control systems involve mainly two approaches, namely, *(i)* the periodic discrete-time modelling approach, and *(ii)* the lifting methodology. This work adopts the latter approach for the following reasons. The main advantage of the lifting approach is that it is conceptually simple and enables a convenient analysis of stability and performance issues of multirate control systems. In addition, the lifting framework translates an MR system into a linear time-invariant (LTI) system, where as the former approach results in a time-varying system. Clearly, it is simpler to analyze LTI systems because of the rich framework of theory that exists in this area (Khargonekar *et al.* 1985, Araki and Yamamoto 1986, Chen and

Qiu 1994, Sagfors and Toivonen 1998). It is for this reason that we have chosen to analyze multirate system using the lifting framework.

Furthermore, the lifting methodology has the following advantages. Firstly, and importantly there is no necessity of estimating intersample outputs either by means of a fast-rate model or using secondary variables. The controller design is based on the lifted model, but not the fast-rate model. Secondly, this method encompasses the case where a fast-rate model is available. Lifted models can be built either from a fast-rate model or through direct identification of a lifted model from the measurements. Since the focus of this work is to illustrate the design technique and the issues involved therein, we will adopt the former case, i.e., building a lifted from the fast-rate or a continuous-time model.

For illustration purposes, we choose a $(2 \times 2)$ distillation column, *i.e.*, two controlled variables (distillate and bottoms compositions) and two manipulated variables (recycle and vapour flows). A distillation column is an appropriate choice as it exemplifies a classical multirate system. While the composition measurements can take 15-30 minutes, flow rate measurements are available at a much faster rate. The nonlinearity and the high interaction among the control loops pose a challenging multirate control problem. The single-rate control problem has been explored in detail by Skogestad (1997*a*). The typical configuration of a distillation column is shown in Fig. 2.5. Detailed analysis and description of distillation columns are elucidated in several publications - see for example Skogestad (1997*b*) and Skogestad and Postlethwaite (1996). The distillation column model used here is provided in Skogestad (1997*b*). The following paragraphs briefly discuss the description of the process system, modelling of this system and the choice of controlled and manipulated variables for this system Skogestad (1997*b*).

In a distillation column, we are interested in separating a mixture of two or more components. In this work, we consider a two component mixture entering the column at a feed flow rate $F$ with a lighter (more volatile) component composition $z_F$. In all the discussions to follow, we only refer to the composition of the lighter component. Mass transfer occurs between the liquid and vapour phases at each stage (tray) in the column and the vapour at the top is condensed to get the distillate $D$ highly rich in the lighter component with a composition $x_D$. A portion of this distillate is recycled to the column at a reflux rate $R$ to achieve higher purities. The liquid at the bottom of the column is partially reboiled to get a bottoms flow rate $B$ with a composition $x_B$ and the vapour boilup $V$. The condenser drum has a holdup of $M_D$ and the bottoms a holdup of $M_B$. There are a total of $N_T + 1$ stages in the column including the total condenser at the top. The reflux flow rate $R$ is a measure of the energy consumption

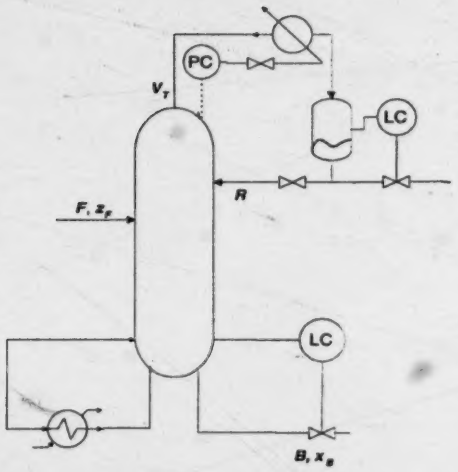


Figure 2.5: *A typical distillation column with the RV-configuration*

in the column and affects the separation (factor) significantly. The column contains a series of stages at each of which, a certain amount of separation take place. As the number of stages become very large, the energy consumption becomes minimum. On the other hand, with a minimum number of stages infinite energy reflux may be required. The external flows ($D$ and $B$) also influence the separation factor but in practice, only small variations in these flows are allowed as $D/F$ is kept close to $z_F$ to get high purity products.

The vapour-liquid equilibrium (VLE) between the two components, assuming to be constant, is given by,

$$\alpha = \frac{y/(1-y)}{x/(1-x)}$$

The quality of the feed, or the amount of liquid in the feed, is denoted by $q_F$ (1 in this example). This notation follows from (Skogestad 1997*b*).

A first-principles model can be developed by writing down the mass and energy balances for the system. The following assumptions are made for the system:

1. Constant relative volatility $\alpha$ (as defined above). This can be re-written as

$$y = \frac{\alpha x}{1 + (\alpha - 1)x}$$

2. The molar flows of the liquid and vapour along the column are constant. This means that the heat of vaporizations for the components will not differ significantly.

3. Constant pressure throughout the column.

4. The liquid dynamics are linear and there is equilibrium at every stage.

The balance equations give rise to a model with four inputs ($R$, $V$, $D$ and $B$) and four outputs ($x_D$, $x_B$, $M_D$, and $M_B$). Disturbances may occur in the system due to changes in ($F$, $z_F$, and $q_F$). Conventionally, the column is first stabilized by closing the level loops associated with the condenser drum and the reboiler drum by manipulating $D$ and $B$, respectively, thus leaving two controlled variables, the product compositions. The remaining inputs available for manipulation are $R$ and $V$. This is known as the RV-configuration which shall be adopted in this work. The open-loop system in this work refers to this $2 \times 2$ system. The column has a total of 41 trays and the steady-state values are given below:

| Quantity | $F$ | $z_F$ | $R$ | $D$ | $V$ | $B$ | $x_D$ | $x_B$ |
|---|---|---|---|---|---|---|---|---|
| Value | 1.0 | 0.5 | 2.7063 | 3.2063 | 0.5 | 0.5 | 0.99 | 0.01 |

All the flow rates are in [kmol/min] and compositions are in mole fractions.

Distillation columns are known to be highly non-linear in nature. mainly due to the nonlinear VLE. The nonlinearity in the distillation column is more pronounced at high purities where the gains drastically drop (in magnitude). Nevertheless, linear models obtained by linearizing around a nominal operating point serve reasonably well for the purpose of controllability and RGA (Relative Gain Array) analysis, and controller synthesis. In fact, linear models based on logarithmic compositions are much less dependent on the operating point. Using the non-linear model, a linear model relating the two inputs ($R$ ,$V$) and the logarithms of compositions ($\log\left(\frac{x_D}{1-x_D}\right)$ , $\log\left(\frac{x_D}{1-x_D}\right)$) is extracted using the **linmod** command in MATLAB. The result is a continuous-time state-space model.

The linear model obtained is stable and contains 82 states (41 tray compositions and 41 holdups). In order to reduce the large number of dimensions in the original model, the balanced truncation technique is employed which allows the reduced order model to retain the strict causality in the system. The reduced order model consists of 5 states. Note that scaling (as described in Skogestad and Postlethwaite (1996)) was done prior to reduction. Figure 2.6 obtained for a step change in $R$ shows that the reduced-order model possesses similar characteristics as the original model. Similarities in responses are seen for all the four cases, *i.e.*, responses of $x_D$ and $x_B$ for step changes in $R$ and $V$. Also, it is clear that for a step change in $R$, this linear model gives a similar response as the non-linear model for the first 10 minutes. The advantage of having a linear model based on logarithmic compositions

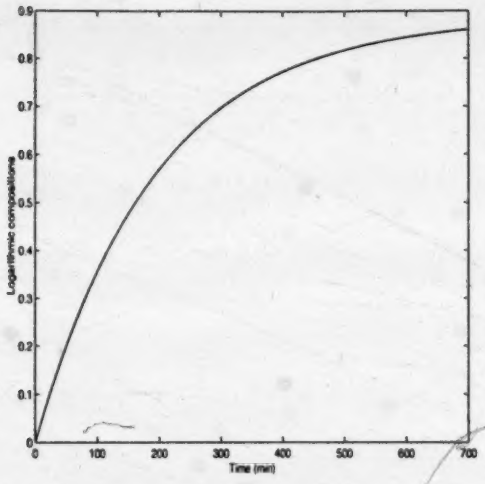


Figure 2.6: *Comparison of the 82-state model and the 5-state model (shown for $x_D$) - hardly differ from each other*

can be seen clearly from Fig. 2.7. Evidently it is useful in a linear controller design problem. The steady-state gains of the reduced-order model differs slightly from the original model as shown below. However, one can always use other techniques such as balanced residualization which preserve the steady-state gain in addition to the model-reduction (Skogestad and Postlethwaite 1996).

Reduced-order

$$G_r(0) = \begin{bmatrix} 88.4936 & -87.0628 \\ 109.4444 & -110.5713 \end{bmatrix} \tag{2.12}$$

Original model

$$G(0) = \begin{bmatrix} 88.4653 & -87.0860 \\ 109.5031 & -110.8809 \end{bmatrix} \tag{2.13}$$

The negative sign suggests that a change in the vapour boilup rate affects the compositions in the opposite direction.

Controllability analysis of the original model reveals 9 controllable states and the reduced-order model has 5 controllable states. The dominant time-constant is 193.05 *min*. Additionally, the original model contains only 6 observable states whereas all the states in the reduced-order model are observable. Thus, the reduced-order model is of great use for controller design.

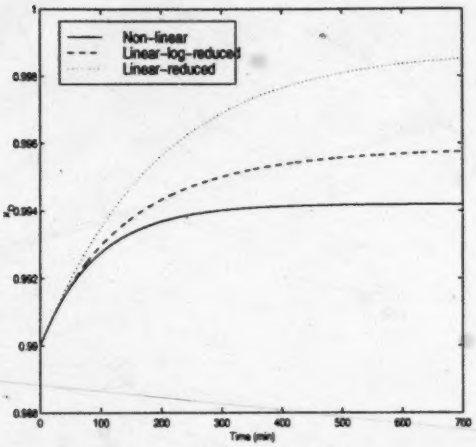


Figure 2.7: *Comparison of the non-linear and linear reduced-order models*

In order to design the controller, it is necessary to assign the appropriate manipulated variable to a controlled variable, based on a user-chosen criterion. Several such combinations arise in a $4 \times 4$ (including the uncontrolled levels) system. In the literature, both the issues, namely, one-point control (perfect control of one of the compositions) and two-point control (both the composition loops are closed) are discussed. Presently, we consider the two-point control. Economically, this is motivating because the optimal operating point generally corresponds to a given purity specification. For the $2 \times 2$ system, we assume the conventional $RV$-configuration to control the compositions. In such a configuration, the recycle flow $R$ is chosen to control the distillate composition $x_D$ while the vapour flow $V$ is chosen to control the bottoms composition $x_B$. There are certain other advantages in choosing this configuration. Firstly, there is hardly any time-delay between the reflux flow rate and the top composition, and similarly between vapour flow and bottoms composition. Secondly, this configuration is shown to be almost independent of the level control tuning (Skogestad 1997*b*), whereas for the other configurations the level control tuning is very important. The levels are controlled, as aforementioned, by manipulating $D$ and $B$ with proportional controllers (integral action assured by the holdups). We consider only the regulatory control problem using an LQG controller assuming that the disturbances are the feed flow rate $F$ and the feed composition $z_F$.

Multirate measurements are comprised of the slow sampled compositions and the fast sampled flow rates. The compositions are assumed to be available over a uniform sampling interval of $n (n \in Z^+)$ minutes while the inputs, *i.e.*, flow rates are assumed

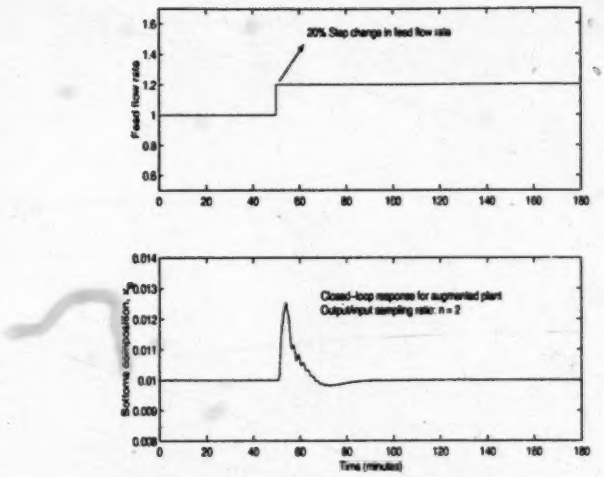
20% Step change in feed flow rate
Feed flow rate
Closed-loop response for augmented plant
Output/input sampling ratio: n = 2
Bottoms composition, $x_B$
Time (minutes)

Figure 2.8: *Closed-loop response of $x_B$ with controller based on augmented plant*

to be available uniformly over a sampling interval of 1 min. We consider two different situations when $n = 2$ and $n = 5$. This situation corresponds to the fast-control, slow-sample case discussed in Section 2.2.

In order to obtain the lifted system, we first discretize the continuous-time model $G_r$ at the fast sample interval $h_b/n$. Using this information in equation (2.7) and substituting $n = 2$ gives the discrete lifted model for the distillation column.

Thus, the lifted system has 4 inputs and 2 outputs. The subsequent step is to design a controller for the lifted system.

For the controller design using LQG techniques, the measurement and state noise covariance matrices are taken as identity. The input weighting is set to a large value compared to the output weighting in order to suppress huge input variations and thus obtain a smooth behaviour in the input moves.

A step-type disturbance is introduced in the feed flow $F$. In order to ensure rejection of step-type disturbances, the closed-loop should contain an integrator. This condition translates to either augmenting the fast-rate plant with a fast-rate integrator, or, by augmenting the lifted plant with the lifted integrator. The closed-loop response for such an augmented system $n = 2$ is shown in Figure 2.8.

In Figures 2.9 and 2.10, we compare the closed-loop responses of $x_D$ and $x_B$ for the multirate and single rate systems. Assuming that no constraints exist on the inputs, the reflux flow rate profiles for both systems are compared in Fig. 2.11.

From the figures, we see that the response of $x_D$ is more aggressive in the case of multirate control. For both values of $n$, the lifted multirate system reaches steady

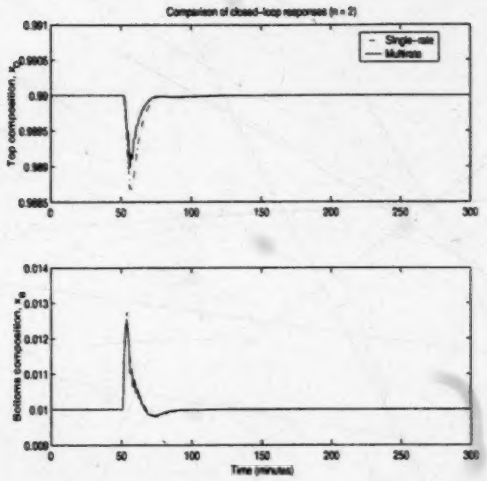


Figure 2.9: *Comparison of closed-loop response of $x_D$ and $x_B$ for multirate and single rate systems ($n = 2$)*

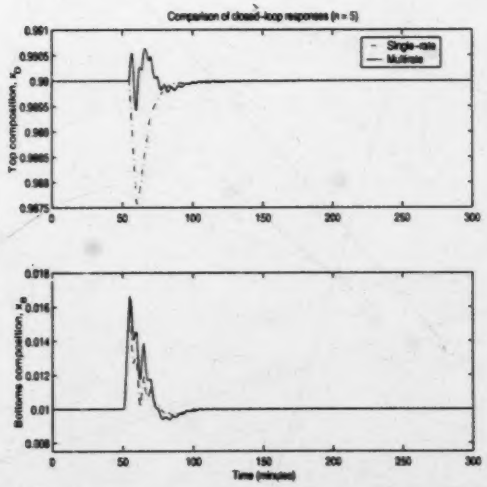


Figure 2.10: *Comparison of closed-loop response of $x_D$ and $x_B$ for multirate and single rate systems ($n = 5$)*

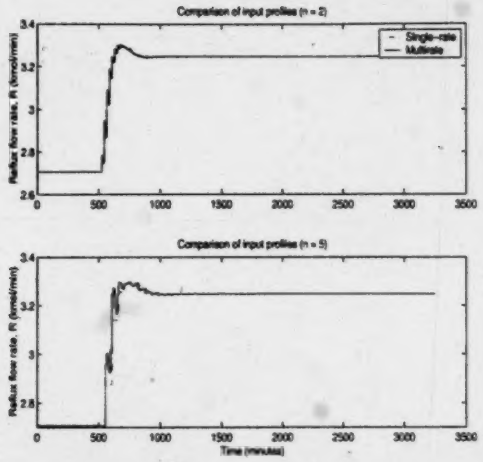


Figure 2.11: *Comparison of input profiles (reflux flow rate) for* $n = 2$ *and* $n = 5$

state not later than the single-rate system. It should be noted that these are just figurative comparisons. It is inappropriate here, however, to decide on the better strategy based on the closed-loop performances due to the lack of a common ground for comparison. A detailed theoretical treatment of the performance comparison problem is discussed later in Chapter 4.

So far, we have illustrated an elegant way of constructing a multirate controller using lifting techniques without the necessity of estimating the intersample outputs. Typically, in a distillation column, inferential control is carried out with the aid of tray temperatures as secondary variables. Also, multirate control using lifting techniques as seen above appears to give a smoother and quicker response than single-rate control scheme. The composition plots shown in the figures are plots of continuous-time outputs. Strictly speaking, in practice only discrete-time outputs are available. In this situation, however, since the column is described by a set of differential and algebraic equations, continuous-time outputs can be computed using integration. The purpose of plotting the continuous-time outputs will prove to be of great value as shown in the following discussion. The multirate control strategy employed earlier for the column included the augmentation of the fast-rate plant with a fast-rate integrator to handle step-type disturbances. Now, moving a step backwards, let us consider the MR control problem for the original plant. As usual, we lift the plant and design an LQG controller yielding a dynamic lifted controller. The resulting closed-loop system (taking $n = 2$) for a step-type disturbance yields the composition plots as sketched in Figure 2.12.

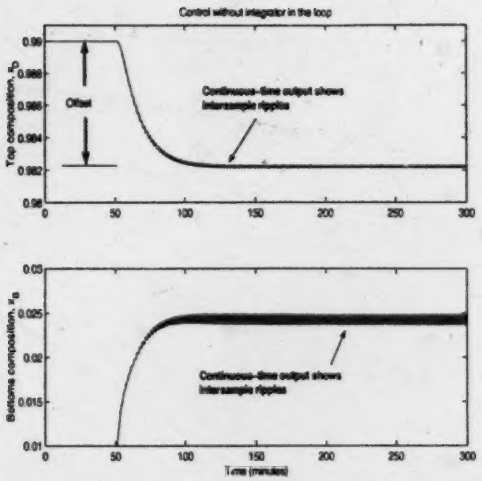


Figure 2.12: *Continuous-time composition plots for MR system without an integrator in the loop ($n = 2$)*

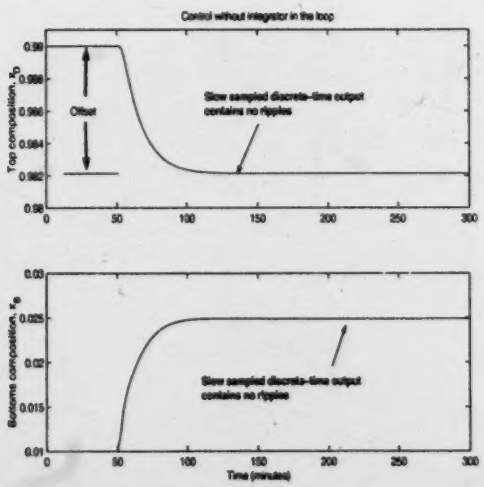
Control without integrator in the loop
Offset
Slow sampled discrete-time output contains no ripples
Slow sampled discrete-time output contains no ripples
Time (minutes)

Figure 2.13: *Slow sampled composition plots for MR system without an integrator in the loop ($n = 2$)*

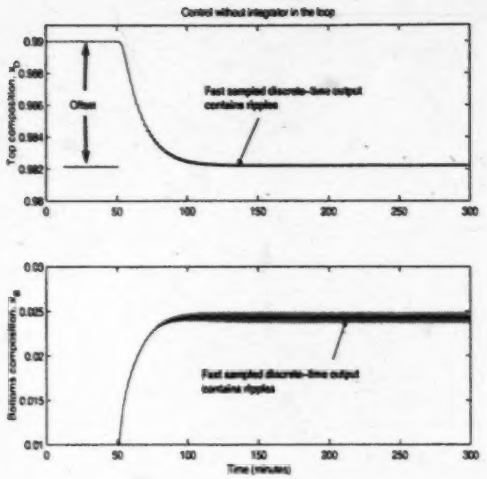
Control without integrator in the loop
Offset
Fast sampled discrete-time output contains ripples
Fast sampled discrete-time output contains ripples
Time (minutes)

Figure 2.14: *Fast sampled composition plots for MR system without an integrator in the loop ($n = 2$)*

There are two important observations that can be made here. Firstly, as expected, due to the absence of an integrator, both the compositions have an offset. However, the second observation is interesting. Both the compositions at their steady states contain regular oscillations or intersample ripples. Therefore, they are not strictly at steady state. Now, let us observe their discrete-time counterparts shown in Figure 2.13.

Not surprisingly, the discrete signals show no oscillations suggesting that the intersample ripples have a period equal to or an integer dividend of the slow sampling interval, $nh$. To verify this conjecture, assume that the outputs are sampled using a fictitious fast-rate sampler $S_f$. The resulting outputs are plotted in Figure 2.14.

Figure 2.14 clearly shows that the fast-sampled outputs contain periodic oscillations. It can be shown that the period of these oscillations is $n$, the ratio of the output/input sampling intervals.

This interesting phenomenon has its roots in the inverse lifting step connecting the lifted moves (made by the lifted controller) and the fast-rate inputs to the plant. In the following chapter, we will discuss this phenomenon in detail - the root cause for such an occurrence and methods to eliminate such intersample ripples in lifted systems. These methods culminate in a set of constraints on the controller gains for stable plants. Also, it is shown that the presence of a fast-rate integrator aids in eliminating these ripples for step-type disturbances and reference signals.

In summary, we have demonstrated an application of a simple and powerful tool

to the multirate control of a commonly occurring chemical engineering system. The application gave birth to two topics that require a broader and more general scope of analysis - the issue of intersample ripples in the closed-loop outputs of lifted multirate systems (discussed in the next chapter), and the issue of the closed-loop performance comparison of multirate and single-rate systems (discussed in Chapter 4).

# Chapter 3

# Ripple-Free Conditions for Lifted Multirate Control Systems

**Purpose:** To present constraints that exist on the gains of the lifted controller to ensure ripple-free conditions in multirate control systems. It is shown that the presence of a fast-rate integrator eliminates these ripples[1].

## 3.1 Introduction

Intersample performance is of prime interest in sampled-data systems analysis, (see, e.g., Grasselli *et al.* (1995), Longman and Lo (1997), Arvanitis (1998)). Generalized sampled-data hold functions (GSHF) (Kabamba 1987) have been used by Arvanitis (1998) to improve intersample performance in sampled-data systems. The focus of this section is on the presence of intersample ripples in closed-loop outputs of multirate sampled-data systems. In this context, Grasselli *et al.* (1995) have presented studies on dead-beat tracking of outputs of closed-loop multirate systems while addressing the elimination of intersample ripples. Grasselli *et al.* (1995) arrived at a set of constraints on the multirate controller by transforming the multirate system into a periodic discrete-time system and imposing the condition of dead-beat tracking of continuous-time signals. They arrived at a set of constraints on the controller from a tracking point of view. However, this study is concerned with the analysis of sampled-data systems in the lifted framework and shows that intersample ripples can exist in the closed-loop outputs. Moreover, the problem of eliminating intersample ripples is tackled in this work from a more fundamental point of view and not only for tracking but also for the regulatory problem.

The main contribution of this chapter is to show that intersample ripples occur

[1]A version of this chapter has been accepted for publication in Automatica, October, 2001 issue

due to the presence of inverse lifting and non-identical gains of the lifted system; and that the imposition of a set of constraints on the controller gains can eliminate these intersample ripples. Results are presented in this work with a primary focus on step-type setpoint and disturbance signals with the idea that these concepts can be extended to other class of reference signals. Furthermore, using the internal model principle (Franklin and Emami-Nacini 1986), for step-type reference signals it is shown that the augmentation of a fast-rate integrator with the plant aids in overcoming these ripples.

By means of theoretical analysis and simulation results, we first show below that intersample ripples can arise in the outputs of closed-loop multirate systems with lifted controllers. The fact that lifted systems have non-identical gains interlinked with inverse lifting is the cause for this phenomenon.

## 3.2 Analysis of Gains

Consider the multirate system shown in Figure 2.1, where it is assumed that the output $\phi$ is sampled at a rate $n$ ($n \in Z^+$) times slower than the input $v$. $G$ represents a continuous-time LTI plant, while $S$ and $H_f$ represent the slow-rate sampler and fast-rate zero-order hold, respectively. Figure 2.1(a) can be converted to Figure 2.1 by using the property $L^{-1}L = I$ and the identity property, $SH_fS_f = S$. As a result of lifting, $\underline{v}$ is of dimension $n$ and the lifted system *(enclosed in the box)* has $n$ transfer functions relating $\phi$ to $\underline{v}$. Equivalently, this can be written as,

$$\phi \;=\; \left[\, G_{L,1} \;\; G_{L,2} \;\; \cdots \;\; G_{L,n} \,\right] \underline{v} \qquad (3.1)$$

where $G_L = SH_fS_fGH_fL^{-1}$ is the lifted system. The following result states that the gains of these $n$ transfer functions are not necessarily identical.

**Proposition 1** *Consider a SISO multirate system $SGH_f$ where $G$ represents a continuous time stable LTI system and the output/input sampling ratio is a positive integer $n$. Then, the gains of the $n$ transfer functions of the lifted system $G_L = SGH_fL^{-1}$ are, in general, not identical.*

**Proof.** Let $G = (A, B, C, D)$ and $G_f = (A_f, B_f, C, D)$ represent the continuous-time and fast-rate discretized state-space models respectively. Using system matrix representations, the transfer function for the lifted system $G_L$ can be obtained in the $\lambda$ ($\lambda = z^{-1}$) domain as

$$\hat{g}_L(\lambda) \;=\; \left[\begin{array}{c|cccc} A_f^n & A_f^{n-1}B_f & A_f^{n-2}B_f & \cdots & B_f \\ \hline C & D & 0 & \cdots & 0 \end{array}\right] \qquad (3.2)$$

Then, the $n$ transfer functions can be written as

$$\hat{g}_{L,1}(\lambda) = \lambda C(I - \lambda A_f^n)^{-1} A_f^{n-1} B_f \tag{3.3}$$

$$\hat{g}_{L,1}(\lambda) = \lambda C(I - \lambda A_f^n)^{-1} A_f^{n-2} B_f \tag{3.4}$$

$$\vdots$$

$$\hat{g}_{L,n}(\lambda) = \lambda C(I - \lambda A_f^n)^{-1} B_f \tag{3.5}$$

where it is assumed that $D = 0$ (for a strictly causal system).

Clearly, the steady-state gains are not identical, or equivalently, in general

$$\hat{g}_{L,1}(1) \neq \hat{g}_{L,2}(1) \neq \cdots \neq \hat{g}_{L,n}(1) \tag{3.6}$$

■

Furthermore, as anticipated, the sum of the lifted gains is identical to the gain of the fast-rate discretized system, $G_f$. The above result is shown for SISO multirate systems with integer output/input sampling ratios. A general result for MIMO systems is shown later. Consequences of non-identical gains in the closed-loop context will be discussed in section 3.3. For SISO and MIMO multirate systems with rational output/input sampling ratios, the observation is slightly different as shown below.

Here, we introduce the notation $S_b$ and $H_a$, denoting the output sampler and input zero-order hold with time periods $T_b$ and $T_a$ respectively. Let the sampling ratio $T_b/T_a$ in its simplest form be represented as $n/m$. The lifted system could then be written as,

$$\begin{aligned} G_L &= L_m S_b G H_a L_n^{-1} \\ &= L_m S_b H_h S_h G H_h S_h H_a L_n^{-1} \\ &= (L_m S_b H_h L_{mn}^{-1})(L_{mn} G_h L_{mn}^{-1})(L_{mn} S_h H_a L_n^{-1}) \end{aligned} \tag{3.7}$$

where $S_h$ and $H_h$ are the sampler and zero-order hold at the fast sampling rate $h$ and $G_h$ with state-space model interval $h$. The fast sampling rate $h$ is essentially the *greatest common divisor* of $T_a$ and $T_b$. $L_{mn}$ is the lifting operator of order $m \times n$, the *least common multiple* of $m$ and $n$. State-space approaches and system matrix representations can be used to arrive at the transfer function for $G_L$.

For example, choosing $T_b = 3h$ and $T_a = 2h$, $G_L$ can be represented as,

$$\hat{g}_L(\lambda) = \left[\begin{array}{c|ccc} A_h^6 & (A_h^5 + A_h^4)B_h & (A_h^3 + A_h^2)B_h & (A_h + I)B_h \\ \hline C & D & 0 & 0 \\ CA_h^3 & C(A_h^2 + A_h)B_h & CB_h + D & 0 \end{array}\right] \tag{3.8}$$

Then, the row sum of the gains relating each of the lifted outputs to the lifted signals are identical. The proof is as follows:

$$\begin{aligned}
\hat{g}^L_{1,1}(1) + \hat{g}^L_{1,2}(1) + \hat{g}^L_{1,3}(1) &= D + C(I - A_h^6)^{-1}(\sum_{k=1}^{5} A_h^k + I)B_h \\
&= D + C(I - A_h)^{-1}B_h \qquad (3.9) \\
\hat{g}^L_{2,1}(1) + \hat{g}^L_{2,2}(1) + \hat{g}^L_{2,3}(1) &= C(A_h^2 + A_h + I)B_h + D + \\
&\quad CA_h^3(I - A_h^6)^{-1}(\sum_{k=1}^{5} A_h^k + I)B_h \\
&= D + C(I - A_h^3)(I - A_h)^{-1}B_h + CA_h^3(I - A_h)^{-1}B_h \\
&= D + C(I - A_h)^{-1}B_h \qquad (3.10)
\end{aligned}$$

In essence, the gains are identical and equal to the gain of the discretized system $G_h$. A more general form of this result is stated below without proof.

**Proposition 2** *Consider a SISO multirate system $S_b G H_a$ with rational output/input sampling ratio $T_b/T_a$ where $G$ is a continuous-time LTI system. The lifted system, $G_L$ has $(n \times m)$ transfer functions where $n/m$ is the least reduced form of $T_b/T_a$. Then the transfer function,*

$$\hat{g}_L(\lambda) = \begin{bmatrix} \hat{g}^L_{1,1}(\lambda) & \hat{g}^L_{1,2}(\lambda) & \cdots & \hat{g}^L_{1,n}(\lambda) \\ \hat{g}^L_{2,1}(\lambda) & \hat{g}^L_{2,2}(\lambda) & \cdots & \hat{g}^L_{2,n}(\lambda) \\ \vdots & \vdots & \vdots & \vdots \\ \hat{g}^L_{m,1}(\lambda) & \hat{g}^L_{m,2}(\lambda) & \cdots & \hat{g}^L_{m,n}(\lambda) \end{bmatrix} \qquad (3.11)$$

*satisfies the property that sums of the gains in each row are identical. In other words,*

$$\hat{g}^L_{1,1}(1) + \cdots + \hat{g}^L_{1,n}(1) = \hat{g}^L_{2,1}(1) + \cdots + \hat{g}^L_{2,n}(1) = \cdots = \hat{g}^L_{m,1}(1) + \cdots + \hat{g}^L_{m,n}(1) \quad (3.12)$$

Next, the case of MIMO systems with integer and rational sampling ratios is considered. For the sake of convenience, a modified version of conventional lifting of multivariable signals is employed in this work and defined as follows. Consider a multivariable signal

$$z(k) = [\ u_1(k) \quad u_2(k) \quad \cdots \quad u_m(k)\ ]^T$$

Then,

$$L_w z = \underline{z} = [\ \underline{u}_1 \quad \underline{u}_2 \quad \cdots \quad \underline{u}_m\ ]^T$$

is the resulting lifted signal of order $w$ due to $z$, where

$$\underline{u}_i = [\ u_1^{(i)} \ \cdots \ u_w^{(i)}\ ]^T$$

is the lifted signal of order $w$ due to $u_i$.

Analysis of MIMO systems in the multirate framework is carried out by using the results for SISO systems.

**Proposition 3** *Consider a MIMO multirate system $SGH_f = SH_fS_fGH_fL^{-1}L$ where $G$ represents a $p$-input, $q$-output, continuous-time stable LTI system. The lifted system has $(q \times np)$ transfer functions. Then, the gains of every $n$ of these $p$ transfer functions of the lifted system $G_L$ are, in general, not identical. In other words, if*

$$\begin{bmatrix} \phi_1 \\ \phi_2 \\ \vdots \\ \phi_q \end{bmatrix}_{q\times 1} = \left[\begin{array}{ccc|ccc|ccc} \hat{g}_{1,1}^{(1)} & \cdots & \hat{g}_{1,n}^{(1)} & \cdots & \cdots & \hat{g}_{p,1}^{(1)} & \cdots & \hat{g}_{p,n}^{(1)} \\ \hline \hat{g}_{1,1}^{(2)} & \cdots & \hat{g}_{1,n}^{(2)} & \cdots & \cdots & \hat{g}_{p,1}^{(2)} & \cdots & \hat{g}_{p,n}^{(2)} \\ \hline \vdots & \vdots & \vdots & \vdots & \vdots & \vdots & \vdots & \vdots \\ \hline \hat{g}_{1,1}^{(q)} & \cdots & \hat{g}_{1,n}^{(q)} & \cdots & \cdots & \hat{g}_{p,1}^{(q)} & \cdots & \hat{g}_{p,n}^{(q)} \end{array}\right]_{q\times np} \begin{bmatrix} \underline{u}_1 \\ \underline{u}_2 \\ \vdots \\ \underline{u}_p \end{bmatrix}_{np\times 1} \tag{3.13}$$

*represents the input-output relation of the lifted system, then every block as partitioned above obeys the result in Proposition 1. In equation (3.13), $\hat{g}_{i,l}^{(j)}$ relates the $j^{th}$ output to the $l^{th}$ lifted component of the $i^{th}$ input signal.*

**Proposition 4** *Consider a MIMO multirate system $S_bGH_a$ with rational output/input sampling ratio $T_b/T_a$ where $G$ is a continuous-time LTI system. The lifted system, $G_L$ has $(np \times mq)$ transfer functions where $n/m$ is the least reduced form of $T_b/T_a$, for a $p$-input, $q$-output system $G$. If the input-output relation of the lifted system is represented by $(mq \times np)$ transfer functions,*

$$\begin{bmatrix} \phi_1^{(1)} \\ \vdots \\ \phi_m^{(1)} \\ \vdots \\ \vdots \\ \phi_1^{(q)} \\ \vdots \\ \phi_m^{(q)} \end{bmatrix}_{mq\times 1} = \left[\begin{array}{ccc|ccc|ccc} \hat{g}_{1,1}^{(1,1)} & \cdots & \hat{g}_{1,n}^{(1,1)} & \cdots & \cdots & \hat{g}_{p,1}^{(1,1)} & \cdots & \hat{g}_{p,n}^{(1,1)} \\ \vdots & \vdots & \vdots & \vdots & \vdots & \vdots & \vdots & \vdots \\ \hline \hat{g}_{1,1}^{(1,m)} & \cdots & \hat{g}_{1,n}^{(1,m)} & \cdots & \cdots & \hat{g}_{p,1}^{(1,m)} & \cdots & \hat{g}_{p,n}^{(1,m)} \\ \hline \vdots & \vdots & \vdots & \vdots & \vdots & \vdots & \vdots & \vdots \\ \vdots & \vdots & \vdots & \vdots & \vdots & \vdots & \vdots & \vdots \\ \hline \hat{g}_{1,1}^{(q,1)} & \cdots & \hat{g}_{1,n}^{(q,1)} & \cdots & \cdots & \hat{g}_{p,1}^{(q,1)} & \cdots & \hat{g}_{p,n}^{(q,1)} \\ \vdots & \vdots & \vdots & \vdots & \vdots & \vdots & \vdots & \vdots \\ \hat{g}_{1,1}^{(q,m)} & \cdots & \hat{g}_{1,n}^{(q,m)} & \cdots & \cdots & \hat{g}_{p,1}^{(q,m)} & \cdots & \hat{g}_{p,n}^{(q,m)} \end{array}\right]_{mq\times np} \begin{bmatrix} u_1^{(1)} \\ \vdots \\ u_n^{(1)} \\ \hline \vdots \\ \vdots \\ \hline u_1^{(p)} \\ \vdots \\ u_n^{(p)} \end{bmatrix}_{np\times 1} \tag{3.14}$$

*then, each block as partitioned above obeys the result in Proposition 2.*

The significance of each result under closed-loop conditions is elucidated below.

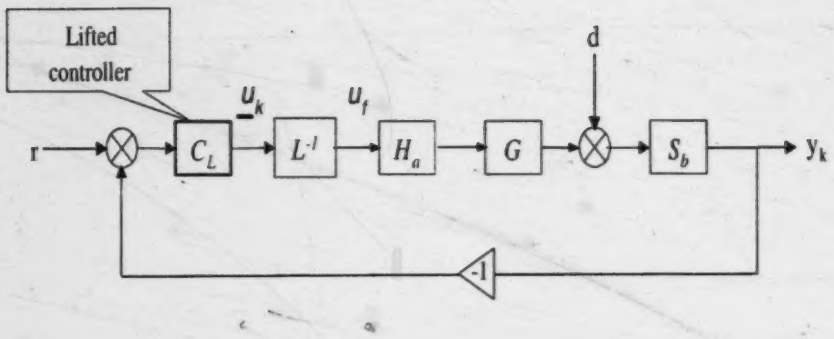


Figure 3.1: *Typical closed-loop multirate system* ($T_b/T_a = n$ ($n \in Z^+$))

## 3.3 Constraints on Controller Gains

Multirate controller design is a challenging problem for several reasons. Existing techniques assume that all the signals are available at a single rate. Hence, conventional methods of discretizing continuous-time models cannot be applied to obtain multirate discrete models. Moreover, the discrete multirate controller has to be periodic unlike the discrete single-rate controller. Lifting techniques bridge the gap between the multirate and single-rate systems by means of a linear transformation. The resulting lifted system is available at a single rate and hence existing techniques can be applied to design a lifted controller. However, causality constraints arise (Meyer 1990, Ravi *et al.* 1990, Chen and Qiu 1994) on the resulting controller which make the design problem relatively more complex.

In addition to the causality constraints, it is shown here as a result of the above analysis and inverse lifting that further constraints arise on the controller gains in order to avoid intersample ripples in the closed-loop outputs. To begin with, the simplest case of a SISO system with integer output/input sampling ratio is considered.

### SISO systems with integer output/input sampling ratio

Lifting a SISO system with $T_b/T_a = n$, an integer, results in a multi-input, single-output (MISO) system with $n$ transfer functions. The lifted controller thus designed yields an $n$-dimensional lifted input signal based on the slow-sampled output. For implementation purposes, the $n$-dimensional lifted signal would have to be inverse lifted to get the fast-rate signal. It is known that at steady-state, for a unit step change in the reference signal, the control signal is proportional to the pseudo-inverse

of the gains of the system. Similarly for a multirate system as shown in Figure 3.1, if $\triangle r(t) = 1$, then at steady-state, $C_L$ would yield a lifted signal $\underline{u}_s$ whose values are proportional to the pseudo-inverses of the gains of the lifted system. In Figure 3.1, $r$ is the reference signal and $C_L$ is the lifted controller designed for the system $S_b G H_a L^{-1}$.

Recall the observation in Proposition 1 that the gains of the $n$ transfer functions are not identical, in general. Therefore, if the steady-state lifted signal

$$\underline{u}_s(k) = [\ u_1 \quad u_2 \quad \cdots \quad u_n\ ]^T$$

then inverse lifting results in the steady-state fast-rate signal

$$u_{fs} = \{u_1, u_2, \cdots, u_n, u_1, u_2, \cdots, u_n, \cdots\} \tag{3.15}$$

which essentially implies that the system is truly not at steady-state. From equation (3.15), it is evident that the input signal is periodic with a period $T_b/T_a = n$. Hence, the closed-loop fast-rate output is oscillatory as well. However, the slow-rate output would not exhibit any oscillatory behaviour.

In order to eliminate these ripples in the output, certain constraints arise on the controller gains such that the fast-rate input is truly at steady-state. One obvious condition is to require that all the $n$ components of the steady-state lifted input share identical values, which leads to the following theorem.

**Proposition 5** *Consider a stable closed-loop system comprising the multirate system $S_b G H_a$ and the lifted controller $C_L$ designed for the corresponding lifted system. If $G$ is strictly stable and $T_b/T_a = n$, a positive integer, then the gains of the $n$ transfer functions arising from $C_L$ need to be identical in order to ensure that there are no intersample ripples in the closed-loop output. Equivalently, if*

$$\hat{c}_L(\lambda) \ = \ [\ \hat{c}_1^L(\lambda) \quad \hat{c}_2^L(\lambda) \quad \cdots \quad \hat{c}_n^L(\lambda)\ ] \tag{3.16}$$

*then the following condition is required to ensure that no intersample ripples are present in the closed-loop output,*

$$\hat{c}_1^L(1) = \hat{c}_2^L(1) = \cdots = \hat{c}_n^L(1) \tag{3.17}$$

**Proof.** For the closed-loop system, the relation between the closed-loop input $u_i$ and the error $e_i$ can be written as,

$$u_i(\lambda) = \hat{c}_i^L(\lambda) e(\lambda) = \frac{\hat{c}_i^L(\lambda)}{1 + \sum_{i=1}^{n} \hat{c}_i^L(\lambda) \hat{g}_i^L(\lambda)} r(\lambda) \tag{3.18}$$

For set-point changes,

$$r(\lambda) = \frac{1}{1-\lambda}$$

If $G$ is stable, the lifted system has finite gains and using the final value theorem, it is straightforward to show that

$$\hat{c}_1^L(1) = \hat{c}_2^L(1) = \cdots = \hat{c}_n^L(1)$$

is necessary for all $u_i$'s to be equal.

If $\hat{c}_i^L$ has an integrator, then a similar condition holds. In such a case, the controller can be written as,

$$\hat{c}_i^L(\lambda) = \frac{\tilde{c}_i^L(\lambda)}{1-\lambda} \tag{3.19}$$

where it is assumed that $\tilde{c}_i^L(1)$ is finite. Substituting equation (3.19) in the closed-loop equation (3.18) for $\hat{c}_i^L(\lambda)$ and using the final value theorem yields the following result

$$\tilde{c}_1^L(1) = \tilde{c}_2^L(1) = \cdots = \tilde{c}_n^L(1)$$

■

In Proposition 5, it is shown that for a stable SISO system, even the presence of controllers with infinite gains does not necessarily eliminate intersample ripples in the output for step type reference signals.

However, a discrete integrator at the input sampling rate $T_a$, present in the plant as shown in Figure 3.12 can ensure a steady output at the fast rate. The following result is stated in this context.

**Proposition 6** *Consider a stable closed-loop system comprising the multirate system $S_bGH_a$ and the lifted controller $C_L$ designed for the corresponding lifted system $G_L$. Assume that $G$ is strictly stable and $T_b/T_a = n$, a positive integer. If $G_a$, the fast-rate discretized system at the rate $T_a$, is augmented with the discrete integrator $G_{Ia}$ at the rate $T_a$, or equivalently, $G_L$ with the lifted integrator $G_{LI} = L_nG_{Ia}L_n^{-1}$, then for step type reference signals, there are no intersample ripples in the steady-state output.*

**Proof.** Augmenting $G_L$ with the lifted integrator $G_{LI}$ is equivalent to lifting the system obtained by augmenting the fast-rate plant $G_a = S_aGH_a$ with the fast-rate discrete integrator $G_{Ia}$. Firstly, since $T_b/T_a = n$, a positive integer, it is easy to note that

$$G_L = S_bGH_aL_n^{-1} = S_bH_aS_aGH_aL_n^{-1} = S_bH_aG_aL_n^{-1}$$

$$G_L G_{LI} = S_b H_a G_a L_n^{-1} L_n G_{Ia} L_n^{-1} = S_b H_a G_a G_{Ia} L_n^{-1} = S_b H_a G_u L_n^{-1}$$

where $G_u$ is the augmented state-space model of $G_a$ with $G_{Ia}$ and the identity property of lifting and inverse lifting is utilized.

Denote the poles of the fast-rate discretized plant $G_a$ by $p_1, p_2, \cdots, p_m$ (need not be distinct). With the augmentation of an integrator, there is an additional pole introduced to $G_a$ at $\lambda = 1$. Thus the augmented plant has poles $p_1, p_2, \cdots, p_m, 1$. From earlier discussions, it can be recalled that lifting preserves the order of the system and that the poles of the lifted system would be raised individually by a power $n$. Thus the resulting lifted system has poles $p_1^n, p_2^n, \cdots, p_m^n, 1$ implying infinite gain for $G_L$.

For step-type reference signals,

$$r(\lambda) = \frac{1}{1-\lambda}$$

With the augmentation of a fast-rate integrator on the plant side, the signals after inverse lifting would be $\Delta u_i$ given by the closed-loop expression

$$\Delta u_i(\lambda) = \hat{c}_i^L(\lambda) e(\lambda) = \frac{\hat{c}_i^L(\lambda)}{1 + \sum_{i=1}^{n} \hat{c}_i^L(\lambda) \hat{g}_i^{LI}(\lambda)} r(\lambda) \tag{3.20}$$

Since $G_{LI}$ has infinite gains, using the final-value theorem it can be observed that the steady state error goes to zero at the sampling instants. This means that $\Delta u_i(1) = \hat{c}_i^L(1) e(1) = 0$, where $\Delta u_i$ is the input to the augmented plant $G_{LI}$. Thus, the fast-rate inputs to the plant are constant at steady-state. With a zero-order hold, the outputs should be steady.

■

The above argument shows that for set-point tracking of step type reference signals and plants with finite gains (Type 0), the controller gains have to be the same in order to avoid intersample oscillations. For plants with infinite gains i.e., the presence of an integrator in the plant, there is no restriction on the controller gains. Simulation and experimental results are illustrated below.

**Experimental and simulation results**

The simulated system is a second-order system

$$G(s) = \frac{1}{(10s+1)(25s+1)} \tag{3.21}$$

with sampling periods $T_b = 5$ and $T_a = 1$ sec. Therefore, $n = T_b/T_a = 5$.

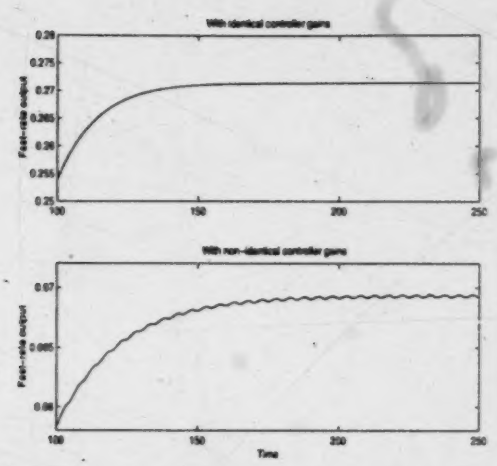

Figure 3.2: *Outputs of the closed-loop system with identical & non-identical controller gains - set point tracking* ($n = 5$)

The lifted system has 5 transfer functions. A lifted controller is designed using LQG techniques and a unit step change is given in the reference signal. The continuous output profile for the closed-loop system for both cases of identical (top) and non-identical (bottom) controller gains are shown in Figure 3.2. In the latter case, the output clearly contains ripples whereas in the former case, the output is ripple-free. Identical controller gains during simulation are ensured by incorporating a linear matrix gain element whose function is to average the outputs of the lifted controller.

The unit step change is given at $t = 50$ and Figure 3.2 is shown for later times. Figure 3.3 shows how inverse lifting introduces oscillations in the inputs. The lifted signal is the output of the lifted controller. The circled points on the multivariable lifted signal are the values at the consecutive instants for the inverse lifted signal. Thus, different steady-states introduce oscillations in the fast-rate input signal due to inverse lifting. Input profiles for both the cases can be seen in Figure 3.4.

In view of the results discussed in Propositions 5 and 6, experimental results of a multirate level control problem on the tank setup shown in Figure 3.5 are presented. For illustration purposes, the level is sampled every 9 seconds while the inlet valve moves are made every 3 seconds. $C_L$ represents the lifted controller yielding the lifted input moves based on the slow-sampled output. The resulting lifted signal is inverse lifted giving a fast-rate signal which passes through a zero-order fast-rate hold (with a period of 3 seconds).

A proportional controller serves to illustrate the main result of interest. First, we

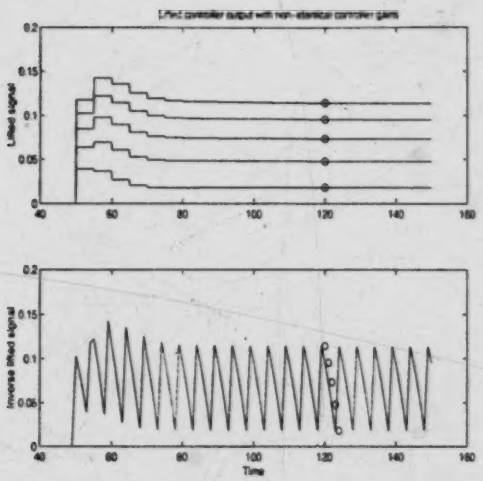

Figure 3.3: *Inverse lifting of the lifted controller output signal introduces oscillations in the inputs* ($n = 5$)

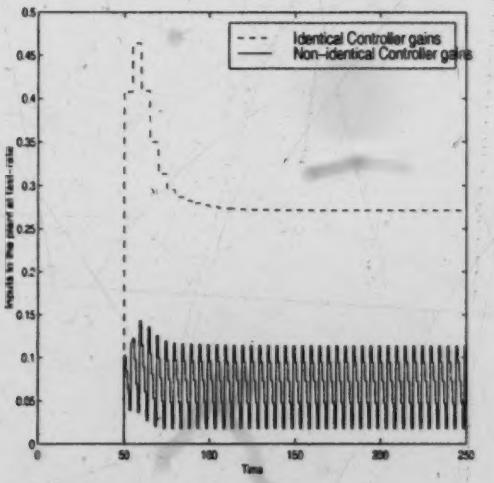


Figure 3.4: *Inputs to the plant for the closed-loop system with non-identical and identical controller gains - set point tracking* ($n = 5$)

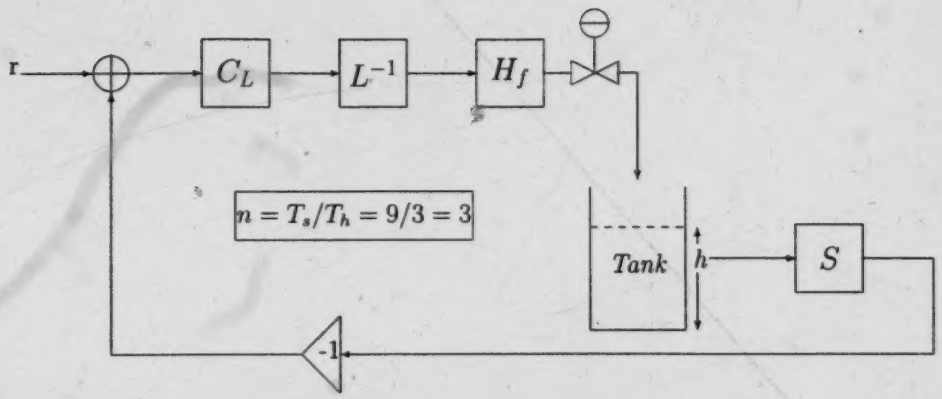


Figure 3.5: *Experimental Tank setup*

consider a lifted proportional controller with $n = 3$ different gains. The open-loop tank is close to an integrator (unstable). Hence, in order to satisfy the assumptions in Propositions 5 and 6, the tank is stabilized by means of proportional feedback (not shown in the figure). Closed-loop experiments are carried out on the stabilized tank.

The fast-rate closed-loop output (sampled every 1 second) and the slow-rate closed-loop output are shown at the top in Figure 3.6. Observe the intersample ripples in the fast-rate output (to the left) while the slow-sampled output is fairly flat (to the right). Presence of minor measurement and process disturbances can be seen in the slow-sampled output. At the bottom are shown the corresponding outputs when the controller gains are identical. In this case, the fast-rate output is ripple free. Thus, experimental results confirm the theoretical results discussed in Proposition 5. It might be misleading to mistake the ripples as noise in the fast-rate output at the top. However, there is hardly any noise as seen in the measurements as observed in the fast-rate output at the bottom.

Figure 3.7 shows the results discussed in Proposition 6. The closed-loop experiment is carried out by augmenting the lifted system with the lifted integrator. Results are shown at the top in Figure 3.7. The plot to the left represents the fast-rate output while the plot to the right shows the slow-rate output. The fast-rate output is ripple free as expected. The output signals at the bottom are obtained when the multirate control strategy is implemented on the unstable tank. For this purpose, the tank was not stabilized prior to carrying out the closed-loop experiment. In this case as well, the fast-rate output is ripple free.

Figure 3.8 shows the output and input profiles for the discretized plant augmented with a fast-rate integrator. Observe that the output tracks the step signal with no

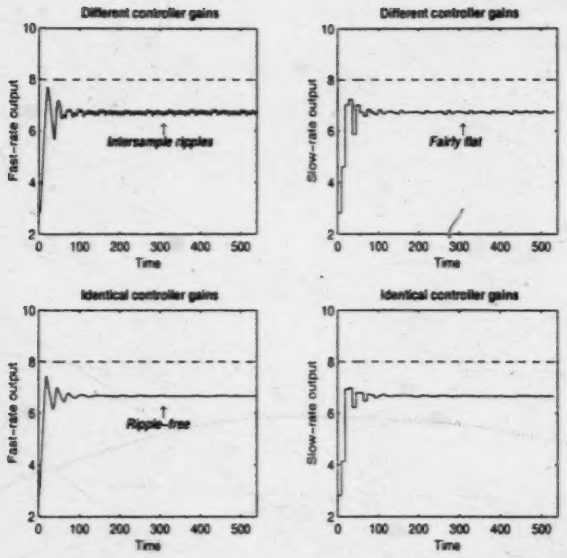


Figure 3.6: *Experimental results - multirate level control: (solid) output, (dashed) setpoint*

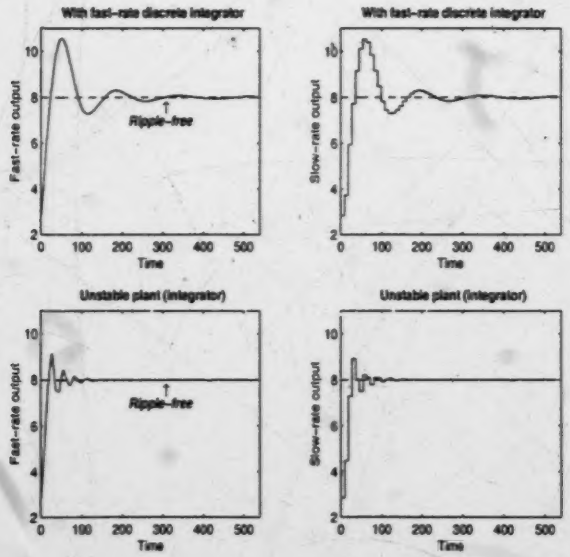


Figure 3.7: *Experimental results - multirate level control: (solid) output, (dashed) setpoint*

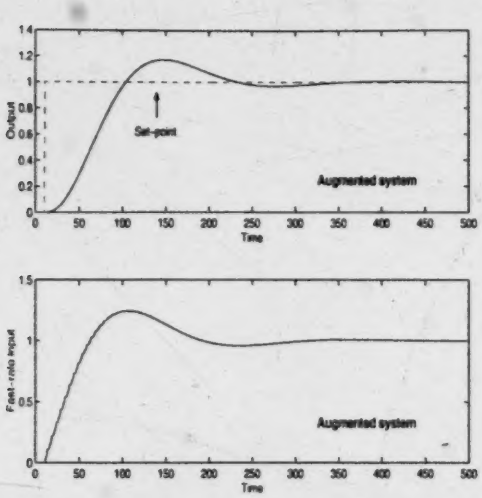


Figure 3.8: *Output and input profiles for set-point tracking in a plant augmented with an integrator - set point tracking* ($n = 5$)

oscillations.

### SISO systems with rational output/input sampling ratio

Typically, the output/input sampling ratio is a rational number rather than an integer. In this section, expressions for controller constraints are given for the case when $T_b/T_a$ is rational.

Let the sampling ratio $T_b/T_a$ in its simplest form be represented as $n/m$. The lifted system, then, would have $(m \times n)$ transfer functions. The lifted controller would have $(n \times m)$ transfer functions relating the lifted input $\underline{u}$ to the lifted error $\underline{u}$. The following theorem states that the sum of gains of the lifted controller in each row should be identical.

**Proposition 7** *Consider a stable closed-loop system comprising the multirate system $S_bGH_a$ and the lifted controller $C_L$ designed for the lifted system $L_nS_bGH_aL_m^{-1}$, where $m/n$ is the simplest form of the output/input sampling ratio $T_b/T_a$. If the controller matrix is represented by*

$$\hat{c}_L(\lambda) = \begin{bmatrix} \hat{c}^L_{1,1}(\lambda) & \hat{c}^L_{1,2}(\lambda) & \cdots & \hat{c}^L_{1,m}(\lambda) \\ \vdots & \vdots & \vdots & \vdots \\ \hat{c}^L_{n,1}(\lambda) & \hat{c}^L_{n,2}(\lambda) & \cdots & \hat{c}^L_{n,m}(\lambda) \end{bmatrix} \tag{3.22}$$

*then the following condition is required to ensure intersample ripple-free output for*

*the the closed-loop,*

$$\hat{c}^L_{1,1}(1) + \hat{c}^L_{1,2}(1) + \cdots + \hat{c}^L_{1,m}(1) = \cdots = \hat{c}^L_{n,1}(1) + \hat{c}^L_{n,2}(1) + \cdots + \hat{c}^L_{n,m}(1) \quad (3.23)$$

**Proof.** Proof of this result is similar to that for Proposition 5 with an additional imposition that the components of the lifted input have to be identical at the output sampling rate $T_b$.

Defining $P = G_L C_L$ and $Q = (I + P)^{-1}$, the closed-loop transfer function can be written as

$$\underline{\phi}(\lambda) = (I + P)^{-1} P \underline{r}(\lambda) \quad (3.24)$$

$$\Longrightarrow \begin{bmatrix} \phi_1(\lambda) \\ \phi_2(\lambda) \\ \vdots \\ \phi_m(\lambda) \end{bmatrix} = (I - Q) \begin{bmatrix} r_1(\lambda) \\ r_2(\lambda) \\ \vdots \\ r_m(\lambda) \end{bmatrix} \quad (3.25)$$

At steady state, it requires that

$$\phi_1 = \phi_2 = \cdots = \phi_m \quad (3.26)$$

Using the final value theorem, for step-type reference signals, the above condition implies that,

$$\hat{q}_{1,1}(1) + \hat{q}_{1,2}(1) + \cdots + \hat{q}_{1,m}(1) = \cdots = \hat{q}_{m,1}(1) + \hat{q}_{m,2}(1) + \cdots + \hat{q}_{m,m}(1) \quad (3.27)$$

The second condition for ripple-free output is similar to that in the proof of Proposition 5, requiring that all the components of the lifted input signal be identical. The relation between $\underline{u}$ and $\underline{r}$ can be written as,

$$\underline{u}(\lambda) = C_L (I + P)^{-1} \underline{r}(\lambda) \quad (3.28)$$

$$\Longrightarrow \begin{bmatrix} u_1(\lambda) \\ \vdots \\ u_n(\lambda) \end{bmatrix} = \begin{bmatrix} \hat{c}^L_{1,1}(\lambda) & \cdots & \hat{c}^L_{1,m}(\lambda) \\ \vdots & \vdots & \vdots \\ \hat{c}^L_{n,1}(\lambda) & \cdots & \hat{c}^L_{n,m}(\lambda) \end{bmatrix} \begin{bmatrix} \hat{q}_{1,1}(\lambda) & \cdots & \hat{q}_{1,m}(\lambda) \\ \vdots & \vdots & \vdots \\ \hat{q}_{m,1}(\lambda) & \cdots & \hat{q}_{m,m}(\lambda) \end{bmatrix} \begin{bmatrix} r_1(\lambda) \\ \vdots \\ r_m(\lambda) \end{bmatrix} \quad (3.29)$$

For ripple free outputs at steady state, the constraint on inputs can be written as

$$u_1 = u_2 = \cdots = u_n \quad (3.30)$$

Applying the final-value theorem to equation (3.29) and using equations (3.27) and (3.30), it is easy to show that the following condition on the controller gains is required to ensure ripple-free outputs with step-type reference signals.

$$\hat{c}^L_{1,1}(1) + \cdots + \hat{c}^L_{1,m}(1) = \hat{c}^L_{2,1}(1) + \cdots + \hat{c}^L_{2,m}(1) = \cdots = \hat{c}^L_{n,1}(1) + \cdots + \hat{c}^L_{n,m}(1) \quad (3.31)$$

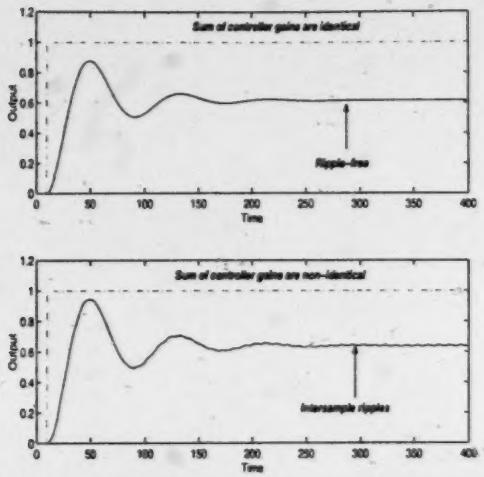


Figure 3.9: *Output (solid) of the closed-loop system with identical & unidentical sums of controller gains - set point (dashdot) tracking; rational sampling ratio* $(n/m = 5/2)$

■

Proposition 7 is corroborated by means of simulation on the system given in equation (3.21). The sampling ratio $n/m$ is set to 5/2. For illustration purposes, a proportional controller is chosen for the lifted controller. Note that causality constraints exist on the controller. Causality constraints essentially imply that the $D$ matrix in the state-space model of the lifted controller has to be block lower-triangular to ensure a causal controller. Keeping this in mind, the controllers with identical and non-identical sums of gains are chosen as

$$\hat{c}_L(\lambda) = \begin{bmatrix} 1.6 & 0 \\ 1.6 & 0 \\ 1.6 & 0 \\ 0.4 & 1.2 \\ 0.6 & 1.0 \end{bmatrix}; \quad \hat{c}_L(\lambda) = \begin{bmatrix} 1.6 & 0 \\ 0.8 & 0 \\ 1.6 & 0 \\ 0.2 & 1.6 \\ 1.0 & 2.0 \end{bmatrix} \tag{3.32}$$

Observe that in the case of identical sums of gains of the controller, at the top in Figure 3.9, the continuous-time output is ripple free. In contrast to this, the output shown in the bottom contains periodic oscillations when the condition in Proposition 7 is not satisfied.

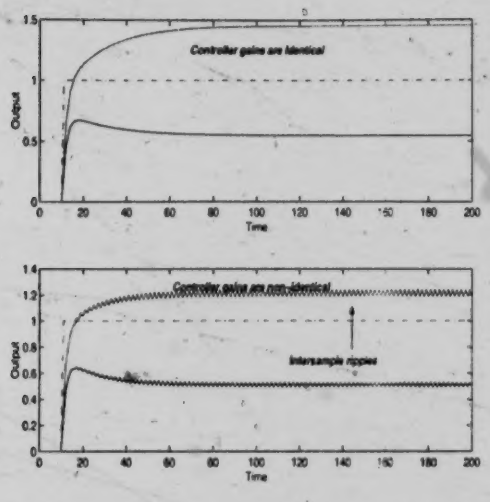


Figure 3.10: *Output (solid) of the closed-loop MIMO* $(2 \times 2)$ *system with identical & non-identical controller gains - set point (dashdot) tracking; integer sampling ratio* $(n = 5)$

### MIMO systems with integer output/input sampling ratio

For MIMO systems with integer sampling ratios, the constraints are similar to those for SISO systems. It is assumed here that all the inputs and outputs are sampled at a uniform rate. The following theorem gives the constraints on the lifted controller for MIMO systems.

**Proposition 8** *Consider a stable closed-loop system comprising the multirate system* $S_b G H_a$ *and the lifted controller* $C_L$ *for the corresponding lifted system* $S_b G H_a L_n^{-1}$, *where* $n = T_b/T_a$, *the output/input sampling ratio is a positive integer and* $G$ *is a MIMO continuous-time LTI system. The lifted system has* $(np \times q)$ *transfer functions if* $G$ *is a* $p$*-input,* $q$*-output system. If* $C_L$ *relates the lifted input to the error as,*

$$\begin{bmatrix} u_1^{(1)} \\ \vdots \\ u_n^{(1)} \\ \hline \vdots \\ \vdots \\ \hline u_1^{(p)} \\ \vdots \\ u_n^{(p)} \end{bmatrix}_{np\times 1} = \left[\begin{array}{c|c|c|c} \hat{c}_{1,1}^{(1)}(\lambda) & \hat{c}_{1,2}^{(1)}(\lambda) & \cdots & \hat{c}_{1,q}^{(1)}(\lambda) \\ \vdots & \vdots & \vdots & \vdots \\ \hat{c}_{n,1}^{(1)}(\lambda) & \hat{c}_{n,2}^{(1)}(\lambda) & \cdots & \hat{c}_{n,q}^{(1)}(\lambda) \\ \hline \vdots & \vdots & \vdots & \vdots \\ \vdots & \vdots & \vdots & \vdots \\ \hline \hat{c}_{1,1}^{(p)}(\lambda) & \hat{c}_{1,2}^{(p)}(\lambda) & \cdots & \hat{c}_{1,q}^{(p)}(\lambda) \\ \vdots & \vdots & \vdots & \vdots \\ \hat{c}_{n,1}^{(p)}(\lambda) & \hat{c}_{n,2}^{(p)}(\lambda) & \cdots & \hat{c}_{n,q}^{(p)}(\lambda) \end{array}\right]_{np\times q} \begin{bmatrix} e_1 \\ e_2 \\ e_3 \\ \vdots \\ \vdots \\ e_q \end{bmatrix}_{q\times 1} \tag{3.33}$$

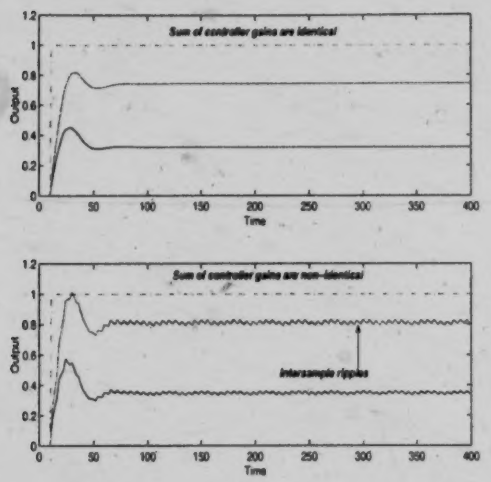


Figure 3.11: *Output (solid) of the closed-loop MIMO* $(2 \times 2)$ *system with identical & non-identical sums of controller gains - set point (dashdot) tracking; integer sampling ratio* $(n/m = 3/2)$

*then, the gains of the controller transfer functions as partitioned above should be identical within each partition to guarantee ripple-free outputs for tracking step-type reference signals.*

**Proof.** Proof of this theorem makes use of the result for SISO systems with integer sampling ratio. In equation (3.33), $\hat{c}^i_{j,k}(\lambda)$ represents the controller transfer function relating the $j^{th}$ component of the $i^{th}$ lifted input to the $k^{th}$ error signal.

The partitions in the transfer function matrix in equation (3.33) represent the controller transfer function when the MIMO lifted system is broken down into MISO lifted systems. The idea is that each block could be viewed as a matrix of controllers for the lifted system formed out of a SISO system with every input-output pair. For example, the first block represents the controller for the lifted system obtained via lifting a SISO system comprised of the input-output pair $(u_1, \phi_1)$ with integer sampling ratio.

Therefore, Proposition 5 holds good for each such partitioned block. Consequently, for step-type reference signals, the following condition ensures ripple-free output

$$\hat{c}^{(\alpha)}_{1,j}(1) = \hat{c}^{(\alpha)}_{2,j}(1) = \cdots = \hat{c}^{(\alpha)}_{n,j}(1) \quad \forall\ \alpha = 1, \cdots, p; \quad \forall\ j = 1, \cdots, q \tag{3.34}$$

■

The above result is illustrated by application to a simulated multivariable system given below:

$$G = \begin{bmatrix} \dfrac{1}{3s+1} & \dfrac{2}{4s+1} \\ \dfrac{3}{5s+1} & \dfrac{4}{6s+1} \end{bmatrix} \tag{3.35}$$

In this case, the causality constraints do not arise because of the nature of the sampling ratio. The controller gains for the identical and non-identical cases are chosen as

$$\hat{c}_L(\lambda) = \left[\begin{array}{c|c} 1.0 & 0.2 \\ 1.0 & 0.2 \\ \hline 0.6 & 0.4 \\ 0.6 & 0.4 \end{array}\right] ; \quad \hat{c}_L(\lambda) = \left[\begin{array}{c|c} 1.0 & 0.2 \\ 0.2 & 1.0 \\ \hline 0.6 & 0.4 \\ 0.4 & 0.6 \end{array}\right] \tag{3.36}$$

Figure 3.10 shows the continuous-time outputs of the closed-loop system when G is a MIMO $2 \times 2$ system given in equation (3.35). The plot in the top depicts the output for the case when the condition in Proposition 8 is satisfied while the plot in the bottom shows the case of non-identical controller gains.

### MIMO systems with rational but uniform output/input sampling ratios

In this section, the case of MIMO systems with rational but uniform output/input sampling ratios is considered, *i.e.*, all inputs are sampled at one common rate and all outputs are sampled at a uniform rate that is different from the input sampling rate. The result with respect to intersample behaviour is obtained by partitioning the controller transfer function matrix into blocks such that Proposition 7 can be applied suitably to get the following result.

**Proposition 9** *Consider a stable closed-loop system comprising the multirate system $S_b G H_a$ and the lifted controller $C_L$ for the corresponding lifted system $L_m S_b G H_a L_n^{-1}$, where $n/m$ is the simplest reduced form of $T_b/T_a$, and $G$ is a MIMO continuous-time LTI system. Assuming that the inputs and outputs are uniformly sampled, the lifted system has $(np \times mq)$ transfer functions if $G$ is a p-input, q-output system. If $C_L$*

*relates the lifted input to the lifted error as,*

$$\begin{bmatrix} u_1^{(1)} \\ \vdots \\ u_n^{(1)} \\ \hline \vdots \\ \hline u_1^{(p)} \\ \vdots \\ u_n^{(p)} \end{bmatrix} = \left[\begin{array}{ccc|c|ccc} \hat{c}_{1,1}^{(1,1)}(\lambda) & \cdots & \hat{c}_{1,m}^{(1,1)}(\lambda) & \cdots & \hat{c}_{1,1}^{(1,q)}(\lambda) & \cdots & \hat{c}_{1,m}^{(1,q)}(\lambda) \\ \vdots & \vdots & \vdots & \vdots & \vdots & \vdots & \vdots \\ \hat{c}_{n,1}^{(1,1)}(\lambda) & \cdots & \hat{c}_{n,m}^{(1,1)}(\lambda) & \cdots & \hat{c}_{n,1}^{(1,q)}(\lambda) & \cdots & \hat{c}_{n,m}^{(1,q)}(\lambda) \\ \hline \vdots & & \vdots & \vdots & \vdots & & \vdots \\ \hline \hat{c}_{1,1}^{(p,1)}(\lambda) & \cdots & \hat{c}_{1,m}^{(p,1)}(\lambda) & \cdots & \hat{c}_{1,1}^{(p,q)}(\lambda) & \cdots & \hat{c}_{1,m}^{(p,q)}(\lambda) \\ \vdots & \vdots & \vdots & \vdots & \vdots & & \\ \hat{c}_{n,1}^{(p,1)}(\lambda) & \cdots & \hat{c}_{n,m}^{(p,1)}(\lambda) & \cdots & \hat{c}_{n,1}^{(p,q)}(\lambda) & \cdots & \hat{c}_{n,m}^{(p,q)}(\lambda) \end{array}\right] \begin{bmatrix} e_1^{(1)} \\ \vdots \\ e_m^{(1)} \\ \hline \vdots \\ \hline e_1^{(q)} \\ \vdots \\ e_m^{(q)} \end{bmatrix} \tag{3.37}$$

*then the sum of controller gains within each block need to be identical to ensure no intersample ripples in the closed-loop output for step-type reference signals.*

**Proof.** In equation (3.37), $\hat{c}_{j,k}^{(i,l)}(\lambda)$ represents the controller transfer function relating the $j^{th}$ component of the $i^{th}$ lifted input to the $k^{th}$ component of the $l^{th}$ error signal.

Following a similar argument as in Proposition 8, each block in the controller transfer function matrix of equation (3.37) represents the controller matrix for the lifted system obtained by every input-output pair. For example, the first block represents the matrix of controllers for the lifted system obtained from the SISO system $(u_1, \phi_1)$ with rational sampling ratio $n/m$. With this view, the following condition needs to hold good for ripple-free output,

$$\hat{c}_{1,1}^{(\alpha,\beta)}(1) + \cdots + \hat{c}_{1,m}^{(\alpha,\beta)}(1) = \hat{c}_{2,1}^{(\alpha,\beta)}(1) + \cdots + \hat{c}_{2,m}^{(\alpha,\beta)}(1) = \cdots = \hat{c}_{n,1}^{(\alpha,\beta)}(1) + \cdots + \hat{c}_{n,m}^{(\alpha,\beta)}(1)$$
$$\forall\ \alpha = 1, \cdots, p;\ \beta = 1, \cdots, q \tag{3.38}$$

■

Figure 3.11 shows the continuous-time outputs of the closed-loop system when $G$ is the continuous-time $2 \times 2$ MIMO system given in equation (3.35). The sampling ratio $n/m$ is set to $3/2$. The controllers for this case are proportional controllers taking into account the causality constraint. It is worthwhile noting here that the controllers have been chosen merely to illustrate the result in Proposition 9. Extra tuning effort could easily be devoted to improve the performance. However, this is beyond the scope of this chapter. Optimal control design requires use of advanced

control strategies which consider the gain and causality constraints on the controller in an algebraic form. For the present, the controllers are chosen as

$$\hat{c}_L(\lambda) = 0.2 \times \left[\begin{array}{cc|cc} 0.5 & 0 & 0.7 & 0 \\ 0.5 & 0 & 0.7 & 0 \\ 0.3 & 0.2 & 0.4 & 0.3 \\ \hline 0.6 & 0 & 0.5 & 0 \\ 0.6 & 0 & 0.5 & 0 \\ 0.3 & 0.3 & 0.3 & 0.2 \end{array}\right] \quad \hat{c}_L(\lambda) = 0.2 \times \left[\begin{array}{cc|cc} 0.5 & 0 & 0.7 & 0 \\ 0.5 & 0 & 0.7 & 0 \\ 0.1 & 0.7 & 0.8 & 0.8 \\ \hline 0.6 & 0 & 0.5 & 0 \\ 0.6 & 0 & 0.5 & 0 \\ 0.6 & 0.3 & 0.7 & 0.2 \end{array}\right] \tag{3.39}$$

Similar observations are made in this case as in the SISO illustrations. When the controller gains do not satisfy the constraints specified in Proposition 9, the output exhibits oscillatory behaviour at steady-state.

The above analysis is now extended by a further result on MIMO systems when the inputs and outputs have distinct sampling rates, *i.e.*, each of the signals has a sampling channel with distinct sampling rates and the ratios of all the output/input sampling intervals are rational numbers. This is the most general result in the present study. All of the earlier results are special cases of this result. From a pedagogical point of view, it makes sense to consider the simpler cases at first. The main result is presented as follows.

### MIMO systems with distinct sampling intervals

Consider a $p$-input, $q$-output continuous-time MIMO system $G$. Each of the $p$ input channel has the respective sampling interval $m_i h$ $(i = 1, \cdots, p)$, while each of the $q$ outputs has the respective sampling interval $n_j h$ $(j = 1, \cdots, p)$. Using the results obtained earlier, the following constraints on the controller need to be satisfied for the multirate system to have desired intersample behaviour. Consider the following new terms for the ensuing discussion.

The MIMO multirate sampler and zero-order hold, $\overline{S_b}$ and $\overline{H_a}$ are defined respectively as:

$$\overline{S_b} = \begin{bmatrix} S_{n_1} & & \\ & \ddots & \\ & & S_{n_q} \end{bmatrix} \quad \overline{H_a} = \begin{bmatrix} H_{m_1} & & \\ & \ddots & \\ & & H_{m_p} \end{bmatrix} \tag{3.40}$$

where $S_{n_i h}$ and $H_{m_j h}$ have sampling intervals $n_j h$ and $m_i h$ respectively.
Let $l$ represent the L.C.M. of all $n_j$ & $m_i$ and the integers $\bar{n}_j = l/n_j$, $j = 1, \cdots, q$; $\bar{m}_i = l/m_i$, $i = 1, \cdots, p$ represent the conjugates of the sampling rates with respect to $l$.

Further, define

$$\overline{L}_b = \begin{bmatrix} L_{\bar{n}_1} & & \\ & \ddots & \\ & & L_{\bar{n}_q} \end{bmatrix} \qquad \overline{L}_a^{-1} = \begin{bmatrix} L_{\bar{m}_1}^{-1} & & \\ & \ddots & \\ & & L_{\bar{m}_p}^{-1} \end{bmatrix} \tag{3.41}$$

The lifted system $\overline{G}_L$ is defined as $\overline{G}_L = \overline{L}_b \overline{S}_b H_h G_h S_h \overline{H}_a \overline{L}_a^{-1}$ where $G_h$ is the discretized model of $G$ at the sampling interval $h$. $S_h$ and $H_h$ are the sampler and zero-order hold at the rate $h$, respectively.

**Theorem 1** *Consider a stable closed-loop system comprising of the multirate system $\overline{S}_b G \overline{H}_a$ and a lifted controller $C_L$ designed for the corresponding lifted system $\overline{G}_L$. If $C_L$ relates the lifted input $\underline{u}$ to the lifted error $\underline{e}$ as,*

$$\left[\begin{array}{c} u_1^{(1)} \\ \vdots \\ u_1^{(\bar{m}_1)} \\ \hline \vdots \\ \hline u_p^{(1)} \\ \vdots \\ u_p^{(\bar{m}_p)} \end{array}\right] = \left[\begin{array}{ccc|c|ccc} \hat{c}_{1,1}^{(1,1)}(\lambda) & \cdots & \hat{c}_{1,1}^{(1,\bar{n}_1)}(\lambda) & \cdots & \hat{c}_{1,q}^{(1,1)}(\lambda) & \cdots & \hat{c}_{1,q}^{(1,\bar{n}_q)}(\lambda) \\ \vdots & & \vdots & & \vdots & & \vdots \\ \hat{c}_{1,1}^{(\bar{m}_1,1)}(\lambda) & \cdots & \hat{c}_{1,1}^{(\bar{m}_1,\bar{n}_1)}(\lambda) & \cdots & \hat{c}_{1,q}^{(\bar{m}_1,1)}(\lambda) & \cdots & \hat{c}_{1,q}^{(\bar{m}_1,\bar{n}_q)}(\lambda) \\ \hline \vdots & & \vdots & & \vdots & & \vdots \\ \hline \hat{c}_{p,1}^{(1,1)}(\lambda) & \cdots & \hat{c}_{p,1}^{(1,\bar{n}_1)}(\lambda) & \cdots & \hat{c}_{p,q}^{(1,1)}(\lambda) & \cdots & \hat{c}_{p,q}^{(1,\bar{n}_q)}(\lambda) \\ \vdots & & \vdots & & \vdots & & \vdots \\ \hat{c}_{p,1}^{(\bar{m}_p,1)}(\lambda) & \cdots & \hat{c}_{p,1}^{(\bar{m}_p,\bar{n}_1)}(\lambda) & \cdots & \hat{c}_{p,q}^{(\bar{m}_p,1)}(\lambda) & \cdots & \hat{c}_{p,q}^{(\bar{m}_p,\bar{n}_q)}(\lambda) \end{array}\right] \left[\begin{array}{c} e_1^{(1)} \\ \vdots \\ e_1^{(\bar{n}_1)} \\ \hline \vdots \\ \hline e_q^{(1)} \\ \vdots \\ e_q^{(\bar{n}_q)} \end{array}\right] \tag{3.42}$$

*and $G_L$ is stable, then the closed-loop output is ripple-free if and only if the sum of controller gains within each block are identical.*

**Proof.** In equation (3.42), the controllers within each partition follow the same definitions as in equation (3.37).

Mathematically, the constraint on the controller gains can be expressed as

$$\hat{c}_{1,1}^{(\alpha,\beta)}(1) + \cdots + \hat{c}_{i,\bar{m}_j}^{(\alpha,\beta)}(1) = \hat{c}_{2,1}^{(\alpha,\beta)}(1) + \cdots + \hat{c}_{2,\bar{m}_j}^{(\alpha,\beta)}(1) = \cdots = \hat{c}_{\bar{n}_i,1}^{(\alpha,\beta)}(1) + \cdots + \hat{c}_{\bar{n}_i,\bar{m}_j}^{(\alpha,\beta)}(1)$$
$$\forall\ \alpha = 1,\cdots,p\ ;\ \beta = 1,\cdots,q \quad \forall\ i = 1,\cdots,p\ ;\ j = 1,\cdots,q \tag{3.43}$$

Using a similar argument as in Proposition 9, it can be easily shown that equation (3.43) gives the required constraint on the controller gains for ripple-free outputs when the reference signal is a step signal. ∎

Although we have focused on the practical case of fast-control slow-sampled system, the general result in (3.43) can be used to arrive at constraints on the controller

for the slow-control fast-sampling case. The following remark states this result for step-type reference signals.

**Remark 1** *In the case of slow-control fast-sampling, the gains of the lifted system are identical when the sampling ratio is an integer. Accordingly, there are no constraints on the controller and the output is guaranteed to be ripple-free. When the sampling ratio is rational, results similar to the fast-control, slow-sampling case can be derived by treating the resulting control problem as a special case of (3.42).*

**Remark 2** *The constraints on the controller gains developed here are applicable to all class of stable plants. Therefore, it is important to note that the constraints are robust with respect to change in model parameters. The robustness result implies that even with the change in model parameters or process operating conditions, it is essential that the lifted controller satisfy the constraints to ensure ripple-free outputs.*

**Remark 3** *As mentioned throughout this work, the results are valid for step-type reference signals only. In the case of non-step type reference signals, the results can be expected to be quite different and are not presented here. Secondly, all the results discussed so far have assumed a strictly stable continuous-time system $G$. However, the stability condition can be relaxed and the above results can be extended to unstable $G$ as well with the sufficient condition of closed-loop stability.*

**Remark 4** *Extensions to unstable plants hold good except for integrating type instabilities. In the case of integrating type instabilities, no constraints exist on the controller as discussed below. Secondly, in all of the above cases, oscillations in the closed-loop output can be eliminated by filtering the inverse lifted input signal. The presence of a moving average filter thus, could aid in ripple-free output. The presence of an integrator (a moving average filter of infinite order) not only eliminates the ripples, but also ensures asymptotic step tracking. The setup for such a configuration when $T_b/T_a = n$, a positive integer, is shown in Figure 3.12. $G_{I_a}$ represents the discrete integrator at the input sampling rate, $T_a$. The following result for a general multirate MIMO system with rational output/input sampling ratio, is given without proof.*

**Theorem 2** *Consider a multirate system $S_bGH_a$. $G$ is a stable continuous-time LTI system and the output/input sampling ratio $T_b/T_a = n/m$, where $n$ and $m$ have no factors in common. Augment the corresponding lifted system, $L_mS_bGH_aL_n^{-1}$ with the lifted integrator $L_nG_{I_a}L_n^{-1}$, where $G_{I_a}$ is the discrete integrator at the input sampling*

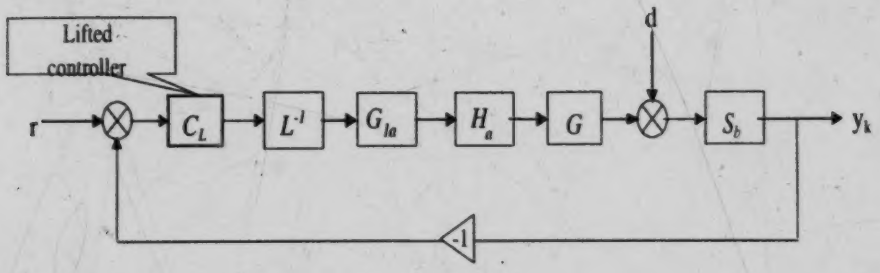


Figure 3.12: *Closed-loop multirate system with augmented discrete integrator* ($T_b/T_a = n\ (n \in Z^+)$)

*rate,* $T_a$. *Then, a controller designed for this augmented system will ensure asymptotic step-tracking and ripple free outputs.*

The above result implies that there are no constraints on the controller gains if the lifted controller is designed for the augmented system described above. In practice, the implementation is done by actually inserting a lifted integrator in the closed-loop. When $m = 1$, Theorem 2 reduces to Proposition 6. Further implications indicate that if $G$ contains an integrator *(integrating type instabilities)*, then the constraints discussed in this work are no longer needed for ripple-free outputs.

Figure 3.13 shows the outputs of the closed-loop system when $G$ is the $(2 \times 2)$ MIMO continuous-time LTI system in equation (3.35). The sampling ratio $n/m$ is set to 3/2 and the lifted plant is augmented with a lifted integrator of appropriate order. A proportional controller not satisfying Proposition 9 is chosen for the purpose. Note that this controller is not an optimal one for the augmented system, but chosen for illustration purposes only. The presence of the lifted integrator according to Theorem 2 ensures ripple-free outputs and asymptotic tracking of unit step changes in the reference signals, evident in Figure 3.13.

A remark is in order here for the class of ramp type reference signals. For a discrete system with zero-order hold, the closed-loop system tracks the discrete ramp with the presence of a discrete double integrator in the closed loop. However, continuous tracking is not guaranteed unless the continuous plant is pre-compensated with a double integrator. Therefore, the mere presence of fast-rate double integrators set-point changes would not suffice to track the continuous output. It is necessary to pre-compensate the continuous plant with an integrator and then further incorporate a fast-rate discrete integrator to ensure continuous tracking and ripple-free output.

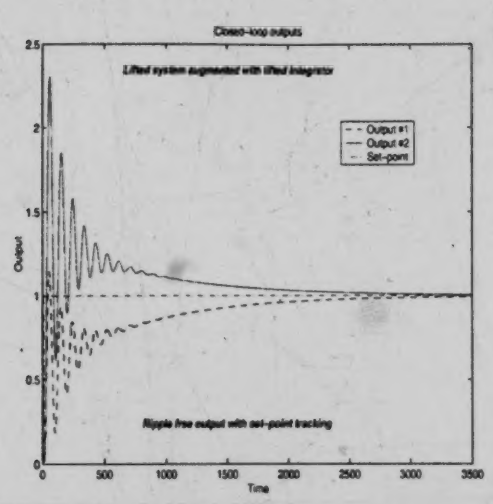


Figure 3.13: *Outputs (solid and dash) of the closed-loop MIMO* $(2\times2)$ *system when the lifted system is augmented with a lifted integrator - unit set point (dashdot) tracking; integer sampling ratio* $(n/m = 3/2)$

### 3.3.1 Intersample Behaviour in the Presence of Disturbances

Here, we discuss the intersample behaviour in the presence of disturbances, in particular, additive type disturbances both at the output and input nodes. For disturbances at the output node *(such as in Figure 3.1)*, it is equivalent to adding another external signal to the output. Therefore, similar results as discussed for step-type reference signals hold good in the case of step-type disturbances. The procedure merely incorporates the disturbance $d$ in the reference signal $r$. In other words, the same constraints are required on the controller gains in order to ensure ripple-free outputs in the presence of step-type disturbances.

In the case of additive type input disturbances, it is not equivalent to adding another external signal. However, we show here that the resulting constraints are the same as in all the previous cases.

Consider the multirate system with disturbances added at the input side, *i.e.*, now the fast-rate input to the plant is $(u_f + d_f)$ instead of $u_f$. We are interested in observing the effect of step-type change in $d_f$ on $u_f$. Let us consider the SISO, integer sampling ratio case first. From Figure 3.1, the closed-loop transfer function between

$\underline{u}$ and $d_f$ *(not shown in the figure)* can be written as *(assuming* $r = 0$*)*

$$\underline{u} = -\frac{C_L S G H_f}{1 + S G H_f L^{-1} C_L} d_f \tag{3.44}$$

$$= -\frac{C_L S G H_f L^{-1}}{1 + S G H_f L^{-1} C_L} \underline{d} \tag{3.45}$$

$$= -\frac{C_L G_L}{1 + G_L C_L} \underline{d} \tag{3.46}$$

where $G_L$ and $C_L$ have their usual meanings. Note that the system is assumed to be closed-loop stable.

Observe that the product $G_L \underline{d}$ is a scalar which allows us to use a similar argument as in Proposition 5 for step-type changes in $d_f$. Using the final value theorem and a similar argument as in Proposition 5, at steady-state we note that the controller gains need to be identical to ensure ripple-free outputs. Additionally, it can be shown that the presence of a fast-rate integrator on the plant side can also eliminate ripples in the closed-loop output.

All the other results shown earlier for MIMO systems with rational and integer sampling ratios can be shown to hold good as well for this class of input disturbances. For MIMO systems, the disturbances have to be lifted accordingly in order to use these results.

Having arrived at the constraints, the next step which is of theoretical importance is parametrization of all such lifted controllers. The following section presents some ideas on parametrization of a class of lifted controller satisfying these constraints.

## 3.4 Parametrization of Lifted Controllers

We have seen so far that the lifted controller has to satisfy certain gain constraints depending on the sampling ratio in order to ensure ripple-free outputs. This section is devoted to designing a lifted controller that satisfies such constraints. We parametrize all such controllers which stabilize the closed-loop system by means of parametrization techniques due to Youla *et al.* (1976) and Kučera (1972). Only stable plants are considered here, as the case of unstable plants is beyond the scope of the discussion. The design problem is formulated in the state-space domain and we make use of the generalized setup as shown in Figure 3.14. The parametrization technique is briefly explained as follows.

Consider the generalized setup as shown in Figure 3.14 where $G_d$ is the generalized

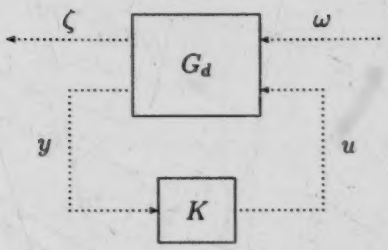


Figure 3.14: *Generalized setup of a discrete-time control system*

plant with

$$\hat{g}_d(\lambda) = \left[\begin{array}{c|cc} A_d & B_{1d} & B_{2d} \\ \hline C_{1d} & D_{11d} & D_{12d} \\ C_{2d} & D_{21d} & 0 \end{array}\right] \tag{3.47}$$

and $K$ represents the controller. Signal $\zeta$ represents the controlled signal while $\omega$ represents the exogenous input comprising of reference signals, disturbances and sensor noise. Measurements from the plant are represented by $y$ while the controller outputs are taken into account by $u$. Note that we have deviated from the earlier use of $G_d$ to represent only an input-output discrete-time system.

Our objective is to parametrize, *i.e.*, express the class of controllers $K$ as a function of a parameter $q$ that achieve internal stability for $G$. This problem is equivalent to internally stabilizing $G_{22}$ (the system from $u$ to $y$) under the assumption that $(A_d, B_{2d})$ is stabilizable and $(C_{2d}, A_d)$ is detectable.

Choose matrices $F$ and $L$ such that $A_d + B_{2d}F$ and $A_d + LC_{2d}$ are stable. Then, all stabilizing controllers for $G$ can be parametrized by a linear fractional transformation of some arbitrary but stable system, as stated by the following theorem.

**Theorem 3** *The set of all (FDLTI and causal) $K$'s achieving internal stability in Figure 3.14 is parametrized by the formula*

$$\hat{k} = \mathcal{F}(\hat{j}, \hat{q}), \quad \hat{q} \in \mathcal{RH}_\infty(D) \tag{3.48}$$

*where*

$$\hat{j}(\lambda) = \left[\begin{array}{c|cc} A_d + B_{2d}F + LC_{2d} & -L & -B_{2d} \\ \hline F & 0 & -I \\ -C_{2d} & I & 0 \end{array}\right] \tag{3.49}$$

The controller $K$ in equation (3.48) is called a *linear fractional transformation* (LFT) of $Q$, which is FDLTI, causal and stable. Such a controller is represented as the input-output transfer matrix of the block diagram

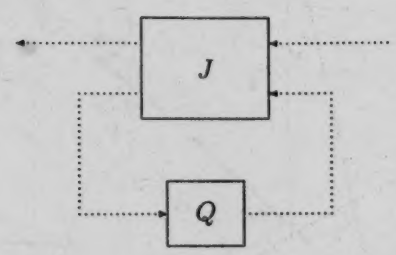


Figure 3.15: *Parametrization of controllers - LFT of Q*

As a special case, if $Q = 0$, $K$ reduces to $J_{11}$ with the transfer matrix

$$\left[\begin{array}{c|c} A_d + B_{2d}F + LC_{2d} & -L \\ \hline F & 0 \end{array}\right] \tag{3.50}$$

which is simply an observer-based controller for $G_{22}$.

Here, we apply Theorem 3 to lifted systems. Assume that the lifted MR system has the generalized form shown in equation (3.47) replaced with the corresponding matrices. Signals $\zeta$, $\omega$, $y$ and $u$ are then represented with their lifted counterparts $\underline{\zeta}$, $\underline{\omega}$, $\underline{y}$ and $\underline{u}$. Thus, replacing $G_d$ by $G_L$ and $K$ by the lifted controller $C_L$, the lifted controller $C_L$ is parametrized by a parameter $Q$ as given in Theorem 3. However, a distinction here follows from the discussion in the earlier section that the class of controllers is restricted to those satisfying the gain constraints. In order to allow this, we have to translate the constraints on the controller gains to constraints on the parameter $Q$, which forms the objective of the following discussion.

We consider the situation when the plant is stable. Therefore, we can choose $L = 0$, $F = 0$. Translation of controller constraints to the parameter $Q$ with $L, F \neq 0$ is a non-trivial problem and beyond the scope of discussion.

### 3.4.1 Stable Plants with $L = 0$, $F = 0$

With the choice of $L$ and $F$, $J$ simplifies to:

$$\hat{j} = \begin{bmatrix} 0 & -I \\ I & \hat{g}_{22} \end{bmatrix} \tag{3.51}$$

First, we consider the case of SISO system with integer sampling ratio. Then, from Proposition 5 we require that $C_L$ satisfies the condition

$$\hat{c}_1^L(1) = \hat{c}_2^L(1) = \cdots = \hat{c}_n^L(1) \tag{3.52}$$

to ensure ripple-free output. Since $C_L$ is an LFT of $Q$, we can write:

$$\begin{aligned} \hat{c}_L &= \hat{j}_{11} + \hat{j}_{12}\hat{q}(I - \hat{j}_{22}\hat{q})^{-1}\hat{j}_{21} \\ &= -\hat{q}(I - \hat{g}_{22}\hat{q})^{-1} \end{aligned} \tag{3.53}$$

after substituting for $\hat{j}$ from equation (3.51). The dimensions of $\hat{g}_{22}$ is $(1 \times n)$ while $\hat{q}$ is $(n \times 1)$. Therefore the matrix that has to be inversed is a scalar, say $p$. Denoting $\hat{c}_{L,i}(1) = c$ (a constant), we get

$$\begin{bmatrix} c \\ c \\ \vdots \\ c \end{bmatrix} = \begin{bmatrix} \hat{q}_1(1) \\ \hat{q}_2(1) \\ \vdots \\ \hat{q}_n(1) \end{bmatrix} p \tag{3.54}$$

which leads to the constraint on $Q$:

$$\hat{q}_1(1) = \hat{q}_2(1) = \cdots = \hat{q}_n(1) = \frac{c}{p} \tag{3.55}$$

Therefore, for a SISO MR system with integer sampling ratio, the class of lifted controllers are parametrized by Theorem 3 along with equation (3.55).

Next we consider the case of SISO systems with rational output/input sampling ratio $n/m$. Then $\hat{g}_{22}$ is of dimensions $(m \times n)$ and $\hat{q}$ has dimensions $(n \times m)$. For the sake of convenience, we choose $n = 3$ and $m = 2$ and later extend it to the general case. Then equation (3.53) can be written as:

$$\begin{aligned} \begin{bmatrix} \hat{c}^L_{1,1} & \hat{c}^L_{1,2} \\ \hat{c}^L_{2,1} & \hat{c}^L_{2,2} \\ \hat{c}^L_{3,1} & \hat{c}^L_{3,2} \end{bmatrix} &= \begin{bmatrix} \hat{q}_{1,1} & \hat{q}_{1,2} \\ \hat{q}_{2,1} & \hat{q}_{2,2} \\ \hat{q}_{3,1} & \hat{q}_{3,2} \end{bmatrix} \begin{bmatrix} \left(1 - \sum_{i=1}^{3} \hat{g}^L_{1,i}\hat{q}_{i,1}\right) & -\sum_{i=1}^{3} \hat{g}^L_{1,i}\hat{q}_{i,2} \\ -\sum_{i=1}^{3} \hat{g}^L_{2,i}\hat{q}_{i,1} & \left(1 - \sum_{i=1}^{3} \hat{g}^L_{2,i}\hat{q}_{i,2}\right) \end{bmatrix}^{-1} \\ &= \begin{bmatrix} \hat{q}_{1,1} & \hat{q}_{1,2} \\ \hat{q}_{2,1} & \hat{q}_{2,2} \\ \hat{q}_{3,1} & \hat{q}_{3,2} \end{bmatrix} \frac{1}{\Delta_L} \begin{bmatrix} \left(1 - \sum_{i=1}^{3} \hat{g}^L_{2,i}\hat{q}_{i,2}\right) & \sum_{i=1}^{3} \hat{g}^L_{1,i}\hat{q}_{i,2} \\ \sum_{i=1}^{3} \hat{g}^L_{2,i}\hat{q}_{i,1} & \left(1 - \sum_{i=1}^{3} \hat{g}^L_{1,i}\hat{q}_{i,1}\right) \end{bmatrix} \end{aligned} \tag{3.56}$$

where we have absorbed the determinant of the rightmost matrix in $\Delta_L$.

Now, recall the constraints on the controller gains from Proposition 7 to ensure ripple-free outputs:

$$\hat{c}^L_{1,1}(1) + \hat{c}^L_{1,2}(1) = \hat{c}^L_{2,1}(1) + \hat{c}^L_{2,2}(1) = \hat{c}^L_{3,1}(1) + \hat{c}^L_{3,2}(1) \tag{3.57}$$

Imposing these conditions on equation (3.56) and making use of Proposition 2, it is easy to see that the constraints on the lifted controller directly translate to the constraints on the parameter $Q$ as:

$$\hat{q}_{1,1}(1) + \hat{q}_{1,2}(1) = \hat{q}_{2,1}(1) + \hat{q}_{2,2}(1) = \hat{q}_{3,1}(1) + \hat{q}_{3,2}(1) \tag{3.58}$$

Constraints on $Q$ for the general $n/m$ case then easily follow from equation (3.58).

Without further discussion, from equations (3.55) and (3.58) it is clear that constraints given on the lifted controller in the most general case in Theorem 1 can be directly delivered to constraints on the parameter $Q$. In other words, for a stable MIMO MR system with $N_i$ inputs and $N_o$ outputs, the constraints:

$$\hat{q}_{1,1}^{(\alpha,\beta)}(1) + \cdots + \hat{q}_{i,\bar{m}_j}^{(\alpha,\beta)}(1) = \hat{q}_{2,1}^{(\alpha,\beta)}(1) + \cdots + \hat{q}_{2,\bar{m}_j}^{(\alpha,\beta)}(1) = \cdots = \hat{q}_{\bar{n}_i,1}^{(\alpha,\beta)}(1) + \cdots + \hat{q}_{\bar{n}_i,\bar{m}_j}^{(\alpha,\beta)}(1)$$
$$\forall\ \alpha = 1, \cdots, N_i\ ;\ \beta = 1, \cdots, N_o \quad \forall\ i = \bar{n}_1, \cdots, \bar{n}_{N_i}\ ;\ j = \bar{m}_1, \cdots, \bar{m}_{N_o}$$
$$\hat{q} \in \mathcal{RH}_\infty(D) \tag{3.59}$$

along with Theorem 3 parametrizes all controllers which ensure ripple-free outputs with $L = 0$, $F = 0$.

In the above parametrization and the discussions, we have implicitly assumed that the lifted controllers are causal. However, as mentioned earlier, as a result of lifting, causality constraints have to be specially imposed during the design process. The following section discusses this issue in detail. The purpose of the next section is to provide the reader with an awareness of this crucial issue that arises during the design process. We do not present a solution to this problem as it is beyond the scope of the discussion and is in itself an active area of research.

## 3.5 Causality Constraints

Causality constraints come into picture during the controller design process. Their presence have attracted the attention of several researchers involved in the application of lifting techniques to resolve the MR control design problem (Al-Rahmani and Franklin 1992, Voulgaris and Bamieh 1993, Chen and Qiu 1994, Qiu and Chen 1995, Colaneri and Nicolao 1995, Shu and Chen 1996, Qiu and Tan 1998, Sagfors and Toivonen 1998). These constraints are seldom an exception in the course of design, except when the ratio of output/input sampling intervals is an integer *(as explained below)*. The issue of causality translates to the imposition of a special structure on the lifted controller. In particular, the feedthrough term should possess a block lower-triangular structure. Several methodologies have been proposed to impose this special structure on the controller.

As the term suggests, these constraints are related to the causality of the controller, *i.e.*, the structure of the controller has to obey the principle of causality explained as follows. Recall the example discussed in Section 2.2 involving an MR system with integer I/O sampling ratio. Upon incorporating lifting and inverse lifting in the appropriate order, we obtain the lifted transfer function of the system $\tilde{G}_L$:

$$\hat{\tilde{g}}_L(\lambda) = \left[\begin{array}{c|cccc} A_f^n & A_f^{n-1}B_f & A_f^{n-2}B_f & \cdots & B_f \\ \hline C & D & 0 & \cdots & 0 \end{array}\right] \tag{3.60}$$

relating the closed-loop output $y$ and the lifted input $\underline{u}$ of dimension $n$.

The structure of the feedthrough term, *i.e.*, the $D$ matrix for the resulting lifted system in equation (3.60) indicates the relationship between the current output and the set of current and future inputs in the slow sampling interval. The $D$ matrix suggests that the current input is not a function of the future inputs in that slow sample interval, which is in accordance with the causality principle. For instance, if $n = 3$, the lifted input is $\underline{u}(0) = [\ u(0)\ \ u(h)\ \ u(2h)\ ]^T$ corresponding to the output $y(0)$, and $\underline{u}(0) = [\ u(3h)\ \ u(4h)\ \ u(5h)\ ]^T$ (the superscript $T$ indicates transpose) corresponding to the output $y(3h)$, and so on. Clearly, $y(0)$ cannot depend on $u(h)$ and $u(2h)$. Similarly, $y(3h)$ cannot depend on $u(4h)$ and $u(5h)$. This is indicated by the zeros in the $D$ matrix in equation (3.60). Therefore, the model obeys the causality principle. Now, let us make a few observations on the structure of the $D$ matrix of the lifted controller.

Since the lifted system is of dimensions $(1 \times n)$, the controller structure would have dimensions $(n \times 1)$, *i.e.*, $n$ outputs and 1 input. Thus, the lifted controller computes the lifted process input based on the slow-sampled process output. Assume that $n = 3$ still holds good. From the earlier discussion, this means that based on the output $y(6h)$, for instance, the lifted controller designs the moves $[\ u(6h)\ \ u(7h)\ \ u(8h)\ ]^T$, which is in accordance again with the causality principle (note that this is not strictly causal which is required for discrete systems). In short, the controller is capable of computing only the future inputs based on the current output. Therefore, the controller obeys the causality principle as well, thus obviating the imposition of any causality constraints.

However, now consider the case of rational sampling ratio. Assuming a SISO system with output and input sampling intervals as $3h$ and $2h$ respectively, we can import the results from Section 2.2. The resulting lifted model is then:

$$\hat{g}_L(\lambda) = \left[\begin{array}{c|ccc} A_h^6 & (A_h^5 + A_h^4)B_h & (A_h^3 + A_h^2)B_h & (A_h + I)B_h \\ \hline C & D & 0 & 0 \\ CA_h^3 & C(A_h^2 + A_h)B_h & CB_h + D & 0 \end{array}\right] \tag{3.61}$$

Let us briefly discuss the impact of such a lifted transfer function. Both the outputs and inputs are lifted unlike the previous case of integer sampling ratio. Therefore, the lifted output $\underline{y}(0) = [\ y(0)\ \ y(3h)\ ]^T$, for instance, is related to the lifted input $\underline{u}(0) = [\ u(0)\ \ u(2h)\ \ u(4h)\ ]^T$. The structure of the $D$ matrix in equation (3.61) reflects two points. The first being that $y(0)$ is dependent on $u(0)$ only and second, $y(3h)$ is dependent on $u(0)$ and $u(2h)$ only. Again, this is in accordance with the causality condition. Thus, the lifted model is causal. Now, consider the requirements of the $D$ matrix structure for the resulting controller. The controller should yield the moves for $\underline{u}$ based on $\underline{y}$. However, at the time instant $t = 0$, only $y(0)$ is available but not $y(3h)$ whereas we need both these measurements to design $\underline{u}(0) = [\ u(0)\ \ u(2h)\ \ u(4h)\ ]^T$. This is the causality constraint problem *(note that this problem did not arise when the sampling ratio was an integer)*. In order to account for this problem, causality constraints are imposed on the controller during the design process. This is done as follows. If a special structure known as the block lower-triangular structure is imposed on the $D$ matrix of the lifted controller, then the causallty problem is overcome. For example, consider the same MR system as in equation (3.61). If the feedthrough term $D$ of the *controller* has the structure:

$$D_{LC} = \begin{bmatrix} D_{11} & 0 \\ D_{21} & 0 \\ D_{31} & D_{32} \end{bmatrix} \tag{3.62}$$

then, $u(0)$ and $u(2h)$ can be designed just based on $y(0)$, while $u(4h)$ makes use of both $y(0)$ and $y(3h)$, which is in line with the causality principle. The structure shown in equation (3.62) is termed as the block lower-triangular structure.

Another situation which can give rise to this problem is when either the inputs or the outputs (or both) are not uniformly sampled, however the sampling ratios are integers. For example, in a $2 \times 2$ MIMO system, if the inputs are uniformly sampled every 2 seconds, but the outputs are sampled every 2 and 4 seconds respectively, then one of the outputs has to be lifted along with the inputs. Then the controller needs the second component (in this case) of the lifted process output in order to design the lifted input moves. In fact, this is a more practical situation than the case of both inputs and outputs sampled uniformly but at different rates.

An optimal solution this problem is far from trivial and handicaps several existing solutions to the optimal control problems. In order to arrive at these structures in an optimal sense, several researchers have employed different approaches. A new framework known as the nest algebra is proposed in (Chen and Qiu 1994, Qiu and Chen 1995) to tackle the optimal $\mathcal{H}_2$ problem with the causality constraint. Constrained model-matching is employed by Voulgaris and Bamieh (1993) to solve the

optimal $\mathcal{H}_2$ problem with the causality constraint. In (Sagfors and Toivonen 1998), the authors achieve this structure by posing the design problem as an $\mathcal{H}_\infty$ optimization problem with additional, nonstandard positive-definiteness constraints and a set of coupling conditions along with a set of algebraic Riccati equations. A direct state-space solution is provided to the $\mathcal{H}_2$ problem by Qiu and Tan (1998) using continuous lifting techniques. The plus points of these methods are evident. They are optimal in nature, rich in theory and yield causal controllers. However, all the schemes are controller specific, meaning $\mathcal{H}_2$ or $\mathcal{H}_\infty$ type controllers. Additionally, these are fairly advanced techniques and difficult to obtain insights. Therefore, from a control engineering point of view and a practical perspective, there is a strong need for a practical, simple and easy-to-understand solution to this problem.

One proposed direction is a two-step method. The first step consists of designing a non causal controller by relaxing the causality constraint, and the second step of approximating this non-causal controller to a causal controller. This could possibly simplify the design procedure and yield a practically appealing method. However, if not optimal, one has to guarantee robustness in terms of stability and performance for the resulting controller. In order to do this, theoretical expressions are necessary to arrive at the loss of performance and analyze the stability of the resulting closed-loop system.

Another direction to this problem is a sequential predictor-corrector method which consists of designing a non-causal controller, but using a predicted value for the unknown process output until it is available. Upon availability, the remaining control moves can be updated. The advantages of this method is it is simple and provides valuable insights into the process and the predictive capabilities of the model. However, it may yield a linear time-varying controller and as mentioned earlier, robustness analysis of stability and performance may become an intractable problem.

In order to evaluate the performance of the resulting controllers from the above schemes, one can compare the performance with the performance of the corresponding lifted system for which the non-causal controller has been designed. In this manner, it is possible to get a measure of the loss of performance.

## 3.6 Summary

Lifting techniques are very powerful tools for designing MR controllers in the discrete domain. However, two issues that arise due to lifting and inverse lifting have to be taken into account. While the former one gives rise to causality constraints, a well known problem, we show that the latter one can give rise to intersample ripples in

the closed-loop outputs. In this chapter we have shown that for step-type reference signals: (1) intersample ripples exist in the closed-loop outputs of lifted MR control systems due to inverse lifting, (2) controller gains have to satisfy certain constraints in order to ensure ripple-free conditions, and (3) the presence of a fast-rate integrator eliminates intersample ripples without the necessity of constraining lifted controllers. As a result, unstable plants with integrating type instabilities allow us to relax these constraints on the controller. Parametrization of all such lifted controllers for stable plants with $L = 0, F = 0$ shows that the constraints on the controller directly translate to the constraints on the parameter $Q$. On the other hand, deriving constraints on $Q$ for observer-based and state-feedback controllers is a non-trivial problem and not considered here.

## 3.7 Future Work

Future work involves research in the following directions:

- Parametrization of state-feedback and observer-based controllers.
- Provision of a practical and simple sub-optimal solution to the causality constraint problem in a tractable framework.
- Exploring the existence of other optimal solutions which yield a causal lifted controller.

# Chapter 4

# Performance Comparison of Multirate Systems vs. Single-rate Systems

**Purpose:** To answer the question: *does multirate control offer incentives over single-rate control? if yes, what are they and in what sense?* To provide a theoretical ground for comparison and establish the conditions under which MR control systems can be compared with single-rate systems[1].

## 4.1 Motivation

One of the primary reasons for moving to MR control from SSR control is the intuitive idea that the former gives better performance than the latter. In general, faster discretization is desired and attractive for emulating continuous-time systems and meeting certain performance specifications.

The question of interest that arises in the context of performance analysis is then: *do MR systems give better performance than SSR systems and if yes, then what is the extent of performance improvement?* It is intuitive on the other hand, that if all the outputs were available at a faster rate than that in the MR system, we could expect better performance than that given by the MR system. It is also for this purpose, that we had introduced in Chapter 2 a fictitious discrete system, $G_f$, at the fast sampling period $h_f$, the *greatest common divisor* of the sampling periods of the multirate system. $G_f$ is referred to as the fast SR system or simply, as FSR system. In an FSR system, control moves are designed assuming that all the signals are available over the sampling interval $h_f$. Hence, from a pedagogical point of view, it is appealing

[1]A version of this chapter has been accepted for publication in the Journal of Dynamics of Continuous, Discrete and Impulsive Systems

to raise the question: *do FSR systems necessarily perform better than MR systems?* In order to address these matters, this chapter considers the comparison by asking: *what is a fair benchmark for comparison?*

Interestingly, there has been no theoretical analysis to compare the closed-loop performance of closed-loop MR and SSR systems. However, there have been only a handful of papers that have addressed a closely related issue (McEachen and Meyer 1991, Berg *et al.* 1988). In both papers (McEachen and Meyer 1991, Berg *et al.* 1988), the comparison is purely on the basis of simulation. The main drawback of the work reported in McEachen and Meyer (1991) is that it lacks a common ground for comparison. For instance, equal importance to input weights in the MR and SSR systems is not ensured because the design problem does not start from a continuous-time cost function, bur rather from a discrete-time one. In Berg *et al.* (1988), although the controllers are derived from the same continuous-time LQG cost function, the comparison is made only on the basis of simulation. Moreover, the MR system is modelled as a periodic discrete-time system, yielding a periodic LQG controller. The work reported in (Berg *et al.* 1988) is case-dependent, *i.e.*, demonstrated for a specific problem and does not constitute a general proof. In contrast, here we give a theoretical proof to show that the performance of MR systems is bounded above by that of single-rate systems at the slow rate and below by single-rate systems at the fast rate. The proof is built in an LTI framework using lifting techniques, with the continuous-time LQR cost function as a benchmark for the state-feedback case and the generalized $\mathcal{H}_2$-norm for the output feedback case.

Performance analysis of multirate control systems can be mainly approached in two ways, namely, *(i)* the periodic discrete-time modelling approach, and *(ii)* the lifting methodology. We adopt the latter approach because of the following reasons. The main advantage of the lifting approach is that it is conceptually simple and enables a convenient analysis of stability and performance issues of multirate control systems. In addition, the lifting framework translates a MR system into an LTI system, whereas the periodic discrete-time modelling approach results in a time-varying system. Clearly, it is simpler to analyze LTI systems because of the rich framework of theory that exists in this area (Khargonekar *et al.* 1985, Araki and Yamamoto 1986, Chen and Qiu 1994, Sagfors and Toivonen 1998). In this work, the advantage of lifting is evident by the theoretical framework it provides for the comparison of performances between MR and SSR (slow single-rate) systems, hitherto not presented.

Although in Berg *et al.* (1988) analysis of the MR control design problem is also done via the discretization of a continuous-time LQR cost function, the approach

followed in this paper markedly differs from that of Berg *et al.* (1988). Firstly, Berg *et al.* (1988) have used the periodic discrete-time modelling approach; while in the present work we have used the lifting scheme. Models obtained using the former method are periodic in nature while lifted models are time-invariant. Additionally, the periodic cost function in Berg *et al.* (1988) yields a periodic/time-varying LQR controller, while the lifted cost function yields an LTI controller. Secondly, in Berg *et al.* (1988) the comparison problem is tackled mainly by applying the design techniques to two different plant models. The performances of MR and SSR systems are then compared by comparing the closed-loop responses and achieved design specifications. In contrast to this, the present work first compares the performances of MR and SSR systems on a theoretical basis, and then the results are illustrated by evaluation on an experimental plant model. Also, we have examined the extent of benefits obtained and the conditions under which such benefits can be expected as one moves from MR to SSR control schemes, with a clear theoretical analysis.

In short, the approach and contributions of this chapter can be summarized as:

- Analysis of MR systems is performed in the lifting framework which yields finally an LTI controller unlike the periodic discrete-time modelling approach.
- The continuous-time cost function is used as a benchmark to overcome the discrepancies with discrete-time benchmarks at the fast or slow sample rates.
- Performance comparison is first performed by establishing the equivalence between the cost functions for the lifted and slow-rate cost functions.
- A proof based on convex optimization ideas that MR systems perform no worse than SR systems at the slow rate and bounded below by the performance of SR systems at the fast rate. The proof is provided in an LTI setup which enables use of the rich theoretical framework available for the controller design of single-rate LTI systems.
- Providing a platform for assessing the benefits of MR systems over SSR systems and FSR systems in a graphical way by plotting the relative improvement (to be defined later) in MR systems vs. the input weight and the sampling ratio.

We consider two separate situations. The first one is that of state-feedback control. An LQR cost function is used for this purpose, presented in Section 4.2. Next, we impose the restriction that the states are not directly accessible and incorporate the state estimation problem in the $\mathcal{H}_2$ setup. This is the second situation. For this purpose, we choose the benchmark as the continuous-time generalized $\mathcal{H}_2$-norm. The

relevant details are discussed in Section 4.5. Since the output feedback problem is more practical, it can be said the results for this case are more general. However, the motivation and the outline for the proof for the output feedback case is derived from the state feedback case.

The objective behind presenting a proof is from an academic point of view to establish the intuitive result in theory, and to pave way for further performance comparison analysis, for example, in the $\mathcal{H}_\infty$ framework and the robustness analysis of performance improvement. The proof is new, non-trivial and established in the lifting framework which preserves the LTI property of the continuous-time system.

The ideas presented in the LQR case are valid for both the regulatory and servo control problems. We first prove the results for the regulatory problem and subsequently import them to the servo problem. The tracking problem covers three classes of signals, *viz*, step, ramp and sinusoidal signals. The import of results from the regulatory problem is made convenient by converting the tracking problem into a disturbance rejection problem by means of suitable transformations. The entire problem is formulated in the state-space framework.

The chapter is organized as follows. Section 4.2 discusses the LQR equivalence of multirate systems and single-rate systems. In Section 4.3, we present the main result, *i.e.*, the proof of the result that the closed-loop performance of MR systems is bounded above by that of SSR systems, and below by the performance of fast-rate control systems. Section 4.4 compares the performance of MR systems vs. SSR systems on an experimental setup comprising a level-control system; the objective is to control the level of water in a continuously stirred tank heater system by manipulating the inlet flow valve. The output feedback case starts to appear in Section 4.5 consisting of the proof of the main result that in general, MR systems perform better than the associated SSR systems. Finally, some concluding remarks with ideas for future work appear in Sections 4.6 and 4.7.

## 4.2 LQR Cost Function for Performance Evaluation

### 4.2.1 Choice of Benchmark

The original sampled-data multirate system requires the design of an optimal linear, causal and periodic controller. However, in the lifted framework, we require an optimal LTI, causal controller. The change of domain from a class of periodic systems to LTI systems simplifies the multirate control design problem, and further elucidated

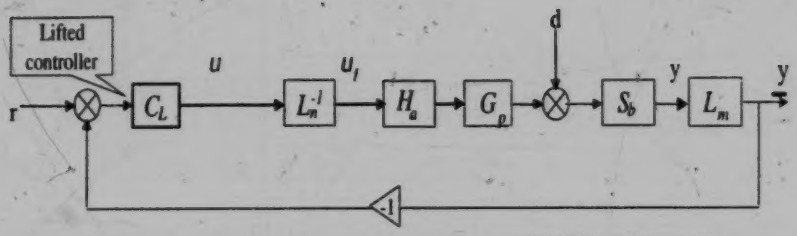


Figure 4.1: *General closed-loop multirate system* ($T_b/T_a = n/m$)

in section 4.3.

For reasons of practical industrial appeal, all the ensuing discussions assume that the inputs are available at a faster rate than the outputs and the term *sampling ratio* shall refer to the ratio of the sampling period of the output to the sampling period of the input. Figure 4.1 shows a block diagram of a general closed-loop system implementing the lifting strategy. In Figure 4.1, $G_p$ represents a continuous-time LTI system and the remaining symbols have their usual connotations.

In the following discussions, the controller outputs in the MR, SSR and FSR systems are denoted by $\underline{u}$, $u_s$ and $u_f$, respectively. Fair comparison and evaluation of the performance of MR systems versus SSR and FSR systems require the choice of a benchmark. For instance, one can compare the variance of controller outputs as a benchmark. However, such a comparison is unfair because the dimension of the controller output signal in the MR system, $\underline{u}$, is different from those in the SSR and the FSR systems, $u_s$ and $u_f$, respectively. Alternatively, if we compare the input signals to the plant, then the signals $u_s$ and the fast-rate signal in the MR system $L^{-1}\underline{u}$ are available at different sampling rates which makes the comparison a difficult task. A similar problem with the sampling rates would arise if we choose the variance of the closed-loop outputs as a performance criterion.

With the above considerations in mind, we approach the problem from a fundamental perspective. The above arguments focus only on discrete-time performance criteria. The motivation for implementing multirate control is to improve the *intersample performance*, or more rigorously, the continuous-time performance of the outputs. Therefore, it seems both intuitive and appropriate to choose a benchmark which includes the continuous-time performance of the system. With these ideas in mind, we choose the continuous-time LQR cost function $J_c$ as a choice for the benchmark problem. Subsequently, we derive the equivalent discrete-time cost functions for the MR, SSR and FSR systems, namely, $J_L$, $J_s$ and $J_f$, respectively, from $J_c$. Essentially, we impose weights on the continuous states and inputs, and arrive at the

equivalent weights on the discrete states and inputs. In this way, all the weights in the discrete-time cost functions arise from one continuous-time cost function. The method of obtaining an equivalent single-rate cost function at a given sample rate from $J_c$ is discussed at length in Chen and Francis (1991*a*). Preliminaries for arriving at an equivalent multirate cost function from $J_c$ are derived in Tangirala *et al.* (1999).

With the design criteria in hand, the achieved closed-loop performance can be measured from the closed-loop data and the lowest of $J_L$, $J_s$ and $J_f$ would indicate the system with the best performance. The following paragraphs discuss this idea in more detail.

### 4.2.2 Performance Based Multirate Controller Design

One of the primary reasons for building a multirate controller is to improve intersample ripples. We had argued earlier that it is not possible to design with an objective function comprising fast-rate states/outputs as it is impractical to measure the output at a faster rate, Hence it is motivating to derive an equivalent discrete-time system given a continuous-time cost function. Besides, this type of design provides a fair benchmark for comparing the closed-loop performances of multirate and single-rate systems. Results for single-rate systems are presented in Chen and Francis (1991*b*). We consider the design problem in the continuous-time domain in the LQR framework and derive the equivalent multirate system.

Consider a SISO sampled-data system with sampling ratio $n/m$ a positive integer, *i.e.*, $m = 1$. Define $h_l$ as the *LCM* of the sampling periods of all the signals comprising the MR system, which is equal to the output sampling period when $m = 1$. Represent the generalized continuous-time LTI system $G$ as:

$$\dot{x} = Ax + Bu \tag{4.1}$$

$$z = C_1 x + D_1 u \tag{4.2}$$

$$y = C_2 x \tag{4.3}$$

where $z$ is the fictitious signal whose $\|.\|_2$ is to be minimized:

$$\|z\|_2 = J_c = \int_0^\infty \begin{pmatrix} x \\ u \end{pmatrix}^T [C_1 \;\; D_1]'[C_1 \;\; D_1] \begin{pmatrix} x \\ u \end{pmatrix} dt \tag{4.4}$$

and the matrices $C_1$ and $D_1$ are chosen such that:

$$[C_1 \;\; D_1]^T[C_1 \;\; D_1] = \begin{pmatrix} Q_c & 0 \\ 0 & R_c \end{pmatrix} \tag{4.5}$$

The *equivalent discrete* single-rate system at a sampling rate $h$, would give rise to the cost function:

$$J_h = \sum_{k=0}^{\infty} \begin{pmatrix} x_k \\ u_k \end{pmatrix}^T \begin{pmatrix} Q_d & N_d \\ N'_d & R_d \end{pmatrix} \begin{pmatrix} x_k \\ u_k \end{pmatrix} \tag{4.6}$$

as given in Chen and Francis (1991*b*). The weighting matrix can be summarized as

$$\begin{pmatrix} Q_d & N_d \\ N'_d & R_d \end{pmatrix} = [\tilde{C}_1 \ \tilde{D}_1]^T [\tilde{C}_1 \ \tilde{D}_1] \equiv M \tag{4.7}$$

where $\tilde{C}_1$ and $\tilde{D}_1$ are the solutions to (4.7) with

$$M = \int_0^h e^{t\bar{A}'} [C_1 \ D_1]^T [C_1 \ D_1] e^{t\bar{A}} dt \tag{4.8}$$

and

$$\bar{A} = \begin{pmatrix} A & B \\ 0 & 0 \end{pmatrix} \tag{4.9}$$

The SSR LQR cost function denoted by $J_s$ *(the weights respectively by $Q_s$, $R_s$ and $N_s$)*, is obtained by setting $h = h_l$ in equation (4.8) and using equations (4.6) through (4.7).

$$J_s = \sum_{k=0}^{\infty} (x_k^T Q_s x_k + u_k^T R_s u_k + 2x_k^T N_s u_k) \tag{4.10}$$

We extend the results here to multirate MIMO systems in the *lifted* framework.

If $\tilde{G}_f$ represents the equivalent system at the fast rate $h_f$, then for the multirate system, we can show using lifting techniques that the lifted system

$$\tilde{G}_L = \begin{pmatrix} L_n & 0 \\ 0 & S_n H_f \end{pmatrix} \tilde{G}_f \begin{pmatrix} L_n^{-1} & 0 \\ 0 & L_n^{-1} \end{pmatrix} \tag{4.11}$$

represents the system from $\underline{u}_m$ to $(\underline{z}_m, y_m)$ where $\tilde{G}_f$ is the equivalent discrete system obtained from $J_c$ by setting $h = h_f$. Here, $\underline{z}_m$ is the lifted fictitious signal obtained in terms of the available states and lifted inputs. $S_n$ is the discrete downsampler with the downsampling factor $n$. The state space model of the lifted system can then be written as

$$\dot{x}_k = A_L x_k + B_L \underline{u}_k \tag{4.12}$$

$$\underline{z}_k = \tilde{C}_{1L} x_k + \tilde{D}_{1L} u_k \tag{4.13}$$

$$y = \tilde{C}_{2L} x_k \tag{4.14}$$

and the matrices $A_L, B_L, \tilde{C}_{1L}, \tilde{C}_{2L}, \tilde{D}_{1L}$ are obtained by using equation (4.11).

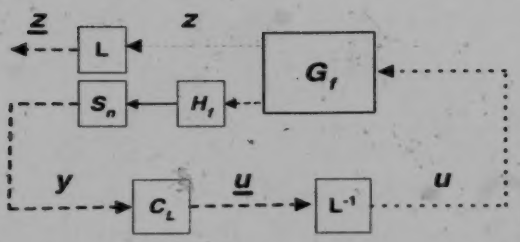


Figure 4.2: *Equivalent multirate system (SISO G and integer sampling ratio)*

Using lifting techniques, we can obtain a state-space model for $L\tilde{G}_f L^{-1}$ (Chen and Francis 1995). Represent this model in transfer function form from $\underline{u}_m$ to $\underline{z}_m$ as

$$\tilde{g}_L = \left[\begin{array}{c|c} \tilde{A}_{L1} & \tilde{B}_{L1} \\ \hline \tilde{C}_{L1} & \tilde{D}_{L1} \end{array}\right]$$

Note that the states are available at the same rate in both the multirate and the single-rate system (at the slow rate) while the inputs are available at the fast rate in the former case.

The following remark is useful to compare the performance of MR and SSR systems in the later sections.

**Remark 5** *If $(A_s, B_s)$ represents the discrete version of $(A, B)$ at the slow rate $h_l$, then it can be shown that $(A_L, B_L)$ and $(A_s, B_s)$ are related as follows:*

$$A_L = A_s \tag{4.15}$$

$$\sum_{j=1}^{n} B_{L_{ij}} = B_{s_i} \quad \forall i = 1 \cdots, n_s \tag{4.16}$$

where $n_s$ is the number of states describing the system. $B_{L_{ij}}$ is the $ij^{th}$ element of the lifted matrix $B_L$ and $B_{si}$ represents the $i^{th}$ element of the column vector $B_s$.

For MIMO systems, $B_s$ is a matrix and therefore equation (4.16) holds good for every column of $B_s$.

Having established a suitable benchmark for the comparison problem and shown the MR control design methodology, the next step is to link the MR and SR control design problem. The importance of the second step will be clear once we establish the proof of the main result.

### 4.2.3 Linking MR and SR Control Design

For the LQR problem, the weights for the cost function $J_L$ for the lifted system are calculated as

$$\begin{pmatrix} Q_L & N_L \\ N'_L & R_L \end{pmatrix} = [\tilde{C}_{1L}\ \tilde{D}_{1L}]'[\tilde{C}_{1L}\ \tilde{D}_{1L}] \ = \ M \tag{4.17}$$

which allows us to write $J_L$ as

$$J_L \ = \ \sum_{r=0}^{\infty} \begin{pmatrix} x_r \\ \underline{u}_r \end{pmatrix}' \begin{pmatrix} Q_L & N_L \\ N'_L & R_L \end{pmatrix} \begin{pmatrix} x_r \\ \underline{u}_r \end{pmatrix} \tag{4.18}$$

Finally, the cost function for the FSR system is obtained by setting $h = h_f$ in equation (4.7):

$$J_f \ = \ \sum_{q=0}^{\infty} \begin{pmatrix} x_q \\ u_q \end{pmatrix}' \begin{pmatrix} Q_f & N_f \\ N'_f & R_f \end{pmatrix} \begin{pmatrix} x_q \\ u_q \end{pmatrix} \tag{4.19}$$

The inputs and states in (4.19) are at the fast rate $h_f$. It can thus be inferred that $J_L$ is identical to $J_c$ because lifting preserves the 2-norm of signals. Hence, all the cost functions $J_s$, $J_L$ and $J_f$ are identical to $J_c$.

The discussions to follow express the relations between the weights for $J_L$ in equation (4.18) and those for $J_s$ in equation (4.10). As usual, we start with the simple case of SISO systems with integer sampling ratios and then proceed towards the general case of MIMO systems with rational sampling ratios.

#### SISO systems with integer sampling ratios

**Theorem 4** *Given a continuous-time cost function $J_c$ for a continuous-time SISO LTI system, $G_p$, the equivalent discrete cost functions $J_s$ for the slow single-rate system at the slow rate and $J_L$, the discrete cost function for the multirate system $SG_pH_f$ arise in such a way that*

$$Q_s \ = \ Q_L \tag{4.20}$$

$$R_s \ = \ \sum_{i=1}^{n}\sum_{j=1}^{n} R_{L_{ij}} \tag{4.21}$$

$$N_{s_i} \ = \ \sum_{j=1}^{n} N_{L_{ij}} \quad i = 1, \cdots, n_s \tag{4.22}$$

*where $R_L = [R_{L_{ij}}]$ and $N_L = [N_{L_{ij}}]$, $n_s$ is the order of the system $G_p$ and $N_{s_i}$ is the weighting between the $i^{th}$ state and the input: $N_s = [N_{s_1}\ N_{s_2}\ \cdots\ N_{s_{n_s}}]^T$.*

**Proof.** Denote the transfer functions between $(z, u)$ and $(z_k, u_k)$ for the continuous-time and the fast rate discretized plants as

$$\hat{g}(s) = \left[\begin{array}{c|c} A & B \\ \hline C_1 & D_1 \end{array}\right] \quad ; \quad \hat{g}(\lambda) = \left[\begin{array}{c|c} A_f & B_f \\ \hline C_{1f} & D_{1f} \end{array}\right]$$

respectively. Also,

$$A_f = e^{Ah_f} \quad ; \quad B_f = \int_0^{h_f} e^{At} dt B$$

If

$$\bar{A} = \begin{pmatrix} A & B \\ 0 & 0 \end{pmatrix}$$

then

$$\cdot \begin{pmatrix} A_f & B_f \\ 0 & I \end{pmatrix} = exp\left\{h_f \begin{pmatrix} A & B \\ 0 & 0 \end{pmatrix}\right\} \tag{4.23}$$

Now, consider the derivation of the equivalent discrete-system at the slow rate $h_b$, given $J_c$. Representing the integral $M$ at the slow rate as $M_s$, and $M_f$ at the fast rate $h_f = h_b/n$, we can write

$$M_s = \int_0^{h_b} e^{t\bar{A}^T} \begin{pmatrix} Q_c & 0 \\ 0 & R_c \end{pmatrix} e^{t\bar{A}} dt \quad ; \quad M_f = \int_0^{h_f} e^{t\bar{A}^T} \begin{pmatrix} Q_c & 0 \\ 0 & R_c \end{pmatrix} e^{t\bar{A}} dt$$

We know from earlier discussion that

$$M_s = \begin{pmatrix} Q_s & N_s \\ N_s' & R_s \end{pmatrix} \quad ; \quad M_f = \begin{pmatrix} Q_f & N_f \\ N_f' & R_f \end{pmatrix} \tag{4.24}$$

Using Cholesky factorization, we can write

$$\begin{pmatrix} Q_c & 0 \\ 0 & R_c \end{pmatrix} = W^T W$$

The integral denoted by $M_s$ can be split into $n$ integrals since $h_b = nh_f$,

$$M_s = \int_0^{h_f} e^{t\bar{A}^T} W^T W e^{t\bar{A}} dt + \cdots + \int_{(n-1)h_f}^{nh_f} e^{t\bar{A}^T} W^T W e^{t\bar{A}} dt \tag{4.25}$$

Note that the first integral in the above equation is $M_f$. Using a change of variable for the rest of the integrals, we can rewrite equation (4.25) as:

$$M_s = M_f + e^{h_f\bar{A}^T} M_f e^{h_f\bar{A}} + \cdots + e^{(n-1)h_f\bar{A}^T} M_f e^{(n-1)h_f\bar{A}} \tag{4.26}$$

Using equation (4.23) in equation (4.26), the $k^{th}$ $(k = 2, \cdots, n)$ term in (4.26) can be written as

$$\begin{pmatrix} A_f^{T^{k-1}} & 0 \\ B_f^T + B_f^T A_f^T + \cdots + B_f^T A_f^{T^{k-2}} & I \end{pmatrix} M_f \begin{pmatrix} A_f^{k-1} & B_f + B_f A_f + \cdots + B_f A_f^{k-2} \\ 0 & I \end{pmatrix}$$

Substituting equation (4.24) in the above equation and equating the individual terms on both the sides in equation (4.26) gives

$$Q_s = Q_f + A_f^T Q_f A_f + A_f^{T^2} Q_f A_f^2 + \cdots + A_f^{T^{n-1}} Q_f A_f^{n-1} \tag{4.27}$$

$$\begin{aligned} R_s = {} & R_f + (B_f^T Q_f B_f + B_f^T N_f + N_f^T B_f + R_f) + \cdots \\ & + (B_f^T Q_f A_f^{n-2} B_f + \cdots \\ & + B_f^T Q_f B_f + B_f^T N_f + N_f^T A_f^{n-2} B_f + \cdots + N_f^T B_f + R_f) \end{aligned} \tag{4.28}$$

$$\begin{aligned} N_s = {} & N_f + (A_f^T Q_f B_f + A_f^T N_f) + (A_f^{T^2} Q_f A_f B_f + A_f^{T^2} Q_f B_f + A_f^{T^2} N_f) + \cdots \\ & + A_f^{T^{n-1}} Q_f A_f^{n-2} B_f + \cdots + A_f^{T^{n-1}} Q_f B_f + A_f^{T^{n-1}} N_f \end{aligned} \tag{4.29}$$

Using Cholesky factorization, we can write

$$\begin{pmatrix} Q_f & N_f \\ N_f^T & R_f \end{pmatrix} = [\ \tilde{C}_{1f} \quad \tilde{D}_{1f}\ ]^T [\ \tilde{C}_{1f} \quad \tilde{D}_{1f}\ ] \tag{4.30}$$

Note that

$$z_k = \tilde{C}_{1f} x_k + \tilde{D}_{1f} u_k$$

is the fictitious signal whose $\|.\|_2$ we seek to minimize.

Observing from our results that for the lifted system, $\tilde{G}_L = L_n G_f L^{-1}$ representing the model between $\underline{z}_k$ and $\underline{u}_k$, we can write,

$$\hat{\tilde{g}}_L(\lambda) = \left[\begin{array}{c|ccc} A_f^n & A_f^{n-1}B_f & A_f^{n-2}B_f & \cdots & B_f \\ \hline \tilde{C}_{1f} & \tilde{D}_{1f} & 0 & \cdots & 0 \\ \tilde{C}_{1f}A_f & \tilde{C}_{1f}B_f & \tilde{D}_{1f} & \cdots & 0 \\ \vdots & \vdots & \vdots & \cdots & \vdots \\ \tilde{C}_{1f}A_f^{n-1} & \tilde{C}_{1f}A_f^{n-2}B_f & \tilde{C}_{1f}A_f^{n-2}B_f & \cdots & \tilde{D}_{1f} \end{array}\right] \tag{4.31}$$

$$= \left[\begin{array}{c|c} A_L & B_L \\ \hline \tilde{C}_{1L} & \tilde{D}_{1L} \end{array}\right] \tag{4.32}$$

Therefore, the equivalent weights in the cost function in the lifted system can be obtained as

$$\begin{pmatrix} Q_L & N_L \\ N_L^T & R_L \end{pmatrix} = [\ \tilde{C}_{1L} \quad \tilde{D}_{1L}\ ]^T [\ \tilde{C}_{1L} \quad \tilde{D}_{1L}\ ] \tag{4.33}$$

where we make use of equations (4.31) and (4.32).

Thus, $Q_L$, $N_L$ and $R_L$ would be $n_s \times n_s$, $n_s \times n$ and $n \times n$ matrices, respectively. From equations (4.27), (4.30) and (4.33), it is easy to see that

$$Q_s = Q_L \tag{4.34}$$

Obtaining $R_L$ from equation (4.33) and adding up all the elements, it can be seen that

$$R_s = \sum_{i=1}^{n}\sum_{j=1}^{n} R_{L_{ij}} \tag{4.35}$$

and similarly, adding up all the columns for each of the rows in $N_L$, we get

$$N_{s_i} = \sum_{j=1}^{n} N_{L_{ij}} \quad i = 1, \cdots, n_s \tag{4.36}$$

■

**Significance**: Given $J_c$, the equivalent single-rate and multirate systems arise in such a way that the states are given the same importance *(which is expected since the states are available at the same rate in both the systems)*. The slow-rate input weights in the SSR system distributes over the lifted inputs in the MR systems such that equation (4.21) is satisfied, while the cross-term weights between the states and inputs in the SSR system translate to those in the MR system as in equation (4.22).

### SISO systems with rational sampling ratios

Here, we consider SISO systems with rational sampling ratio $T_b/T_a = n/m$. For the sake of brevity and without further discussion we state that the result in Theorem 4 applies to the case of rational sampling ratios as well. Proof of this result is similar to that as in the case of integer sampling ratio in Theorem 4.

However, the lifted system defined in equation (4.11) needs to be re-defined for this case as:

$$\tilde{G}_L = \begin{pmatrix} L_l & 0 \\ 0 & L_m S_n H_f \end{pmatrix} \tilde{G}_f \begin{pmatrix} L_l^{-1} & 0 \\ 0 & S_f H_m L_m^{-1} \end{pmatrix} \tag{4.37}$$

where $l$ is the *l.c.m.* of the sampling intervals, $nh$ and $mh$ are the output and input sampling intervals respectively, and the subscript $f$ stands for the fast rate system over the sampling interval $h$.

As a result, $B_L$ in equation (4.12) and $\tilde{D}_{1L}$ in equation (4.33) have to be modified accordingly. For instance, if the output and input sampling intervals are $3h$ and $2h$ respectively, then the modified $B_L$ and $\tilde{D}_{1L}$ are obtained as:

$$B_L = B_L \left[\begin{array}{ccc} 1 & 0 & 0 \\ 1 & 0 & 0 \\ \hline 0 & 1 & 0 \\ 0 & 1 & 0 \\ \hline 0 & 0 & 1 \\ 0 & 0 & 1 \end{array}\right]; \quad \tilde{D}_{1L} \triangleq \tilde{D}_{1L} \left[\begin{array}{ccc} 1 & 0 & 0 \\ 1 & 0 & 0 \\ \hline 0 & 1 & 0 \\ 0 & 1 & 0 \\ \hline 0 & 0 & 1 \\ 0 & 0 & 1 \end{array}\right] \tag{4.38}$$

The relations between the weights in $J_L$ and $J_f$ can be then obtained by substituting the modified $\tilde{D}_{1L}$ from equation (4.38) into equation (4.33).

### MIMO systems

Relations between the weights discussed so far also apply to MIMO systems. In this work, we lift multivariable signals by lifting individual signals and then augmenting them together. Multivariable lifting defined this way is particularly useful for generalizing the SISO case equivalence presented in Theorem 4 to MIMO systems. The weighting matrices in the cost functions are now of different dimensions. Therefore, the relations given in equations (4.20)-(4.22) need some generalization. Consider, for example, a *2-output, 2-input* system, with integer sampling ratio, $n = 2$. Then $R_s$ will be a $(2 \times 2)$ matrix, whereas $R_L$ will be a $(4 \times 4)$ matrix partitioned into 4 sub-blocks as shown below:

$$R_s = \begin{bmatrix} R_{d11} & R_{d12} \\ R_{d21} & R_{d22} \end{bmatrix} \tag{4.39}$$

Here, $R_s$ is the weighting matrix for $[\ u_1(k) \quad u_2(k)\ ]$. On the other hand, $R_L$ is the weighting matrix for $[\underline{u}_1(k) \quad \underline{u}_2(k)]$ :

$$R_L = \left[\begin{array}{cc|cc} R_{L11} & R_{L12} & R_{L13} & R_{L14} \\ R_{L21} & R_{L22} & R_{L23} & R_{L24} \\ \hline R_{L31} & R_{L32} & R_{L33} & R_{L34} \\ R_{L41} & R_{L42} & R_{L43} & R_{L44} \end{array}\right] \tag{4.40}$$

Here, $\underline{u}_i(k)$ represents the $i^{th}$ lifted input at the $k^{th}$ instant. The relation between $R_s$ and $R_L$ is that the sum of the elements in each of the blocks in $R_L$ is equal to the corresponding element in $R_s$. In other words, $R_{s11} = R_{L11} + R_{L12} + R_{L21} + R_{L22}$ and so on. The cross-term weight between the states and lifted inputs $N_L$ can be similarly partitioned into 2 blocks, one for each lifted input. Then, $N_{s11} = N_{L11} + N_{L12}$ and so on. The general result with the assumption that all the inputs are uniformly sampled with sampling interval, $T_a$, and all the outputs are uniformly sampled over one sampling interval, $T_b$, is stated as follows.

**Theorem 5** *Consider a (q-output, p-input) MIMO system $S_bGH_a$, where $G$ is a continuous-time LTI system, and the ratio of sampling intervals $T_b/T_a = n$, a positive integer. Given a continuous-time LQR performance criterion, $J_c$, then for impulse type disturbances, the weights in the equivalent discrete-time SR and MR LQR cost*

*functions are related as follows:*

$$Q_s = Q_L \tag{4.41}$$

$$R_{sij} = \sum_{\text{block } ij} R_{Lij} \tag{4.42}$$

$$N_{sij} = \sum_{\text{block } ij} N_{Lij} \quad i = 1, \cdots, n_s \tag{4.43}$$

*Proof of the above result is not given here for the sake of brevity.*

As in the case of SISO systems, Theorem 5 can be generalized to MIMO systems with rational sampling ratios as well.

Now, we return to the comparison problem. The LQR design problem for the discrete-time systems consists of minimizing the corresponding objective functions subject to the corresponding models. The relations between the weights given in Theorems 4 and 5 are useful to observe the connection between the LQR optimization problems for the MR, SSR and FSR systems. The following remark establishes the link between $J_L$ and $J_s$.

**Remark 6** *Given that both the MR and SSR cost functions are derived from the same $J_c$ (therefore the weights satisfying Theorem 5); then with the constraint that all the fast-rate input moves in a MR system are identical over the sampling period $l$, the MR cost function $J_L$ in equation (4.18) becomes identical to the SSR cost function $J_s$.*

We illustrate this by a simple example for a SISO system. The validity of the above remark for MIMO systems is then a straightforward extension. Consider, for example, a multirate SISO system, with $n = 2$, and a $J_c$ such that we arrive at

$$J_s = \sum_{k=0}^{\infty} (x^2 + u^2 + 2xu) \tag{4.44}$$

Denoting the lifted input by $\underline{u} = [u_1 \;\; u_2]'$, we arrive at

$$J_L = \sum_{k=0}^{\infty} \left( x^2 + [u_1 \; u_2] \begin{pmatrix} 1/4 & 1/4 \\ 1/4 & 1/4 \end{pmatrix} [u_1 \; u_2]' + 2x[1/2 \; 1/2]] u_1 \; u_2]' \right) \tag{4.45}$$

Observe that the relations in Theorem 4 are satisfied. Now, impose the constraint on $J_L$ that $u_1 = u_2$. Then, it is clear after substitution that the constrained $J_L$ is identical to $J_s$.

Note that if the relations between the weights as in Theorem 4 are satisfied, it is not necessary that they should arise from the same $J_c$. In other words, the converse of

Theorem 4 need not necessarily hold good. The above example is to merely illustrate Remark 6.

The following remark relate $J_L$ to $J_f$ for the rational case.

**Remark 7** *Given that both the MR and FSR cost functions are derived from the same $J_c$ (therefore the weights satisfying the relations given in equation (4.33); then with the constraint that all the fast-rate input moves in an FSR system are identical over the input sampling period $mh$, $J_f$ in equation (4.19), the constrained FSR cost function $J_f$ is identical to the MR cost function $J_s$ derived from $J_c$.*

For example, if the output and input sampling intervals are $3h$ and $2h$ respectively, the fast-rate control strategy updates the control moves every $h$ units. If we now restrain that the moves are updated every $2h$ units instead of $h$ units, then we get the lifted MR control strategy (which updates control moves every $2h$ units). This is because the same continuous-time cost function and fast-rate model are used in deriving the individual cost functions and also given the assumption that there is no model-plant mismatch.

**Remark 8** *All the resulting three discrete-time cost functions are convex in nature because of the positive semi-definiteness of the weights.*

Intuitively one would expect that MR systems can outperform SSR systems in terms of optimal closed-loop performance. This is because of the extra degrees of freedom available in MR systems *(e.g. in manipulating u)*. Similarly, one can expect FSR systems to outperform MR systems. In the following section, we present the main results for the state-feedback case; the proof that the optimal performance of MR systems is, in general, better than that of SSR systems and bounded below by that of FSR systems.

## 4.3 Multirate Control vs. Single-Rate Control

### 4.3.1 Regulatory Problem

First, we relate the performances of MR and SSR systems. Using previous results and ideas in optimization, the following result is stated in the LQR framework *(assuming full knowledge of the states)* and no model-plant mismatch.

**Theorem 6** *Consider a closed-loop multirate sampled-data system comprising of a MIMO continuous-time LTI system $G_p$, a sampler $S_h$, and a zero-order hold $H_a$.*

*Given a continuous-time LQR cost function $J_c$ and that $T_b/T_a = n/m$, a rational number, then the optimal performance of multirate systems is bounded above by the optimal performance of slow single-rate systems and below by the optimal performance of fast single-rate systems. In other words, if $J_f$,, $J_L$ and $J_s$ are the cost functions for the FSR, lifted MR and SSR systems respectively, then for impulse type disturbances,*

$$J_{opt,f} \leq J_{opt,L} \leq J_{opt,s} \tag{4.46}$$

*Remarks and Significance:* The proof is relatively straightforward based on results in Section 2. The idea is to show that the class of controllers for the SSR systems belong to a subspace of controllers for the MR systems which themselves belong to a subspace of controllers for the FSR systems. We consider the regulatory problem for impulse type disturbances.

**Proof.**

*Part 1:*

The controller design problem for SSR systems can be stated as:

$$\min J_s \tag{4.47}$$

subject to the model $(A_s, B_s)$ among the class of LTI, causal controllers; and for MR systems as,

$$\min J_L \tag{4.48}$$

subject to the model $(A_L, B_L)$ among the class of LTI, causal controllers.

Next, we impose the constraint on MR systems that all the fast-rate input moves are equal,

$$\underline{u}_1(k) = \underline{u}_2(k) = \cdots = \underline{u}_n(k) \tag{4.49}$$

where $\underline{u}_j(k)$ is the $j^{th}$ component of the lifted signal $\underline{u}$ at the $k^{th}$ instant. Then, the model $(A_L, B_L)$ reduces to $(A_s, B_s)$ and from Remark 6, $J_L$ reduces to $J_s$. Therefore, the objective function in (4.48) takes the form of that in (4.47).

It is well known that the minimum value of a constrained convex cost function cannot be lesser than that of the corresponding unconstrained cost function. Therefore, from Remark 8 and the above observations, the right-hand inequality follows,

$$J_{opt,L} \leq J_{opt,s}$$

*Part 2:*

The proof for the lower bound is as follows.

The controller design problem for FSR systems can be stated as:

$$\min J_f \tag{4.50}$$

subject to the model $(A_f, B_f)$ among the class of LTI, causal controllers.

When the sampling ratio is rational, Remark 7 indicates that $J_L$ is a special case of $J_f$ (*i.e.*, with the constraint of identical control moves over each input sampling interval $mh$). Therefore, based on similar arguments as in Part 1,

$$J_{opt,f} \leq J_{opt,L}$$

■

**Remark 9** *For the integer sampling ratio case, the optimization problems for the FSR and MR systems in (4.50) and (4.48) are identical (no model-plant mismatch and control moves are made at the same fast rate). Hence, the optimal performances of both the systems for the integer case are identical (equality sign).*

The importance of Theorem 6 is that it provides a benchmark for a fair comparison of FSR, MR and SSR systems and establishing the superiority of one system over other on a theoretical basis. Besides, it can illustrate the relative benefits one can achieve with FSR over MR systems or MR over SSR systems with the changes in sampling ratio and the tuning parameters, for example, the input weight $R_c$. Later in Section 4.4, we illustrate this point by means of simulation on an experimental model.

In the next section, we deal with the tracking problem.

### 4.3.2 Servo Problem

Firstly, we convert the given step-tracking servo problem into an equivalent regulatory problem (see Problem 4.3-5, Anderson and Moore (1990)) and then compare the performances for the regulatory problem. Then, these ideas are extended to the class of ramp and sinusoidal signals. The transformation of the servo to regulatory problem is equivalent to augmenting the continuous-time system with the reference model. Thereby, continuous-time tracking is ensured.

#### Step tracking

To ensure step tracking, the continuous-time plant is augmented with the reference model of the step signal, which is an integrator. Thus, the inputs to the augmented

system would be $\dot{u}$ where $u$ is the input to the unaugmented system. The state space model for the augmented plant takes the form:

$$\begin{pmatrix} \dot{x} \\ \dot{u} \end{pmatrix} = \begin{pmatrix} A & B \\ 0 & 0 \end{pmatrix} \begin{pmatrix} x \\ u \end{pmatrix} + \begin{pmatrix} 0 \\ I \end{pmatrix} \dot{u} \qquad y = Cx \tag{4.51}$$

Therefore, the cost function for step tracking is accordingly defined as:

$$J_c = \int_0^\infty \begin{pmatrix} y - \tilde{y} \\ \dot{u} \end{pmatrix}^T \begin{pmatrix} Q_c & 0 \\ 0 & R_c \end{pmatrix} \begin{pmatrix} y - \tilde{y} \\ \dot{u} \end{pmatrix} dt \tag{4.52}$$

where $\tilde{y}$ represents the reference signal. Defining $W = (CA^{-1}B)^{-1}$, and using the following transformation (Anderson and Moore 1990),

$$w = \begin{pmatrix} x - A^{-1}BW\tilde{y} \\ u + W\tilde{y} \end{pmatrix} \tag{4.53}$$

the cost function in (4.52) can be converted to the regulatory cost function:

$$J_c = \int_0^\infty \begin{pmatrix} w \\ \dot{u} \end{pmatrix}^T \begin{pmatrix} \hat{Q}_c & 0 \\ 0 & R_c \end{pmatrix} \begin{pmatrix} w \\ \dot{u} \end{pmatrix} dt \tag{4.54}$$

with the new state-space model as:

$$\dot{w} = \begin{pmatrix} A & B \\ 0 & 0 \end{pmatrix} w + \begin{pmatrix} 0 \\ I \end{pmatrix} \dot{u} \qquad y - \tilde{y} = [\ C \quad 0\ ] w \tag{4.55}$$

In (4.54), $\hat{Q}_c = [\ C \quad 0\ ]^T Q_c [\ C \quad 0\ ]$. Thus, if $w \to 0$, $y \to \tilde{y}$ and tracking is ensured.

The new cost function described in (4.54) along with the state-space model in (4.55) forms a standard LQR problem and the solution is a state-feedback controller relating $\dot{u}$ to $(u, x, \tilde{y})$. Thus, for the step-tracking problem we can derive the corresponding continuous-time LQR cost function as described in (4.54) and its equivalent slow-rate and lifted counterparts. Consequently, a similar result as stated in Theorem 6 holds good for the step-tracking situation as well. In the discussion to follow, we suggest suitable transformations for ramp and sinusoidal signals to arrive at similar results for these types of signals as well.

### Ramp tracking

Since ramp signals have a non-zero constant time-derivative the transformation used in the case of step-signals has to be slightly modified with the inclusion of one more state. Also, now since the plant is augmented with a double integrator, the cost function changes its form to:

$$J_c = \int_0^\infty \begin{pmatrix} y - \tilde{y} \\ \ddot{u} \end{pmatrix}^T \begin{pmatrix} Q_c & 0 \\ 0 & R_c \end{pmatrix} \begin{pmatrix} y - \tilde{y} \\ \ddot{u} \end{pmatrix} dt \tag{4.56}$$

After some suitable manipulations, the required transformation can be arrived at as:

$$w = \begin{pmatrix} x + k_1\tilde{y} + k_2\dot{\tilde{y}} \\ u + k_3\tilde{y} + k_4\dot{\tilde{y}} \\ \dot{u} + k_5\dot{\tilde{y}} \end{pmatrix} \tag{4.57}$$

where the constants $k_i's$ are given as:

$$k_1 = -A^{-1}Bk_3 \tag{4.58}$$

$$k_2 = A^{-1}(k_1 - Bk_4) \tag{4.59}$$

$$k_3 = (CA^{-1}B)^{-1} \tag{4.60}$$

$$k_4 = (CA^{-1}B)^{-1}CA^{-1}k_1 \tag{4.61}$$

$$k_5 = k_3 \tag{4.62}$$

giving rise to the new state-space model:

$$\dot{w} = \begin{pmatrix} A & B & 0 \\ 0 & 0 & I \\ 0 & 0 & 0 \end{pmatrix} w + \begin{pmatrix} 0 \\ 0 \\ I \end{pmatrix} \ddot{u} \qquad y - \tilde{y} = [\ C \ \ 0 \ \ 0\ ]w \tag{4.63}$$

The modified cost function takes the form:

$$J_c = \int_0^\infty \begin{pmatrix} w \\ \ddot{u} \end{pmatrix}^T \begin{pmatrix} \bar{Q}_c & 0 \\ 0 & R_c \end{pmatrix} \begin{pmatrix} w \\ \ddot{u} \end{pmatrix} dt \tag{4.64}$$

where $\bar{Q}_c = [\ C \ \ 0 \ \ 0\ ]^T Q_c [\ C \ \ 0 \ \ 0\ ]$.

Arguing in a similar way as in the case of step-tracking, Theorem 6 can be extended to the ramp tracking problem as well.

### Sinusoidal signals

Finally, we deal with the class of sinusoidal signals. Sinusoidal signals are of special interest since they introduce complex modes in the eigenvalues of the augmented system. It is well-known that complex eigenvalues of continuous-time systems can impose restrictions on the sampling rates in order to retain controllability and observability of their discrete-time MR and SR counterparts.

The Laplace transform of the sinusoid $\sin(\omega t)$ is $\frac{1}{s^2+\omega^2}$ implying we should minimize both the input moves and its second derivative. This suggests the following continuous-time cost function for minimization purposes:

$$J_c = \int_0^\infty \begin{pmatrix} y - \tilde{y} \\ u \\ \ddot{u} \end{pmatrix}^T \begin{pmatrix} Q_c & 0 & 0 \\ 0 & R_{c1} & 0 \\ 0 & 0 & R_{c2} \end{pmatrix} \begin{pmatrix} y - \tilde{y} \\ u \\ \ddot{u} \end{pmatrix} dt \tag{4.65}$$

The transformation and the transformed cost function are of the form:

$$w = \begin{pmatrix} x + k_1\tilde{y} + k_2\dot{\tilde{y}} \\ u + k_3\tilde{y} + k_4\dot{\tilde{y}} \\ \dot{u} + k_5\tilde{y} + k_6\dot{\tilde{y}} \end{pmatrix} \tag{4.66}$$

$$J_c = \int_0^\infty \begin{pmatrix} w \\ u \\ \ddot{u} \end{pmatrix}^T \begin{pmatrix} \tilde{Q}_c & 0 & 0 \\ 0 & R_{c1} & 0 \\ 0 & 0 & R_{c2} \end{pmatrix} \begin{pmatrix} w \\ u \\ \ddot{u} \end{pmatrix} dt \tag{4.67}$$

The constants in equation (4.66) are given as the solution of:

$$\begin{bmatrix} A & -\omega^2 I & B & 0 \\ -I & A & 0 & B \\ C & 0 & 0 & 0 \\ 0 & C & 0 & 0 \end{bmatrix} \begin{bmatrix} k_1 \\ k_2 \\ k_3 \\ k_4 \end{bmatrix} = \begin{bmatrix} 0 \\ 0 \\ -I \\ 0 \end{bmatrix} \tag{4.68}$$

$$k_5 = -\omega^2 k_4 \tag{4.69}$$

$$k_6 = k_3 \tag{4.70}$$

such that the new state-space model takes the shape:

$$\dot{w} = \begin{pmatrix} A & B & 0 \\ 0 & 0 & I \\ 0 & -\omega^2 I & 0 \end{pmatrix} w + \begin{pmatrix} 0 & 0 \\ 0 & 0 \\ \omega^2 I & I \end{pmatrix} \begin{pmatrix} u \\ \ddot{u} \end{pmatrix} \qquad y - \tilde{y} = [\, C \;\; 0 \;\; 0 \,] w \tag{4.71}$$

With the above transformation, it can be observed that MR systems can outperform SR systems at the slow rate in the case of sinusoid-tracking as well.

More generally, the results stated in Theorem 6 can be stated for the servo problem as follows.

**Theorem 7** *Consider a closed-loop multirate sampled-data system comprising a MIMO continuous-time LTI system $G_p$, a sampler $S_b$, and a zero-order hold $H_a$. Given a continuous-time LQR cost function $J_c$ and that $T_b/T_a = n/m$, a rational number, then for tracking the class of step, ramp and sinusoidal signals, the optimal performance of the multirate system is bounded above by the optimal performance of slow single-rate systems and below by the optimal performance of fast single-rate systems.*

Although Theorem 6 focuses on impulse type disturbances, it can be shown with marginal effort that similar arguments hold good for step-type, ramp and sinusoidal class of disturbances as well. This can be shown by appropriately modifying the LQR cost function for these class of signals as well.

From the relations derived in Theorem 5 and equation (4.33), it can be expected that as the input weight, $R_c$ and hence $R_s$, $R_L$ and $R_f \to \infty$, $J_L \to J_s$ and $J_L \to J_f$.

In other words, for very large input weights $R_c$, all the optimal performances of FSR, MR and SSR control systems should be expected to be identical.

In the next section, we illustrate the results for the regulatory problem in accordance with Theorem 6 on an experimental model of a SISO system.

## 4.4 Results on an Experimental Model

The setup is a $(2 \times 2)$ continuously stirred tank heater system in which the level is maintained by manipulating the input valve position. For the present, we are interested in only controlling the level. Disturbances are due to a a sudden change in the outlet flow rate or a sudden change in the level.

The following first-order model describes the relation between the level and inlet flow valve position in the discrete time

$$G_f(z) = \frac{0.1416}{z - 0.9868} \tag{4.72}$$

at the fast-sample period of $h = 4$ seconds.

Define the relative improvement in the closed-loop performance of FSR system (over MR system) and the MR system (over SSR system) as

$$J_{f,rel} = \frac{J_L - J_f}{J_f} \quad ; \quad J_{L,rel} = \frac{J_s - J_L}{J_L} \tag{4.73}$$

First, let us consider the FSR and MR systems. Figure 4.3 shows the relative improvement $J_{f,rel}$ in the fast-rate system over the multirate system as we change two parameters - the input weight $R_c$ and the sampling ratio $n/m$. While $R_c$ varied on a log scale from $10^{-2}$ to $10^3$, the set of sampling ratios $n/m$ were $(1, 5/4, 3/2, 2, 7/3, 8/3, 3, 11/3, 4, 9/2, 19/4, 5)$. The state-weighting $Q_c$ was set to 100.

As Remark 7 indicates, whenever the sampling ratio is an integer, the relative improvement is zero $\forall$ $R_c$, implying identical performances for the FSR and MR systems. In the non-integer case, the plot confirms the result stated in Theorem 6. As we can see, the improvement is not linear in the sampling ratio. In fact, we can see three sets of identical peaks. The identical nature is clear for those sets corresponds to the input sampling intervals $3h$ and $4h$, while the pair corresponding to to $2h$ is somewhat hidden. This point corroborates our arguments in Remark 7 and Theorem 6 that the difference in performances between both these systems is only due to the difference in the input sampling rates.

Now let us turn towards Figure 4.4 which shows the 3-D plot of $J_{L,rel}$ vs. $R_c$ and $n/m$. The plot confirms our observations in Theorem 6. As in the earlier plot, the

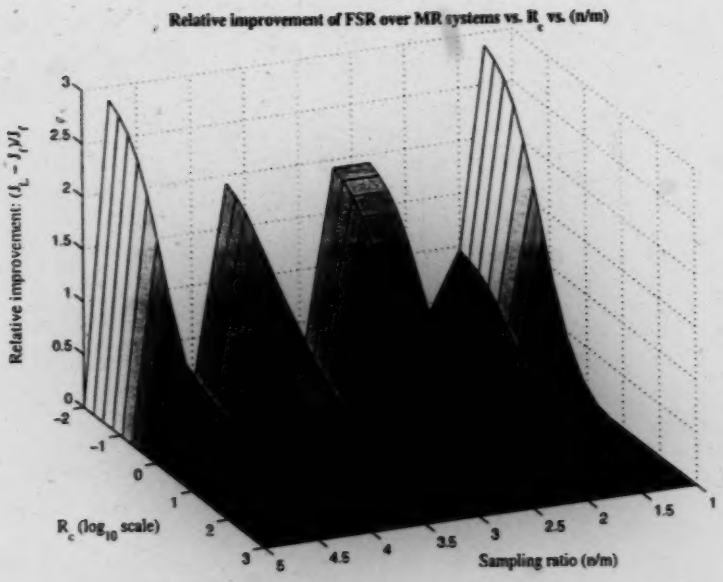


Figure 4.3: *Variation of relative improvement in the closed-loop performance of FSR over MR systems with input weight $R_c$ and sampling ratio $n/m$.*

improvement is not linear in sampling ratio. In fact, the largest peak corresponds to that ratio with the largest *l.c.m.*, which is 68 ($n/m = 19/4$). This is expected as the SSR system operates at the *l.c.m.* of the sampling intervals. Therefore, the improvement can be said to increase as the *l.c.m.* increases. When the sampling ratio is unity, all the systems are identical as confirmed in the plots.

An important observation to note is that as the input weight $R_c$ becomes very large, all the three systems give identical performances. As mentioned earlier, this is due to the fact that the corresponding input weights also become very large rendering all the input moves highly damped. Then, although the inputs are made at the fast rate, the magnitude is considerably small making the controller very sluggish. In other words, the extra degrees of freedom available with the FSR and MR system are curbed to such an extent that they behave like a SSR system. Theoretically speaking, as $R_c \rightarrow \infty$, the optimal controller gains for each of these systems become identical and hence the optimal performances also tend to be identical.

So far, we have assumed that all the states are accessible for the LQR problem. Under these conditions, we proved that FSR systems give a lower bound for the optimal performance of MR systems which in turn gives a lower bound for that of SSR systems.

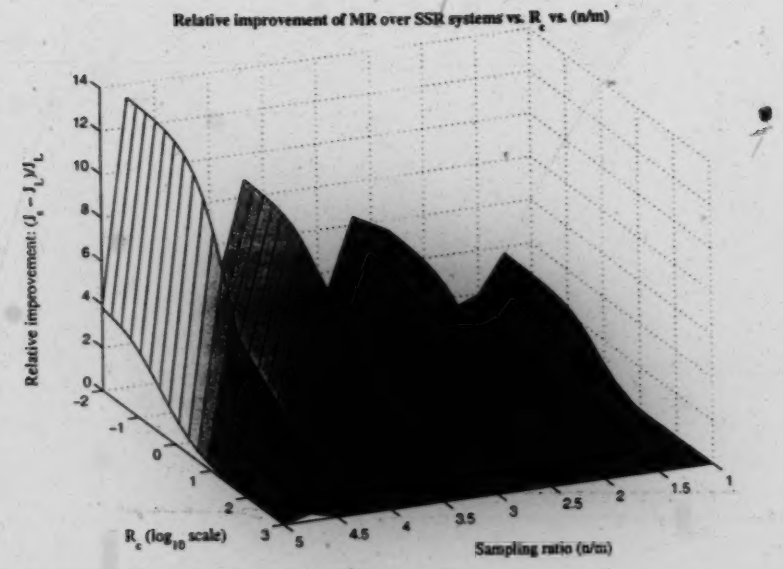


Figure 4.4: *Variation of relative improvement in the closed-loop performance of MR over SSR systems with input weight $R_c$ and sampling ratio $n/m$.*

In the next section, we impose a practical restriction that the states are not available and hence include the state estimation problem. However, we only compare the performances of MR and SSR systems. The reason for such a choice is that with the approach presented below, the comparison of FSR and MR systems is more complex than the problem of comparing MR and SSR systems.

## 4.5 A Step Further: Output Feedback Control

Here, we choose the sampled-data (SD) setup to represent MR and SSR systems. The continuous-time generalized $\mathcal{H}_2$-norm for SD systems (Bamieh and Pearson 1992, Khargonekar and Sivashankar 1992) is proposed as a benchmark. The main result is a proof that the superiority of MR systems over SSR systems in the state-feedback case holds for the output feedback case as well. The proof is constructed using lifting techniques and optimization ideas.

The design problem for SR SD systems is well known (Levis *et al.* 1971, Chen and Francis 1991*b*, Bamieh and Pearson 1992, Khargonekar and Sivashankar 1992) and for dual-rate SD systems (Chen and Francis 1991*a*). Optimal design of multirate SD systems has also been widely addressed (Araki and Yamamoto 1986, Voulgaris and Bamieh 1993, Chen and Qiu 1994, Chen and Francis 1995, Qiu and Chen 1995, Sagfors

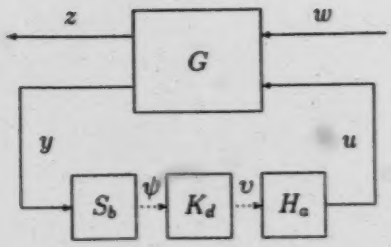


Figure 4.5: *A general sampled-data system*

and Toivonen 1998). The novelty in this work is the comparison problem.

The main result is arrived at by showing that the set of optimal, causal and FDLTI controllers for SSR systems is a subset of the optimal, causal and FDLTI controllers for the lifted MR systems.

The choice of sampled-data setup is due to a few important reasons. SD systems allow us to obtain the benefits of digital technology while taking into account the continuous-time performance and design specifications. Besides, many practical situations give rise to sampled-data systems. Another relevant factor is that both multirate and single-rate systems can be conveniently viewed as special cases of sampled-data (SD) systems.

A typical sampled-data system as shown in Figure 4.5 consists of a continuous-time plant, $G$, coupled with a digital controller, $K_d$. As a combination, $H_a K_d S_b$ quantize a continuous-time signal $y$, process that digital signal $\psi$ using a digital computer or based on a discrete-time control law, and then convert the resulting digital signal $v$ back into a continuous-time one, $u$. A few references for good reading are Ragaziini and Franklin (1958), Åström and Wittenmark (1984) and Chen and Francis (1995).

Moving from state-feedback control to output feedback control involves the state estimation problem is well known. It seems obvious at this stage that LQG schemes would be the immediate choice for this situation. However, we deviate here and pose the comparison problem in the $\mathcal{H}_2$ setup. Due to the periodic and hybrid nature of SD systems, the continuous-time generalized $\mathcal{H}_2$-norm defined for SD systems (Bamieh and Pearson 1992, Khargonekar and Sivashankar 1992) appears more appropriate as a benchmark than the $\mathcal{H}_2$-norm or the classical LQG cost function. This choice accounts for the entire sampling period over which both MR and SSR systems are periodic, instead of merely looking at the initial time $t = 0$. Besides, $\mathcal{H}_2$ is a more general case and encompasses the LQG scheme as well. The additional benefit is that the state estimation problem is easily integrated into the comparison problem than

in the LQG framework.

In Figure 4.5, assume $G$ is FDLTI, causal with a state-space model:

$$\hat{g}(s) = \left[\begin{array}{c|cc} A & B_1 & B_2 \\ \hline C_1 & 0 & D_{12} \\ C_2 & 0 & 0 \end{array}\right] \tag{4.74}$$

Note that we have taken $D_{11}$ and $D_{21}$ as zero to ensure finiteness of the $\mathcal{H}_2$ norm and for the reason that $S$ is not defined on impulsive functions.

The generalized $\mathcal{H}_2$ measure (Bamieh and Pearson 1992, Khargonekar and Sivashankar 1992) for an $h$-periodic SD system is given as,

$$J = \left(\int_0^h J_\tau^2 d\tau\right)^{1/2} \tag{4.75}$$

where

$$J_\tau = \left(\sum_i \|T_{zw}\delta_\tau e_i\|_2^2\right)^{1/2} \tag{4.76}$$

with $\delta_\tau = \delta(t-\tau)$ and $e_i$ $(i = 1, \cdots, m)$ are the $m$ unit basis vectors in $R^m$. Note that the quantity $\bar{J} = J/\sqrt{h}$ can be interpreted as the root-mean square of $J_\tau$. We shall use this normalized performance index rather than simply $J$ itself.

The generalized performance spec defined above is very useful when the time of applying the input is unknown. This is a practical situation as the input can enter at any instant in the interval over which the SD system is periodic.

The controller design methodology employed here is similar to that of Voulgaris and Bamieh (1993) in their work on hybrid multirate systems. The methodology involves continuous lifting of exogenous signal and the controlled signal, and discrete lifting of input/output signals. Continuous lifting results in a system with infinite input/output spaces. To find a solution, this infinite-dimensional system is associated with a finite-dimensional system. In Voulgaris and Bamieh (1993), a solution is given to this optimal generalized $\mathcal{H}_2$ control problem. These results are directly imported here to prove the final result.

The following section gives the main result for the output feedback case. The novelty in the main result is the theoretical establishment of the superiority of MR control systems over SSR control systems in the absence of model-plant mismatch.

Problem formulation is done in the state-space domain. The notation followed here is standard. Discrete lifting with a factor $n$ is denoted as $L_n$, while continuous lifting with a period $nh$ is denoted as $W_{nh}$. All lifted signals and systems shall be denoted by an underline; for example, a fast rate signal $v$ upon lifting becomes $\underline{v}$.

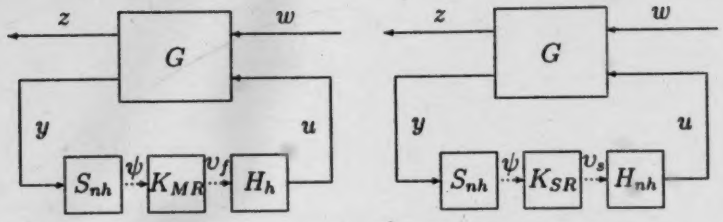


*(a) MR sampled-data system* *(b) Associated SSR sampled-data system*

Figure 4.6: *MR system with integer sampling ratio and its associated SSR system*

Subscripts on the sampler and zero-order hold indicate their period of operation; for instance, $S_h$ is a sampler with period $h$.

### 4.5.1 Main Result: Performance Comparison

In Figures 4.6(a) and 4.6(b) are shown the corresponding MR system with integer sampling ratio and the associated SSR system, respectively. Blocks $S_{nh}$ and $H_{nh}$ are the slow sampler and zero-order hold, respectively, while block $H_h$ takes the place of a fast-rate zero-order hold. The multirate controller is represented by $K_{MR}$ while the corresponding slow single-rate controller is represented by $K_{SR}$. It is assumed that $G$ is a continuous-time, FDLTI, causal, MIMO system. The subscripts $f$ and $s$ on $v$ refer to the fast and slow rate signals, respectively.

For the sake of simplicity, initially a proof for the case of integer sampling ratio is given with the aid of Figures 4.6(a) through 4.7. The proof for the rational case is then briefly sketched on similar lines as the integer case. The following result (Bamieh and Pearson 1992, Khargonekar and Sivashankar 1992, Voulgaris and Bamieh 1993, Chen and Francis 1995) is useful for later analysis.

**Remark 10** *The optimal performances of the MR and SSR systems shown in Figure 4.6 are identical to those of shown in Figure 4.8.*

**Theorem 8** *For the SD system shown in Figure 4.5, choose a continuous-time generalized $\mathcal{H}_2$ cost function as in equation (4.75) with period $nh$. Then, in general, the optimal performance of the MR system is better than the optimal performance of the associated single-rate system at the slow rate and in the worst case, identical to that*

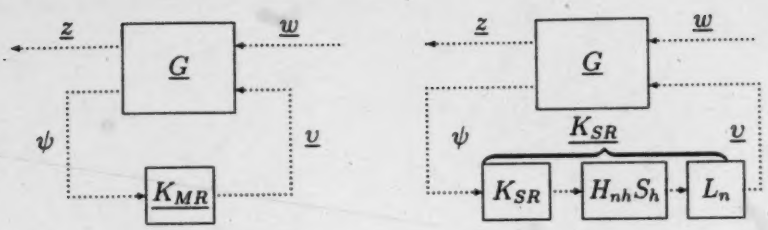


*(a) Lifted MR system* *(b) Lifted SSR system*

Figure 4.7: *Introducing lifting operators in the fast-rate channels of MR and SSR systems*

*of the SSR system. Equivalently,*

$$\textit{Optimal } \|\hat{t}^{MR}_{\zeta\omega}\|_2 \leq \textit{Optimal } \|\hat{t}^{SSR}_{\zeta\omega}\|_2 \tag{4.77}$$

*where $\hat{t}^{MR}_{\zeta\omega}$ and $\hat{t}^{SSR}_{\zeta\omega}$ are the transfer functions from $\omega$ to $\zeta$ for the MR and SSR SD systems shown in Figure 4.8.*

**Proof.** Initially, assume that the sampling ratio is an integer, $n$.

Starting with Figures 4.6(a) and 4.6(b), notice that both are $nh$-periodic system ($h$ is the fast sampling interval). The set of admissible controllers for the MR system are linear, $nh$-periodic meaning $K_{MR}U = U^n K_{MR}$ ($U$ is the time delay operator over $h$) and causal; while for the SSR system, the admissible controllers are linear, time-invariant and causal.

For the SSR system, we can write the output of the slow-rate zero order hold as $H_h S_h H_{nh}$. Then, continuously lift $z$ and $w$ with a period $nh$, and discretely lift the outputs of the fast-rate samplers in both the systems. With this step, we obtain the configurations shown in Figure 4.7.

The hybrid lifted system $\underline{G}$ and the controllers in Figure 4.7 are defined as,

$$\begin{aligned} \underline{G} &= \begin{bmatrix} W_{nh} & 0 \\ 0 & S_{nh} \end{bmatrix} G \begin{bmatrix} W_{nh}^{-1} & 0 \\ 0 & H_h L_n^{-1} \end{bmatrix} \\ \underline{K_{MR}} &= L_n K_{MR} \\ \underline{K_{SR}} &= L_n S_h H_{nh} K_{SR} \end{aligned} \tag{4.78}$$

The resulting system is infinite-dimensional due to the presence of continuous lifting operators. Hence, we need one more step before proving the main result. This final step is to associate this resulting system with a finite-dimensional system. Details of this step and a controller design procedure for the associate finite-dimensional LTI

system are provided in Voulgaris and Bamieh (1993), Figure 4.8 shows the resulting SD setup where the FDLTI lifted system is represented as $\underline{\tilde{G}}$ and the exogenous signals are now represented as $\underline{\zeta}$ and $\underline{\omega}$. The associated FDLTI system is arrived at by ensuring that the resulting finite-dimensional SD system will have the same $\mathcal{H}_2$-norm as the infinite-dimensional one.

Denoting $J_{MR} = \|\hat{t}_{\zeta\omega}^{MR}\|_2^2$ and $J_{SSR} = \|\hat{t}_{\zeta\omega}^{SSR}\|_2^2$, the optimal performances for the individual systems in Figure 4.8 can be written as,

$$J_{MR}^{\bullet} = \min_{\underline{K_{MR}}} \|\hat{t}_{\zeta\omega}^{MR}\|_2^2 \quad J_{SSR}^{\bullet} = \min_{\underline{K_{SR}}} \|\hat{t}_{\zeta\omega}^{SSR}\|_2^2$$

Observe that by performing the $\mathcal{H}_2$ equivalent discretization, we have ensured equivalence between both the cost functions.

The key point to note is that,

$$\underline{K_{MR}} = \begin{bmatrix} K_1 \\ K_2 \\ \vdots \\ K_n \end{bmatrix} \; ; \; \underline{K_{SR}} = \begin{bmatrix} I \\ I \\ \vdots \\ I \end{bmatrix} K_{SR} \tag{4.79}$$

In arriving at equation (4.79), we have made use of equation (4.78) and the relation (Chen and Francis 1995),

$$L_n S_h H_{nh} = \begin{bmatrix} I \\ I \\ \vdots \\ I \end{bmatrix}$$

Therefore, $\underline{K_{SR}}$ is a special case of $\underline{K_{MR}}$

$$\Longrightarrow J_{MR}^{\bullet} \leq J_{SSR}^{\bullet}$$

For the rational case, assume sampling intervals $2h$ and $3h$ for the hold and sampler, respectively. Then, the *g.c.d.* and *l.c.m.* of the sampling intervals are $h$ and $6h$, respectively. As in the integer case, introduce fast-rate (at $h$) samplers and hold in the measurement and output channels of both systems. Following this, discrete lifting is done by a factor of 6 and continuous lifting at the period of $6h$. The infinite-dimensional lifted system and the lifted controllers for both systems can be written as:

$$\underline{G} = \begin{bmatrix} W_{6h} & 0 \\ 0 & L_6 S_h \end{bmatrix} G \begin{bmatrix} W_{6h}^{-1} & 0 \\ 0 & H_h L_6^{-1} \end{bmatrix}$$

$$\underline{K_{MR}} = L_6 S_h H_{2h} K_{MR} S_{3h} H_h L_6^{-1} \tag{4.80}$$

$$\underline{K_{SR}} = L_6 S_h H_{6h} K_{SR} S_{6h} H_h L_6^{-1} \tag{4.81}$$

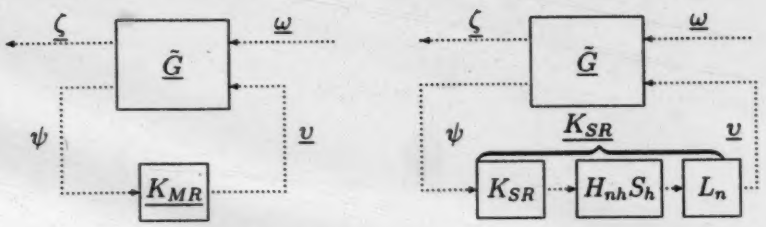


*(a) Lifted MR system* *(b) Lifted SSR system*

Figure 4.8: *Associated finite-dimensional systems for the lifted MR and SSR control systems*

The associated finite-dimensional system can be found in similar ways as earlier. Using properties of lifting, $\underline{K_{SR}}$ can be easily simplified to:

$$\underline{K_{SR}} = \begin{bmatrix} K_{SR} & 0 & \cdots & 0 \\ K_{SR} & 0 & \cdots & 0 \\ \vdots & \vdots & \vdots & \vdots \\ K_{SR} & 0 & \cdots & 0 \end{bmatrix}_{6\times 6} \tag{4.82}$$

For the MR system, we can write:

$$\begin{aligned} \underline{K_{MR}} &= L_6 S_h H_{2h} K_{MR} S_{3h} H_h L_6^{-1} \\ &= L_6 S_h H_{2h} L_3^{-1} L_3 K_{MR} L_2^{-1} L_2 S_{3h} H_h L_6^{-1} \\ &= \begin{bmatrix} K_{11} & 0 & 0 & K_{12} & 0 & 0 \\ K_{11} & 0 & 0 & K_{12} & 0 & 0 \\ K_{21} & 0 & 0 & K_{22} & 0 & 0 \\ K_{21} & 0 & 0 & K_{22} & 0 & 0 \\ K_{31} & 0 & 0 & K_{32} & 0 & 0 \\ K_{31} & 0 & 0 & K_{32} & 0 & 0 \end{bmatrix} \end{aligned} \tag{4.83}$$

where we have assumed a causal LTI controller:

$$L_3 K_{MR} L_2^{-1} = \begin{bmatrix} K_{11} & K_{12} \\ K_{21} & K_{22} \\ K_{31} & K_{32} \end{bmatrix}$$

Looking at equations (4.83) and (4.82), it can be clearly inferred that $\underline{K_{SR}}$ is a special case of $\underline{K_{MR}}$. Hence,

$$\Longrightarrow J^*_{MR} \leq J^*_{SSR}$$

■

The equality sign occurs when the optimal performances are identical, or equivalently, when the optimization problems yield the same controller. Also, heavy input

weighting can dampen the extra degrees of freedom that are possessed by the MR and FSR systems. As a result, both the systems start to behave like the SSR system. In essence, the equality sign comes into play when the weighting on the inputs goes to infinity. Although in chemical processes weighting on the inputs are necessary, such large weighting factors on input weights are rare as it practically implies an open-loop situation. Similar arguments hold for the rational case as well. Therefore, it can be concluded without much loss of generality that MR systems yield better performance than the associated SSR systems.

## 4.6 Conclusions and Summary

In this chapter, we have addressed the performance comparison problem for the multirate and the associated slow and fast single-rate systems from a theoretical point of view which has been so far considered on the basis of simulations.

By means of theoretical analysis and the equivalence between the derived MR and SR discrete-time cost functions, we have proved the fundamental result that with state feedback control and for impulse type disturbances, FSR systems provide a lower bound for the optimal performance of MR systems which in turn are bounded above by the optimal performance of SSR systems. In addition, for the output-feedback case (stochastic case), we have shown that with the continuous-time generalized $\mathcal{H}_2$-norm as the benchmark, MR systems perform better than the associated SSR systems in absence of model-plant mismatch. They yield identical performance, in the presence of large input weights. In practice, the input weights $R_c$ can be relatively small, implying that for all practical purposes, MR systems indeed perform better than SSR systems and FSR systems perform better than MR systems.

The results of this chapter provide upper and lower bounds on the quadratic cost function for MR systems. In case of large input weights, we show that $J_L \simeq J_s$, however, with small input weights, the results show a definite advantage on implementing MR control. In our opinion, these are theoretical results of great interest with practical appeal and not necessarily obvious. Finally, our analysis gives a picture of the extra benefits one can achieve by implementing MR control over SSR control depending on the input weights and the sampling ratio.

With marginal effort, results in this work can be shown to hold good even when each of the inputs and outputs sampling rates are distinct. Also, since step-type disturbances can be transformed into impulse-types by means of suitable transformations, the results need not necessarily be restricted to the class of impulse-type disturbances only.

## 4.7 Journey Ahead

With the provision of a new benchmark for comparing the performances of FSR, MR and SSR systems, it is important to explore the doorways to other possible benchmarks for this cause. This is in itself a non-trivial problem.

Future work consists of:

- Comparing FSR and MR systems in the output feedback case.
- Analyzing the output feedback problem in the $\mathcal{H}_\infty$ setup.
- Considering the presence of model-plant mismatch. The measure $J_{rel}$ is sensitive to the model parameters in $G$ or $G_f$. Thus, it is both of practical importance and challenging to perform a robustness analysis on the relative improvement in the closed-loop performance of MR systems. Such a robustness analysis of the performance comparison problem is more difficult and challenging than the comparison problem discussed so far.

# Chapter 5

# Robustness Analysis of the Performance Comparison Problem

**Purpose:** To analyze and assess the superiority of fast single-rate (FSR) over multi-rate (MR) control systems and MR over slow single-rate (SSR) control systems using LQR control in presence of model-plant mismatch.

## 5.1 Motivation

In the previous chapter, it was shown that the performance of FSR systems is, in general, better than that of MR systems which is in turn better than that of the SSR systems. This is true provided the design is based on a continuous-time LQR cost function and there is no model-plant mismatch. However, what is of practical interest is the performance comparison in the presence of a model-plant mismatch. Then, the natural question to consider is: does the fast-rate control strategy (that is if there was a scope for sampling the measurements at the same fast rate as the inputs) always give a better performance than the multirate strategy (where the measurements are usually sampled at a slower rate than the inputs)? Or, is the performance of MR control systems always better than that of SSR systems in the presence of model-plant mismatch? In this chapter, we tread this path. Our objective is to gain an insight into the comparison problem in the presence of mismatch; check for those uncertainty regions where the superiority of one over another does not hold and finally, arrive at analytical expressions (if possible) for these uncertainty regions in terms of known model and design parameters.

It is a commonly held belief that faster sampling rates can yield better performance. On the other hand, it is also widely known that faster sampling rates can push the zeros of discrete system outside the unit circle (cf Åström *et al.* (1984)),

which means non-minimum phase zeros. That non-minimum phase zeros pose limitations on the closed-loop performance of LTI systems is a well known and widely addressed issue. However, it has been shown that with the aid of periodic digital controllers, one can arbitrarily increase the gain margin especially for unstable plants (Francis and Georgiou 1988). Additionally, periodic control allows for the possibility of relocating the non-minimum phase zeros (Khargonekar *et al.* 1985, Lee *et al.* 1987). These results lead us to believe the possibility of improving closed-loop performance using multirate control instead of single-rate control.

With the advances in digital technology and the theories for multirate systems, it is interesting and challenging to analyze performance benefits with multirate sampling especially when we desire to make fast control moves at the expense of sampling the outputs at a faster rate. From a practical point of view, it is necessary to understand whether a benefit is achieved by moving from MR to fast-rate systems given the presence of model uncertainties. On similar grounds, it is important to know whether we can achieve any benefit when we opt for MR control rather than SSR control in the presence of uncertainties. This is indeed an open problem and demands a rigorous analysis.

This work is partly motivated by some interesting results on the superiority of multirate inferential schemes over fast-rate single-rate schemes in the context of robust stability by Li *et al.* (2000*a*).

We consider only parametric uncertainties here. This is a preliminary analysis that is helpful in providing an initial insight into the robustness problem. The novelty in this work lies in the fact that we show that slower output sampling rates can be beneficial from a performance point of view when it is intended to make control moves at the fast rate in the presence of model uncertainty.

To carry out this analysis we require two pieces of information: (1) a benchmark for evaluation, and (2) an uncertainty structure. Here, we use the continuous-time LQR cost function as a benchmark and employ a simple parametric additive uncertainty representation. To arrive at a general analytical result and make conclusions for MIMO systems is a difficult task and beyond the scope of the discussion. Therefore, in this thesis, we consider only a first-order SISO system. Parametric uncertainties are introduced in the gain and pole parameters.

## 5.2 Robustness Analysis

In order to assess the robustness, we obtain expressions for the difference in the LQR cost functions for the fast-rate and MR systems in terms of the model uncertainty. We

will compare the robustness of these two systems for both performance and stability.

The notation in the following sections has its usual meaning. However, since we consider only first-order SISO systems, all matrices are treated as scalars, *i.e.*, the uncertain continuous-time state space model is represented as $(a, b, c, d)$. Estimated parameters are denoted with a hat; for example, an estimated pole is represented as $\hat{a}$ whereas the corresponding uncertain pole is $a$.

### 5.2.1 FSR systems vs. MR systems

In order to design a controller using the LQR technique, two items are essential: *(i)* the input and state weights, and *(ii)* a state-space model of the plant. Following the approach in Chapter 4, we start from continuous-time LQR cost function and then obtain equivalent discrete lifted multirate and single-rate cost functions. The following cost-functions are then equivalent:

$$J_c = \int_0^\infty (x^T q_c x + u^T r_c u) dt \tag{5.1}$$

$$J_L = \sum_{l=0}^{\infty} (x_l^T q_L x_l + \underline{u}_l^T r_L \underline{u}_l + 2x_l^T n_L \underline{u}_l) \tag{5.2}$$

$$J_f = \sum_{k=0}^{\infty} (x_k^T q_f x_k + u_k^T r_f u_k + 2x_k^T n_f u_k) \tag{5.3}$$

where the weights in equations (5.2) and (5.3) are obtained using results obtained in Section 4.2.2.

The objectives of the LQR problems are:

$$\min_{k_L} J_L \quad \text{s.t.} \quad x_{l+1} = \hat{a}_L x_l + \hat{b}_L \underline{u}_l \tag{5.4}$$

$$\min_{k_f} J_f \quad \text{s.t.} \quad x_{k+1} = \hat{a}_f x_k + \hat{b}_f u_k \tag{5.5}$$

#### Integer sampling ratio

We have already observed that for integer sampling ratios, (5.4) and (5.5) yield identical optimal performance indices in absence of model plant-mismatch. This is natural since the lifted model consists of lumping together the intermediate states over the slow-sampled interval using the fast-rate model.

Assume $d = \hat{d} = 0$ and that the sampling ratio is an integer, $n$. The state-feedback control law for the MR and SFR systems yields:

$$x_{l+1} = (a_L - b_L k_L) x_l \quad (\text{denote } \gamma_L = (a_L - b_L k_L)) \tag{5.6}$$

$$x_{k+1} = (a_f - b_f k_f) x_k \quad (\text{denote } \gamma_f = (a_f - b_f k_f)) \tag{5.7}$$

Therefore, the achieved cost function (obtained by implementing the control law on the plant) equals the estimated (optimal) cost functions:

$$J_L = x_0^T(\sum_{l=0}^{\infty} \hat{\gamma}_L^{l^T} w_L \hat{\gamma}_L^l)x_0 \quad \text{and} \quad J_f = x_0^T(\sum_{k=0}^{\infty} \hat{\gamma}_f^{k^T} w_f \hat{\gamma}_f^k)x_0 \tag{5.8}$$

where

$$w_L = (q_L + k_L^T r_L k_L - 2n_L k_L) \quad ; \quad w_f = (q_f + k_f^T r_f k_f - 2n_f k_f) \tag{5.9}$$

In the absence of model-plant mismatch, from the previous section it is known that $J_L = J_f$. Hence, it can be shown that over a period of $nh$, the corresponding terms in (5.2) and (5.3) are identical. This is explained as follows. Assuming $x_0 = 1$, $w_L$ is the cost incurred for the lifted system during the first $nh$ period (by putting $l = 0$ in (5.2)) and $w_f + \hat{\gamma}_f^T w_f \hat{\gamma}_f$ (by putting $k = 1$ in (5.3) and model equals plant) is the cost incurred for the FSR systems during the first $nh$ period. Then,

$$\begin{aligned} w_L &= w_f + \hat{\gamma}_f^T w_f \hat{\gamma}_f + \cdots + \hat{\gamma}_f^{T(n-1)} w_f \hat{\gamma}_f^{(n-1)} \\ &= w_f \underbrace{(1 + \hat{\gamma}_f^2 + \cdots + \hat{\gamma}_f^{2(n-1)})}_{\alpha} \end{aligned} \tag{5.10}$$

However, with the introduction of model-plant mismatch, the achieved cost functions given in (5.8) differ from their designed optimal ones and also from each other. We first consider those class of plants due to a mismatch in the parameter $\hat{b}_f$, i.e., $b_f = \hat{b}_f + \Delta b$. All other parameters are fixed.

## Mismatch in the gain parameter:

For a first-order SISO system, the difference in the achieved cost functions $\Delta J = J_f - J_L$, can be written as:

$$\begin{aligned} \Delta J = J_f - J_L &= \frac{w_f}{1 - \gamma_f^2} - \frac{w_L}{1 - \gamma_L^2} \\ &= \frac{w_f}{(1 - \gamma_f^2)(1 - \gamma_L^2)}[(1 - \gamma_L^2) - \alpha(1 - \gamma_f^2)] \end{aligned} \tag{5.11}$$

where (5.11) is obtained by using (5.10). From the definition of $\gamma_f$,

$$\gamma_f = a_f - b_f k_f = \hat{a}_f - \hat{b}_f k_f - (\Delta b) k_f = \hat{\gamma}_f - (\Delta b) k_f \tag{5.12}$$

From the equivalence of the cost functions for the nominal plant, the controllers $k_f$ and $k_L$ can be related as,

$$k_L = [\ 1 \quad \hat{\gamma}_f \quad \cdots \quad \hat{\gamma}_f^{n-1}\ ]^T k_f \tag{5.13}$$

Further define $\mathbf{A} = [\ a_f^{n-1}\ \ a_f^{n-2}\ \ \cdots\ \ 1\ ]^T$ and $\mathbf{\Gamma} = [\ 1\ \ \hat{\gamma}_f\ \ \cdots\ \ \hat{\gamma}_f^{n-1}\ ]^T$. With equation (5.13) we can write,

$$\gamma_L = a_L - b_L k_L = \hat{a}_L - \mathbf{A}^T b_f \mathbf{\Gamma} k_f = \hat{a}_L - \beta(\hat{b}_f + \triangle b) = \hat{\gamma}_L - \beta(\triangle b) \tag{5.14}$$

where $\beta = \mathbf{A}^T \mathbf{\Gamma} k_f$ is a scalar. Also, using equation (5.13), it can be shown that

$$\hat{\gamma}_L = \hat{\gamma}_f^n \tag{5.15}$$

From equation (5.11), we can translate the condition,

$$\triangle J \geq 0 \Longleftrightarrow (1 - \gamma_L^2) - \alpha(1 - \gamma_f^2) \geq 0 \tag{5.16}$$

Substituting equation (5.15) into equation (5.14) and using equation (5.12) in equation (5.16), we obtain a quadratic inequality in terms of $\triangle b$,

$$p(\triangle b)^2 + 2q(\triangle b) \geq 0 \tag{5.17}$$

where $p$, and $q$ are known quantities, expressed as,

$$p = (\alpha k_f^2 - \beta^2); \quad q = (\beta \hat{\gamma}_f^n - \alpha k_f \hat{\gamma}_f) \tag{5.18}$$

Let us carefully look at the solution of the above quadratic problem, *i.e.*, the situation when the performances of both the systems are identical. Firstly, it is clear that when $\triangle b = 0$, $\triangle J = 0\ \forall\ n,\ k_f$. However, it is interesting to notice that a non-zero value of $\triangle b$ can also yield $\triangle J = 0$. This means that in presence of a model-plant mismatch, sampling the output signal at a slower rate can yield the same performance as when the output signal is sampled at a faster rate. In fact, four cases arise depending on the values of $p$ and $q$, which in turn depend on the sampling ratio $n$ and feedback gain $k_f$:

1. If $p$ and $q \neq 0$, then $\triangle J = 0 \Longleftrightarrow \quad \triangle b = 0$ or $\triangle b = -\dfrac{2q}{p}$
2. If $p = 0$, then $\triangle J = 0 \Longleftrightarrow \quad \triangle b = 0$
3. If $q = 0$, then $\triangle J = 0 \Longleftrightarrow \quad \triangle b = 0$

It can be easily shown that the case when $p = 0,\ q = 0$ does not arise because there is no solution satisfying these conditions. For the second and third cases, it is not possible to arrive at explicit solutions in terms of $n$ and $k_f$. Therefore, they would have to be numerically computed. However, our primary interest is the first case. Given $n$ and $k_f$, the value of $\triangle b$ is computable from equation (5.17) as:

$$\triangle b = -\frac{2q}{p} = 2\left(\frac{\alpha k_f \hat{\gamma}_f - \beta \hat{\gamma}_f^n}{\alpha k_f^2 - \beta^2}\right) = \theta_2 \ \text{(say)} \tag{5.19}$$

It is clear that the roots of equation (5.17) are real $\forall\ Q_c, R_c, n$. Therefore, we can conclude that in situations excepting cases 2 and 3 discussed above, the superiority of FSR systems over MR systems holds iff,

$$\min(0, \theta_2) < \Delta b < \max(0, \theta_2) \tag{5.20}$$

To summarize, we are able to give expressions for those intervals of uncertainty where MR systems can perform better than FSR systems, in terms of model and design parameters. Next, we consider the case of pole mismatch with all other parameters fixed.

## Mismatch in the pole parameter:

Consider the class of plants arising when $a_f = \hat{a}_f - (1-\epsilon)\hat{a}_f$, where $\epsilon \in \mathcal{R}$, the set of real numbers. Then,

$$\gamma_f = a_f - b_f k_f = \hat{\gamma}_f - (1-\epsilon)\hat{a}_f \tag{5.21}$$

and

$$\gamma_L = \epsilon^n \hat{a}_f^n - \left[\ \epsilon^{n-1}\hat{a}_f^{n-1} \quad \epsilon^{n-2}\hat{a}_f^{n-2} \quad \cdots \quad 1\ \right] \hat{b}_f k_f \tag{5.22}$$

Equation (5.22) can be in fact rearranged to give,

$$\begin{aligned}
\gamma_L &= \hat{\gamma}_L - \left[\ \hat{a}_f^n \quad \cdots \quad \hat{a}_f\ \right] \underbrace{\begin{bmatrix} -(\epsilon^n - 1) & 0 & \cdots & \cdots \\ 0 & (\epsilon^{n-1} - 1) & 0 & \vdots \\ \vdots & \vdots & \ddots & \vdots \\ \cdots & \cdots & 0 & (\epsilon - 1) \end{bmatrix}}_{\mathbf{E}} \hat{b}_f \mathbf{\Gamma} k_f \\
&= \hat{\gamma}_L - \hat{a}_f \mathbf{A}^T \mathbf{E} \hat{b}_f \mathbf{\Gamma} k_f \\
&= \hat{\gamma}_L - f(\epsilon)\hat{a}_f \\
&= \hat{\gamma}_f^n - (1-\epsilon)g(\epsilon)\hat{a}_f
\end{aligned} \tag{5.23}$$

where $g(\epsilon)$ is a polynomial in $\epsilon$ of order $(n-1)$ such that $g(1) \neq 0$. The last equation is a result of the fact that $f(\epsilon) = 0$ iff $\epsilon = 1$.

Recalling equation (5.16), we again consider the situation when $\Delta J = 0$. This can happen only when $(1-\gamma_L^2) - \alpha(1-\gamma_f^2) = 0$. Using equations (5.21) and (5.22), we can write this condition as:

$$(1-\gamma_L^2) - \alpha(1-\gamma_f^2) = F(\epsilon) = (1-\epsilon)^2\hat{a}_f^2(\alpha - g^2(\epsilon)) + 2(1-\epsilon)\hat{a}_f(\hat{\gamma}_f^n g(\epsilon) - \alpha\hat{\gamma}_f) = 0 \tag{5.24}$$

From equation (5.24), as expected, it is clear that $\epsilon = 1$ is a root of $F(\epsilon) = 0$. Moreover, as observed in the earlier case of mismatch in $b$, in this case too there exist

values of $\epsilon$ different from unity that yield identical performances for both systems. Since $g(\epsilon)$ is a polynomial of order $(n-1)$, there are a total of $2n$ roots for equation (5.24) including $\epsilon = 1$.

Although the $(2n-1)$ values of $\epsilon$ cannot be computed explicitly, it is of interest to compare the situation with the earlier case of gain mismatch. In the former situation, there was only one point beside the trivial solution $\Delta b = 0$ for which both the systems gave identical performances. Thus, the number of solutions were independent of the sampling ratio, $n$. In contrast, here the uncertainty region is divided into $(2n-1)$ (unequal) intervals, at the nodes of which, MR control achieves identical performance as the fast-rate control. This implies that as the sampling ratio increases, the uncertainty interval encompasses more and more such points of identical performance. However, it should be noted that if the roots are complex, the number of intervals would be different from $(2n-1)$.

Due to the dependency of the number of zeros of $F(\epsilon)$ on $n$, it is not possible to arrive at an explicit condition as in equation (5.20). The winner among the MR and fast-rate control systems in the given uncertainty interval for the parameter $a$ depends on the sign of $F(\epsilon)$ in that interval. A positive sign would indicate that MR system is a better choice than fast-rate systems.

### Rational sampling ratio

Now, consider the above situations (gain and pole mismatches) when the sampling ratio is rational. From Chapter 4, we know that the performance of fast-rate systems gives a lower bound on the performance of MR systems. The strict equality holds good for integer sampling ratios. When the sampling ratio is rational, the inequality comes into role. Therefore, equation (5.10) does not hold good in this case. Define, $\tilde{\alpha} = 1 + \hat{\gamma}_f^2 + \cdots + \hat{\gamma}_f^{2l}$ ($l$ is the *l.c.m.* of the sampling intervals). Also, the relations in equations (5.13) and (5.15) no longer hold good. Hence, we define $\tilde{\beta} = \tilde{\mathbf{A}}^T k_L$ where

$$\tilde{\mathbf{A}} = [\ (a_f^{l-1} + a_f^{l-2} + \cdots + a_f^{l-m}) \ \cdots \ (a_f^{l-(n-1)m-1} + a_f^{l-(n-1)m-2} + \cdots + 1)\ ]^T$$

to write $\gamma_L = \hat{\gamma}_L - \tilde{\beta}(\Delta b)$. Then, the difference between the optimal performances can be written as:

$$\begin{aligned} \Delta J = J_f - J_L &= \frac{w_f}{1-\gamma_f^2} - \frac{w_L}{1-\gamma_L^2} \\ &= \frac{1}{(1-\gamma_f^2)(1-\gamma_L^2)}(\tilde{p}(\Delta b)^2 + 2\tilde{q}(\Delta b) + \tilde{r}) \end{aligned} \tag{5.25}$$

where $\tilde{p}$, $\tilde{q}$ and $\tilde{r}$ are defined as,

$$\tilde{p} = (w_L k_f^2 - w_f \tilde{\beta}^2)\ ;\quad \tilde{q} = (w_f \tilde{\beta}\hat{\gamma}_L - w_L \hat{\gamma}_f k_f)\ ;\quad \tilde{r} = w_f(1-\hat{\gamma}_L^2) - w_L(1-\hat{\gamma}_f^2) \tag{5.26}$$

In the integer case, $l = n$, $w_L = \tilde{\alpha} w_f$ and equation (5.15) simplifies to equation (5.18) with $\tilde{r} = 0$.

The sign of $(J_f - J_L)$ is determined by the sign of the quadratic expression in equation (5.25). Note that the denominator is always positive for stable closed-loop systems. Also, since $\triangle J \leq 0$ when $\triangle b = 0$, $\tilde{r} \leq 0\ \forall\ R_c$.

As earlier, we investigate conditions when $\triangle J = 0$. Four possibilities arise:

1. If $\tilde{p}$ & $\tilde{q} \neq 0$, then $\triangle J = 0$ iff $(\triangle b) = (\triangle b)_1$ or $(\triangle b) = (\triangle b)_2$.
2. If $\tilde{p} = 0$, then $\triangle J = 0$ iff $\triangle b = -\dfrac{\tilde{r}}{2\tilde{q}}$
3. If $\tilde{q} = 0$, then $\triangle J = 0$ iff $(\triangle b)^2 = -\dfrac{\tilde{r}}{\tilde{p}}$
4. If $\tilde{p} = \tilde{q} = 0$, then $\triangle J = 0$ iff $r = 0$

where $(\triangle b)_1$ and $(\triangle b)_2$ are the roots of quadratic expression in (5.25). Cases 2 and 3 assume that $\tilde{r} \neq 0$. We are mainly interested in the case $\tilde{p},\ \tilde{q} \neq 0$. In fact, the last case arises only when the input weight becomes large.

In order for $(\triangle b)_1$ and $(\triangle b)_2$ to be real, we require that $(\tilde{q}^2 - \tilde{p}\tilde{r}) \geq 0$. It is hard to comment on the sign of $(\tilde{q}^2 - \tilde{p}\tilde{r})$ given the known parameters. However, it can be said that as $R_c$ becomes large, one of the roots will tend to zero (since $\tilde{r}$ tends to zero).

From the above discussion, it can be stated that for the rational sampling ratio case, FSR systems perform better than MR systems iff,

$$(\triangle b)_1 < \triangle b < (\triangle b)_2 \qquad \text{where } (\triangle b)_1 < (\triangle b)_2 \tag{5.27}$$

Again, these intervals can be estimated with the help of known model and design parameters.

Now, consider the pole-parameter mismatch case. The results are similar to those in the integer sampling ratio case, except that now we would have $2l$ nodes where the MR systems will yield identical performance as the FSR systems. Additionally, the quantity $\mathbf{E}$ has to be modified to a new quantity $\tilde{\mathbf{E}}$ in accordance with the definition of $\tilde{\mathbf{A}}$.

**Robust stability**

So far, we have analyzed and compared the performance of these systems in presence of a model-plant mismatch. However, we have assumed inherently that both systems obey the conditions of closed-loop stability. Here, we include the stability conditions in an explicit fashion as they are crucial to the earlier analysis. We only consider the gain mismatch case as the pole-mismatch case is beyond the scope of this discussion.

The common interval for which both the control systems are stable and $J_f < J_L$ is given by (for the rational case)

$$\max\left(\frac{\hat{\gamma}_f - 1}{k_f}, \frac{\hat{\gamma}_L - 1}{\tilde{\beta}}, (\Delta b)_1\right) < \Delta b < \min\left(\frac{\hat{\gamma}_f + 1}{k_f}, \frac{\hat{\gamma}_L + 1}{\tilde{\beta}}, (\Delta b)_2\right) \tag{5.28}$$

Given the model and design parameters, the above interval can be easily computed.

Using the expression given above, we can compare the robust stabilities of MR and FSR system. Since $\hat{\gamma}_L$ is closer to zero than $\hat{\gamma}_f$, it turns out that lifted MR systems are more robustly stable than the associated FSR systems whenever $\tilde{\beta} << k_f$. Additionally, whenever $\tilde{\beta} > k_f$, the MR system is more robust on the lower bound, with the FSR system on the upper bound.

It is interesting to compare this result with that given by Li *et al.* (2000*a*), where it was shown that dual-rate inferential systems are, in general, more robustly stable than their associated FSR systems.

In the next section, we perform a similar analysis for MR systems vs. SSR systems.

### 5.2.2 MR vs. SSR systems

Define,

$$w_s = (q_s + k_s^T r_s k_s - 2n_s k_s) \tag{5.29}$$

$$\tilde{\Omega} = (\sum_i \tilde{\mathbf{A}}_i) k_s \tag{5.30}$$

Then, $\gamma_s = \hat{\gamma}_s - \tilde{\Omega}(\Delta b)$. Note that $\tilde{\Omega} \geq \tilde{\beta}$ and hence, $\hat{\gamma}_L \geq \hat{\gamma}_s$.

We directly analyze the rational sampling ratio case. The difference in performances can be written as:

$$\begin{aligned} \Delta J = J_L - J_s &= \frac{w_L}{1-\gamma_L^2} - \frac{w_s}{1-\gamma_s^2} \\ &= \frac{1}{(1-\gamma_L^2)(1-\gamma_s^2)}(\tilde{p}(\Delta b)^2 + 2\tilde{q}(\Delta b) + \tilde{r}) \end{aligned} \tag{5.31}$$

where $\tilde{p} = (w_s\tilde{\beta}^2 - w_L\tilde{\Omega}^2)$, $q = (w_L\tilde{\Omega}\hat{\gamma}_s - w_s\tilde{\beta}\hat{\gamma}_L)$ and $r = w_L(1-\hat{\gamma}_s^2) - w_s(1-\hat{\gamma}_L^2)$. Here, as per earlier discussion, $r \leq 0$ since $J_L - J_s \leq 0$ when $\Delta b = 0$.

Based on our earlier analysis, we can directly state that MR systems perform better than SSR systems iff,

$$(\Delta b)_1 < \Delta b < (\Delta b)_2, \qquad (\Delta b)_1 < (\Delta b)_2 \tag{5.32}$$

where $(\Delta b)_1$ and $(\Delta b)_2$ are the roots of the quadratic expression in equation (5.31). It is not guaranteed that the roots are always real.

For the pole mismatch case, as in earlier situations, it is easy to see that we would have $2l$ nodes at which the SSR systems can give identical performance as the MR systems.

In the following discussion, we show that MR systems are more robustly stable than SSR systems in presence of gain mismatch.

**Robust stability**

As in the earlier analysis, we can write the common interval for which both the control systems are stable and $J_L < J_s$ as (for the rational case)

$$\max\left(\frac{\hat{\gamma}_s - 1}{\tilde{\Omega}}, \frac{\hat{\gamma}_L - 1}{\tilde{\beta}}, (\Delta b)_1\right) < \Delta b < \min\left(\frac{\hat{\gamma}_s + 1}{\tilde{\Omega}}, \frac{\hat{\gamma}_L + 1}{\tilde{\beta}}, (\Delta b)_2\right) \tag{5.33}$$

Recall that $\tilde{\Omega} \geq \tilde{\beta}$ and hence $\hat{\gamma}_L \geq \hat{\gamma}_s$. Therefore, we can rewrite the above condition as,

$$\max\left(\frac{\hat{\gamma}_s - 1}{\tilde{\Omega}}, (\Delta b)_1\right) < \Delta b < \min\left(\frac{\hat{\gamma}_s + 1}{\tilde{\Omega}}, (\Delta b)_2\right) \tag{5.34}$$

From the above expression, an interesting conclusion arises - MR systems are more robustly stable than SSR systems to gain mismatches.

In the next section, we present simulation results that allow us to gain more insight into the behaviour of these systems in presence of a gain mismatch.

## 5.3 Simulation Results

Consider the experimental model used in Chapter 4 at the fast sample rate $h = 4$:

$$G_f(z) = \frac{0.1416}{z - 0.9868} \tag{5.35}$$

For illustration purposes, choose the control interval $m = 3$ and output sampling interval $n = 5$ fast sample units. The state weight $Q_c$ is set to 10 and the input weight $R_c$ is varied on a log scale from 0.01 to 1000 in 30 intervals.

First, observe the plot of $\tilde{p}$, $\tilde{q}$ and $\tilde{r}$ vs. $\log_{10} R_c$ shown in Figure 5.1(a). As expected, $\tilde{r} < 0 \; \forall \; R_c$. Moreover, $\tilde{p}$ and $\tilde{q}$ pass through zero once and tend to zero as

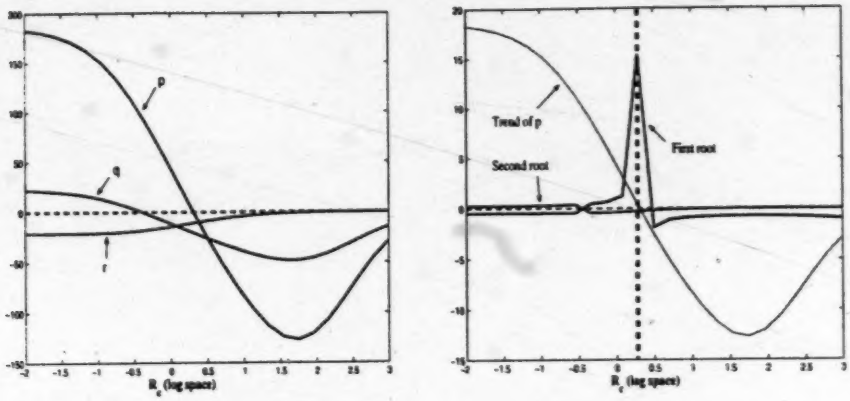


*(a) Variation of $\tilde{p}$, $\tilde{q}$ and $\tilde{r}$ with $R_c$* *(b) Trajectory of roots with $R_c$*

Figure 5.1: *FSR vs. MR systems - performance comparison*

$R_c \rightarrow \infty$. As $p \rightarrow 0$, one root tends to zero and the other root tends to $\infty$. This point is illustrated in Figure 5.1(b) where the roots of the quadratic expression in equation (5.25) are plotted along with the trend of $\tilde{p}$.

The robust stability bounds along with the roots are plotted in Figure 5.2(a). It is seen that while the root with smaller magnitude always remains within the robust stability bounds, the other root reverses its sign and remains out of these bounds. Another point to note is that the roots for all values of $R_c$ are real. Adjacent to this plot is shown how the bounds for robust stability are decided depending on $\tilde{\beta}$ and $k_f$. A flag value of "1" is used to indicate that the bounds of the FSR system decide the boundaries of robust stability while a value of "2" indicates that the bounds are decided by that of the MR system. This means that when the flag value is "1", for example, then the bounds of the MR system are wider than that of the FSR system - meaning that the MR system is more robustly stable than the FSR system. As mentioned earlier, Figure 5.2(b) illustrates that for almost all situations when $\tilde{\beta} < k_f$, MR systems are more robust than FSR systems with respect to stability.

Now, we compare MR systems with SSR systems. Similar plots are shown in Figures 5.3 and 5.4. An interesting observation to make is that Figure 5.4(b) shows that MR systems can tolerate larger intervals of uncertainty in the gain estimate than SSR systems for closed-loop stability. Our earlier theoretical analysis yielded the same conclusion.

The important point to note here is that a few complex roots were obtained with

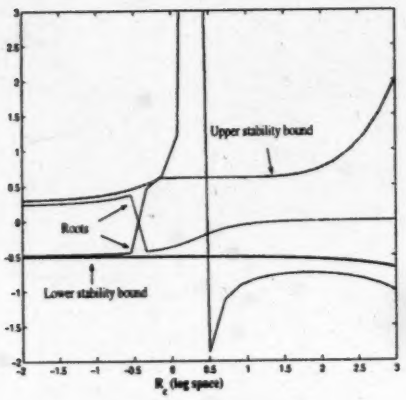


*(a) Intervals for robust stability and optimal performance*

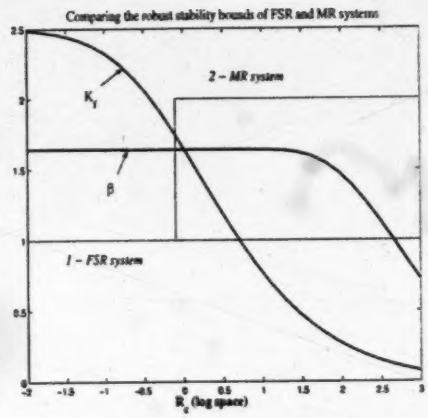


*(b) Comparison of robust stability of FSR & MR systems - $\tilde{\beta}$ and $k_f$ vs. $R_c$*

Figure 5.2: *Effect of input weighting on MR and FSR systems (robustness analysis)*

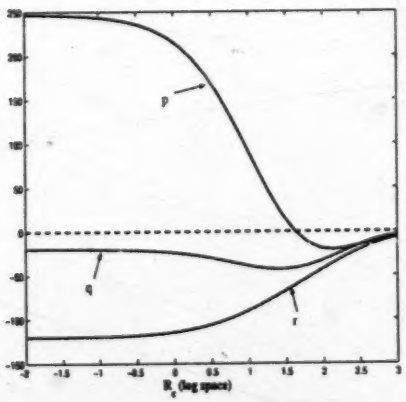


*(a) Variation of $\tilde{p}$, $\tilde{q}$ and $\tilde{r}$ with $R_c$*

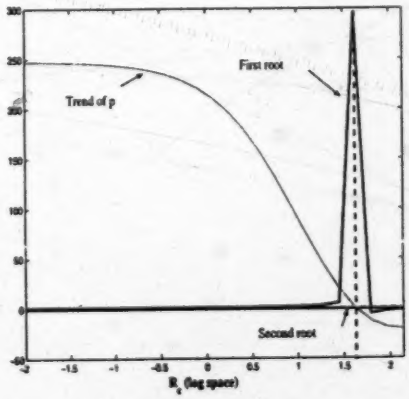


*(b) Trajectory of roots with $R_c$*

Figure 5.3: *Effect of input weighting on MR and SSR systems (robustness analysis)*

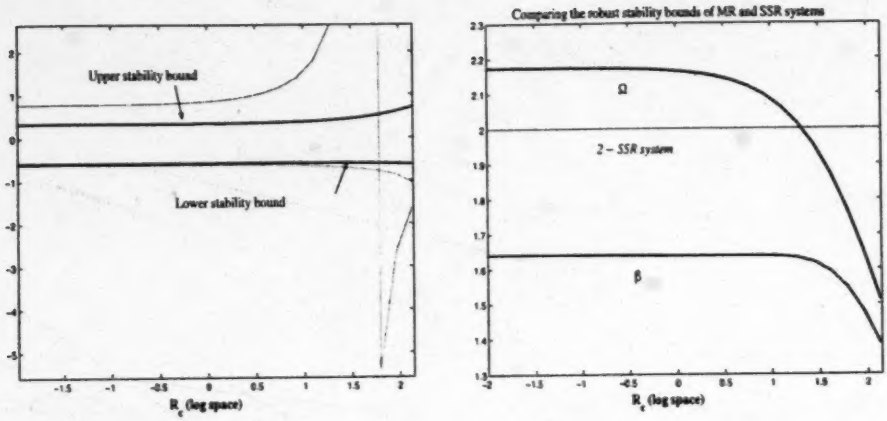


*(a) Intervals for robust stability and optimal performance*

*(b) Comparison of robust stability of MR & SSR systems - $\tilde{\beta}$ and $\tilde{\Omega}$ vs. $R_c$*

Figure 5.4: *MR vs. SSR systems - performance comparison*

the last few large values of $R_c$. However, one cannot make any general conclusions about the nature of roots (complex or real) as $R_c$ is varied.

## 5.4 Summary

In summary, for first-order SISO systems in the presence of model-plant mismatch:

- Given model and design parameters, we can calculate intervals for parametric uncertainty from which one can directly infer the better of the FSR, MR and SSR systems for optimal performance and robust stability.
- MR systems are more robustly stable than FSR systems for almost all cases of $\tilde{\beta} < k_f$ with a gain mismatch.
- MR systems are more robustly stable than SSR systems in the presence of a gain mismatch.
- In the presence of a pole mismatch, with the increase in $l$, there is an increase in the number of nodes of uncertainty at which among each pair of MR and FSR, MR and SSR systems give identical performance. However, it is hard to comment on the robustness of stability in such a situation.

- As input weight $R_c$ becomes large, even in the presence of model-plant mismatch, all three systems tend to give identical performance.

## 5.5 Future work

Although the analysis here is based only on first-order SISO systems, it provides an insight into the robust stability comparison and optimal performance comparison problems. Comparison of robust stability of these systems for higher-order SISO systems and MIMO systems involves a well-known problem known as the stability radius problem. Inclusion of such an analysis is intended in the future so that a generalized inference can be made.

In the future, the objectives would be *(i)* to arrive at a general result for higher-order SISO systems and MIMO systems, and *(ii)* tackle this problem for output feedback systems.

# Chapter 6

# Multiscale Analysis Using Wavelets

**Purpose**: To introduce the reader to wavelet theory from a filtering perspective with illustrated applications to process industry.

## 6.1 Multiscale Systems

So far in Chapters 2-5, we have discussed issues arising in the design of multirate control systems and the related performance benefits in comparison with single-rate systems both with and without model-plant mismatch. In Chapter 1, we noted that multirate systems are in fact, a special class of what are termed as *multiscale systems*.

Multiscale (MS) systems as defined in Chapter 1, are those class of systems whose variables evolve over different/multiple time-frequency scales or, equivalently those which possess significantly differing time constants. Examples of such systems are in series chemical reactors with different residence times, chemical vapour deposition reactors (where coupling of fast and slow reaction occurs), *etc.* Another commonly occurring system is the ubiquitous distillation column with large number of trays where the effect of vapour boilup on the top product occurs relatively slowly than recycle flow. In fact, many industrial processes involve physico-chemical phenomena that occur in separate time scales.

Multiscale nature can also be introduced in the data for several reasons. First due to different sampling rates, which is none other than the multirate sampling scheme. Secondly, in the process industry, seldom do measured data contain contributions from a single scale since the overall contributions to a sample usually come from different localizations in time and frequency. In addition, the data is corrupted with noise due to stochastic events such as measurement noise, disturbances, faults, etc. that often occur in different time zones in different frequency bands. For example, a typical process signal can be a combination of a constant frequency disturbance

with high-frequency noise, in the presence of slow equipment degradation added with intermittent abrupt sensor failures, *etc.* (Bakshi 1999). Clearly, these components occur at different times and belong to different frequency bands.

Identification, control and monitoring of multiscale systems can be more complicated and cumbersome than that of single-scale systems. Many a time, complicated system models are used to represent these type of systems. It is well-known that a direct application of standard control methods, or even modern control methods to such multiscale system models can lead to complicated or ill-conditioned controllers (high sensitivity), closed-loop instability, *etc.* (Christofides and Daoutidis 1996*b*, Kokotovic *et al.* 1986). To circumvent these problems, multiscale systems can be represented as a combination of models with fast and slow dynamics (Luse and Khalil 1985). This decomposition is advantageous for the reason that the design criteria for the slow dynamics differs considerably from that of the fast dynamics. Moreover, the degree of accuracy with which slow dynamics are identified is quite higher than that with the fast dynamics. In this context, singular perturbation theory has found a comfortable place in the theory of multiscale systems (Kokotovic *et al.* 1976, Saksena *et al.* 1984, O'Reilly 1980, Kokotovic *et al.* 1986, Khalil 1987). Frequency domain techniques have also found a strong application in this area. In this work, however, we are concerned with the analysis of multiscale systems in the time and frequency domains simultaneously using process data.

Representing measured data in terms of basis functions at a single scale is not efficient in separating the different frequency components of a signal, for example, dynamics from the stochastic component. In fact, any single-scale method is inherently forced to trade-off the extent of noise removal with the quality of the retained features (see for *e.g.*, Bakshi (1999)). Now, let us look at it from a frequency domain point of view. Raw measurements typically provide a good picture of the time variation, but, obscure the frequency information. Fourier transforms, which belong to the class of single-scale methods, give us an excellent picture of the underlying frequency information at the cost of losing the knowledge of time variations. This is acceptable for stationary signals, *i.e.*, those signals whose frequency content does not vary with time. But, in reality, is stationarity a practical assumption? Chemical processes seldom give rise to stationary signals. In speech recognition or musical tones where different scales (pitches) appear at different times, stationarity is far from being true. Non-stationary signals emphasize the need for a tool that enables us to view the frequency variations in time.

Therefore for multiscale systems, a more natural scheme would be the one that is capable of taking into account the underlying different time-frequency scales while

achieving good separation between the deterministic and stochastic parts of a signal. In filtering terminology, the multiscale method of interest should be capable of providing varying time-frequency resolution depending on the signal features.

Recently, the theory of wavelets has occupied a prominent place mainly in the analysis of non-stationary signals and data pre-processing. The wavelet transform is a powerful tool that allows decomposition of data into components whose frequency resolutions are matched to their scale. In other words, the low frequency components are well resolved in frequency, while the high frequency components are well resolved in time. In essence, they separate the slow and fast components of a signal in a way that is suitable for effective control and monitoring of MS systems. They also possess other attractive properties that have made them a popular choice for the analysis of multiscale systems. In the wavelet literature, the term *scale* is a synonym for *frequency*, despite the difference in their connotations.

Fault detection, needless to say is a crucial component of the safe operation of a plant. Existing fault detection methods are based on the stationarity assumption. Again, this assumption is more often impractical due to several reasons. Faults occurring in process industry rarely occur simultaneously. Besides, depending on the nature of the fault, they fall in different frequency categories. Conventional PCA (including its variations) assume that measurements possess single-scale characteristics, thus resolving different types of faults at the same level. Multiscale PCA (MSPCA) described by Bakshi (1998) first separates the characteristics of measurements into different time-frequency scales using wavelets and then builds PCA models on each of these scales.

In the ensuing section, we present an illustrative introduction to wavelets - the motivation, brief mathematical background and the filtering algorithm to implement wavelet transformations. These transformations form the basis of the multiscale analysis discussed in this chapter.

## 6.2 Introduction to Wavelets

Over the last decade, the scientific literature has been inundated with a myriad of perspectives on wavelet theory. The theory of wavelets is not new, but rather known to mathematicians, physicists and scientists in various forms for several decades. It is the work by Morlet *et al.* (1982) that brought researchers from different disciplines together to provide a more unified framework of wavelet theory. In some school of thought, it is also believed that Fourier, in a way, laid foundation with his pioneering work on frequency domain analysis. Fourier transforms are a foundation for many of

the frequency domain techniques that have appeared in several disciplines.

Although wavelets can be introduced in many ways, an intuitive way is to begin with Fourier transforms. This is particularly useful for engineers and scientists as the motivation for wavelet transforms becomes clearly visible with the type of signals encountered in engineering and scientific systems. Because frequency domain analysis has close relations with filtering and the ease of implementation of wavelet transforms, we focus on the filtering perspective of wavelet transforms. For detailed historical details behind the development of wavelets, the reader is referred to Meyer (1986), Daubechies (1992) and Mallat (1998).

### 6.2.1 The Need for Wavelets: Why?

Process data is usually recorded as variations with time giving a direct view of the changes in the time domain. On many occasions, we are interested in how "fast" or "slow" a particular variable changes with time leading us to the frequency regime. Ideally, we would like to convert the existing time information into frequency information. Joseph Fourier (1807) in his pioneering work addressed and solved this problem by proving that a periodic signal $f(t)$ can be decomposed into building blocks made up of sines and cosines. Fourier transforms (FT), as they are popularly known since then played a vital role in almost every engineering and scientific application. The Fourier transform of a signal $f(t)$ is defined as:

$$\hat{f}(\omega) = \int_{-\infty}^{+\infty} f(t) e^{-i\omega t} dt \quad \text{(Continuous)} \tag{6.1}$$

$$\hat{f}[n] = \sum_{k=-\infty}^{k=\infty} f[k] \exp\left(-\frac{i2\pi nT}{k}\right) \quad \text{(Discrete)} \tag{6.2}$$

where $f(t)$ is sampled with interval $T$. The set of values $f[k]$ is the measurement of $f(t)$ in discrete-time. Equation (6.2) is of practical interest as it deals with sampled signals. In essence, a data sequence $f[n]$ is convolved with a class of compiex exponential functions at different frequencies. Alternatively, it can be said that the sequence $f[n]$ is decomposed into a set of building blocks that are sinusoidal waves, infinitely long in time and perfectly localized in frequency. The magnitude of each building block is a direct measure of the "strength" of the signal at that frequency. The basis functions or the building blocks come from the so-called *transformation kernel*: $K(t,\omega) = e^{-i\omega t}$.

In practice, we look at the magnitude of the complex FT to assess the frequency content of a signal. Also, note that the inverse of Fourier transform provides a perfect reconstruction of the original signal.

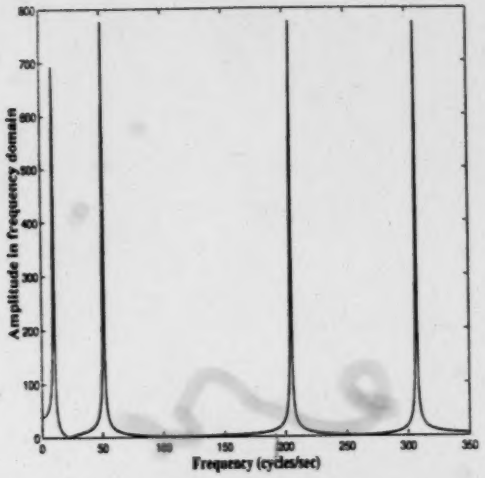


Figure 6.1: *Fourier transform of signal:* $f(t) = sin(2\pi 10t) + sin(2\pi 50t) + sin(2\pi 200t) + sin(2\pi 300t)$ *- provides good frequency resolution*

Figure 6.1 shows the FT of a signal $f(t) = sin(2\pi n_1 t) + sin(2\pi n_2 t) + sin(2\pi n_3 t) + sin(2\pi n_4 t)$ with $n_1 = 10$; $n_2 = 50$; $n_3 = 200$; and $n_4 = 300$ sampled at a frequency of 1000 Hz (cycles/sec) ($T = 1$ ms). The plot clearly illustrates the capability of Fourier transform. The frequency resolution achieved with FT is high and evidently improves with the increase in sampling frequency. The upper limit to frequency resolution is decided by the sampling frequency of the discrete signal at hand, or by the Nyquist frequency. The term *resolution* is intuitively understood as the degree of detail in the respective domains.

Now, observe Figure 6.2 showing the FT of two signals. The transforms look similar with the exception of small ripples and the smaller amplitude in the second plot. The question is: *could the underlying signals be similar in nature?*. We already know the underlying time domain signature for signal 1. So, do the plots indicate a close resemblance of signal 2 with signal 1? Figure 6.3 answers our question indicating that signals 1 & 2 differ considerably from each other. While signal 1 contains four frequencies at all times, signal 2 contains these four frequencies over different non-overlapping time intervals. Essentially, the FT fails to distinguish between two signals which contain identical frequencies but with different frequency distributions. What could be the reason for this drawback? Recall from the definition in equation (6.2) that the FT decomposes a signal into building blocks that are infinitely long in time, and, perfectly localized in frequency (sinusoidal waves never die with time but oscillate with a fixed frequency). By integrating (or summing) over the infinite time domain,

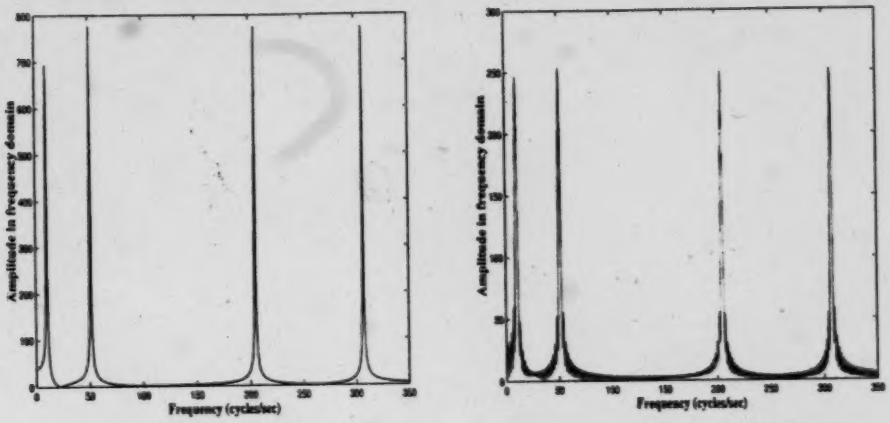


*(a) Fourier transform of signal 1* *(b) Fourier transform of signal 2*

Figure 6.2: *Fourier transforms of two signals - look almost identical*

we are unable to focus on the local features of this signal. This is a major drawback of FT in many situations. In situations that do not require the knowledge of frequency variations in time, FT is a powerful tool. Signal 1 is an example of a signal whose frequencies do not change with time while signal 2 is an example of a signal whose frequencies evolve with time. To summarize, FT provides perfect frequency resolution but loses out entirely on the time resolution.

In order to overcome this drawback, Gabor (1946) introduced what is known as the Short-Time Fourier transform (STFT) or the *Gabor transform*. Although the idea is simple - slicing the signal using a finite length of the window and then performing its FT and STFT provides a good solution to the problem. Mathematically, the STFT is defined as:

$$Sf(u,\xi) = \int_{-\infty}^{+\infty} f(t)g(t-u)e^{-it\xi}dt \;=\; \frac{1}{2\pi}\int_{-\infty}^{+\infty} \hat{f}(\omega)\hat{g}(\omega-\xi)e^{-iu(\omega-\xi)}d\omega \quad (6.3)$$

The *transformation kernel* in this case is the window function: $K(u,\xi) = g(t-u)e^{-it\xi}$. It is the function $g(t-u)$ which selects that slice of $f(t)$ in the neighbourhood of $u$. Both the expressions are identical in equation (6.3) by virtue of Parseval's theorem. The identity also means that the effect of windowing a function in time and performing the Fourier transform is equivalent to multiplying the FT of the window function with the FT of the signal in the frequency domain. Thus, STFT localizes the FT of the function, $\hat{f}(\omega)$ in the neighbourhood of $\xi$. The length of the window $g(t-u)$ decides the time resolution of the resulting STFT. Because we have gained a resolution in

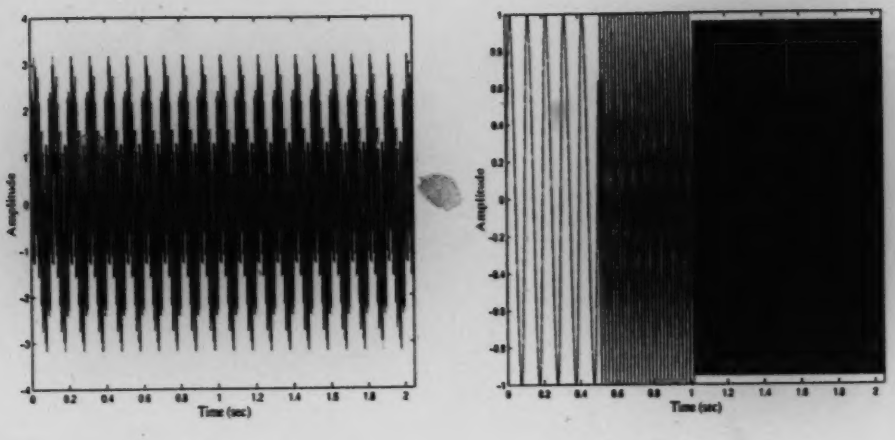


*(a) Signal 1* *(b) Signal 2*

Figure 6.3: *Signals 1 & 2 - quite different from each other*

time over the pure FT, it is intuitive that we lose out on the frequency resolution. In fact, the pure frequencies in the original FT become frequency bands localized in the neighbourhood of $\xi$. Figures 6.4(a) and 6.4(b) illustrate the STFT of the two signals discussed earlier. The plots clearly show the capability of STFT in distinguishing these signals. A Hanning window with a width of 32 units was chosen for this purpose. Upon an increase in window width to 512 units (one-fourth of the signal length), the STFT appears as in Figure 6.5. The plot shows marked improvement in frequency resolution at the loss of time resolution.

Based on Figures 6.2, 6.4 & 6.5, let us make a quick comparison with FT. While we had pure frequencies in FT, we now have frequency bands in STFT, but at the benefit of additional time information. The excellent frequency resolution in FT is now divided into good time and lower frequency resolution with STFT. However, on increasing the window length, we begin to improve on the frequency resolution but at the loss of distinction in time (note the overlaps in time in Figure 6.5).

As in the earlier case, the *upper limit* to the frequency resolution is limited by the Nyquist frequency of the discrete signal. As the window size gets larger the frequency resolution gets better and the transform asymptotically takes the shape of FT. However, the key observation to make is that we could not achieve both good time and frequency resolution simultaneously. In fact, the resolutions are governed by *Heisenberg's uncertainty principle* that states that the energy spreads in the time and frequency domains, $\sigma_t$ and $\sigma_\omega$ cannot be arbitrarily small simultaneously and are

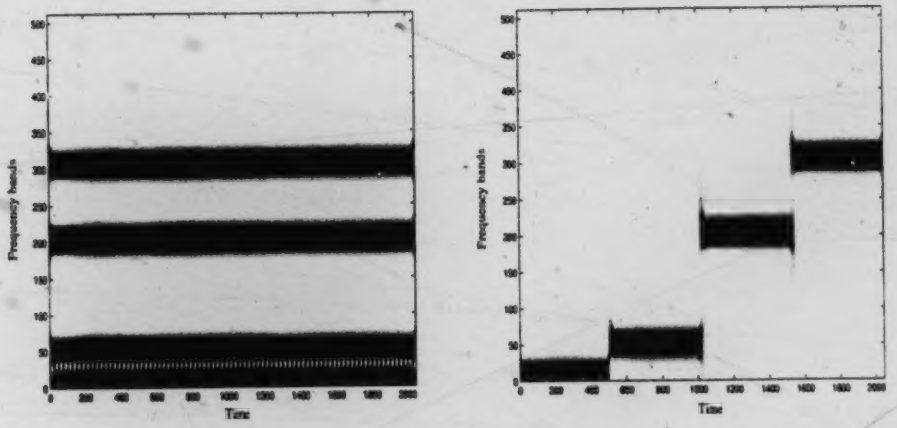


*(a) STFT of signal 1* *(b) STFT of signal 2*

Figure 6.4: *STFT of signals 1 & 2 using Hanning window (window width = 32 units) - capable of distinguishing signals 1 & 2*

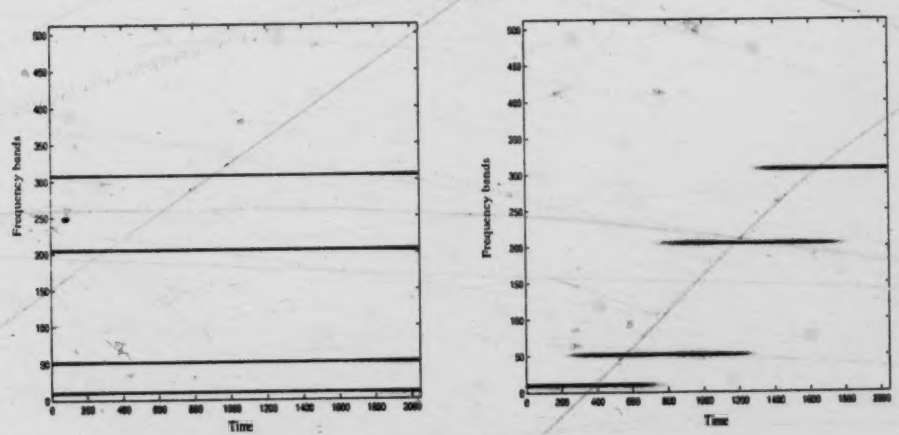


*(a) STFT of signal 1* *(b) STFT of signal 2*

Figure 6.5: *STFT of signals 1 & 2 using Hanning window (window width = 512 units) - loss in time resolution with increase in frequency resolution*

related ay the formula,

$$\sigma_t \sigma_\omega \geq \frac{1}{2} \tag{6.4}$$

where

$$\sigma_t = \int_{-\infty}^{+\infty} t^2 |g(t)|^2 dt \quad ; \quad \sigma_\omega = \int_{-\infty}^{+\infty} \omega^2 |g(\omega)|^2 d\omega \tag{6.5}$$

Here, we assumed that the window is normalized meaning $\|g\|_2 = 1$.

Equation (6.5) carries an important connotation: $\sigma_t$ and $\sigma_\omega$ are independent of the parameters $u$ and $\xi$. This means that once the window characteristics are fixed, the frequency resolution is fixed in the STFT. A useful way of looking at it is that the entire time-frequency domain is divided into boxes of same size. But, this is not the desired division of time-frequency plane. Ideally in order to capture the high-frequency features, we need to look through a narrow window and on the other hand, the low frequency or slow changes can be resolved well only by looking through a wide window. In other words, we need good time resolution for capturing the high-frequency components and good frequency resolution for capturing low frequencies. These conflicting requirements make the problem of time-frequency transform very challenging and interesting. The question remains: how do we accomplish these different resolutions? One way is to perform several STFT analyses with different window sizes. However, this can result in a highly redundant representation of the original signal and involves a large amount of bookkeeping.

Wavelet transforms offer an elegant solution to this problem by choosing a constant *relative bandwidth*:

$$r = \frac{\triangle \omega}{\omega} \tag{6.6}$$

in contrast to the *constant bandwidth* as in STFT. It is important to note that the uncertainty relationship given in equation (6.5) still holds good. The difference lies in the fact that now, $\sigma_t$ and $\sigma_w$ are each scaled by a factor $\frac{1}{s}$ and $s$ respectively. However, the product remains invariant. The large amount of bookkeeping is avoided due to the fact that the different window sizes are obtained from the same mother wavelet function by varying the scaling factor.

In the next section, we give a detailed discussion on the mathematical background behind these transforms.

### 6.2.2 Wedding Time and Frequency: Wavelets

The idea behind wavelet transforms is similar to that of performing STFT analyses with different window sizes. However, the low frequency component of $f(t)$ is

extracted using a wide window and the high frequency component using a narrow window. These windows (basis functions) in a wavelet transform are obtained by scaling and translating only one *scaling* function $\phi(t)$. Such a commonness is absent in STFT. This is the basic difference between a wavelet transform and STFT. The role of the scaling function will be clear once we are familiar with wavelet functions.

The wavelets meaning "little waves" arise by scaling and translating a finite energy "mother" wavelet function $\psi(t)$ with zero mean. The mother wavelet itself can be expressed as a linear combination of the scaling function (as seen later), and the wavelets can be then expressed as:

$$\psi_{s,u} = \frac{1}{\sqrt{|s|}}\psi\left(\frac{t-u}{s}\right), \qquad s, u \in R \;\; s \neq 0 \tag{6.7}$$

The values of *scaling* parameter $s$ determines whether a compression or dilation of the mother wavelet takes place. If $s > 1$, there is a stretching of $\psi(t)$ along the time axis, resulting in a wide window that is suitable for analyzing the low frequency features of a signal. On the other hand, if $0 < s < 1$, $\psi(t)$ is in a compressed state that is suitable to analyzing the high-frequency components of the signal. The parameter $u$ as in STFT is the *translation* parameter, used to traverse along the length of the signal. The factor $\frac{1}{\sqrt{|s|}}$ is a normalization factor so that the energy of the wavelets is the same as mother wavelet. The Continuous Wavelet Transform (CWT) is then given by the formula,

$$Wf(u,s) = \langle f, \psi_{u,s} \rangle = \int_{-\infty}^{+\infty} \psi^*_{u,s}(t) f(t) dt \tag{6.8}$$

From above, it is clear that CWT is the correlation at lag $b$ between $f(t)$ and the wavelet dilated to a scale factor $s$. A classical example of a wavelet is the *Mexican hat* wavelet function obtained by taking the second derivative of the negative *Gaussian* function $-e^{-t^2}/2$,

$$\psi(t) = (1 - 2t^2)e^{-t^2} \tag{6.9}$$

As in FT, the original signal $f(t)$ can be restored perfectly using,

$$f(t) = \frac{1}{C_\psi} \int_0^\infty \int_{-\infty}^{+\infty} Wf(u,s)\psi_{s,u}\frac{1}{s^2} ds du \tag{6.10}$$

where $C_\psi$ is called the *admissibility constant* and is given by,

$$C_\psi = \int_0^\infty \frac{\hat{\psi}^*(\omega)\hat{\psi}(\omega)}{\omega} d\omega \qquad C_\psi < \infty \tag{6.11}$$

The reproducing kernel in this case is: $k_{u,s} = \frac{1}{\sqrt{s}}\psi\left(\frac{t-u}{s}\right)$. Equation (6.11) implies that $\hat{\psi}(0) = 0$ (assuming $\psi(.)$ is real) meaning $\psi(.)$ should have a zero average. Another way of interpretation is that the mother wavelet should be a small wave that should die off quickly with $t$. The zero average also indicates that the wavelet characteristics can be related to the impulse response of a band-pass filter $g[n]$. In fact, equation (6.8) can be written as a convolution equation:

$$Wf(u,s) = f(t) \star \bar{\psi}_s(u) \qquad \psi_s(t) = \frac{1}{\sqrt{s}}\psi^*\left(\frac{-t}{s}\right) \tag{6.12}$$

Equation (6.12) is of crucial importance in implementing wavelet transforms. The convolution results in filtering of $f(t)$ with a series of dilated band-pass filters.

The wavelet coefficients produced using equation (6.12) reflect the amount of correlation of the signal with the basis function at that scale and position.

### Scaling function

Recall that since wavelets are zero average functions, wavelet transformation is identical to band-pass filtering. Furthermore, filtering is equivalent to approximating the signal at a particular frequency resolution. Therefore, with wavelet transformations, we are in essence building approximations of a signal at different time-frequency resolutions. It is intuitive that it requires infinite number of wavelets to decompose a function and reconstruct it without loss of information (since wavelet filters are band-pass filters). Assume that the we have built an approximation of a function $Wf(u,s)$ up to a scale $s < s_0$. Then, we need a complement of information corresponding to $Wf(u,s)$ $s > s_0$. This aggregate information is obtained by introducing a *scaling* function corresponding to scales $s > 1$, with its modulus defined as,

$$|\hat{\phi}(\omega)|^2 = \int_1^{+\infty} |\hat{\psi}(s\omega)|^2 \frac{ds}{s} = \int_\omega^{+\infty} \frac{|\hat{\psi}(\xi)|^2}{\xi} d\xi \tag{6.13}$$

The above definition is reflective of our earlier representation of the mother wavelet function as a linear combination of the dilations and translations of a scaling function. Using the above definition and the admissibility condition, it is easy to show that $\lim_{\omega \to 0} \hat{\phi}(\omega) = C_\psi$ indicating that the scaling function can be interpreted as an impulse response of a low-pass filter $h[n]$.

With the introduction of a scaling function, now any finite energy signal $f(t)$ can be expressed as a combination of finite number of scaling and wavelet functions. This is the basic idea behind the wavelet decomposition of a signal. The scaling function transformation or low-pass filtering builds an approximation of the signal

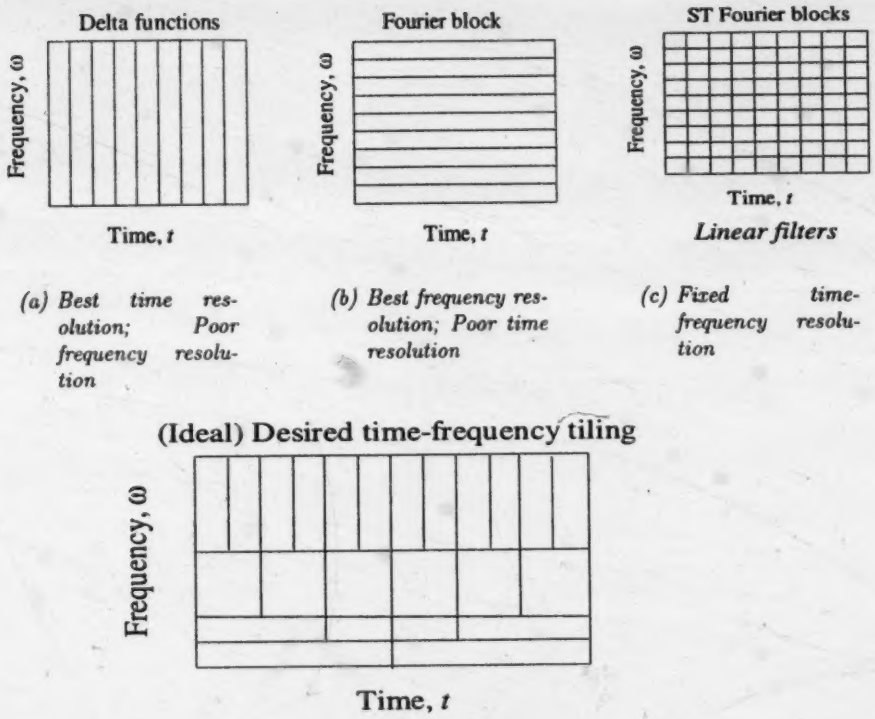


*(a) Best time resolution; Poor frequency resolution*

*(b) Best frequency resolution; Poor time resolution*

*(c) Fixed time-frequency resolution*

*(d) Ideal time-frequency resolution*

Figure 6.6: *Time frequency tiling with Delta, Fourier, STFT and Wavelet basis functions*

while the wavelet transformation (high-pass filtering) gives the details (the remaining information) of the signal. Further, the approximation can be decomposed in a similar way. Thus, we achieve a multilevel approximation of the signal as the scale parameter $s$ assumes different values.

Figure 6.6 shows a comparison of the abilities of FT, STFT and CWT in dividing the time-frequency plane.

The raw sampled data belongs to the space spanned by delta functions, where the time resolution achieved is the best and limited by the sampling interval, however, with poor frequency resolution. In contrast, Fourier transformation rearranges the time-frequency tiling with the best possible frequency resolution limited by the sampling frequency. However, there is an entire loss of time information in the Fourier domain. Next, with the STFT, the information is re-arranged in time-frequency tiles

of fixed area. The STFT is equivalent to linear filtering as we can write,

$$Sf(u,\xi) = \int_{-\infty}^{+\infty} f(t)g(t-u)e^{-it\xi}dt = e^{-iu\xi}\, f \star \bar{g}_\xi(u) \tag{6.14}$$

where $\bar{g}_\xi(u) = g(-t)e^{it\xi}$.

But the desired tiling as we noticed earlier is that low-frequency components need wide windows in time and high-frequency windows need narrow windows. This ideal time-frequency tiling is given in the last plot, which is achieved with wavelet basis functions.

The CWT is a redundant representation of the signal as it maps a 1-D signal to a 2-D space. But, it is a translation-invariant representation, meaning if $f_\tau(t) = f(t-\tau)$ is a translation of $f(t)$ by $\tau$, then,

$$Wf(u,s) = f_\tau \star \bar{\psi}_s(u) = Wf(u-\tau, s) \tag{6.15}$$

But, in practice, we use only the discrete version of the CWT by computing the transforms only at intermediate scales, in particular, at dyadic scales. This is accomplished by discretizing the scaling parameter $s = a_0^j$ and making translations in time proportional to that scale of the wavelet, $u = kb_0a_0^j$.

$$\psi_{j,k} = \frac{1}{a_0^j}\psi\left(\frac{t - kb_0a_0^j}{a_0^j}\right) \tag{6.16}$$

In this way, low frequency analyzing windows (meaning large values of $j$) will be shifted over large steps whereas high frequencies (small values of $j$) will require small steps to capture the quick variations in the signal. In this way, the discrete wavelet transform (DWT) achieves the trade-off between time and frequency resolutions. The most popular DWT that is implemented is the dyadic one by setting $a_0 = 2$ and $b_0 = 1$. Note that the DWT is still the transform of a continuous-time signal. The DWT mentioned here should not be confused with the *dyadic wavelet transform* in the wavelet literature in which only the scale parameter $s$ is discretized in dyadic levels, but not the translation parameter $u$. The dyadic wavelet transform maintains the translation-invariance of the CWT unlike the DWT.

Next, we are concerned with the implementation of wavelet transforms. The discrete wavelet transform (DWT) is a discrete convolution equation implemented using a two-step procedure known as the pyramidal algorithm due to Mallat (1989). The algorithm consists of first convolving the data with the low-pass and high-pass filters. The second step is the downsampling of the resulting convolved data. This is the key step and an attractive feature of wavelet transforms. At a first glance, it

appears that downsampling might result in a loss of information. However, as we will see in the next section, downsampling in fact is a solution to remove the redundancy in the wavelet transforms.

### 6.2.3 Wavelet Filtering

Wavelet transform decomposes a signal into successive bands of low to high frequency. This decomposition is obtained by consecutive two channel filtering and downsampling operations applied only on the low frequency band at each stage of the decomposition.

We begin with a simple example. Consider a data sequence $x_1, x_2, x_3, \cdots, x_n$ of interest. Let us consider the *decomposition* of this sequence into an approximation and detail. Choose a set of low-pass and high-pass filters known as the Haar filters (Haar 1910) whose impulse responses are $h = [\frac{1}{\sqrt{2}} \frac{1}{\sqrt{2}}]$ and $g = [\frac{1}{\sqrt{2}} \frac{-1}{\sqrt{2}}]$ respectively. Then, the filtered data sequence is $\tilde{a}_1 = \frac{x_0+x_1}{\sqrt{2}}, \frac{x_1+x_2}{\sqrt{2}}, \frac{x_2+x_3}{\sqrt{2}}, \cdots$, and $\tilde{d}_1 = \frac{x_0-x_1}{\sqrt{2}}, \frac{x_1-x_2}{\sqrt{2}}, \frac{x_2-x_3}{\sqrt{2}}, \cdots$, respectively. Next, downsample by a factor of 2 (remove every other sample) to obtain $a_1 = \frac{x_0+x_1}{\sqrt{2}}, \frac{x_2+x_3}{\sqrt{2}}, \frac{x_5+x_6}{\sqrt{2}}, \cdots$, and $d_1 = \frac{x_0-x_1}{\sqrt{2}}, \frac{x_2-x_3}{\sqrt{2}}, \frac{x_4-x_5}{\sqrt{2}}, \cdots$, respectively. But we can still *reconstruct* the original sequence with this downsampled sequence as $x_1 = \frac{a_1(1)+d_1(1)}{\sqrt{2}}, x_2 = \frac{a_1(1)-d_2(1)}{\sqrt{2}}, \cdots$,. In fact, this is exactly the same as upsampling $a_1$ and $d_1$ by a factor of 2 (insert zero in between samples) followed by convolution with $\tilde{h} = [\frac{1}{\sqrt{2}} \frac{1}{\sqrt{2}}]$ and $\tilde{g} = [\frac{1}{\sqrt{2}} \frac{-1}{\sqrt{2}}]$. The combination of filtering and downsampling steps can be repeated on the sequence $a_1$ until the desired stage. This is exactly the multiscale representation of a signal.

The above procedure of analysis (transformation) and synthesis (reconstruction) reflects the underlying principle of the pyramidal algorithm for the implementation of DWT. It was suggested by Mallat (1989). The idea is to obviate the need to convolve every sample of the original sequence with a long scale wavelet filter to obtain approximation and details at any given level. Instead, as we go to higher scales, the convolution sequences become shorter increasing the speed of the algorithm.

Each scale of wavelet ensembles a distinct band of frequencies in such a way that there is a minimum overlap of information among adjacent scales. This *band-limitation* of the wavelet is performed by dividing the time-frequency space into *proportional* width bandpass filters. In contrast, FT and STFT divide the time-frequency space into sequences of equal width bandpass filters. In the above decomposition, notice the filters satisfy the conditions $\langle h, g \rangle = 0$ and $h^2 + g^2 = 2$. Filters that satisfy these conditions are termed as *quadrature mirror filters* (QMF). These are a special pairs of low- and high-pass filters whose every stage of filtering results in slicing out

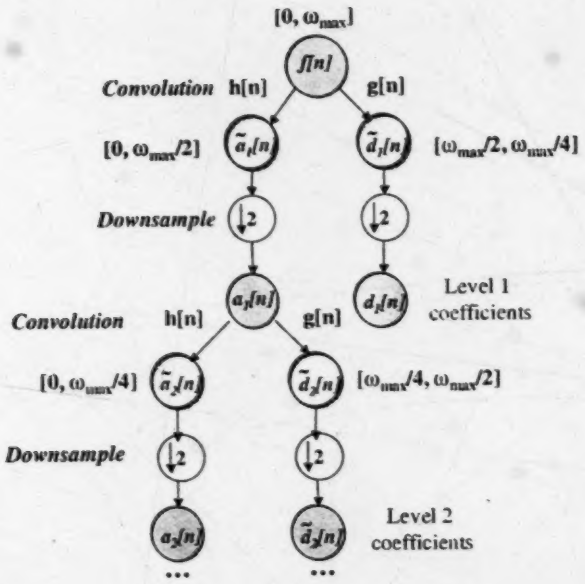


Figure 6.7: *Splitting data into low and high frequency components - Wavelet filtering tree: Mallat's pyramidal algorithm*

the frequency band of the signal into two halves. Figure 6.7 is illustrative of this multistage filtering using the pyramidal algorithm.

Starting from a data sequence $f[n]$, convolution with filters $h[n]$ and $g[n]$ results in splitting the original frequency band in approximately half frequency bands. The side-effect is a redundancy which is removed by downsampling by a factor of 2. Due to this step, the total number of samples at any level is the same as the number of samples in the low and high frequency bands put together at a lower level. For instance, if $f[n]$ has 1024 samples, then each of $a_1[n]$ and $d_1[n]$ would contain 512 samples.

The tree-like structure in Figure 6.7 is referred to as the wavelet tree. One could also follow the path along the details at every level and apply the same steps as to the approximation. Then, the resulting tree would have branches on both sides and the resulting transform is known as the wavelet packet (WP) transform. The wavelet tree is then a subset of the wavelet packet tree. The wavelet packet approach is a generalization of Mallat's algorithm. The WP transform gives the user the freedom to zoom into the specific frequency bands of the data. Thus, WP enables application-dependent frequency band splitting. Another advantage is that through arbitrary band splitting it can have frequency resolutions different from the octave band con-

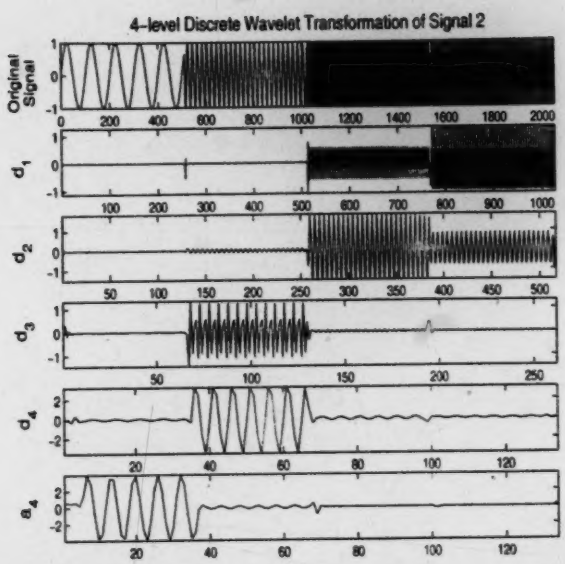


Figure 6.8: *Wavelet transformation of signal 2 using D8 wavelets*

stant relative bandwidth present in the wavelet transform. Nevertheless, in this work, we focus only on the wavelet tree algorithm because of its wide applications and most importantly, its relevance to many chemical processes. Data from chemical processes contain mainly low frequency components due to dynamics of the process, slow equipment degradation, etc. and relatively minor contributions from measurement noise, disturbances, etc. As we are mainly concerned with the separation of dynamic and stochastic components of a signal, the wavelet tree algorithm suffices for our situation.

Illustrated in Figure 6.8, is a wavelet transformation of signal 2 mentioned at the beginning of this chapter. The wavelet filter is a Daubechies filter with 8 coefficients (discussed in Section 6.3). We have divided the frequency band of the original signal into 5 octave bands. The original sequence contains 2048 samples. Scaling coefficients obtained in the lowest frequency band are plotted at the bottom of the figure. The higher frequency band wavelet coefficients $d_1 - d_4$ also appear in the Figure. The first stage of convolution followed by downsampling yields $a_1$ and $d_1$. In the second stage, $a_1$ is subjected to the same operation to obtain $a_2$ and $d_2$. This process continues until we reach the desired level. Observe how the number of samples decrease by a factor of 2 as one progresses from one level to another.

The natural topic of interest here is concerned with the design of wavelets to enable efficient separation, isolate singularities, etc. As we saw earlier, scaling and wavelet functions are characterized by the impulse responses of low and high-pass

filters. Therefore, it is natural to build these filters which will then help us visualize the scaling and wavelet functions. These filters are constructed by tailoring certain properties of the wavelet to suit the needs of the application at hand. Most applications of wavelet bases involve those wavelets which are capable of producing a few non-zero scaling coefficients $\langle f, \phi_{j,k} \rangle$. This is true for most of the chemical engineering applications where a majority of the signal content is in the low frequency regime. Then, the design of $\psi$ must be in such a way that the maximum number of close-to-zero wavelet coefficients $\langle f, \psi_{j,k} \rangle$ are produced. This property is useful for example, in data compression. Again, this depends on the regularity of $f$, the number of vanishing moments of $\psi$ and the size of its support (the range over which $\psi$ is non-zero). Starting from a conjugate mirror filter, we relate the wavelet properties to conditions on the filter $\hat{h}[\omega]$.

In the next section, we see how the design of wavelet filters is related to the generation of embedded subspaces, popularly known as *multiresolution analysis* (MRA).

## 6.3 Multiresolution/Multiscale Analysis

To begin with, we recall some useful mathematical definitions for multiresolution analysis and then discuss the design of wavelet filters. Finally, we review the fast wavelet transform algorithm due to Mallat (1989) with some examples.

### 6.3.1 Multiresolution Spaces

One can recall the analogy of the map discussed in Section 6.1 to understand the theory of multiresolution or multistage approximation of a function. Each stage of resolution can be considered as a *space* and a subset of the resolution at a higher space. For instance, an approximation (say at level 1) of the signal (level 0) is a subset of the signal, while a further approximation (say at level 2) is a subset of the approximation at level 1. The approximation of a function at a resolution $2^{-j}$ is specified by a discrete grid of samples that provides local averages of $f$ over neighbourhoods of size proportional to $2^j$. A multiresolution approximation is thus composed of embedded grids of approximation.

In mathematical terms, the approximation of a function at a level $j$ can be defined as an orthogonal projection of the function on a space $V_j \subset \mathbf{L}^2(\Re)$. Then the detail at that level spans a subspace $W_j$. At a lower level $j+1$, the approximation spans the subspace $V_{j+1}$. The following definition is due to Mallat (1989) and Meyer (1986):

**Definition 1** *A sequence $\{V_j\}_{j \in Z}$ of closed subspaces of $\mathbf{L}^2(\Re)$ is a multiresolution*

*approximation if the following properties are satisfied.*

$$\forall (j,k) \in Z^2, \quad f(t) \in V_j \iff f(t-2^j k) \in V_j, \tag{6.17}$$

$$\forall j \in Z, V_{j+1} \in V_j \tag{6.18}$$

$$\forall j \in Z, \quad f(t) \in V_j \iff f\left(\frac{t}{2}\right) \in V_{j+1}, \tag{6.19}$$

$$\lim_{j \to +\infty} V_j = \cap_{j=-\infty}^{+\infty} V_j = 0 \tag{6.20}$$

$$\lim_{j \to -\infty} V_j \quad = Closure\left(\cup_{j=-\infty}^{+\infty} V_j\right) \quad = \mathbf{L}^2(\Re) \tag{6.21}$$

*There exists a function called a scaling function $\phi(t)$ such that $\{\phi(t-k), k \in Z\}$ is a basis for $V_0$.*

The first property implies that $V_j$ is translation invariant by an amount proportional to $2^j$. The second property implies causality for the space $V_j$. Dilating functions by 2 expands the details by 2 and the third property is the definition of approximation at a coarser resolution $2^{-j-1}$. When the resolution goes to 0, the fourth property implies that we lose all the details of $f$,

$$\lim_{j \to +\infty} \|P_{V_j} f\| = 0 \tag{6.22}$$

On the other hand, the fifth property indicates that when the resolution $2^{-j}$ goes to $+\infty$, the signal approximation converges to the original signal,

$$\lim_{j \to +\infty} \|f - P_{V_j} f\| = 0 \tag{6.23}$$

The final property requires that there be a scaling function $\phi(t)$ such that the set $\{\phi(t-k), k \in Z\}$ is linearly independent and any function $f(t) \in V_0$ is expressible as,

$$f(t) = \sum_{n=-\infty}^{n=+\infty} a(0,n)\phi(t-n) \tag{6.24}$$

where $a(0,n)$ belongs to the set of scalars.

An important class of MRA results when the set of $\phi(t)$ and its integer translates form an orthonormal set. Further, notice that the above definition of MRA does not contain any mention of wavelet functions. Yet, based on the relations between the wavelet and scaling functions, MRA provides a natural setting for the wavelet functions.

Practically, the raw measurements is at the finest time resolution and assumed to be level 0. Then we build a level 1 approximation using the scaling function (low-pass filter) and the remaining information as detail at level 1. Now, we split the

approximation spanning $V_1$ into $V_2$ and $W_2$. This process continues depending on the length of the data at hand.

From above, it is clear that

$$\cdots V_1 \subset V_0 \subset V_{-1} \subset \cdots \tag{6.25}$$

form a *nested* sequence. Since $V_0 \subset V_{-1}$, every vector in $V_0$ belongs to $V_{-1}$ as well. Then, the scaling function $\phi(t)$ belonging to $V_0$ must also be $V_{-1}$. Therefore, it should be possible to express $\phi(t)$ as a linear combination of the basis for $V_{-1}$, namely, $\phi(2t-n)$. With this property, the familiar dilation equation can be written as (Daubechies 1990, Strang 1989, Mallat 1989),

$$\phi(t) = \sum_{n=-\infty}^{+\infty} c(n)\phi(2t-n) \tag{6.26}$$

Equation (6.26) is known as the *dilation* equation or the *two-scale* equation because $\phi(t)$ is expressed as a function of its own dyadic dilation and translation. In general,

$$\phi(2^{-j}t) = \sum_{n=-\infty}^{+\infty} c(n)\phi(2^{-(j-1)}t-n) \tag{6.27}$$

which justifies the concept of nested sequences. Similarly, one can also write for the wavelet function

$$\psi(t) = \sum_{n=-\infty}^{+\infty} d(n)\phi(2t-n) \tag{6.28}$$

due to the fact that $W_0 \subset V_{-1}$.

The dilation equation is very useful in the design of wavelet filters.

### 6.3.2 Design of Wavelet Filters

The following discussion is related to the design of wavelet filters. We recall the basic properties of a set of orthonormal scaling functions which will be then suitably translated to conditions on filter coefficients.

1. The area of the scaling function should be unity,

$$\int_{-\infty}^{+\infty} \phi(t)dt = 1 \tag{6.29}$$

2. It has unit energy:

$$\|\phi(t)\|_2^2 = \int_{-\infty}^{+\infty} |\phi^2|(t)dt = 1 \tag{6.30}$$

3. The set of $\phi(t)$ and its integer translates forms an orthonormal set

$$\langle \phi(t), \phi(t-n) \rangle = \delta(n) \tag{6.31}$$

4. $\psi(t)$ is zero-mean:

$$\int_{-\infty}^{+\infty} \psi(t)dt = 0 \tag{6.32}$$

5. $\psi(t)$ is normalized to unity:

$$\int_{-\infty}^{+\infty} |\psi(t)|^2 dt = 1 \tag{6.33}$$

6. The set of $\psi(t)$ and its integer translates forms an orthonormal set

$$\langle \psi(t), \psi(t-n) \rangle = \delta(n) \tag{6.34}$$

7. Subspace $V_j$ is orthogonal to $W_j$:

$$\langle \psi(t), \phi(t-n) \rangle = 0 \tag{6.35}$$

An additional condition imposed is that the wavelet function exactly fits a polynomial of a certain degree. This degree is directly related to the vanishing moments of the wavelet.

$$\int_{-\infty}^{+\infty} t^k \psi(t)dt = 0 \qquad \text{for } 0 \leq k < p \tag{6.36}$$

The vanishing moments of the wavelet determines how well it can capture the regularity of $f$. It can be proved that if $f$ is regular and $\psi$ has enough vanishing moments then the wavelet coefficients $[\langle f, \psi_{j,k} \rangle]$ are small at fine scales.

Using the dilation equation (6.26) and the above conditions, we can arrive at conditions on the coefficients $c[n]$ and $d[n]$. For implementation purposes, we are concerned with FIR filters. The associated filters can be then obtained as:

$$h[n] = \frac{c[n]}{\sqrt{2}} \qquad g[n] = \frac{d[n]}{\sqrt{2}} \tag{6.37}$$

$$\tilde{h}[n] = h[-n] \qquad \tilde{g}[n] = g[-n] \tag{6.38}$$

where the pairs $(h[n], g[n])$ and $(\tilde{h}[n], \tilde{g}[n])$ are the analysis (transformation /decomposition) and synthesis (reconstruction) filters respectively. Additionally, for the case of conjugate mirror filters,

$$g[n] = (-1)^{1-n} h[1-n] \tag{6.39}$$

The first set of orthonormal wavelets that appeared were the Haar wavelets (Haar 1910) described by the wavelet filters used at the beginning of Section 6.3,

$$\psi(t) = \begin{cases} 1 & 0 \leq t < \frac{1}{2} \\ -1 & \frac{1}{2} \leq x < 1 \\ 0 & \text{otherwise} \end{cases} \tag{6.40}$$

whose scaling function is,

$$\phi(t) = \begin{cases} 1 & 0 \leq t < \frac{1}{2} \\ 0 & \text{otherwise} \end{cases} \tag{6.41}$$

The Haar wavelet is related to the scaling function as:

$$\psi(t) = \phi(2t) - \phi(2t-1) \tag{6.42}$$

The Haar basis is special in the sense they were the first orthogonal wavelets to appear and are simple to comprehend. It is probably the only wavelet basis for which an explicit formula exists. Unfortunately, it is not so in general for most wavelet functions. Usually only an equation of the form given in (6.28) is given. On the other hand, the Haar wavelet is not suitable for description of smooth functions. However, it is very useful for detecting sharp/abrupt changes in the signal. The Haar filter is the only real compactly supported conjugate mirror filter that has a linear phase.

Daubechies wavelets were the first orthogonal and compactly supported smooth wavelets that appeared in the literature due to a pioneering work by Daubechies (1988). Daubechies wavelet filters exist for different number of coefficients. The number of coefficients for each filter is equal to $2p$ where $p$ is the number of vanishing moments of that wavelet. With $p = 1$, we obtain the Haar wavelets. Figure 6.9 shows the sketch of Daubechies' wavelets for different vanishing moments. Notice how the smoothness increases as $p$ increases. So far, we have discussed the decomposition or the analysis using wavelet filters. However, what constitutes MRA is the reconstruction of the original signal from their transformation using the synthesis filters. This is the inverse wavelet transform (IWT). With conjugate mirror filters, we attain perfect reconstruction of the original signal using FIR filters (Smith and Barnwell III 1986, Vetterli 1986). The algorithm for both wavelet transformation and reconstruction is reviewed in the next section with illustrative examples. The term *decomposition* is sometimes used synonymously with the therm *transformation*. However, strictly speaking, the decomposition step first involves transformation and then the reconstruction of the components in the individual frequency bands.

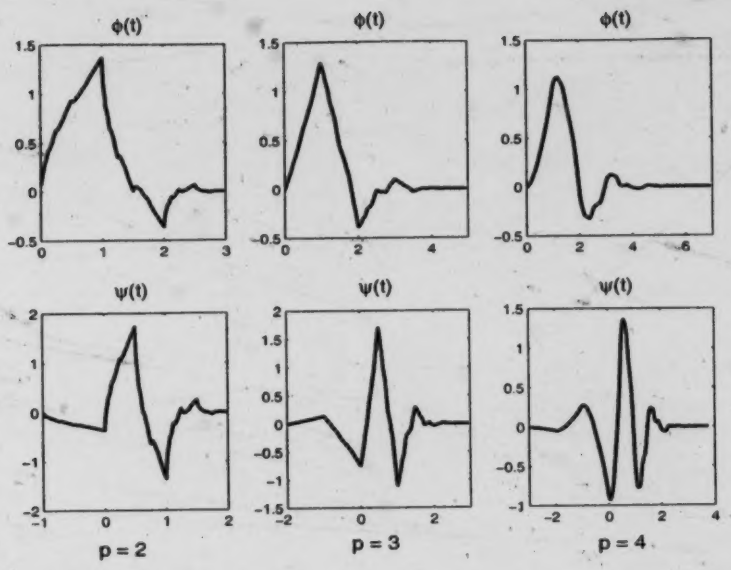


Figure 6.9: *Daubechies scaling function $\phi$ and wavelet $\psi$ with p vanishing moments*

### 6.3.3 Fast Orthogonal WT and IWT

In this section, we review Mallat's fast algorithm (Mallat 1989) for orthogonal wavelet transforms and inverse wavelet transforms.
Define,

$$f(t) = \sum_{k=-\infty}^{+\infty} a_0[n]\phi(t-k) \tag{6.43}$$

Since $\{\phi(t-k)\}_{k\in Z}$ is orthonormal, in general,

$$a_j[n] = \langle f(t), \phi_{j,k}\rangle = f \star \bar{\phi}(k) \tag{6.44}$$

The associated discrete wavelet coefficients are then defined as,

$$d_j[n] = \langle f(t), \psi_{j,k}\rangle \tag{6.45}$$

In the last equation, $d_j[n]$ is non-zero only for $j > 0$.

A fast wavelet transform decomposes successively each approximation or successively projects $f$ as $P_{V_j}f$ into a a coarser approximation $P_{V_{j+1}}f$ plus $P_{W_{j+1}}f$, the projection onto the wavelet space. The reconstruction proceeds in the opposite direction, combining both the spaces into a space with higher time-resolution. Denoting $\bar{x}[n] = x[-n]$ and

$$\tilde{x}[n] = \begin{cases} x[p] & \text{if } n = 2p \\ 0 & \text{if } n = 2p+1 \end{cases} \tag{6.46}$$

Then the following Theorem due to (Mallat 1989) prescribes the algorithm for the wavelet transform (decomposition) and the inverse wavelet transform (reconstruction).

**Theorem 9** *At the decomposition,*

$$a_{j+1}[p] = \sum_{n=-\infty}^{+\infty} h[n-2p]a_j[n] = a_j \star \bar{h}[2p] \tag{6.47}$$

$$d_{j+1}[p] = \sum_{n=-\infty}^{+\infty} g[n-2p]a_j[n] = a_j \star \bar{g}[2p] \tag{6.48}$$

*At the reconstruction,*

$$a_j[p] = \sum_{n=-\infty}^{+\infty} h[p-2n]a_{j+1}[n] + \sum_{n=-\infty}^{+\infty} g[p-2n]d_{j+1}[n] \tag{6.49}$$

$$= \tilde{a}_{j+1} \star h[n] + \tilde{d}_{j+1} \star g[n] \tag{6.50}$$

The theorem above shows that the orthogonal wavelet decomposition and reconstruction are performed with discrete convolutions with downsampling and upsampling respectively. The upsampling (insertion of zeroes) is necessary to cancel the frequency folding (aliasing) created during downsampling (Mallat 1998). For practical implementations of DWT, the original signal is assumed to be at level 0, the finest resolution. Therefore, the set of coefficients $\{a_0\}$ is the original signal.

We consider two illustrative examples. The first example is to compare the properties of Haar and Daubechies wavelet transforms for a function $f(t) = 2 + \sin(\pi t) + 0.6\sin(2\pi t)$. In Figure 6.10, we build a multiresolution approximation of this smooth function with two different wavelets using Haar filters and Daubechies filters (4 coefficients). The decomposition is performed upto level 3, to obtain the scaling coefficients $a_3$ and details $d_3, d_2, d_1$.

The way MRA is performed is that we start from the coarsest approximation and then gradually add details at every level. For a perfect reconstruction of the original signal, we need all the coefficients $a_3, d_3, d_2$ and $d_1$. The coarsest approximation is obtained by reconstructing using $a_3$ and setting $d_1 = d_2 = d_3 = \mathbf{0}$. This yields $A_3$, the component of the original signal in that frequency band. At the next step, we include $a_2$ and $d_2$, setting all the other details to zero to get $A_2$. Next we get $A_1$ and then finally reconstruct the original signal.

Each of the four plots show the original function against approximations $A_3$, $A_2$ and $A_1$. Observe that as we add each level of detail, we gradually approach the true form of the curve. Comparing Figures 6.10 and 6.11, it is clear that the convergence is

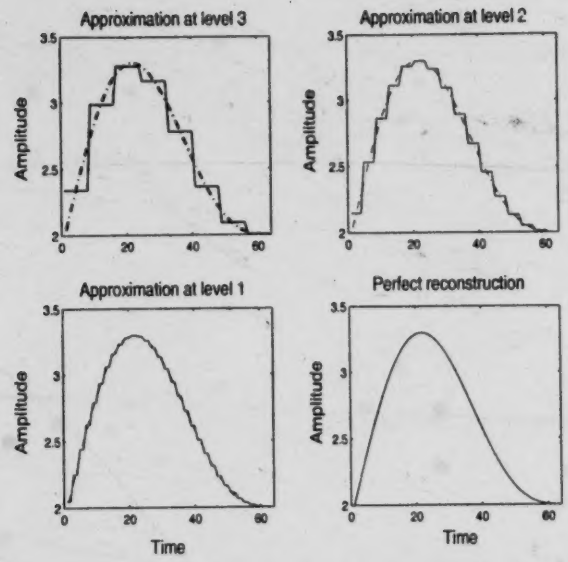


Figure 6.10: *Reconstruction at each level starting from the coarsest level - using Haar basis*

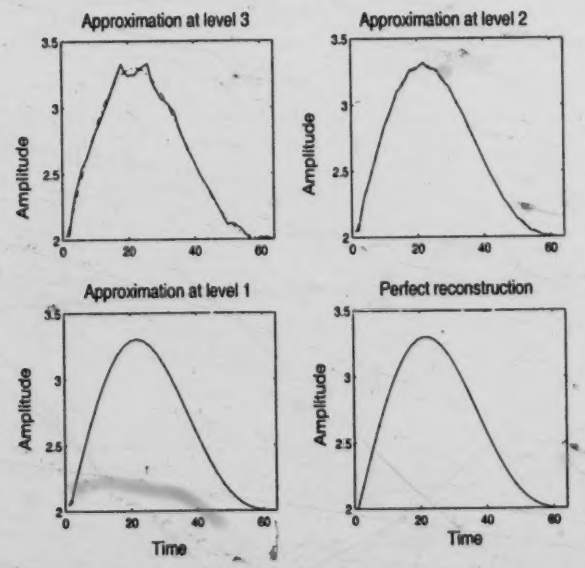


Figure 6.11: *Reconstruction at each level starting from the coarsest level - using Daubechies basis*

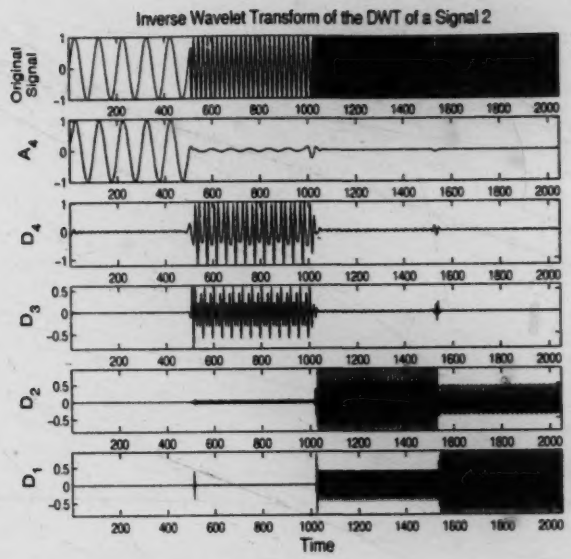


Figure 6.12: *IWT - reconstruction of each component of the wavelet decomposition of signal 2 using D8 wavelets*

much faster with Daubechies basis than with the Haar basis. The convergence rate is indicative of the influence of the number of vanishing moments on the approximation abilities of the wavelet. Here, the difference in the number of vanishing moments is one. In addition, D4 wavelets (Daubechies filters with 4 coefficients) are smooth functions unlike Haar wavelets.

We conclude this next section with the second example that is concerned with the signal 2 used at the beginning of this chapter. A 4-level wavelet decomposition is performed with D8 (Daubechies filters with 8 coefficients). First we show the reconstruction of individual components of the decomposition in Figure 6.12. In other words, we sketch $A_4$, $D_4$, $D_3$, $D_2$ and $D_1$. Then, in a separate plot in Figure 6.13, we show $A_4$, $A_3 = A_4 + D_4$, $A_2 = A_3 + D_3$, $A_1 = A_2 + D_2$, $A_0 = f(t) = A_1 + D_1$.

In the next section, we discuss a few engineering applications particularly useful to process industry.

## 6.4 Application of Wavelets

The applications are mainly categorized into four sections. Many other applications exist, to include all of which is beyond the scope of discussion. Several books have

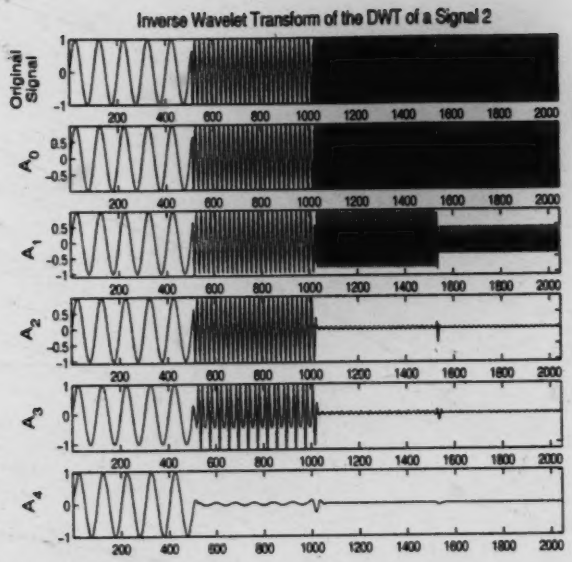


Figure 6.13: *MRA of signal 2 using D8 wavelets*

been written addressing specific applications in this area. Here, we particularly focus on those applications which have close relevance to process applications.

### 6.4.1 Data Compression

One of the most well understood and widely applied application of WT is data compression. Data compression could also mean image compression. The basic idea is to utilize the potential of wavelets in capturing most of the signal information in a small set of coefficients.

Data storage is increasingly growing to be an important issue for data historians. Huge volumes of data are collected every day to document/record routine process operation. The data archive is useful for many purposes such as research, modelling, improved control, performance assessment, process monitoring, etc. Therefore, efficient storage of data is of crucial importance to the industrial community. It is known that there is a strict relationship between the number of bytes needed in the storage of a function and its smoothness.

Process measurements are typically corrupted with sensor noise, measurement noise, process disturbances, *etc.* The dominant signal contains process characteristics, usually in the low frequency bands relative to that of the stochastic component. Using wavelet transformations we can achieve a separation between the dynamic and

the stochastic components of these measurements. In particular, With orthonormal wavelet basis, we know that we can perfectly reconstruct the signal. However, in process industry, typically we are interested in discarding a fair amount of noise while extracting the information pertinent to the dynamic behaviour of the process from the routine data. The dynamic components are typically captured in a few scaling coefficients. By storing the low-frequency scaling coefficients which can typically contain 80-90 % of the signal content, we can achieve a remarkable efficiency in the storage requirements. This is known under the data/image compression problem. If we consider signal 2, the original sequence contains 2048 samples. Then with a 4-level decomposition, the number of samples reduce by a factor of $\frac{1}{2^4} = 16$. The compression ratio can get larger with the number of data samples.

In data compression, we also use the term *quantization* where we restrict the number of possible wavelet coefficients by varying them over a finite (preferably small) set of possible values. The $B$-spline wavelet is particularly useful in this regard. When the concern is only storage, the wavelet coefficients are further compressed methods using Huffman decomposition (Storer 1988). Ideally, we would be able to recreate the original signal given the compressed data, *i.e.*, a lossless compression; otherwise, it is said to be a lossy compression. For the latter case, an objective measure of distortion or the quality of reconstruction is the mean squared value of error signal. However, the drawback with such objective measures is the lack of ability to reflect the magnitude of distortion as perceived by our senses. To overcome this, further work by Jayant and Noll (1984) lead to the characterization of compression as the removal of redundancy and irrelevancy. While the former results in lossless compression, the latter results in lossy compression. The key theoretical result related to the maximal amount of lossless compression possible for a given source is related to the *entropy rate* which is an important concept in information theory (Cover and Thomas 1991).

A benefit of linear compression is that it is still possible to apply many multivariate statistical techniques to the compressed data itself.

### 6.4.2 Wavelet Denoising

The term *denoising* finds its origin in the signal estimation problem. Estimating the underlying signal can be of great value to many applications that are either sensitive to the presence of noise or inapplicable due to a lack of understanding of the underlying signal. The arrival of wavelets have brought in with them a new tool for signal estimation. The principal work by Donoho *et al.* (1995) based on the idea of thresholding and then reconstructing the signal is instrumental to the widely

implemented wavelet denoising algorithm.

Most of the noise present in process measurements takes its seat in the higher frequency bands or at the finer scales. Filtering is a well-known technique for extracting the underlying signal. However, conventional filtering results in discarding these wavelet coefficients. This can be detrimental in many situations where the finer scales carry the information on abrupt changes in the process, sudden sensor failures, edge information, *etc.* To avoid complete disposal of wavelet coefficients (Donoho *et al.* 1995, Donoho 1995) introduced a thresholding method in which the wavelet coefficients below a certain thresholding are set to zero. There are two kinds of thresholding: (1) *soft* thresholding and (2) *hard* thresholding. Soft thresholding leads to less distortion of the object of interest.

Several methods have been suggested to compute the threshold. A common approach is to compute the sample variance of the coefficients in a particular frequency band and set the threshold to a multiple of the standard deviation, $\sigma$. The general procedure to denoise a deterministic signal contaminated by stationary stochastic errors can be described as a three-step method:

1. Decompose measured data on a selected family of basis functions
2. Eliminate wavelet coefficients at finer scales that are smaller than a selected threshold
3. Reconstruct the rectified signal

The *Visushrink* method determines the threshold at unit scale as

$$\gamma_j = \sigma_j \sqrt{2 \log N} \tag{6.51}$$

where $\sigma_j$ is the standard deviation of the errors at scale $j$, $N$ being the length of the signal. The IWT of the scaling coefficients along with the thresholded coefficients gives the denoised signal. The higher the threshold, the better the noise removal. The statistical properties of this approach have been studied by Donoho *et al.* (1995). The factor $\sqrt{2 \log N}$ is included in equation (6.51) to improve the appearance of the rectified signal. The reason is that for uncorrelated Gaussian errors $e_i$, the probability of not eliminating a coefficient representing the error decreases as the number of samples increases:

$$\Pr\{\max(|e_i| > \sqrt{\log N})\} \to 0, \quad \mathrm{N} \to \infty \tag{6.52}$$

It is shown by Donoho *et al.* (1995) that the thresholding method gives a nearly optimal estimation of the underlying signal for a wide variety of theoretical objectives

such as various error norms and smoothness. In many practical situations, the variance of the coefficients at each scale is taken to be the variance of errors, $\sigma_j$ and may be estimated by the robust absolute median deviation as:

$$\sigma_j = \frac{1}{0.6745}\text{median}(|d_j|) \tag{6.53}$$

The above equation is valid assuming that in many practical situations, most of the wavelet coefficients in a multiscale decomposition of a measured signal correspond to errors.

Noise removal is always accompanied by some degradation of the underlying signal. Increasing the threshold results in more of the signal component being zeroed out along with the noise. Soft thresholding minimizes the contribution of the residual noise to some extent by reducing the magnitude of the residual noise in the thresholded high-frequency outputs. Also, the number of scales to which the signal is decomposed determines the quality of the signal. contaminating the rectified signals. On the other hand, if the decomposition goes too low in scale, then the details at the coarsest signal may hardly contain any contribution from the errors. The smoothness is highly influenced by the smoothness of the wavelet. Therefore, Daubechies filters are more efficient in maintaining the smoothness than the Haar filters.

Another practical approach for threshold estimation is the cross-validation. In this approach, the measured data is divided into training and testing data. The threshold is selected in such a way that the error is minimized for the testing data. The details of this method is discussed in the work by Nason (1996). The cross-validation method is claimed to give a better rectification, but involves intensive computations since different values of the threshold need to be calculated for selecting the best value.

The above two methods convey the basic philosophy of denoising based on thresholding. The problem of denoising is closely related to another well-known problem - outlier detection. This latter problem is also known as data rectification. In the next section, we discuss the wavelet application to this problem.

### 6.4.3 Outlier Detection

Outlier detection is one of the most common and difficult problems faced by multivariate data analysts in dealing with process data. There are several factors that induce outliers into process data. Unfortunately, these outliers have a great influence on the process modelling capabilities both for control and monitoring. Because of the complexity of the problem, the detection of outliers still remains an open problem. Here, we discuss the application of wavelet thresholding to outlier detection.

Outliers are of two types: *(i)* additive outliers and *(ii)* innovative outliers. Additive outliers affect the measurement level at the time of disturbance and influence model selection and prediction capabilities. Innovative outliers affect the measurement level with a memory and can be generally neglected unless multiple ones are present. Most of the existing methods for outlier detection are cumbersome to use as the number of variables increases. In general, they assume the data is representative of that generated from an ARIMA model. As a result, they are difficult to automate. Wavelet thresholding based outlier detections are in that sense easy to automate and can be extended to multivariate systems easily. Outliers are, by their very nature, localized high-frequency phenomena. If they occurred as anything other than isolated aberrations in the data, they would be considered part of the signal's structure, but not an outlier. In such a case, they are extremely difficult to detect. In the rest of the discussion, we will deal with additive outliers and assume that they are detectable.

The basic idea in wavelet based outlier detection remains the same. We still choose a threshold and reconstruct the signal with the coefficients that pass the threshold test. The reconstructed signal is sometimes called the rectified signal.

Wavelet thresholding for rectification can create spurious features near large changes in the measured signal. This is related to the variation in the wavelet decomposition with the signal translation. One of the approaches that have been suggested to make the wavelet transform invariant to signal translations is that of Mallat and Zhong (1992). However, these methods assume that: *(i)* the batch of data is of dyadic length and *(ii)* the errors are Gaussian. Moreover, if the values at the beginning and end are very different, artificial discontinuities can set in leading to errors in the signal ends. Several extensions to the wavelet-thresholding approach have also been developed for removing other types of errors (von Sachs and Schneider 1996).

Multiscale median filtering proposed by Nounou and Bakshi (1999) takes into account non-Gaussian errors. In the same work, a method for on-line rectification is proposed. The methodology comprises of decomposing the measured data on the selected family of wavelets or wavelet packets in the largest possible window of dyadic length. As new samples are collected, the window is translated so that the most recent sample is at a dyadic location for at least one translated window. As more samples are collected, the window size is increased to the largest possible dyadic length. The assumption is that the nature of random errors does not change over time. The resulting wavelet transform is translationally invariant.

In another development, Bilen and Huzurbazar (2000) consider the problem of detecting outliers in time series data and propose a general framework based on wavelets. Their method is not based on time-series models, and not restricted to data

generated from ARIMA processes. Again, the underlying idea is to use a thresholding approach. In their work, they propose a new estimate for $\sigma_j$ based on the mean absolute deviations from the median of the wavelet coefficients. It is claimed that their method is superior to that of the existing methods or at worse identical in performance to detection tests based on likelihood ratio tests.

Elsewhere, wavelets have been used in econometrics for outlier detection particularly from an economist's point of view (Greenblatt 1994). The method looks at the application of an order statistic outlier test to the most detailed level of wavelet coefficient computed using the Haar wavelet. In general, the Haar wavelet is good because it has good local properties and this application has no need for the greater regularity of smoother wavelets.

### 6.4.4 Process Identification, Control & Monitoring

Compared to the applications discussed so far, wavelets have been more extensively applied to empirical modelling, process control and monitoring. Of these three areas, we are primarily concerned with the application to process monitoring.

It is well known that the quality of empirical model depends on the quality of the measured data used for modelling. Preprocessing or prefiltering is a common approach to eliminate the effects of noise and other less relevant signal features. Since most data contain contributions from multiple scales, multiscale methods are expected to yield better empirical models than those obtained by conventional methods.

In the area of identification, the usual idea is straightforward. Perform wavelet thresholding of the measured data and then employ regression techniques. In Fourier regression, a regression model is built relating the power spectra and a dependent variable. Similarly, the wavelet transform can be used as a pre-processing step prior to regression. Essentially, this is a *scale-dependent* regression. In this way, we can shape the model features in a certain frequency regime. A PLS-based regression technique with wavelet transformation is discussed in Alsberg *et al.* (1997). Other approaches to using wavelet in connection with regression are also available (Engel 1994, Sjoberg *et al.* 1995, Ogden and Parzen 1996). In other developments, wavelets have been used for identification of linearly time-varying systems (cf. Tsatsanis and Giannakis (1993)).

In control, wavelets are combined with existing control design tools to enhance their quality and provide additional features. One of the most popular ones is the Multiscale MPC (MSMPC) (Krishnan and Hoo 1999, Stephanopoulos *et al.* 1998). In (Stephanopoulos *et al.* 1998), the data is first projected on multiple scales and

then, the objective functions, state equations, output equations and constraints on inputs and outputs are transformed into the multiscale domain. The resulting Multiscale MPC satisfies all the input/output constraints given the problem feasibility and satisfies the frequency response specifications on the controlled outputs. In the same work, it is also claimed that MSMPC reduces the computational load through effective mechanisms.

At a higher level of hierarchy in the plant operation, process monitoring is a crucial task. As discussed earlier, process events occur at different times with different frequencies. Wavelets are capable of localizing these faults in an effective way. Wavelet based multiscale methods for Statistical Process Monitoring (SPM) have been recently shown to be very effective in providing enhanced sensitivity towards detecting process faults. One such method is Multiscale PCA (MSPCA) that combines the properties of wavelet and PCA by decomposing each variable on a selected wavelet basis. Following this, thresholding can be introduced as a part of data rectification. Finally, the matrix of coefficients is subjected to PCA which then gives a separate chart for each scale. The individual charts give the detection limits for each frequency band. While abrupt faults usually fall in the high frequency bands, incipient and persistent faults lie in the low frequencies. This effective separation of faults makes MSPCA superior to PCA in many ways (Bakshi 1998, Luo *et al.* 1999, Zhang *et al.* 1999). The next chapter is devoted to discussing the methodology of MSPCA and its theoretical benefits over PCA. In Chapter 8, we present an application of MSPCA to an important industrial problem - the sheet-break diagnosis problem.

## 6.5 Summary

In summary, multiscale systems are a common occurrence and provide a more generalized description of chemical processes. In these systems, events occur with different frequencies at different times. In this context, wavelet transforms are powerful tools for analyzing non-stationary signals. Existing methods extract all frequency bands at the same resolution. In contrast, wavelet transforms give a trade-off between the conflicting time and frequency resolutions as described by Heisenberg's uncertainty principle. WT provide good time resolution for the high frequency and good frequency resolution for the low frequency components of a signal. In this way, they evolve as useful tools and provide effective results when combined with existing single-scale methods for many applications such as data compression, signal estimation, outlier detection, modelling, control and monitoring of processes.

# Chapter 7

# Multiscale Process Monitoring Using Wavelets

**Purpose:** To give a detailed treatment of off-line MSPCA highlighting its key features that are advantageous over conventional PCA.

## 7.1 Introduction

Recent advances in computer technology and instrumentation techniques have enabled us to collect large amounts of data from chemical processes. With the increasing data dimensionality, multivariate statistical tools such as Principal Component Analysis (PCA), Partial Least Squares (PLS), *etc.* have gained much attention in recent years. PCA or PLS can be exploited to express the essential information contained in these measurements using a relatively small number of latent variables, thus reducing the dimensionality of the monitoring problem significantly. The idea of PCA was first introduced by Pearson (1901), and developed by Hotelling (1933). These ideas were further reviewed by Jackson (1980) and Wold *et al.* (1987). In recent years, PCA has been used in the statistical process control area such as process monitoring (Kresta *et al.* 1991), gross error detection (Tong and Crowe 1995), sensor fault identification (Dunia *et al.* 1996), etc.

Statistical Process Monitoring (SPM) via PCA involves the use of Hotelling $T^2$ and $Q$ (also known as Square Prediction Error or SPE) charts. Time-independency and normal distribution of the measurements and residuals of PCA model are required for obtaining the statistical limits for the $T^2$ and $Q$ charts, respectively. In practice, measurements from dynamic chemical processes do not satisfy the assumptions on the measurements resulting in the loss of statistical basis for the $T^2$ charts. However, not enough attention has been paid to these underlying assumptions (Luo *et al.* 1999).

Wise *et al.* (1990) showed that the underlying distribution of data can vary substantially from normality without affecting the results, while autocorrelated measurements would certainly influence the results. Consequently, conventional PCA is not suitable for monitoring dynamic processes due to the presence of non-stationarities and time dependencies.

Wavelet decomposition of a signal results in approximately decorrelated wavelet coefficients of the stochastic part of the signal and a few set of large coefficients containing the trend of the process. Thus, wavelets provide a good separation between the deterministic and stochastic parts of a measured signal (Donoho *et al.* 1995). Typically, measurements from chemical processes are autocorrelated making them unsuitable for SPM by PCA. Conventional PCA is ideally suited for monitoring steady state processes based on the assumption that the measurements are time independent (uncorrelated) and normally distributed. Typically, most of the processes are in dynamic state, with various events occurring such as abrupt process changes, low drifts, bad measurements due to sensor failures, human errors, etc. Data from these processes are not only cross-correlated, but also auto-correlated. Applying steady-state PCA directly to dynamic systems can raise false alarms, making it insensitive to detect and discriminate different kinds of events.

Every event is associated with a certain frequency band according to its power spectrum. Wavelets are emerging tools to decompose a signal into various frequency bands providing simultaneous time-frequency domain analysis. In this work, we combine the potential of wavelets with the congeniality of PCA to monitor dynamic multivariate processes at different scales (frequencies). This multiscale monitoring strategy extends the suitability of PCA to statistically monitor processes based on autocorrelated measurements. Additionally, the resulting PCA models are more sensitive in detecting changes in a process.

It is shown here that this strategy helps in overcoming the shortcomings of conventional PCA by retaining the statistical basis for the monitoring charts. Moreover, since each event occurs over a certain frequency band, MSPCA possesses greater sensitivity in fault detection and process changes.

## 7.2 PCA and Statistical Assumptions

Consider a data matrix (zero-mean, unit variance) $X$ $(m \times n)$, where $m$ is the number of observations, and $n$ is the number of process variables. Then, $X$ can be decomposed

as

$$X = TP^T + E \tag{7.1}$$

where the columns of $P$ $(n \times p)$ are the principal component loadings, and the columns of $T$ $(m \times p)$ are the scores for each observation. The residual term $E$ can be expressed as

$$E = X(I - PP^T) \tag{7.2}$$

PCA methodology involves the computation of the loadings and scores using the covariance matrix of $X$. If the original variables are correlated, it is possible to summarize most of the variability present in the $n$ variable space, in terms of a lower $p$ dimensional subspace ($p << n$). Here, $p$ represents the number of principal components. Two dimensional score plots (usually $T_1$ vs. $T_2$), Hotelling $T^2$ and $Q$ statistics (SPE) are usually used to monitor the process. If the first two principal components can explain a large part of the variance, the two dimensional scores plot provides an intuitive insight into process variations. Any abnormal shift in the process will cause the scores to move out of the confidence limits in the 2-D scores plot. However, the $T^2$ statistic, which contains the information from all PCs retained in the model, may prove a better quantity to monitor when the number of retained PCs is much greater than two. The $T^2$ statistic based on the first $p$ PCs is defined as

$$T^2 = \sum_{i=1}^{p} \frac{t_i^2}{\lambda_i} \tag{7.3}$$

where $\lambda_i$ is eigenvalue of the covariance matrix of $X$. The $T^2$ statistic given in eqn. (7.3) can be considered as an ellipsoid in a $p$-dimensional space. Confidence limits for $T^2$ at confidence level $(1 - \alpha)$ relates to the $F$-distribution as follows:

$$T^2_{m,p} = \frac{(m-1)p}{m-p} F_{p,m-p} \tag{7.4}$$

where $F_{p,m-p}$ is the upper $100\alpha\%$ critical point of the $F$ distribution with $p$ and $(m - p)$ degrees of freedom.

Variations in the process could be associated with the breakdown of the correlation structure among the measured variables while still within the confidence regions of $T^2$ charts. For this reason, monitoring the process only via $T^2$ charts alone is not sufficient. To overcome this problem, SPE charts are usually used together with $T^2$ charts.

Let $x_i$ $(1 \times n)$ denote the $i^{th}$ multivariate observation whose corresponding score is $t_i = x_i P$. The prediction from PCA model for $x_i$ is given by $\widehat{x}_i = t_i P^T = x_i P P^T$. The $p$ dimensional error vector is given by $e_i = x_i - \widehat{x}_i$. The SPE is then defined as

$$SPE = e_i e_i^T \tag{7.5}$$

SPE can be considered as a measure of the plant-model mismatch. The confidence limits for SPE are given by Jackson and Mudholkar (1979). This test suggests the existence of an abnormal condition when $SPE > Q_\alpha$, where $Q_\alpha$ is defined as:

$$Q_\alpha = \Theta_1 \left[ 1 + \frac{c_\alpha h_0 \sqrt{2\Theta_2}}{\Theta_1} + \frac{\Theta_2 h_0 (h_0 - 1)}{\Theta_1^2} \right]^{\frac{1}{h_0}} \tag{7.6}$$

where

$$\Theta_i = \sum_{j=p+1}^{n} \lambda_j^i; \quad for\ i = 1, 2, 3 \tag{7.7}$$

$$h_0 = 1 - \frac{2\Theta_1 \Theta_3}{3\Theta_2^2} \tag{7.8}$$

$c_\alpha$ is the confidence limits for the $1 - \alpha$ percentile in a normal distribution.

Note that the confidence limits calculated in equations. (7.4) are based on the assumptions that the measurements are time independent and normally distributed in the multivariate sense. The confidence limits in (7.6)-(7.8) were derived assuming that errors are random with zero mean and Gaussian distribution. In practice, the underlying distribution of the residuals and the scores can vary substantially from the Gaussian assumption without affecting the results due to the central limit theorem (Wise *et al.* 1990). The highly autocorrelated data would certainly affect the confidence limits for $T^2$ chart. On the other hand, improper choice of number of PCs retained in the model may lead to the autocorrelated residuals, which will influence the confidence limits for SPE chart.

In order to account for the autocorrelation among measured variables, dynamic PCA (DPCA) was proposed by Ku *et al.* (1995). The dynamics are accounted for by including the lagged variables in the data matrix. However, the dynamic PCA model suffers from certain drawbacks. Firstly, the order of the process and the associated time delay are usually unknown quantities. Time delay estimation of chemical processes is quite difficult in practice. Therefore, the lagged data matrix in many situations may not capture the true dynamics of the process.

Equally important to note is that the incorporation of lagged variables does not aid in obtaining scores that are decorrelated. Thus, the assumption of time independency

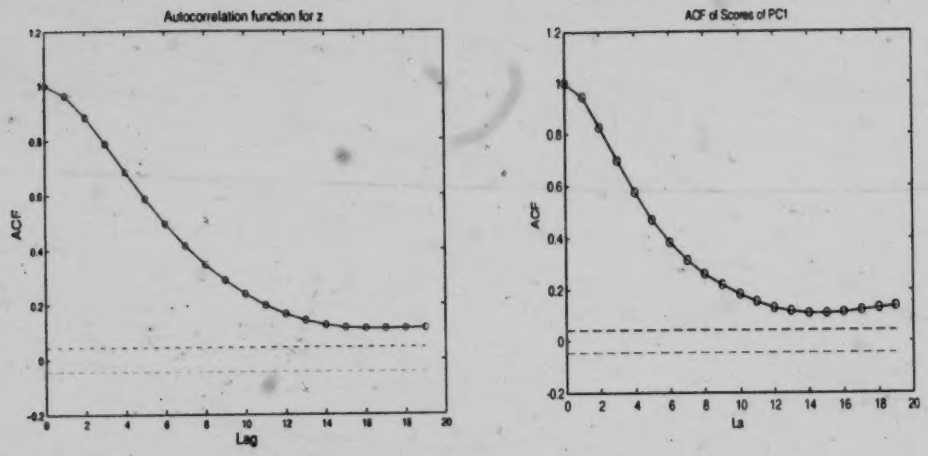


*(a) Autocorrelation function for z* *(b) Autocorrelation function for PC-1*

Figure 7.1: *ACF plots of z and the scores from PCA*

is still violated hence invalidating the statistical basis obtained with the dynamic PCA model.

We illustrate this point by means of an example where the autocorrelated measurements: $u$, $z$ and $p$ are given by

$$u(k) = 0.7u(k-1) + w(k-1) \tag{7.9}$$

$$z(k) = 0.8z(k-1) + 0.3u(k-1) \tag{7.10}$$

$$p(k) = 0.5p(k-1) + 0.2u(k-1) \tag{7.11}$$

where $w(t)$ is the white noise with unit variance. The data matrix, $X$ for a steady-state PCA analysis is arranged as follows:

$$X = [u(k)\ z(k)\ p(k)] \tag{7.12}$$

The autocorrelation function (ACF) of $z$ is shown in Figure 7.1(a). The strong autocorrelated feature indicates the strong time-dependence of the data. Consequently, the first PC also exhibits significant autocorrelation as shown in Figure 7.1(b). In this case, statistical control limits obtained for the $T^2$ chart based on the time independency assumption are not valid. In order to account for the dynamics/autocorrelation, we consider the lagged data matrix for the dynamic PCA model given in Ku *et al.*

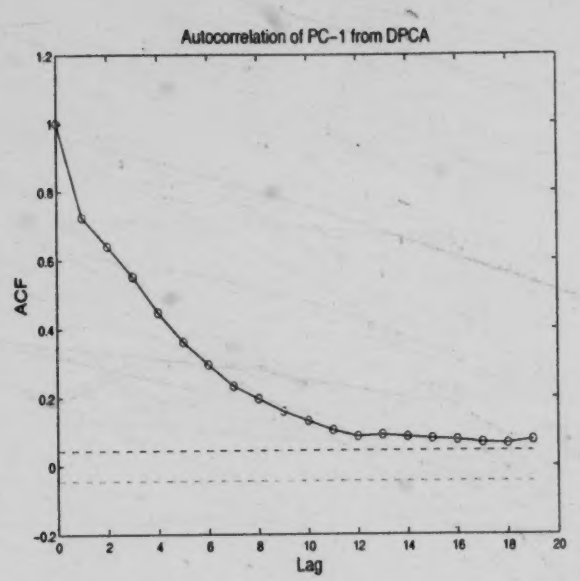


Figure 7.2: *Autocorrelation function of PC-1 from DPCA*

(1995):

$$X = [u(k)\ z(k)\ p(k)\ u(k-1)\ z(k-1)\ p(k-1)] \tag{7.13}$$

However, as shown in Figure 7.2 the first principal component still exhibits time-dependency. The autocorrelation in the scores are not eliminated by including the lagged variables. However, the inclusion of lagged variables can be useful for system identification purposes. Since any process measurement from a dynamic process invariably contains autocorrelation, total elimination of autocorrelation in the scores is not possible. Nevertheless, one can separate the correlated dynamics from its stochastic counterpart and then build PCA models separately for each component. This is the basic philosophy of MSPCA. The following section discusses this philosophy in detail.

## 7.3 MSPCA for Dynamic Process Monitoring

### 7.3.1 Philosophy

Measured variables from a dynamic process may contain contributions from several events, such as process dynamics, sensor noise and fault, parameter drifts, and operator-induced actions. Every event has its own frequency and time features. For

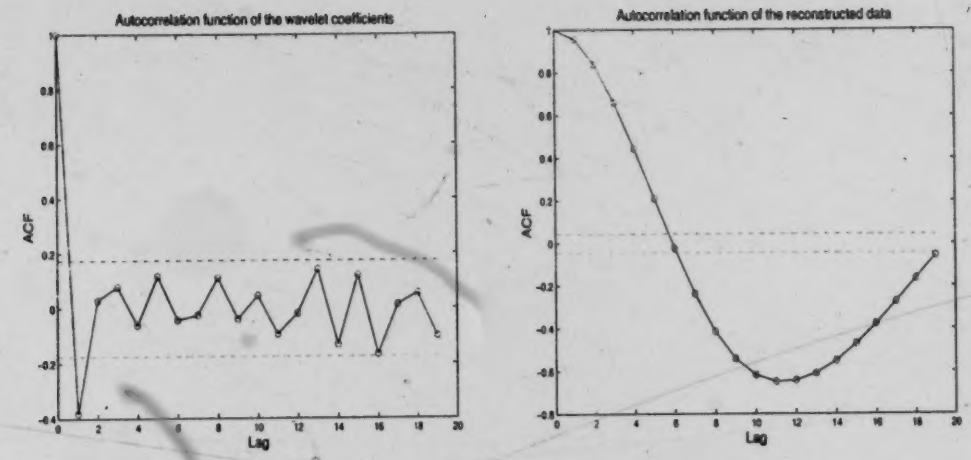


*(a) Autocorrelation function of the wavelet coefficients $d_{4,z}$*

*(b) Autocorrelation function of reconstructed data from $d_{4,z}$*

Figure 7.3: *ACF plots of wavelet coefficients and their reconstruction*

instance, components of measurement noise are mainly localized in the high frequency band, while basic process dynamics are mainly localized in low frequency band. Since the data from practical processes are multiscale in nature, analyzing a process signal over various frequency ranges or scales may provide a multiscale, hierarchical description of the signal (Bakshi and Stephanopoulos 1994). Consequently, PCA models built on wavelet transformed data at various scales or frequency bands would have some advantages.

Each PCA model at a certain scale can be expected to have more ability to detect the events whose spectrum is most significant at that scale. Here, PCA models are based on the wavelet coefficients rather than the reconstructed data over certain frequency bands. The benefit of monitoring the wavelet coefficients is that these coefficients contain no significant correlation, while the reconstructed data still retains some time-dependent features. These issues are illustrated using the data generated in the earlier example. A 4-level wavelet transformation of the data is carried out yielding the representation of the signals over 5 frequency bands ($a_4$ and $d_1$ to $d_4$). Figure 7.3(a) shows the ACF of the wavelet coefficients $d_{4,z}$ and the corresponding reconstructed data. This figure illustrate the decorrelating ability of wavelet transforms. Notice that the reconstructed signal still contains significant correlation.

The idea of multiscale PCA is to build individual models based on the wavelet

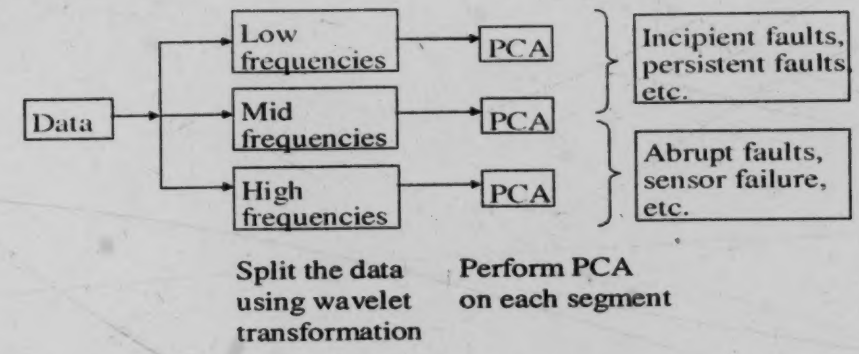


Figure 7.4: *Typical illustration of the MSPCA methodology*

coefficients at each scale. A typical methodology is illustrated in Figure 7.4 where we break up the data into three bands - low, medium and high frequency bands followed by feature extraction using PCA. The PCA model at each scale provides a breakdown of the signal pattern in that frequency band. Consequently, MSPCA is expected to be more sensitive to abnormal events than conventional PCA. Off-line MSPCA involves the pattern search for an abnormal event in one or more frequency bands. In the on-line MSPCA, the dyadic data length required by wavelet decomposition poses computational problems and can induce detection delays. Recently, Bakshi (1998) has given an effective method for an on-line application of this technique that overcomes the hindrance of data length.

The enhanced sensitivity of MSPCA when compared to DPCA is highlighted in the next section, where we illustrate an application comparing MSPCA and DPCA in detecting a sensor failure over a short period of time.

### 7.3.2 Comparison with Dynamic PCA

Consider our earlier example in equations (7.9)-(7.11). A sensor failure is simulated by introducing a sudden mean shift of magnitude 1.0 in $z$ between sample times 200-800.

The SPE and $T^2$ charts obtained using dynamic PCA are shown in Figures 7.5(a) and 7.5(b), respectively, where we have employed the same lagged data matrix as in equation (7.13). Both the charts fail to detect the sensor fault. A slight indication is given by the SPE chart; however, it is hard to draw any inferences based on the chart.

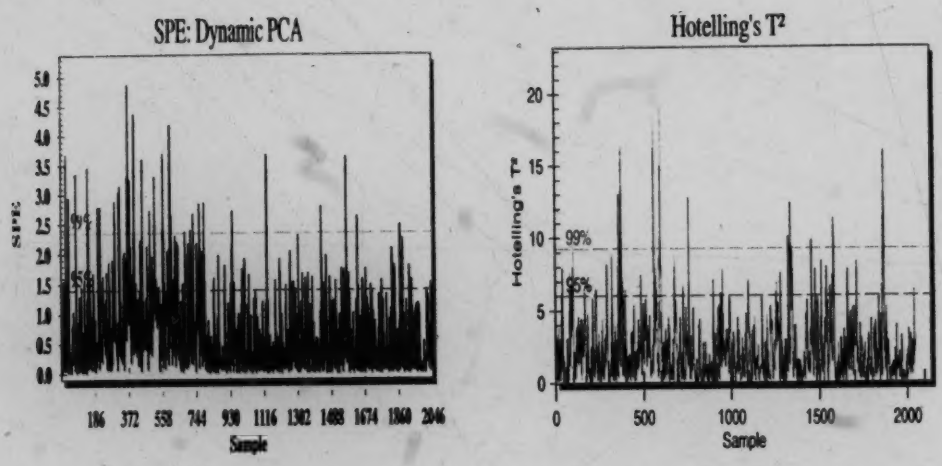


*(a) $T^2$ plot from DPCA*

*(b) SPE plot from DPCA*

Figure 7.5: *Results from DPCA*

Since sudden changes in processes contain mainly high frequency components, the beginning and end of abrupt events are expected to reflect in the PCA model based on the wavelet coefficients at a finer scale (first level of decomposition). The SPE chart shown in Figure 7.6(b) clearly indicates this point. Adjacent to this figure is the $T^2$ chart with MSPCA at finer scale is shown as well but it is insensitive to such a change. A note of caution is required while interpreting the time axis in the monitoring charts obtained using PCA on wavelet coefficients. At finer level, the time resolution is halved and therefore should be doubled when going back to the original time domain.

While the wavelet coefficients at finer level (the highest frequency band) are primarily sensitive to sudden changes, the ones at the lower frequency bands detect the persistence in the fault. For this purpose, we make use of the $T^2$ and SPE charts using the coefficients at the coarser levels. Here, we only show the charts using the coarsest level coefficients. Figure 7.7 contains the SPE and $T^2$ charts corresponding to the coarsest level (lowest frequency band) of wavelet transformation. The SPE chart is clear in showing the persistence of the fault while the $T^2$ chart is insensitive to the fault. Since the original signals have been decomposed to four levels (5 frequency bands) in this example, we need to multiply the time index in the Figure 7.7 by $2^4$ to get the interval of fault persistence in the original time domain. The ACF of wavelet coefficients at the coarsest level is shown in Figure 7.8. The scaling function

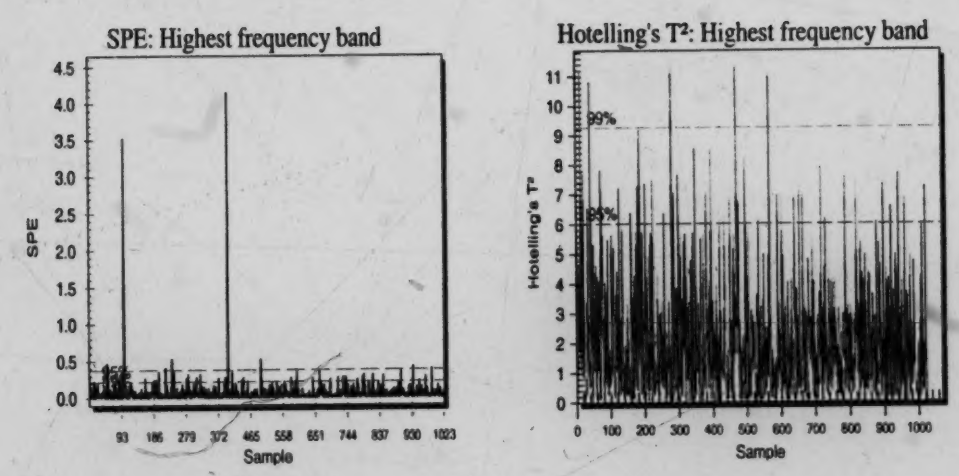


*(a) SPE plot from MSPCA* *(b) $T^2$ plot from MSPCA*

Figure 7.6: *Results from MSPCA - highest frequency band*

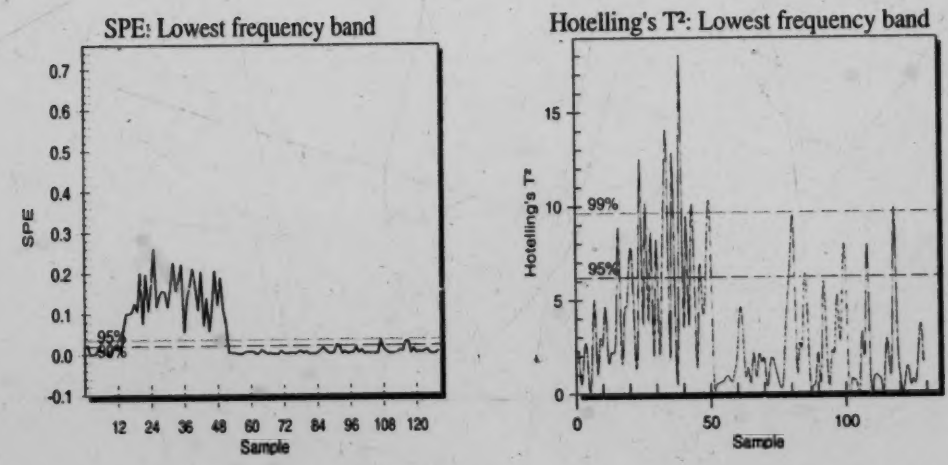


*(a) SPE plot from MSPCA* *(b) $T^2$ plot from MSPCA*

Figure 7.7: *MSPCA - lowest frequency band; SPE chart clearly captures the fault*

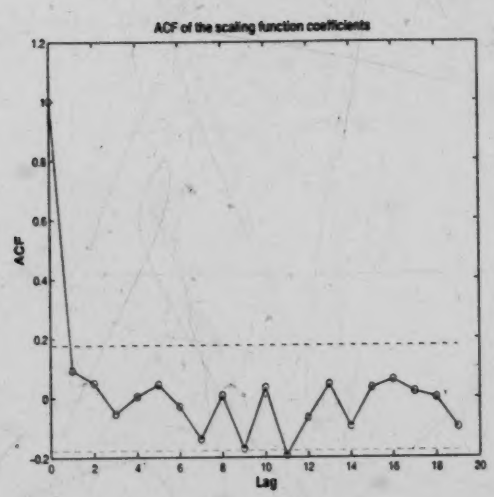


Figure 7.8: *ACF of the scaling function coefficients - approximately decorrelated*

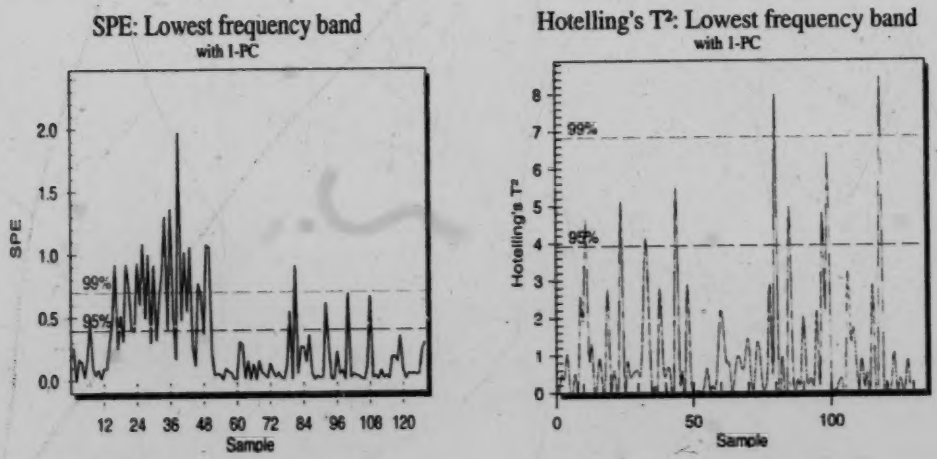


*(a) SPE plot from MSPCA*

*(b) $T^2$ plot from MSPCA*

Figure 7.9: *MSPCA - lowest frequency band; 1-PC SPE is unable to capture the persistent fault*

coefficients (lowest frequency coefficients) at this level are almost decorrelated. Thus, the confidence limits for the monitoring charts can be correctly calculated in this case, providing a sound statistical criteria to detect an abnormal event.

An important observation to be made for the lowest frequency band is by the comparison of situations in Figures 7.7 and 7.9. In the former case, 2-PCs were chosen (which explained 99.82%) to be included in the model, whereas in the latter, only 1-PC which explained 96.4% of the variance. In the latter case, both the SPE and $T^2$ charts fail to detect the fault unequivocally. In fact, Figure 7.9 indicates that one has to be careful in choosing the number of principal components for correctly showing the fault in the SPE chart. At this level since the coefficients are almost noise-free, the 80% criteria for choosing the number of PCs cannot be conveniently applied as in the highest frequency band which mainly represents noise. Note that in this case, 2-PCs are chosen keeping in mind that there are two linear relationships present in the model. The underlying message here is that in practice, one has to be cautious in deciding on the number of PCs at the coarsest level and make best use of the *apriori* information that is available.

## 7.4 Conclusion & Discussion

The underlying assumptions of applying PCA have not received enough attention in the past years. Since most industrial processes are dynamic systems, the measurements are usually time dependent. Results of applying PCA to monitoring these systems will be severely affected without taking into account the time-dependency of the measurements. Wavelet transformation of measurements result in signals with no significant correlation. Monitoring charts with PCA models based on the transformed data comply with the underlying statistical assumptions. Furthermore, we have shown by example that MSPCA is more sensitive to small disturbances than dynamic PCA .

Typically, the wavelet coefficients at the coarsest level would primarily contain the deterministic part of a signal while the higher frequency bands contain mainly the stochastic part. In this example, it is a matter of coincidence that the wavelet coefficients at the coarsest level are approximately decorrelated as well. In practice, for reasons mentioned above, the confidence limits for the charts in Figure 7.7 may not be valid. In such a case, we could monitor deterministic or low-frequency changes with heuristics based on process knowledge. This point is clearly illustrated in the ensuing chapter on an application to detection of sheet-breaks in a major pulp and paper mill.

In this work, we have discussed the issues involved in conventional PCA and a way to overcome some of the drawbacks therein. Extensions of off-line MSPCA to on-line MSPCA is possible with some enhancements in the methodology (Bakshi 1998).

# Chapter 8

# Application of Multiscale PCA to Sheet Break Diagnosis

**Purpose**: to illustrate the power of combining an innovative tool such as MSPCA with process knowledge in the detection of process problems.

Multiscale Principal Component Analysis (MSPCA) is an emerging multivariate statistical data analysis tool for fault detection and isolation. It is a result of the combination of wavelets, the emerging signal processing tool, with a widely familiar fault detection technique, PCA. Sheet breaks have attracted increasing attention among the industrial pulp and paper community for several reasons. Economically, they can degrade the efficiency of production and increase downtimes. In addition, they also pose a safety risk for plant personnel. With this motivation, in this chapter we show the capability of MSPCA in diagnosing the sheet break problem involved with a world scale paper producer. The MSPCA methodology involves breaking up data into different frequency bands of interest and then performing PCA on each of these bands. Use of available process knowledge is made wherever appropriate.

## 8.1 Introduction

The paper production process is complex and intricate due to the influence of several variables in the consistent and successful formation of a sheet. The mode of influence of all the variables in such a process is far too complicated to be explicitly assessed using process knowledge alone. Nevertheless, a great deal of process behaviour and variable interaction can be understood by a thorough analysis of process measurements. In this respect, multivariate data analysis has played a key role in process industry especially in the areas of process monitoring and control loop performance assessment. Besides, with the increase in on-line data acquisition systems in manu-

facturing processes, the collection of process data during production runs is becoming routine. With the enormous amount of stored data rich in process information far from being utilized to its full potential, there is a strong need for the blending of multivariate data analysis with process knowledge.

It is of increasing importance both to the academic community and industry that the tools developed in the research division are translated to useable technology that is able to identify important causal relationships between breaks and historical process data. In this work we demonstrate the potential that lies in a blend of multivariate data analysis with process knowledge in solving process problems.

This present work is concerned with the off-line diagnosis of sheet-breaks occurring in a major pulp and paper mill. Off-line diagnosis is appealing mainly because, from a process benefit point of view, it is certainly meaningful and economical to eliminate causes for failure and thus streamline the process. In this way a significant portion of the process bottlenecks can be eliminated by careful off-line analysis resulting in relatively trouble-free process operation.

The results presented here are from a preliminary analysis of the enormous amount of data that was collected as a part of this project. Although the present analysis is mainly diagnostic in nature, our experience with MSPCA and the citations in the literature encourage us to believe that with additional work and quality data, an on-line process monitoring scheme can be constructed.

This chapter is organized as follows. Section 8.2 presents our motivation behind the project and this paper. Section 8.3 gives a substantial description of the problem of interest. Sections 8.4 and 8.5 cover the analysis of the results obtained by applying MSPCA to the sheet-break problem. Conclusions are given in Section 8.6.

## 8.2 Motivation

The issue of sheet break reduction is one of considerable interest to pulp and paper manufacturers. Sheet break is a significant contributor to lost market opportunity as well as increased downtime and greater operating expense. Besides these factors, the motivation for this work comes from the fact that sheet breaks are associated with a myriad of problems including decreased reliability and efficiency of pulp production, large financial cost, impaired paper quality control, safety concerns for plant personnel, etc. A pulp mill in Alberta, for example, reported a total of seventeen sheet-breaks in one month at an average cost of $25,000 per break. In more extreme cases, paper machines sheet-breaks have been documented to cause downtime in excess of two to four hours at a cost of up to $40,000 per hour. On higher-grade

machines, the cost may be greater.

Based on the magnitude of this problem in the industry and the tremendous ROI (return on investment) associated with the prevention of sheet breaks, there has been a significant amount of research carried out in this area both in academia and industry. It is important to note, the focus of research in this area is only on breaks related to, or caused by slow process excursions or incipient upsets.

From an engineering point of view, the enormity and complex variability of a paper manufacturing process involves contributions from several events, such as process dynamics, sensor noise and fault, parameter drifts, operator-induced actions, etc. Every event can be associated with different time-frequency zones (scales). For instance, components of measurement noise are mainly localized in the high frequency band, while basic process dynamics are mainly localized in low frequency band. Similarly, sudden and/or short-lived faults such as machine breakdown, sensor failure, etc. live in the high-frequency domain while long-lived abnormalities such as persistent faults, equipment degradation, process drifts, etc. are located in the low-frequency regions. Due to this inherent multiple time-frequency scales, it is natural to analyze process signals over various frequency ranges or scales in a multiscale, hierarchical descriptive framework (Bakshi and Stephanopoulos 1994).

Multiscale analysis of signals is related to signal spectral separation and study of the effects of such signals in different time-frequency scales within a system. In this regard, wavelet filters (Morlet *et al.* 1982, Daubechies 1988, Mallat 1989, Daubechies 1990) have emerged as powerful tools, and have been widely used in several disciplines of engineering for over a decade now. While the raw measurements present no clear picture of the spectral content, Fourier transforms of these measurements reveal excellent spectral information, but with a loss of information on variations in time domain. Wavelet transforms with certain attractive properties strike a compromise between these two representations by achieving a trade-off between the time and frequency resolutions. They are capable of separating the stochastic and deterministic parts of a signal by means of what is termed as multiscale decomposition or multiresolution analysis (Mallat 1989).

In mill-wide process monitoring systems, the ability to reduce data storage requirements is of great benefit. For this purpose, wavelets are being widely used as powerful data compression tools. Other applications to the pulp and paper industry include the work of Nesic *et al.* (1980) and Keller *et al.* (1999). This representation allows improved estimation and visualization of the machine direction and cross machine variations. Other areas of wavelet applications are signal estimation, image processing, estimation of missing data, outlier detection, etc.

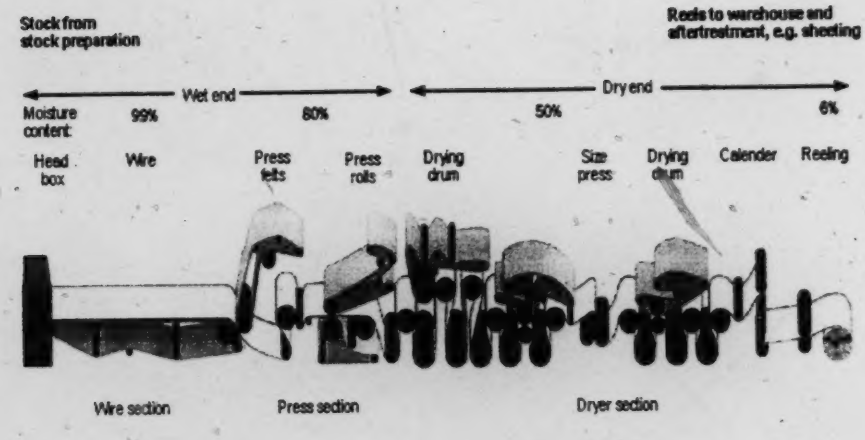


Figure 8.1: *Typical flowsheet of a paper machine*

More importantly, wavelets have a strong potential as a beneficial data preprocessing tool for fault detection and diagnosis by providing useful insights into process characteristics. In this work, their potential is combined with the powerful ability of PCA to project measurements onto an orthogonal subspace with reduced dimensionality. PCA is amongst the most popular methods for extracting information or features from process measurements, and is applied extensively in a wide range of disciplines. In process operations and control, PCA is used to carry out data rectification, gross-error detection, disturbance detection and isolation, statistical process monitoring (SPM) and fault detection and diagnosis. In this regard, it has been shown by Zhang *et al.* (1999) and Bakshi (1998) that a combination of wavelets with PCA, termed multiscale PCA (MSPCA), has conceptual advantages over conventional, single-scale PCA.

With this motivation, we state the objectives of this work: (1) to uncover causes of breaks purely from a data analysis perspective, by analyzing massive volumes of data of a plant seated thousands of miles away from the mill, (2) to provide a strong ground for the development and installation of a process monitoring tool aimed at the reduction of breaks in the sheets from a paper machine and (3) illustrate the role of wavelet filtering as a tool in providing valuable insights into process characteristics.

## 8.3 Problem description

Figure 8.1 gives a compact sketch of the paper manufacturing unit[1].

[1] `http://www.skogsverige.se/MassaPapper/Faktaom/eng/massaopapptillv/paptillv.cfm`

Paper is produced on large, intricate machines, with the wood fibers introduced into the process as a dilute water mixture, then passing at high speed through a sequence of sheet formation, pressing, drying and finishing steps. The process is complicated by water and fiber recycles, and requires tight control of feed consistency, chemical addition, moisture content, rotation speeds, and tension in order to meet product quality specifications.

One of the main challenges of successful paper machine operation is avoiding breakages in the sheet. When a sheet break occurs (usually without warning), production time is lost, waste material must be recycled, and the sheet must be "re-threaded" manually in order to resume production. This provides strong economic and safety incentives for the mill operators and technical support staff to understand the causes of sheet breaks, in order to modify or control the process to minimize their occurrence. Large volumes of operating data are typically collected and stored electronically, and this work is concerned with the problem of extracting useful information from such data to shed light on sheet breaks in a particular machine.

Sheet breaks occur due to various reasons. Literature highlights a variety of causes (Fisher 1975, Locke 1966, Rochealeau 1965, Mardon *et al.* 1969, Ibrahim 1981, Blimke *et al.* 1995, Li 1997) such as:

- White water re-circulation.
- Broke re-circulation.
- Paper machine stock system instability.
- High moisture profile of the sheet.
- Problems with sheet formation.
- Pulp quality of the stock.
- Wrinkles in the paper sheet.

Breaks are usually classified according to the location of their occurrence. They can occur mainly in the dryer section, couch section, press and wire sections. In Li (1997), the author reports that about 61% of sheet breaks in an 11-month period took place in the dryer section, and various causes of sheet break in the dryer section are clearly explained. Therefore, sheet breaks can be caused by many factors and may also result from the contribution of several factors simultaneously.

The focus in this work is only on those sheet breaks occurring in the dryer section. Again sheet breaks can be classified as wet or dry breaks depending on whether they

occur upstream or downstream respectively. Here, we consider wet sheet breaks in the dryer section, designated "type 4" breaks. In the subsequent discussions, we show by means of an application, the key role that wavelet filtering plays in extracting the dynamics of the process and in complementing the ability of PCA to compress enormous amounts of data into a compact space. Further, since wavelet transformations take into account the time-varying nature of the signal, it suffices to use steady-state PCA for constructing template models.

The following section illustrates the application of MSPCA to the sheet-break data with a detailed analysis.

## 8.4 Data Analysis

### 8.4.1 Objective

Our main objective in conducting this data analysis was to demonstrate the ability of the analytical techniques to locate valuable information in the data, with respect to diagnosing the root causes of sheet breaks.

The data contained a number of on-off sheet break indicator signals, each corresponding to a different location on the paper machine. By visual inspection of these signals, and by comparing the total counts of break types, it was found that breaks in the dryer section, designated "type 4", had the highest occurrence. There were also significant operating periods during which type 4 breaks did not occur. This presented the opportunity to develop a PCA model of break-free operation for comparison with upset conditions

### 8.4.2 Variable Selection and Data Cleaning

The initial data set contained process measurement and controller setpoint and output signals numbering 900 tags, covering the entire paper machine and ancillary equipment. Through a series of steps, as shown in Figure 8.2, the number of tags was reduced to 120, 70, and ultimately 10 key variables.

The initial reduction from 900 to 120 tags was performed by discarding variables known to be downstream of the type 4 break indicator, then discarding all setpoints, all controller outputs with an associated flow measurement, and variables with insufficient information to contribute to the analysis. This last category includes signals with large amounts of missing values, constant signals, and signals that were archived with a wide data compression band. Data compression involves storing a new signal value only when it differs from the previously stored value by a specified amount.

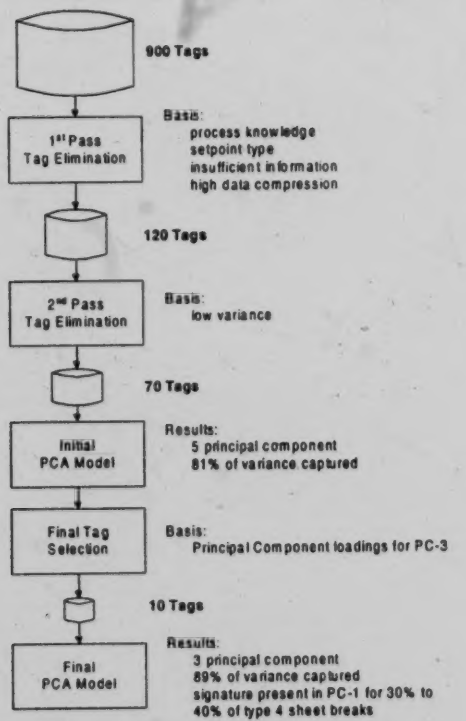


Figure 8.2: *Procedure for data analysis*

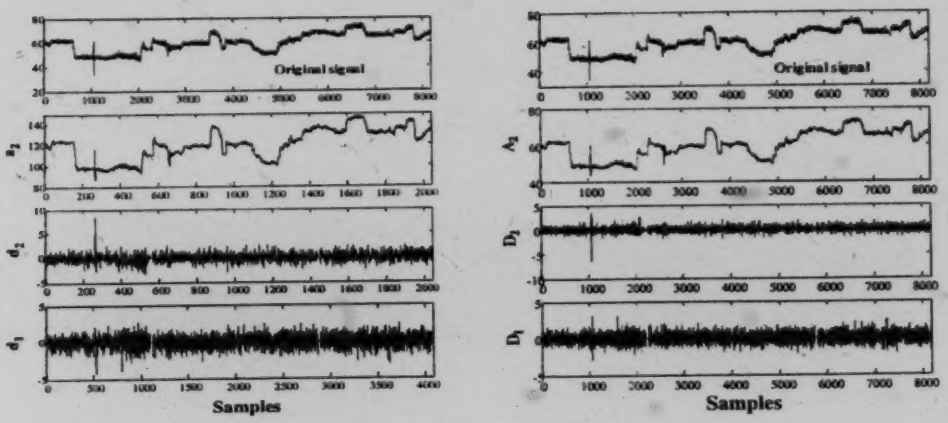


*(a) 2-level wavelet transformation* *(b) 2-level wavelet decomposition*

Figure 8.3: *2-level wavelet transformation and decomposition of a process measurement*

While the intent is to minimize storage requirements, there is a danger that the specified deviation can be so large that most of the useful information in the signal is lost.

By keeping or eliminating variables on the basis of the condition of each signal, it is likely that a number of important variables were excluded from the subsequent analysis. The final results should therefore be considered very preliminary.

### 8.4.3 Wavelet Filtering

The remaining 120 tags were then passed through a wavelet filter to remove the high-frequency variations. All measurements were subjected, using WAVELAB[2], to a 2-level wavelet filtering yielding three non-overlapping frequency bands. Daubechies filter with 6 coefficients was used for this purpose.

The wavelet filtering resulted in a set of coefficients, which were spread over three different frequencies. The lowest frequency coefficients primarily contained contributions from process dynamics and slow process drifts, while the coefficients in the remaining bands contained energies from the stochastic part such as measurement noise, disturbances, etc.

Several filtered signals were found to have low variance, and were rejected from the analysis, bringing the total number of tags to 70. This reduced set of signals

[2]Department of Statistics, Stanford University, `http://playfair.stanford.edu`

made up the input data for the initial principal component analysis.

Figure 8.3 shows the 2-level wavelet transformation and decomposition of a measurement (among the 70 measurements) using Daubechies filter with 6 coefficients. The plots clearly depict the power of wavelets in separating the deterministic and stochastic parts of a real-time signal corrupted with noise. The left panel shows the transformation starting with the high-frequency coefficients at level 1, $d_1$ at the bottom going up to the low-frequency coefficients at level 2, $a_2$. The transformation rightly shows that most of the information (or energy) of the measurement lies in the low-frequency region. Observe how the number of samples reduces by half as one moves across levels. On the right panel is shown the multiscale decomposition of the same measurement. The decomposition is equivalent to passing the original signal through a set of 5 band-pass filters. Signal $A_2$ is obtained by reconstructing only that part of the original signal corresponding to $a_2$ (by setting the coefficients $d_1$ & $d_2$ to zero). Signals $D_1$ and $D_2$ are obtained in a similar fashion. Perfect reconstruction can be verified by checking that the original signal is equal to $A_2 + D_1 + D_2$.

It is of theoretical advantage to use the wavelet coefficients shown in Figure 8.3(a) for the next step of PCA in lieu of the decomposed signal shown in Figure 8.3(b). An additional benefit is that data analysis is conducted on a much smaller number of samples, relative the original sample size, without significant loss of information.

Our implementation of PCA differed from the conventional way in that we performed a two-phase PCA. Further, in both phases we preferred to analyze the scores directly rather than the $T^2$ or SPE charts. The motivation behind this implementation is explained later in Section 8.4.6. It suffices here to note that the first phase of PCA consisted of a data set that contained a normal operating region and a break. The second phase of PCA consisted of data that arose out of only the normal process operation.

### 8.4.4 Initial PCA Model

As mentioned in Section 8.2, the focus of this work is only on the influence of slow process phenomena on sheet breaks. Therefore, only the low-frequency coefficients were chosen for PCA analysis The initial PCA model captured 81% of the variance in the 70 input signals in 5 principal components. Trend plots of the scores for each component were compared with the sheet break signal to see if there were any consistent patterns associated with the breaks. As illustrated in Figure 8.5(a), the third principal component (PC-3) tended to ramp up immediately prior to type 4 breaks. Principal component loadings for PC3 indicated that only 10 tags were significant in

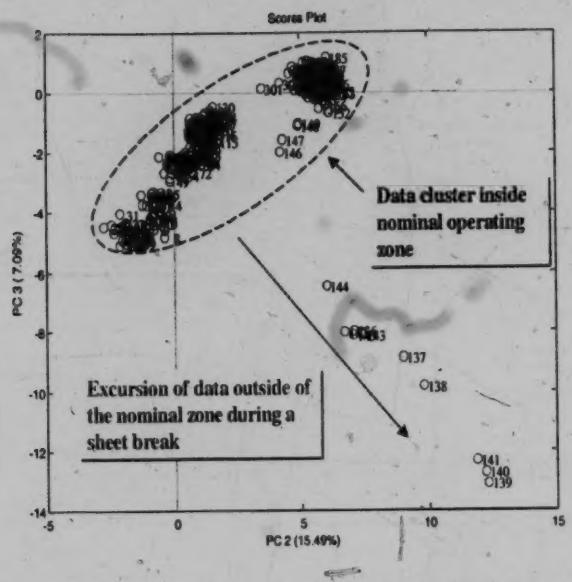
Scores Plot
Data cluster inside nominal operating zone
Excursion of data outside of the nominal zone during a sheet break
PC 3 (7.09%)
PC 2 (15.49%)

Figure 8.4: *MSPCA revealing the process drifts due to a sheet break*

the calculation of this score.

It is interesting to note that PC-3 accounted for only 7% of the total variance observed in the 70 signals, after a cumulative 70% of the variance had already been explained by the first two principal components. The PCA modelling technique removes the variance explained by a given principal component before attempting to find the next principal component in the modified data. This example highlights the ability of PCA to extract valuable information from large amounts of data. In this case 15% of the signals, weighted to represent 7% of the total information in the time domain, yielded a derived signal bearing some relationship to the problem at hand.

The 10 important tags in PC-3 were then used as the input data for the final principal component analysis.

### 8.4.5 Final PCA Model

The final PCA model captured 89% of the variance in the 10 remaining signals in 3 principal components. Scores for PC-1 of the final model were found to move abruptly, either up or down, prior to 30% to 40% of type 4 sheet breaks, as shown in Figure 8.5(b). Principal component loadings indicated that all 10 signals contributed to PC-1. All of the tags were recognized as belonging to a group of closely related variables in a specific area of the plant.

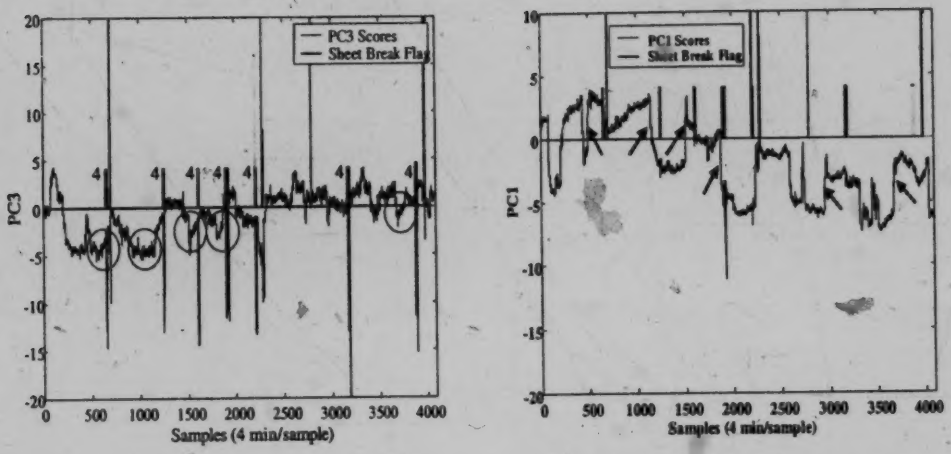


*(a) PC3 scores based on 70-variable PCA model*

*(b) PC1 scores based on 10-variable PCA model*

Figure 8.5: *Scores plots due to initial and final phases of PCA*

### 8.4.6 Remarks on PCA Implementation in the First Phase

We performed a PCA on the data set that consisted of a normal operating region and a break. The conventional way is to only include the normal operating region. The second phase consisted of PCA of data that covered only the normal operating regime. The motivation for a two-phase analysis is as follows. Since we were interested in capturing the signature of those patterns leading to a sheet break, including a break would certainly serve the purpose. Once the signature is obtained and the important variables that indicate or affect an impending sheet break may be identified. This can be done using the loadings plot and then verifying the cause and effect relationships using process knowledge. The first phase therefore formed the basis in providing a set of important tags for our second phase PCA analysis, which was concerned with purely building template models for normal operating regimes.

In both the phases, a graphical plot of the scores was preferred to the conventional Hotelling $T^2$ and SPE charts. The preference came from the fact that we were mainly interested in identifying the signatures among the measurements (or a linear combination of the measurements) that could reveal some of the underlying causes of the sheet breaks. Moreover, since the PCA models were built on low-frequency coefficients, the scores would also be autocorrelated and hence the statistical limits are not reliable for monitoring purposes.

## 8.5 Results

By visual inspection of the individual signals, the abrupt features corresponding to the breaks were located in a subset of the tags. Process knowledge was used to determine the root cause, which cannot be revealed for reasons of confidentiality, but which was related to operating practice in the mill. Interpretation of the root cause was confirmed by mill personnel.

The value in this analysis was in diagnosing the possible cause of type 4 sheet breaks, giving mill personnel the opportunity to focus on the problem to find a solution. At this time of writing, we are unable to report on any corrective action. However, it appears that modification to process equipment, process control or operating practice could potentially reduce the occurrence of one type of sheet break by at least 30%.

In cases where a solution requires improved process control to avoid certain conditions, or forewarning of undesirable conditions, MSPCA can be deployed on-line to monitor the process. Development of a reliable on-line break predictor, which is beyond the scope of this study, involves considerable data analysis to maximize successful predictions, and minimize false predictions. Software and hardware currently exist to deploy this type of process monitoring reliably and economically.

## 8.6 Conclusions

Multiscale principal component analysis (MSPCA) was shown to be an effective means of locating the potential root cause of a particular type of paper machine sheet break, by extracting a small quantity of highly pertinent information from a large quantity of operating data.

The contribution of MSPCA in this project is summarized as follows.

- Principal component analysis (PCA) condensed the information in a multitude of process signals into a small set of scores. Variation in each score is inherently independent from the variation in all other scores. This feature of PCA allowed process variations correlated with sheet breaks to be retained and further analyzed, and unimportant information to be rejected from the analysis.

- Conversion of the raw signals to a set of wavelet coefficients provided a multiscale view of the data. This enhanced the effectiveness of PCA, by restricting the analysis to process variations in a narrower frequency band. Since the objective of this work was to detect gradual process changes that were correlated with

sheet breaks, only the lower frequency range was studied. Medium- and high-frequency variations were removed from the analysis, and the number of samples to be analyzed was reduced by a factor of four.

- Consistent patterns in principal component scores were found to occur prior to 30% to 40% of one type of sheet break, as detected by visual inspection. Furthermore, application of process knowledge was required in the final interpretation of the potential root cause of the sheet breaks. MSPCA therefore served to complement human interpretation by highlighting the statistical importance of a small number of key process variables.

# Chapter 9

# Conclusions and Future Work

In this work, we have mainly focused on two classes of systems that are commonly encountered in process industry, namely, *multirate* and *multiscale* systems. The former class of systems are in fact, a special case of the latter. Multirate sampling introduces explicit multiple time scales in the data due to multiple sampling intervals and therefore, is only one way of representing the underlying multiple time-scales in the process. Multiscale methods on the other hand, not only allow to deal with explicit multiscale nature in the data but also allow to capture the inherent multiple scales in a methodical way. Conventional methods are not appropriate for control or monitoring of multiscale systems as they assume availability of data at a uniform rate and project measurements onto a time-frequency plane that contains tiles of fixed resolution (single-scale).

Design of multirate controllers is challenging and complex due to their periodically time-varying (PTV) nature and lack of data at one uniform rate. Traditional methods make use of inferential strategies that estimate intersample outputs using a fast-rate model built on primary and/or secondary measurements. In contrast, in this work, *lifting techniques*, which design the fast-rate input moves based merely on the slow sampled outputs, were employed for the control of MR systems. The lifting strategy provides a more practical approach since it is independent of the existence of a fast-rate model and does not need any secondary measurement(s). The elegance in this method is due to the fact that it bridges the gap between the PTV and LTI systems by the transformation of an MR system into a fictitious single-rate system. In doing so, one can make use of well-established controller design tools for LTI single-rate systems. The resulting controller termed as the *lifted controller* gives the set of fast rate input moves (*lifted input*) that can be made over one slow sampling interval.

In arriving at a lifted controller, one has to take certain design issues into account. In this thesis, it has been shown that due to the nature of inverse lifting operator,

outputs of closed-loop lifted linear MR systems can contain intersample ripples when tracking step-type reference signals. Although the controller yields a steady lifted input, from the viewpoint of the plant, the inputs are oscillatory thereby rendering the continuous-time output of the plant oscillatory. In order to eliminate these ripples, the lifted controllers have to satisfy certain gain constraints depending on the sampling ratio. On the other hand, pre-compensation of the plant with an integrator at the input sampling rate obviates these constraints and produces ripple-free outputs. What remains of interest is to check the impact of a linear lifted controller built for a non-linear system. In future, the question that needs investigation is: *do linear lifted controllers for non-linear MR systems yield intersample ripples?* and *if yes, how can they be eliminated?* An inevitable issue with lifting strategy is the causality constraint on the controller, attributed to the non-casual nature of the lifting operator. A substantial amount of research has progressed in this direction involving the use of some advanced concepts with some computable solutions. However, there still remains a strong need for more practical solutions. Future work is concerned with exploring the existence of exact or approximate solutions to the causality constraint problem.

A strong factor that favours lifting techniques is the potential it holds as a tool for analyzing MR systems. This potential was explored in the work on the performance comparison of MR vs. SR systems. Using lifting techniques, a proof has been given to show that the closed-loop performance of MR systems is limited below by the performance of fast single-rate systems and above by that of slow single-rate systems. The proof provides a benchmark for the comparison of the performances of these systems, which in itself is a non-trivial problem, and provides a clear theoretical base for a result that has been so far only intuitively understood. Further, it also carries with it ideas useful when other benchmarks such as the $\mathcal{H}_\infty$-norm are used for performance comparison. However, the superiority of one system over another is true at all times only in the absence of model-plant mismatch. In a practical situation when the model cannot capture the behaviour of the plant accurately, it is important to analyze the robustness of this superiority. In this context, preliminary results for first-order systems were obtained with the continuous-time LQR cost function as the benchmark. The focus of this analysis was mainly to highlight the fact that faster sampling rates need not necessarily yield better performance in the presence of model-plant mismatch. The next step in this direction is to provide a more thorough analysis that allows us to provide definitive answers to the performance comparison problem in presence of uncertainties for higher-order and MIMO systems. This analysis may involve the well-known stability radius problem. At this stage, however, it is hard to

provide an intuitive answer to this problem.

On that note, we move on to briefly mention the multirate monitoring problem. Although not discussed elsewhere in this work, monitoring of multirate systems rightfully deserves the attention of a process engineer. Despite the huge accumulation of multirate data in many process industries, there is still a need for a practical method that can fuse these multirate measurements together in a simple way, allowing easy application of existing SR monitoring techniques. For this purpose, the lifting methods can prove an appropriate choice due to their ability to transform an MR system to an SR system. The resulting lifted data matrix can then be used for monitoring using well-known techniques such as PCA, PLS, etc. If successful, this idea can be beneficial to industrial applications where one is frequently faced with the monitoring of multirate systems.

Multirate sampling introduces multiple scales (resolutions) in the data, thus making MR systems a special case of MS systems. MS systems are more general in the sense that the evolution times and frequencies of the physical variables may substantially differ from each other. Conventional methods fall under the single-scale category and therefore fail to exploit the multiscale nature of the data. A consequence of this drawback, for example in process monitoring, is that they provide equal sensitivity to different kinds of faults. In practice, however, it may be necessary to monitor some faults earlier than others.

In this work, we employed wavelet transformations, one of the foremost emerging techniques that allow multiscale representations of signals. The potential of wavelet transformation in providing a multiresolution analysis of signals was illustrated with an application of MSPCA to process monitoring. While the wavelet filtering allows us to zoom into data and separate the dynamics from the stochastic component of that measurement, PCA optimally re-orients most of the cross-correlated information in a subspace with much fewer dimensions. Thus, MSPCA combines the properties of wavelet transformations with PCA to yield template models for different frequency bands. In this way, MSPCA is able to provide enhanced sensitivity to different kinds of faults when compared to the conventional PCA. The main difference between wavelet filtering and conventional filtering is that it provides a time-frequency splitting in accordance with the frequency regime. Low frequency components are resolved well in frequencies while the high frequency components are resolved well in time. The pyramidal algorithm makes the computation of wavelet transformation very efficient and fast. Another advantage is that it is not required to recalculate the filter coefficients at every level. On the theoretical aspect, since wavelet coefficients in the high frequency bands are approximately decorrelated, the assumption of time-independency

on the principal components is rightly justified using wavelet filtering. The present version of MSPCA discussed here is restricted to off-line analysis only. While off-line analysis is helpful in eliminating a significant portion of the bottlenecks in the process, it is equally important to detect and diagnose process faults on-line. The focus of future work would consist of developing MSPCA to meet the requirements of on-line detection and diagnosis.

The hierarchical decomposition in a wavelet transform results in compaction of energy in the lowest resolution scale which was exploited in early image coders. Recently the frequency-space characteristics of wavelet transform coefficients have been exploited by making use of spatial structuring of wavelet coefficients. This has resulted in the wavelet packet transform which is a generalization of wavelet transform basis. It offers a rich set of decomposition structures so that wavelet decomposition can be performed according to a subset of wavelet packet bases. This subset can be selected as the one which minimizes a predefined, application specific cost function. For process monitoring applications, this can be useful especially if one has *a priori* information about the frequency localization of process upsets. Future research involves the exploration of the ability of a wavelet packet based MSPCA and comparison of its performance with that of wavelet transform based MSPCA in the monitoring of multiscale systems.

In summary, lifting and wavelet transformation hold a strong potential in the analysis, control and monitoring of multirate/multiscale systems. This thesis gave a flavour of these techniques both in theory and practice using several examples. The underlying potential of these techniques, however, awaits exploration of their application to solving several other theoretical and real-life problems.

# Bibliography


Al-Rahmani, H.M. and G.F. Franklin (1992). Multirate control: A new apporach. *Automatica* **28**, 35–44.

Alsberg, B.K., A.M. Woodward and D.B. Kell (1997). An introduction to wavelet transforms for chemometricians: A time-frequency approach. *Chemometrics and Intelligent Laboratory Systems* **37**, 215–239.

Anderson, B. D. O. and J. B. Moore (1990). *Optimal Control - Linear Quadratic Methods*. Information and Systems Sciences. Prentice Hall, Inc.. Eaglewood Cliffs, New Jersey, USA.

Araki, M. and K. Yamamoto (1986). Multivariable multirate sampled-data systems: State-space description, transfer characteristics and Nyquist criterion. *IEEE Transactions on Automatic Control* **AC-31**(2), 145–154.

Arvanitis, K. G. (1998). On the localization of intersample ripples of linear systems controlled by generalized sampled-data hold functions. *Automatica*, **34**(8), 1021–1024.

Åström, K.J. and B. Wittenmark (1984). *Computer Controlled Systems*. Prentice-Hall. Eaglewood Cliffs, New Jersey, USA.

Åström, K.J., P. Hagander and J. Sternby (1984). Zeros of sampled-data systems. *Automatics* **20**(1), 31–38.

Bakshi, B. R. (1998). Multiscale PCA with application to multivariate statistical process monitoring. *AIChE J.*, **44**(7), 1596–1610.

Bakshi, B. R. (1999). Multiscale analysis and modelling using wavelets. *Journal of Chemometrics* **13**, 415–434.

Bakshi, B.R. and G. Stephanopoulos (1994). Representation of process trends-iii: Multiscale extraction of trends from process data. *Computers and Chemical Engineering* **18**(4), 267–302.

Bamieh, B. and J.B. Pearson (1992). The $\mathcal{H}_2$ problem for sampled-data systems. *Systems & Control Letters* **19**, 1–12.

Bamieh, B., J. B. Pearson, B. A. Francis and A. Tannenbaum (1991). A lifting technique for linear periodic systems with applications to sampled-data control. *Systems & Control Letters* **17**, 79–88.

Berg, M. C., N. Amit and J. D. Powell (1988). Multirate digital control system design. *IEEE Transactions on Automatic Control* **33**(12), 1139–1150.

Bilen, C. and S. Huzurbazar (2000). Wavelet based detection of outliers in time series. To appear in Journal of Computational and Graphical Statistics.

Blimke, D., T. Chen, D. Ford, G. Moreside, G. Navaro, G. Riger, P. Petryhyn and B. Watson (1995). The quality improvement story. *Weyerhaeuser C.L. internal memo* p. 1.

Brosilow, C. B. and M. Tong (1978). Inferential control of part ii. the structure and dynamics of inferential control systems. *AIChE Journal* **24**, 492–500.

Chaplais, F. and K. Alaoui (1996). Two time scaled parameter identification by coordination of local identifiers. *Automatica* **32**(9), 1303–1309.

Chen, T. and B. Francis (1991*a*). Linear time-varying $\mathcal{H}_2$-optimal control of sampled-data systems. *Automatica* **27**, 963–974.

Chen, T. and B. Francis (1991*b*). $\mathcal{H}_2$-optimal sampled data control. *IEEE Transactions on Automatic Control* **36**(4), 387–397.

Chen, T. and B. Francis (1995). *Optimal Sampled-Data Control Systems*. Springer-Verlag. London.

Chen, T. and L. Qiu (1994). $\mathcal{H}_\infty$ design of general multirate sampled-data control systems. *Automatica*, **30**(7), 1139–1152.

Christofides, P. D. (1998). Output feedback control of nonlinear two time-scale processes. *Ind. Eng. Chem. Res.* **37**, 1893–1909.

Christofides, P. D. and P. Daoutidis (1996*a*). Feedback control of two time-scale nonlinear systems. *International Journal of Control* **63**, 965–994.

Christofides, P.D. and P. Daoutidis (1996*b*). Feedback control of two time-scale nonlinear systems. *International Journal of Control* **63**, 965–994.

Colaneri, P. and G. De Nicolao (1995). Multirate lqg control of continuous-time stochastic systems. **31**, 591–596.

Cover, T.M. and J.A. Thomas (1991). *Elements of Information Theory*. Wiley Interscience. New York.

Daubechies, I. (1988). Orthogonal bases of compactly supported wavelets. *Commun. Pure Appl. Math* **41**(7), 909–996.

Daubechies, I. (1990). The wavelet transform, time-frequency localization and signal analysis. *IEEE Trans. Inf. Theory* **36**, 961–1005.

Daubechies, I. (1992). *Ten Lectures in Wavelets*. Society for Industrial and Applied Mathematics. Philadelphia, Pennsylvania.

D'Hulster, F. M. and A. R. van Cauwenberghe (1981). Application of parameter adaptive inferential control to non-continuously measurable quality variables. In: *Proceedings of the Second World Congress of Chemical Engg.*. Montreal, Canada.

Donoho, D. (1995). De-noising by soft-thresholding. *IEEE Transactions on Information Theory* **41**(3), 613–627.

Donoho, D. L., L. M. Johnstone, G. Kerkyacharian and D. Picard (1995). Wavelet shrinkage: Asymptopia?. *J. R. Stat. Soc. B* **57**, 301–309.

Doroslovacki, M. J. and H. Fan (1996). Wavelet-based linear system modelling and linear filtering. *IEEE Transactions on Signal Processing* **44**(5), 1156–1167.

Dunia, R., S.J. Qin, T.F. Edgar and T.J. McAvoy (1996). Identification of faulty sensors using principal component analysis. *AIChE J.* **42**(10), 2797–2811.

Dyer, M. S., O. Karsligil and G. Stephanopoulos (1998). Multiscale state estimation and its applications to process operations analysis and model predictive control. AIChE.

Engel, J. (1994). A simple wavelet approach to nonparametric regresson from recursive partitioning schemes. *Journal of Multivariate Analysis* **49**(2), 242–254.

Fisher, D. (1975). Experiences with paper machine stock system instability. *Spring Conference CPPA Technical Section, Pacific Coast and Western Branches* pp. 1–5.

Francis, B.A. and T.T. Georgiou (1988). Stability theory for linear time-invariant plants with periodic digital controllers. *IEEE Transactions on Automatic Control* **33**(9), 820–832.

Franklin, G. F. and A. Emami-Nacini (1986). Design of ripple-free multivariable robust servomechanisms. *IEEE Transactions on Automatic Control,* **31**, 661–664.

Freidland, B. (1961). Sampled-data control systems containing periodically varying members. In: *IFAC World Congress.* Vol. 37. pp. 361–367.

Glasson, D. P. (1983). Development and applications of multirate digital control. *IEEE Control Systems Magazine* **3**(4), 2–8.

Glasson, D.P. (1980). *Research in Multirate Estimation and Control.* Analytic Sciences Corporation. Six Jacob Way, Reading, Massachussets, USA.

Grasselli, G.M., L. Jetto and S. Longhi (1995). Ripple-free dead-beat tracking for multirate sampled-data systems. *International Journal of Control,* **61**(6), 1437–1455.

Greenblatt, S.A. (1994). Wavelets in econometrics: An application to outlier testing. Report 23. University of Reading. http://econwpa.wustl.edu/eprints/em/papers/9410/9410001.abs.

Grossman, A. and J. Morlet (1984). Decomposition of hardy functions into square integrable wavelets of constant shape. *SIAM J. of Anal. Math.* **15**(4), 723–736.

Gudi, R. D. (1995). Multirate Estimation, Control and Monitoring of Fed-Batch Fermentation. PhD thesis. Department of Chemical and Materials Engg., University of Alberta. Edmonton, Alberta, Canada.

Guilandoust, M. T., A. J. Morris and M. T. Tham (1987). Adaptive inferential control. *IEEE Proceedings* **134**, 492–500.

Haar, A. (1910). Zur theorie der orthogonalen funktionen-systeme. *Math. Ann.* **69**, 331–371.

Hotelling, H. (1933). Analysis of a complex of statistical variables into principal components. *Journal of Educational Pyschology* **24**, 417–441.

Ibrahim, A. (1981). Formation and basis weight uniformity through headbox control: Art or science?. In: *Technical Association of the Pulp and Paper Industry*. pp. 95–117.

Jackson, J.E. (1980). Principal components and factor analysis: I. principal components. *Journal of Quality Technology* **12**(4), 201–213.

Jackson, J.E. and G. Mudholkar (1979). Control procedures for residuals associated with principal component analysis. *Technometrics* **21**, 341–349.

Jayant, N.S. and P. Noll (1984). *Digital Coding of Waveforms*. Prentice-Hall. Englewood Cliffs, NJ.

Jury, E. I. and F. J. Mullin (1959). The analysis of sampled-data control systems with a periodically time-varying sample rate. *IRE Transactions on Automatic Control* **AC-24**, 15–21.

Kabamba, P. T. (1987). Control of linear systems using generalized sampled-data hold functions. *IEEE Transactions on Automatic Control*, **AC-32**, 772–783.

Kalman, R. E. (1960). A new approach to linear filtering and prediction problems. *Trans. ASME Journal of Basic Engineering*, **82**, 34–45.

Kalman, R. E. and J. E. Bertram (1959). A unified approach to the theory of sampling systems. *J. Franklin Inst.*, **267**, 405–436.

Karsligil, O., M. Dyer and G. Stephanopoulos (1999). Multiscale model predictive control. AIChE Annual Meeting, Los Angeles.

Keller, D.S., J. Lewalle and P. Luner (1999). Analysis of paper variability using the continuous wavelet transform. *Paperi ja Puu Paper and Timber* **81**, 440–446.

Khalil, H.K. (1987). Output feedback control of linear two-time-scale systems. *IEEE Transactions on Automatic Control* **AC-32**, 784–792.

Khargonekar, P. P., K. Poolla and A. Tannenbaum (1985). Robust control of linear time-invariant plants using periodic compensation. *IEEE Transactions on Automatic Control* **30**, 1088–1096.

Khargonekar, P.P. and N. Sivashankar (1992). $\mathcal{H}_2$-optimal control for sampled-data systems. *Systems & Control Letters* **18**, 627–631.

Kokotovic, P.V., H. K. Khalil and J. O'Reilly (1986). *Singular Perturbations in Control: Analysis and Design*. Academic Press. London.

Kokotovic, P.V., R.E. O'Malley, Jr. and P. Sannuti (1976). Singular perturbation and order reduction in control theory - an overview. *Automatica* **12**, 123–132.

Kosanovich, K. A. and M. J. Piovoso (1997). PCA of wavelet transformed process data for monitoring. *Intelligent Data Analysis*.

Kranc, G. M (1957). Input-output analysis of multirate feedback systems. *IRE Transactions on Automatic Control* **3**, 21–28.

Kresta, J., J. F. MacGregor and T. E. Marlin (1991). Multivariate statistical monitoring of process operating performance. *Canadian J. Chem. Engg.*

Krishnan, A. and K.A. Hoo (1999). A multiscale model predictive control strategy. *Industrial Engineering Chemistry Research* **38**(5), 1973–1986.

Ku, W., R.H. Storer and C. Georgakis (1995). Disturbance detection and isolation by dynamic principal component analysis. *Chem. Intell. Lab. Sys.* **30**, 179–196.

Kučera, V. (1972). The discrete riccati equation of optimal control. *Kybernetica* **8**, 430–447.

Lakshminarayanan, S., A. K. Tangirala, S. L. Shah, K. Akamatsu and S. Ooyama (1998). Soft sensor design using partial least squares and neural networks: Comparison and industrial applications. AIChE Annual Meeting, Miami, FL, USA.

Lee, J.H. and M. Morari (1992). Robust inferential control of multirate sampled-data systems. *Chemical Engineering Science* **47**(4), 865–885.

Lee, S., S.M. Meerkov and T. Runolfsson (1987). Vibrational feedback control: Zeros placement capabilities. *IEEE Transactions on Automatic Control* **AC-32**, 604–611.

Levis, A.H., R.A. Schlueter and M. Athans (1971). On the behaviour of optimal linear sampled-data regulators. *International Journal of Control* **13**(2), 343–361.

Li, D., S. L. Shah and T. Chen (2000*a*). Robustness analysis of multirate inferential control systems. In: *Proceedings of the Asian Control Conference*. Shanghai, China. pp. 2768–2772.

Li, D., S. L. Shah and T. Chen (2001). Identfication of fast-rate models from multirate data. *International Journal of Control* **74**(7), 680–689.

Li, D., S.L. Shah and T. Chen (2000*b*). Identification of fast-rate models from multirate data. Accepted for publication in the International J. of Control.

Li, I. (1997). Prediction and prevention of sheet break using partial least squares and an expert system. Master's thesis. University of British Columbia, Department of Chemical Engineering. Vancouver.

Li, W., H.H. Yue, S.V. Cervantes and S.J. Qin (2000*c*). Recursive pca for adaptive process monitoring. *Journal of Process Control* **10**, 471–486.

Locke, I. (1966). The effect of hydraiulic properties of the fluid on the formation on a high speed fourdriner. *Paper Trade Journal* pp. 42–48.

Longman, R.W. and C. Lo (1997). Generalized holds, ripple attenuation, and tracking additional outputs in learning control. *Journal of Guidance Control and Dynamics* **20**(6), 1207–1214.

Lu, W. and D. G. Fisher (1990). Multirate constrained adaptive control. *International Journal of Control* **51**, 1439–1456.

Luo, R., M. Misra and D.M. Himmelblau (1999). Sensor fault detection via multiscale analysis and dynamic pca. *Industrial and Engineering Chemistry Research* **38**(4), 1489–1495.

Luse, D.W. and H.K. Khalil (1985). Frequency domain results for systems with slow and fast dynamics. *IEEE Transactions on Automatic Control* **AC-30**(12), 1171–1178.

MacGregor, J. F. (1994). Statistical process control of multivariate processes. In: *IFAC ADCHEM*. Kyoto (Japan).

Mallat, S. G. (1989). A theory for multiresolution signal decomposition : The wavelet representation. *IEEE Trans. on Pattern Analysis and Machine Intelligence* **11**, 674–693.

Mallat, S.G. (1998). *A Wavelet Tour of Signal Processing*. Academic Press. london, UK.

Mallat, S.G. and S. Zhong (1992). Characterization of signals from multiscale edges. *IEEE Transactions on Pattern Recognition and Machine Intelligence* **14**(7), 710–732.

Mardon, J., R.E. Mohanan and B.I. Howe (1969). The operation of paper machine headboxes. *Pulp and Paper Magazine of Canada* pp. 57–80.

McEachen, J.C. and D.G. Meyer (1991). Tradeoffs for multi-rate controller design and exact comparisons with single-rate control. *IEEE Control Systems Magazine* **11**(6), 30–35.

Meyer, D. G. (1990). A parametrization of stabilizing controllers for multirate sampled-data systems. *IEEE Transactions on Automatic Control* **AC-35**, 233–236.

Meyer, D. G. (1992). Cost translation and a lifting approach to the multirate LQG problem. *IEEE Transactions on Automatic Control*, **AC-37**, 1411–1415.

Meyer, R. A. and C. S. Burrus (1975). A unified analysis of multirate and periodically time-varying digital filters. *IEEE Transactions on Circuits and Systems* **22**, 162–168.

Meyer, Y. (1986). Ondelettes et fonctions splines. Seminaire EDP. Ecole Polytechnique. Paris.

Mirkin, L. and H. Rotstein (1997). On the characterization of sampled-data controllers in the lifted domain. *Systems and Control Letters* **29**, 269–277.

Morlet, J., G. Arens, I. Fougean and D. Glard (1982). Wave propagation and sampling theory. *Geophysics* **47**, 203–236.

Nason, G.P. (1996). Wavelet shrinkage using cross-validation. *J. R. Statist. Soc. B.* **58**, 463–479.

Nesic, Z., M. Davies and G. Dumont (1980). Paper machine data analysis and compression using wavelets. *TAPPI Journal* **80**(10), 191–204.

Nomikos, P. and J.F. MacGregor (1994). Monitoring batch processes using multiway principal component analysis. *AIChE J.* **40**(8), 1361–1375.

Nounou, M.N. and B.R. Bakshi (1999). Online multiscale filtering of random and gross errors without process models. *AIChE Journal* **45**(5), 1041–1058.

Nyquist, H. (1928). Certain topics in telegraph transmission theory. *AIEE Transactions* **47**, 617–644.

Ogden, T. and E. Parzen (1996). Data dependent wavelet thresholding in non-parametric regression with change-point application. *Computational Statistical Data Analysis* **22**, 53–70.

O'Reilly, J. (1980). Dynamical feedback control for a class of singularly perturbed systems using a full-order observer. *International Journal of Control* **31**, 1–10.

Pearson, K. (1901). On lines and planes of closest fit to systems of points in space. *Phil. Mag., Ser. B.* **2**, 559–572.

Qiu, L. and K. Tan (1998). Direct state-space solution of multirate sampled-data $\mathcal{H}_2$ optimal control. *Automatica* **34**, 1431–1437.

Qiu, L. and T. Chen (1995). $\mathcal{H}_2$-optimal design of multirate sampled-data systems. *IEEE Transactions on Automatic Control* **AC-39**, 2506–2511.

Ragaziini, J.M. and G.F. Franklin (1958). *Sampled-Data Control Systems*. Mc-Graw Hill. New York, USA.

Ravi, R., P. P. Khargonekar, K. D. Minto and C. N. Nett (1990). Controller parametrization for time-varying multirate plants. *IEEE Transactions on Automatic Control* **AC-35**, 1253–2162.

Rochealeau, A. (1965). A practical approach to the reduction of machine direction and cross direction basis weight variations. *Phil. Mag., Ser. B.* **48**, 48–57.

Sagfors, M. F. and H. T. Toivonen (1998). $\mathcal{H}_\infty$ control of multirate sampled-data systems: A state-space approach. *Automatica* **34**, 415–428.

Saksena, V.R., J. O'Reilly and P.V. Kokotovic (1984). Singular perturbation and time scale methods in control theory: Survey 1976-1983. *Automatica* **20**(3), 273–293.

Shannon, C. E. (1949). Communications in the presence of noise. In: *Proceedings of the IRE*. Vol. 37. pp. 10–21.

Shu, H. and T. Chen (1996). State-space approach to discrete-time $\mathcal{H}_2$ optimal control with a causality constraint. *Systems Control Letters* **26**, 69–77.

Sjoberg, A., Q.H. Zhang, L. Ljung, A. Benveniste, B. Delyon, P.Y. Glorennec, H. Hjalmarsson and A. Juditsky (1995). Non-linear black box modeling in system-identification: A unified overview. *Automatica* **31**, 1691–1724.

Sklansky, J. and J. R. Ragazzini (1955). Analysis of errors in sampled-data feedback systems - part ii. *AIEE Transactions* **74**, 65–71.

Skogestad, S. (1997*a*). Dynamics and control of distillation column - a critical survey. *Modeling, Identification and Control*, **18**(3), 177–217.

Skogestad, S. (1997*b*). Dynamics and control of distillation column - a tutorial introduction. Technical report. Department of Chemical Engineering, Norwegian University of Science and Technology.

Skogestad, S. and I Postlethwaite (1996). *Multivariable Feedback Control*. John Wiley and Sons. West Sussex, England.

Smith, M.J. and T.P. Barnwell III (1986). Exact reconstruction for tree structured sub-band coders. *IEEE. Transactions on Acoustic Speech and Signal Processing* **34**(3), 431–441.

Stephanopoulos, G., M. Dyer and O. Karsligil (1997). Multi-scale modelling, estimation and control of processing systems. *Comput. Chem. Engg.* **21**, S797–S803.

Stephanopoulos, G., O. Karsligil and M.S. Dyer (1998). Multiscale aspects in model predictive control. In R. Berber & C. Kravaris, Nonlinear Model Based Control NATO ASI. The Netherlands: Kluwer Academic Publishers. 667-734.

Storer, J.A. (1988). *Data Compression, Methods and Theory.* Computer Science Press. Rockville, MD.

Strang, G. (1989). Wavelets and dilation equations: A brief introduction. *SIAM Review* **31**, 614–627.

Tabaru, T. and S. Shin (1997). Dead-time detection by wavelet transform of cross-spectrum data. In: *IFAC ADCHEM.* pp. 311–316.

Tangirala, A. K., D. Li, R. S. Patwardhan, S. L. Shah and T. Chen (1999). Some issues in multirate process control. In: *ACC Proceedings.* San Diego, CA, USA. pp. 2771–2775.

Tangirala, A. K., D.Li, R. S. Patwardhan, S. L. Shah and T. Chen (2001). Ripple-free conditions in lifted multirate control systems. To appear in Automatica.

Tangirala, A.K., R.S. Patwardhan, S.L. Shah and T. Chen (2000). LQR performance comparison of multirate vs. single-rate systems. Presented at ACC, San Diego, CA. - Accepted for publication in the *Journal of Dynamics of Continuous, Discrete and Impulsive Systems.*

Tong, H. and C.M. Crowe (1995). Detection of gross errors in data reconciliation by principal component analysis. *AIChE J.* **41**(7), 1712 1722.

Tsatsanis, M. K. and G. B. Giannakis (1993). Time-varying system identification and model validation using wavelets. *IEEE Transactions on Signal Processing* **41**(12), 3512–3523.

Vetterli, M. (1986). Filter banks allowing perfect reconstruction. *Signal Processing* **10**(3), 219–244.

von Sachs, R. and K. Schneider (1996). Wavelet smoothing of evolutionary spectra by nonlinear thresholding. *Journal of Applied and Computational Harmonic Analysis* **3**(3), 268–282.

Voulgaris, P.G. and B. Bamieh (1993). Optimal $\mathcal{H}_\infty$ and $\mathcal{H}_2$ control of hybrid multirate systems. *Systems & Control Letters* **20**, 249–261.

Whittaker, J. (1935). Interpolatory function theory. *Cambridge Tracts in Mathematical and Mathematical Physics.*

Wise, B.M., N.L. Ricker, D.F. Veltkamp and B.R. Kowalski (1990). A theoretical basis for the use of principal component models for monitoring multivariate processes. *Process Control and Quality* **3**(1), 41–51.

Wold, S., K. Esbensen and P. Geladi (1987). Principal component analysis. *Chem. Intell. Lab. Sys* **2**, 37–52.

Youla, D.C., H.A. Jahr and J.J. Bongiorno (1976). Modern weinet-hopf design of optimal controllers: part2. *IEEE Transactions on Automatic Control* **AC-21**, 319–338.

Zhang, H., A.K. Tangirala and S.L. Shah (1999). Dynamic process monitoring using multiscale pca. In: *Canadian Conference on Electrical and Computer Engineering*. Vol. 3. pp. 1579–1584.